Compound Specific Concentration and Stable Carbon Isotope Ratio Measurements of Secondary Organic Aerosols

Marina Sonia Saccon

A Dissertation submitted to the Faculty of Graduate Studies in Partial Fulfillment of the Requirements for the Degree of

Doctor of Philosophy

Graduate Program in Chemistry

York University

Toronto, Ontario

October 2013

Abstract

The formation, composition and processing of secondary organic aerosols (SOA) in the atmosphere is poorly understood and is of great interest to the scientific community. It has been proposed that the use of concentration and isotope ratios measurements from precursors and products can test the applicability of laboratory results to the atmosphere. A method has been developed for the determination of concentration and stable carbon isotope ratios of SOA in the atmosphere. Nitrophenols, formed specifically from the photooxidation of aromatic volatile organic compounds (VOC), are the target compounds in this study. These compounds are semi-volatile in nature, and therefore can exist in both the gas phase and in particulate matter (PM). Consequently, two types of filters, uncoated quartz filters and quartz filters coated with XAD-4^{TM} resin, were used for the collection of nitrophenols. Filters were extracted with acetonitrile with an HPLC and solid phase extraction (SPE) clean up step followed by derivatization with N,O-bis(trimethylsilyl) trifluoroacetamide (BSTFA). Samples were analyzed for concentrations by GC-MS at York University and isotope ratio analysis was conducted at Environment Canada using GC-IRMS.

The developed method gave a precision of 5 % for concentration measurements and 0.3 ‰ for isotope ratio measurements. The detection limits achieved for concentration measurements were in the pg m^{-3} range. Through comparison of concentration measurements in each phase, the majority of nitrophenols was found to be in the gas phase, consistent with findings from Facca (2013). The isotope ratios of the nitrophenols were used to find their photochemical ages (PCA), during which they were

formed by oxidation of the precursor, which is the time the precursor has been exposed to the HO radical in the atmosphere. With the inclusion of possible isotopic fractionation that could occur during the reaction mechanism of the precursor and possible loss reactions of the product, the PCA were found to be comparable to those found from precursor isotope ratios by Kornilova (2012). Ambient yields of the nitrophenols were found to be orders of magnitude lower than predicted from laboratory studies, indicating that the quantitative extrapolation of laboratory studies to the atmosphere may not necessarily be acceptable.

Acknowledgements

The success of this research project was made possible due to the support of several individuals over the years. First and foremost, I would like to thank my supervisor, Dr. Jochen Rudolph. His enthusiasm for this research is what made me interested in atmospheric chemistry to begin with, and his constant support, guidance and patience thereafter is what has helped me to where I am today. I would also like to thank him for teaching me the importance of having more than two watches.

I would also like to thank Dr. Geoff Harris and Dr. Robert McLaren for being a part of my supervisory committee members over the past few years. Their input and suggestions have been helpful and appreciated. I would also like to sincerely thank Dr. Yongsheng Chen and Dr. Habil Astrid Kiendler-Scharr for being a part of my defense committee.

I appreciate the tremendous support from Dr. Lin Huang and Dr. Douglas Lane during my time at Environment Canada. I would like to acknowledge their meaningful scientific discussions and allowing me to use their laboratories and resources. This research would not have been possible without them.

I have been very fortunate to have wonderful and supportive group members in the Rudolph group during my time here. I would like to thank Anna Kornilova and Christine Facca for their daily discussions, support, laughter and friendships. They have truly made an imprint on my life and I will forever cherish their friendship. I would also like to take this opportunity to thank past and present group members Rosalyne, Sophie, Xueping, Satoshi, Richard and Yasamin, all of the previous undergraduate students that have passed through our laboratory, as well as other CAC members, especially Amanda, Dana, Kim, Mehrnaz, Zena, Zoë and Zoya. A special thanks also goes out to Carol Weldon and all CAC work study students for their support throughout the years.

Lastly, I would like to thank my parents, Lorenzo and Gloria, my sister, Daniela and my fiancé, Joseph. These individuals have shown remarkable love, support and patience through the years. It has been their encouragement that has pushed me to where I am today. Thank you.

Table of Contents

List of Figures

List of Tables

Commonly Used Abbreviations and Special Notations

[HO]t	photochemical age
^{12}C	carbon-12 isotope of carbon
^{13}C	carbon-13 isotope of carbon
2,6-dime-4-NP	2,6-dimethyl-4-nitrophenol
2,6-dime-ph	2,6-dimethylphenol
2-me-3-NP	2-methyl-3-nitrophenol
2-me-4-NP	2-methyl-4-nitrophenol
2-me-5-NP	2-methyl-5-nitrophenol
2-me-ph	2-methylphenol
3-me-2-NP	3-methyl-2-nitrophenol
3-me-4-NP	3-methyl-4-nitrophenol
3-me-ph	3-methylphenol
4-me-2-NP	4-methyl-2-nitrophenol
4-me-ph	4-methylphenol
4-NP	4-nitrophenol
5-me-2-NP	5-methyl-2-nitrophenol
6-me-2-NP	6-methyl-2-nitrophenol
A	area of filter
AU	arbitrary units
BET	Brunauer, Emmett and Teller
BSTFA	N,O-bis(trimethylsilyl) trifluoroacetamide

C17	heptadecane
C18	octadecane
C19	nonadecane
Cal	response from calibration curve
C_C	Cunningham slip correction factor
D_p	particle diameter
DL	detection limit
F	reaction coordinate
f_{om}	weight fraction absorbing in organic matter
FID	flame ionization detector
G	gaseous-associated concentration
GC-MS	gas chromatography mass spectrometry
GC-IRMS	gas chromatography isotope ratio mass spectrometry
HLB	hydrophilic-lipophilic balanced
HPLC	high performance liquid chromatography
i.d.	inner diameter
IS	internal standard
k	rate constant
K_p	partitioning coefficient
KIE	kinetic isotope effect
m	mass
MTBSTFA	N-methyl-N-tert-butyldimethylsilylfluoroacetamide

MW	molecular weight
n	moles
NA	not available
ND	not detected
o.d.	outer diameter
om	organic matter
P	particle-associated concentration
p_A	partial pressure of component A in solution
p_A *	vapour pressure of pure liquid A
PA	peak area
PCA	photochemical age
PM	particulate matter
PM2.5	particulate matter with an aerodynamic diameter less than 2.5 μm
POM	particulate organic matter
QL	quantification limit
R	gas constant
SD	standard deviation
SEM	standard error of the mean
SIF	sorbent impregnated filter
SIM	selective ion monitoring
SOA	secondary organic aerosols
SPE	solid phase extraction

SVOC	semi-volatile organic compounds
T	temperature
TLC	thin layer chromatography
TMS	trimethylsilyl
TSP	total suspended particulate
u	flow rate of air sampler
V	sampling volume
V-PDB	Vienna-peedee belemnite scale
VOC	volatile organic compounds
VWD	variable wave detector
w	width of impactor jet
$\delta^{13}C$	delta value
ϵ	efficiency of air sampler
ε	kinetic isotope effect in per mille
ρ	particle density
μ	viscosity of air
μ_{FV}	face velocity of filter
χ	mixing ratio
χ_A	mole fraction of component A
ζ_A	activity of component A

List of Equations

Eq. 2.1 $$K_P = \frac{P/TSP}{G}$$

Eq. 2.2 $$p_A = \chi_A p_A^*$$

Eq. 2.3 $$p_A = \zeta_A \chi_A p_A^*$$

Eq. 2.4 $$n_A = \frac{P_A}{MW_A 10^9}$$

Eq. 2.5 $$n_{Tot} = \frac{f_{om} TSP}{MW_{om} 10^6}$$

Eq. 2.6 $$K_P = \frac{f_{om} 760RT}{MW_{om} \zeta_i p_{L,A}^0 10^6}$$

Eq. 2.7 $$\delta^{13}C = \frac{(^{13}C/^{12}C)_{sample} - (^{13}C/^{12}C)_{V-PDB}}{(^{13}C/^{12}C)_{V-PDB}} \times 1000‰$$

Eq. 2.8 $$\varepsilon = \frac{k_{12} - k_{13}}{k_{13}} \times 1000‰$$

Eq. 2.9 $$F = \frac{\chi_0 - \chi_{amb}}{\chi_0}$$

Eq. 2.10 $$\chi_{proc} = \chi_{amb} \frac{F}{1 - F}$$

Eq. 2.11 $$\delta^{13}C_{pre} = \delta^{13}C_0 + k_{12} \varepsilon [HO] t$$

Eq. 2.12 $$\chi_{amb} = \chi_0 \exp(-k_{12}[HO]t)$$

Eq. 2.13 $$F = 1 - exp\left(-\frac{\Delta\delta^{13}C}{\varepsilon}\right)$$

Eq. 2.14 $$F = \frac{\delta^{13}C_0 - \delta^{13}C_t^{pre}}{\delta^{13}C_t^{prod} - \delta^{13}C_t^{pre}}$$

Eq. 3.1 $$\epsilon = \frac{2u}{w}\left(\frac{C_c \rho D_p^2}{18\mu}\right)$$

Eq. 3.2 $$D_{p2}^2 = \frac{D_{p1}^2 u_1}{u_2}$$

Eq. 3.3 $$\mu_{FV} = \frac{u}{A}$$

Eq. 3.4 $$m_T = \frac{PA_T Cal_{IS}}{Cal_T PA_{IS}} m_{IS}^{Der} \frac{MW_T^{free}}{MW_T^{Der}}$$

Eq. 3.5 $$C_T = \frac{m_T - m_B}{V}$$

Eq. 3.6 $$\delta^{13}C_{free} = \frac{\#C_{deriv}}{\#C_{free}} \times \delta^{13}C_{deriv} - \frac{\#C_{TMS}}{\#C_{free}} \times \delta^{13}C_{TMS}$$

Eq. 5.1 $$\delta^{13}C_{prod} = \frac{\delta^{13}C_o - \exp(-k_{HO}[HO]t)(\delta^{13}C_o + k_{12}\varepsilon[HO]t)}{1 - \exp(-k_{HO}[HO]t)}$$

Eq. 5.2 $$\delta^{13}C_{prod} = \left(\frac{^{13}C}{^{12}C}\right)prod - 1 \times 1000\ ‰$$

Eq. 5.3a $$d^{12}C_{prod} = -^{12}C_{prod}[HO]dt + {}^{12}C_{int}[HO]dt$$

Eq. 5.3b $$d^{13}C_{prod} = -^{13}C_{prod}[HO]dt + {}^{13}C_{int}[HO]dt$$

Eq. 5.4a $$d^{12}C_{int} = -^{12}C_{int}[HO]dt + {}^{12}C_{pre}[HO]dt$$

Eq. 5.4b $$d^{13}C_{int} = -^{13}C_{int}[HO]dt + {}^{13}C_{pre}[HO]dt$$

Eq. 5.5a $$d^{12}C_{pre} = -^{12}C_{pre}[HO]dt$$

Eq. 5.5b $$d^{12}C_{pre} = -^{12}C_{pre}[HO]dt$$

1. Introduction

Volatile organic compounds (VOC) are emitted in large quantities into the atmosphere by both biogenic and anthropogenic sources. Anthropogenic VOC emissions in Canada have been estimated to decrease from 2.4 Tg Yr^{-1} in 1995 to less than 2 Tg Yr^{-1} in 2005 (Environment Canada, 2012[b]). Consisting of thousands of different compounds, VOC, once emitted, can undergo photooxidation in the atmosphere to produce products of lower volatility, known as semi-volatile organic compounds (SVOC), which can exist in the gas phase and in particulate matter (PM). One of the still poorly understood processes in the atmosphere is the formation of secondary organic matter from the photooxidation of atmospheric VOC. PM has been confirmed to have adverse effects on climate and health and a better understanding in their formation and atmospheric processing is needed in order to develop effective mitigation strategies. In fact, a direct correlation has been observed between the rate of mortality and PM levels. Specifically PM with an aerodynamic diameter less than 2.5 μm (PM2.5), has been found to negatively impact human health (Dockery et al., 1993; Pope et al., 1995).

Nitrophenols are products formed specifically from the photooxidation of aromatic VOC, such as toluene, benzene and m-xylene (Forstner et al., 1997; Atkinson, 2000; Jang and Kamens, 2001; Hamilton et al., 2005; Sato et al., 2007) and are the target compounds in this study. This class of compounds has only been studied in the atmosphere by a limited number of studies (Herterich and Hermann, 1990; Nishioka and Lewtas, 1992; Lüttke and Levsen, 1997; Cecinato et al., 2005; Moukhtar et al., 2011).

Laboratory studies have been conducted to quantify their yields (Forstner et al., 1997; Irei, 2008); however, the yields reported in these studies differ substantially and due to using unrealistically high precursor mixing ratios and seeded particles, large uncertainties are introduced. Based on laboratory yields, atmospheric concentrations are predicted to be in the range of several ng m^{-3} but have often been found in the sub ng m^{-3} range in ambient measurements (Nishioka and Lewtas, 1992; Lüttke and Levsen, 1997; Moukhtar et al., 2011).

It has recently been proposed that the combination of concentration and isotope ratio measurements can be used to gain insight into formation and processing of secondary organic products in the atmosphere, differentiate between chemical processing and mixing and to gain insight into true ambient yields (Goldstein and Shaw, 2003; Rudolph, 2007; Irei, 2008). To accomplish this, the target compounds should be formed specifically from one type of reaction, as the nitrophenols are, so that they can be traced back to the precursor. To limit the number of possible precursors, only ring retaining products were considered as target compounds in this work. Furthermore, the target compounds should have an isotope ratio that can be predicted from known isotope effects and the precursor isotope ratios. It has been found in laboratory studies that the isotope ratio of methylnitrophenols formed from the gas phase oxidation of toluene is very close to that of the isotope ratio of the sum of all products (Irei, 2008). This allows a first order prediction of the isotope ratio of atmospheric methylnitrophenols for comparison with observations. Lastly, the precursor should be emitted in large quantities since numerous compounds can be formed as secondary products, often resulting in low ambient yields.

This is important since the sample mass needed to quantify isotope ratios is orders of magnitudes larger than needed to quantify concentrations.

Stable carbon isotope ratios have been used extensively to gain insight into environmental processes, but only in the past two decades have been used to study the ambient processing of atmospheric VOC (Rudolph et al., 1997; Tsunogai et al., 1999; Czuba, 2000; Czapiewski et al., 2002; Rudolph et al., 2002; Saito et al., 2002; Rudolph et al., 2003; Thompson, 2003; Kornilova, 2012; Kornilova et al., 2013). Research results presented in these studies have proven useful to characterize different environments using isotope ratios and applying them in determining the photochemical age (PCA) of a species. Research using the isotope ratios of secondary organic matter are lacking and have only been occasionally studied in the laboratory (Irei, 2008; Fisseha et al., 2009[b]; Irei et al., 2011) and in the atmosphere (Fisseha et al., 2009[a]; Li et al., 2010; Moukhtar et al., 2011).

This work presents the development of a method to quantify concentration and stable carbon isotope ratio measurements of nitrophenols that is based on the method described by Moukhtar et al. (2011). High volume air samplers have been used extensively for the collection of trace compounds in PM. Due to its high flow rate of 1.13 m^3 min^{-1}, a volume of air upwards of 1600 m^3 can be collected in a 24 hour period. This is important given the relatively low concentrations of ambient nitrophenols previously found in the atmosphere (Herterich and Hermann, 1990; Nishioka and Lewtas, 1992; Lüttke and Levsen, 1997; Cecinato et al., 2005; Moukhtar et al., 2011) and the

relatively high mass of carbon needed for isotope ratio measurements (Rudolph, 2007). Quartz filters are traditionally used for the high-volume collection of PM due to their ability to support a high mass without creating a significant pressure difference and having low levels of artifacts. Busca (2010) has found strong evidence that nitrophenols in the Toronto area exist mainly in the gas phase. Since gas phase nitrophenols cannot be collected using quartz filters alone, Busca developed a method to use sorbent impregnated filters (SIF) to do so. XAD-4™ was the adsorbent chosen to coat quartz filters to collect nitrophenols due to its success in being used as an adsorbent for phenols in ambient air and aqueous solutions from other studies (Herterich and Hermann, 1990; Nishioka and Lewtas, 1992; Ku and Lee, 2000; Morville et al., 2004). Both types of filters were extracted according to a procedure originally developed by Moukhtar et al. (2011) and modified in this work.

All air sampling was conducted at York University in Toronto, Canada which is a location that is on the outskirts of Toronto with pollution sources dominated by transportation. PM sampling occurred from 2009 to 2012 and gas phase and PM sampling occurred from 2011 to 2012. Concentration data were determined for each of the filters, which allowed for the observation of correlations in concentration with atmospheric pollutants and meteorological factors. Isotope ratio measurements could only be acquired for samples that had a large enough mass. Although several of the collected samples thus were eliminated, the reduced data set still provided valuable information from the isotope ratios such as the PCA of secondary products as well as their ambient yields.

The formation mechanisms of the target nitrophenols, as proposed from laboratory studies, their possible losses in the atmosphere and background information on isotope ratios, the kinetic isotope effect (KIE) and PCA are explained in Section 2 (Theory). The experimental method, including the preparation of coated and uncoated quartz filters, the sampling and extraction of the filters as well as analysis by gas chromatography mass spectrometry (GC-MS) and gas chromatography isotope ratio mass spectrometry (GC-IRMS) are described in Section 3 (Methodology). Method validation and evaluation tests are presented in Section 4 (Results) along with a summary of ambient results from concentration measurements and isotope ratio measurements in each phase. Section 5 (Discussion) discusses the overall uncertainty of the method, the comparison and insight into possible differences in concentration and isotope ratio measurements of nitrophenols in each phase, the PCA of nitrophenols, as determined from isotope ratios and the ambient yields of phenols. Conclusions are made in Section 6 as well as suggestions for future directions of this work.

2. Theory

2.1. Chemical Formation of Nitrophenols

Nitrophenols are compounds that can be formed in the atmosphere through the photooxidation of aromatic VOC. Several laboratory studies have found methylnitrophenols to be products of the toluene + HO reaction (Fig 2.1) (Atkinson, 1994; Forstner et al., 1997; Jang and Kamens, 2001; Sato et al., 2007). This reaction is initiated by an addition of a HO radical to the ring, which has a branching ratio of 90 % of reactions and can produce both ring-retaining and ring-fragmentation products (Atkinson et al., 1992). The addition of the HO radical to form a methyl hydroxycyclohexadienyl radical has been found to be most favourable when added in the ortho position (Andino et al., 1996). Atmospheric oxidants such as O_2 or NO_2 can then react with this radical to form methylphenols (cresols) (Atkinson, 1994). A HO radical can react with the cresol, followed by a reaction with NO_2 to form nitrophenols (Forstner et al., 1997). The major pathway was found to be by a HO addition to the ring (Atkinson et al., 1980). 2,6-dimethyl-4-nitrophenol, hypothesized to be formed by the photooxidation of m-xylene, is proposed to follow the same reaction pathway as the HO induced oxidation of toluene (Forstner et al., 1997; Bennett, 2010).

The formation mechanism of 4-nitrophenol in the atmosphere has three proposed mechanisms. Each mechanism begins with phenol as a precursor, which can be emitted directly from anthropogenic sources or can be formed through the photooxidation of benzene, which is also emitted from similar sources (Section 2.2). Atkinson et al. (1992)

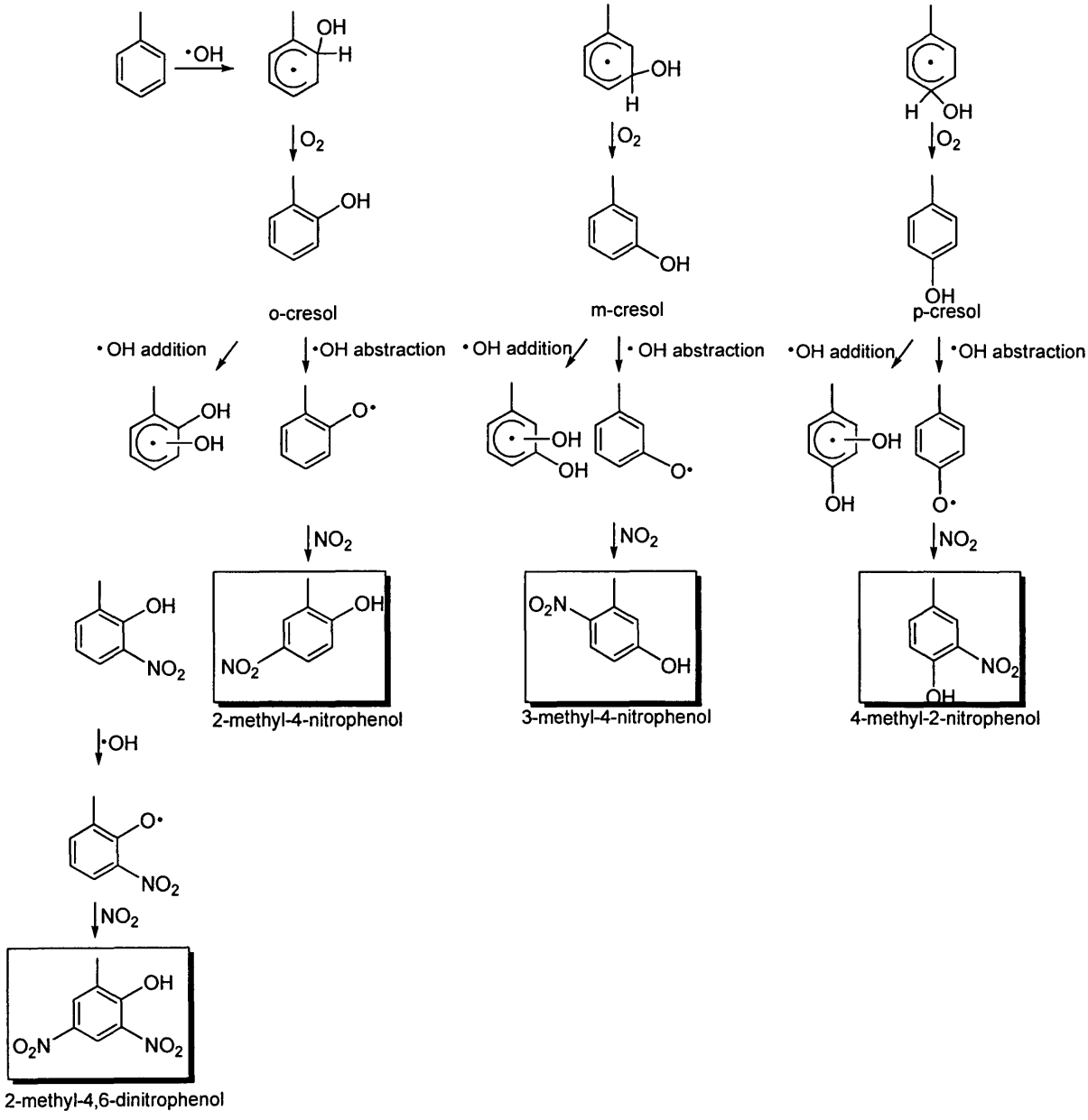

Figure 2.1 Proposed formation mechanism of methylnitrophenols from toluene (adapted from Forstner et al., 1997).

suggested that a phenoxy radical is formed through a hydrogen abstraction from the HO group by reaction with a HO radical followed by reaction with NO_2 to form 4-nitrophenol (Fig 2.2). Bolzacchini et al. (2001), on the other hand, suggested an addition of NO_3 to the HO carbon of phenol, followed by the addition of NO_2 to the para carbon and final loss of HNO_3, forming 4-nitrophenol. Carter (1990) proposed that a phenoxy radical, once produced, reacts with NO_2 to form 4-nitrophenol.

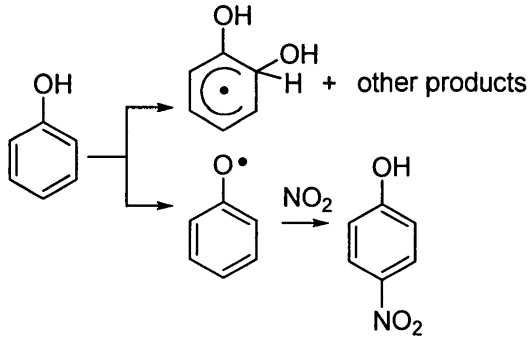

Figure 2.2. Proposed reaction mechanism for 4-nitrophenol formation (Atkinson et al., 1992).

Table 2.1. Rate constants for reactions of aromatic VOC with HO and NO_3 radicals at 298 K (unless otherwise stated) (Calvert et al., 2002).

Precursor	k_{HO} x 10^{12} (cm^3 $molec^{-1}$ s^{-1})	k_{NO3} x 10^{12} (cm^3 $molec^{-1}$ s^{-1})
toluene	5.63	7×10^{-5}
benzene	1.39	$< 1 \times 10^{-5}$
m-xylene	23.1 (250 – 315 K)	2.6×10^{-4}
phenol	27	3.8
2-me-ph	41	14
3-me-ph	68	11
4-me-ph	50	11

Rate constants for the reactions of aromatic VOC with the HO radical are shown in Table 2.1. Rate constants for the reactions of the methyl hydroxycyclohexadienyl radicals from toluene photooxidation with NO_2 and O_2 are found to be 3 x 10^{-11} cm^3 $molec^{-1}$ s^{-1} and 5 x 10^{-16} cm^3 $molec^{-1}$ s^{-1}, respectively (Seinfeld and Pandis, 2006). As the number of substituted groups on a benzene ring increases, the reactivity of the species increases exponentially (Calvert et al., 2002).

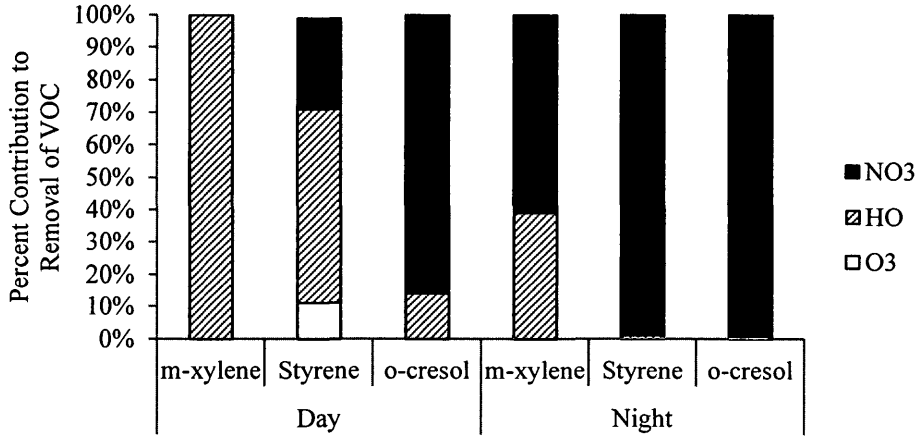

Figure 2.3. Contribution to the removal of VOC by atmospheric oxidants NO_3, HO and O_3 during the day and night in an urban environment (adapted from Calvert et al., 2002).

The removal of aromatic VOC by reaction with the NO_3 radical is insignificant for most of the nitrophenol precursors (Table 2.1, Fig 2.3). However, the NO_3 addition reaction seems to be more significant with the cresols and provides another reaction pathway for the formation of nitrophenols. The reaction pathway is similar to that shown in Fig 2.1 once the cresol is formed and the reaction with NO_3 to from the methyl nitrophenol proceeds through the abstraction pathway (Grosjean, 1984).

The primary removal of aromatic VOC in the atmosphere is through the reaction with the HO radical, however, the competing pathways that can occur with nitrophenol formation is for the reaction to proceed through the hydrogen abstraction pathway, occurring 10 % of the time, as previously mentioned or the formation of ring-opening products following the HO-addition reaction. The o-cresol formed from this reaction through an ortho-addition of HO is thought to comprise only 20 % of the initial reaction products (Atkinson et al., 1980). Furthermore, it was found that the sum of yields of aromatic products is approximately 20 % to 40 % while the remainder are ring fragmentation products. Atkinson et al. (1980) found that the reaction of the cresols, specifically o-cresol, with the HO radical was found to form methylnitrophenols with yields that were less than 5 %. The major pathway, and believed to be the reason for low methylnitrophenol yields, occurs when the radical formed from the cresol and HO reaction reacts with O_2 rather than NO_2.

2.2. Precursor and Product Emissions

Aromatic VOC are emitted into the atmosphere in large quantities by both biogenic and anthropogenic sources. Globally, toluene emissions are approximately 6.9 Tg C $year^{-1}$ (Henze et al., 2008). It was estimated that VOC emissions in Canada reached almost two teragrams in 2005 (Environment Canada, 2012[b]) and by source apportionment, transportation was found to be the most dominant contributor (Fig. 2.4). The main VOC of concern in this research are toluene, benzene and m-xylene, which are all precursors of the target compounds and are amongst the most abundant species in fossil fuels. All three VOC have been found in rural, semi-urban and urban locations in

sub ppbv to several ppbv levels (Lawrimore et al., 1995; Hagerman et al., 1997; Derwent et al., 2000; Pankow et al., 2003; Thompson, 2003; Legreid et al., 2007; Kornilova, 2012).

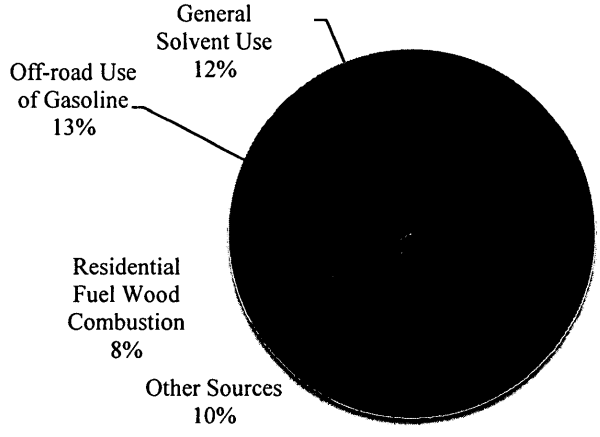

Figure 2.4. Estimated VOC emission contributions without open sources in Canada in 2005 (adapted from Environment Canada, 2012[b]).

Table 2.2. Source apportionment for select VOC in Hong Kong (Guo et al., 2004).

	Vehicle Emission (%)	Solvent Use (%)	Petroleum Gas or Natural Gas Leakage + Industrial Sources (%)	Industrial Sources 2 (%)
benzene	29.9 ± 17.8	33.6 ± 31.9	25.1 ± 58.0	11.3 ± 17.1
toluene	29.9 ± 17.8	61.3 ± 51.8	12.1 ± 27.8	-3.2 ± 4.8
p,m-xylene	7.5 ± 4.5	81.1 ± 76.9	5.1 ± 11.7	6.3 ± 9.4

Source apportionment studies for select VOC were done in Hong Kong, specifically in a location that combines residential, commercial and light industrial uses in 2001 (Guo et al., 2004). In this study, it was found that benzene and toluene have sources dominated by vehicle emissions and solvent use, while p,m-xylene were found to mainly derive from solvent use (Table 2.2). It is expected that VOC emissions in Toronto and the surrounding area are characterized by transportation and from gas stations.

Methylnitrophenols, the products of aromatic VOC oxidation and the target compounds of this study, have only been listed in one reference as components of primary emissions (Tremp et al., 1993) and 4-nitrophenol was found to be emitted in vehicle exhaust in small quantities (Nojima et al., 1983). In this study, methylnitrophenols were found to comprise approximately 40 % of the cresols when no catalytic converter was used on a vehicle and dropped to approximately 2 % when a catalytic converter was used. Typically, nitrophenol emissions were found to be less than 2 $\mu g\ L^{-1}$ exhaust gas.

2.3. Yields of Nitrophenols from Precursor Oxidation

Although there have been several studies to identify products from the photooxidation of aromatic VOC, there has only been one publication (Forstner et al., 1997) and one study (Irei, 2008) to determine yields of nitrophenols. Each of these studies determined the yields in secondary organic aerosols (SOA) and did not quantify the gas phase (Table 2.3). Forstner et al. (1997) used a 60 m^3 outdoor smog chamber with

initial VOC mixing ratios ranging from 200 ppbv to 900 ppbv and initial propene mixing ratios, used to enhance photochemical activity, of 100 ppbv to 340 ppbv. The initial ratios of hydrocarbon to NO_x were from 3 ppbv C ppb^{-1} to 14 ppbv C ppb^{-1} and ammonium sulfate seed aerosols were used to induce condensation of the products formed. The particles were then collected on quartz filters after approximately four hours. Irei (2008) used flow reactor experiments to determine the product yields. Isopropyl nitrate was used as a HO source and had an initial mixing ratio of 230 ppmv. The mixing ratios of toluene and nitrogen oxide were 20 ppbv to 40 ppbv and 5 ppmv, respectively. The residence time within the tube was between 0.6 minutes and 3.2 minutes and the PM was sampled upon exit of the tube onto filters. The unreacted toluene was also monitored to determine the true yields.

Table 2.3. Yields of nitrophenols determined from smog chamber studies.

Product	Yield (%)
4-me-2-NP	4.4[a]
3-me-4-NP	6.8[a], 0.096[b]
2-me-4-NP	10[a], 16.3[b]
2,6-dime-4-NP	3.3[a]

[a] Forstner et al., 1997; [b] Irei, 2008

2.4. Atmospheric Loss Processes of Nitrophenols

The loss processes of methylnitrophenols in the atmosphere have not been widely studied, however, it is expected that the dominant gas phase loss is due to the reaction with the HO radical. The known rate constants for the target compounds or isomers of them are listed in Table 2.4. With these rate constants and an average HO radical mixing ratio of 10^6 molec cm^{-3}, the lifetime of the phenols should be in the order of days.

Furthermore, the half-life of the direct photolysis of nitrophenols in water has been found to be in the order of months (Palm et al., 1999).

Table 2.4. Rate constants for loss reactions of phenols with the HO radical.

Compound	$k_{HO} \times 10^{12}$ (cm^3 $molec^{-1}$ s^{-1})	Reference
2-me-ph	41	Calvert et al., 2002
4-me-ph	50	Calvert et al., 2002
4-NP	0.34	Grosjean, 1991
3-me-2-NP	3.69	Bejan et al., 2007
4-me-2-NP	3.59	Bejan et al., 2007
5-me-2-NP	6.72	Bejan et al., 2007
6-me-2-NP	2.7	Bejan et al., 2007

Due to the relatively long lifetime of the nitrophenols, they have been thought to be in the accumulation mode of particles. This mode includes particles with aerodynamic diameters from approximately 0.1 μm to 2 μm. Aitken nuclei, with diameters as large as 0.1 μm have a lifetime that is often in the order of minutes, due to losses by coagulation or condensation. The accumulation mode in the troposphere has a lifetime that can be several days and has losses due to wet deposition (Finlayson-Pitts and Pitts, 2000). The reason for the longer lifetime of the accumulation mode is that these particles are large enough that diffusion is low and small enough that gravitational settling is insignificant.

2.5. Ambient Sampling of Nitrophenols

Nitrophenols in air have only been studied by a limited number of research groups (Herterich and Hermann, 1990; Nishioka and Lewtas, 1992; Lüttke and Levsen, 1997; Morville, et al., 2004; Cecinato et al., 2005; Moukhtar, et al., 2011) and the results of these studies are summarized in Table 2.5. Sampling sites for these studies ranged from

remote locations on a hill in Garmisch-Partenkirchen, Germany (Herterich and Hermann, 1990) to urban locations in Rome, Italy (Cecinato et al., 2005) and Strasbourg, France

Table 2.5. Summary of ambient nitrophenol data from literature (all concentration measurements are expressed in ng m^{-3}).

Compound	Herterich and Hermann (1990)	Nishioka and Lewtas (1992)		Lüttke and Levsen (1997)	Morville et al. (2004)	Cecinato et al. (2005)		Moukhtar et al. (2011)
	Gas	Gas	PM	Gas	Gas + PM	Gas	PM	PM
phenol					18.97			
m-cresol					0.5			
p-cresol					0.83			
o-cresol					0.36			
2-NP	6.9-18.1	2.4	ND	0.8-7.47		10.4	3.5	
3-NP					ND			
4-NP	2.8-4.2	0.85	2.7	<0.005-20.4		3.9	18	
2-me-3-NP		ND	ND		0.09			
2-me-4-NP		2.7	1.2					0.06-0.23
2-me-5-NP		ND	ND					
3-me-2-NP		0.23	ND		0.35			
3-me-4-NP		0.54	0.77		0.69	2.2	7.8	
4-me-2-NP	12.3-27.6	1.8	ND		0.58	6.9	2.9	
4-me-3-NP		ND	ND					
5-me-2-NP		0.59	ND		0.12	4.8	1.7	
5-me-3-NP		ND	ND					
6-me-2-NP		1.7	ND					
6-me-3-NP		ND	ND					
2,6-dime-4-NP						2.0	5.9	
6-me-2,4-DNP	1.0-5.9							
2,4-DNP	1.8-11.0			0.1-0.54	0.65			
2,5-DNP					ND			
2,6-DNP					0.22			
3,4-DNP					ND			

ND = not detected

(Morville et al., 2004). Unlike this work, the main motivation to determine nitrophenol concentrations in ambient air was due to their phytotoxicity (Shea et al., 1983; Shafer and Schönherr, 1985; Rippen et al., 1987) and their adverse health effects (Bruce, 1987). Herterich and Hermann (1990) sampled air through a column filled with XAD-2^{TM} resin with a glass fibre filter in front. Extraction of the phenols from XAD-2^{TM} was done with

pentane, diethyl ether and hexane, followed by analysis with a GC coupled with an electron capture detector. Nishioka and Lewtas used 200 g of XAD-2™ for gas phase collection and a PM10 sampler with a Teflon glass filter for PM collection. Both denuder and filter were extracted with dichloromethane, separated with high performance liquid chromatography (HPLC) and analyzed with Chemical Ionization GC-MS. Lüttke and Levsen (1997) sampled gas phase nitrophenols on Great Dun Fell, England using scrubbers to separate the gas phase from cloud droplets. Extraction was done with solid phase extraction (SPE) followed by analysis with GC-MS. Gas phase and PM nitrophenols were separated by Cecinato et al. (2005) using KOH coated denuders and a Teflon filter. Extraction was done with a 50:50 mixture of dichloromethane and acetone and the sample was subsequently evaporated, derivatized with N-methyl-N-tert-butyldimethylsilylfluoroacetamide (MTBSTFA) and analyzed by GC-MS. Morville et al. (2004) sampled both gas and PM nitrophenols in Strasbourg, France using a high volume air sampler with a glass fibre filter and 20 g of XAD-2™. Soxhlet extraction was done for 12 hours using a hexane and dichloromethane mixture. The sample was evaporated to dryness, derivatized with MTBSTFA and analyzed by GC-MS. Moukhtar et al. (2011) sampled nitrophenols in PM in Toronto, ON using a quartz filter and PM2.5 air sampler. The extraction procedure included filter extraction with acetonitrile, an HPLC and SPE step, several evaporation steps, derivatization with N,O-bis(trimethylsilyl) trifluoroacetamide (BSTFA) and analysis with GC-MS.

2.6. Use of XAD-4^{TM} as an Adsorbent

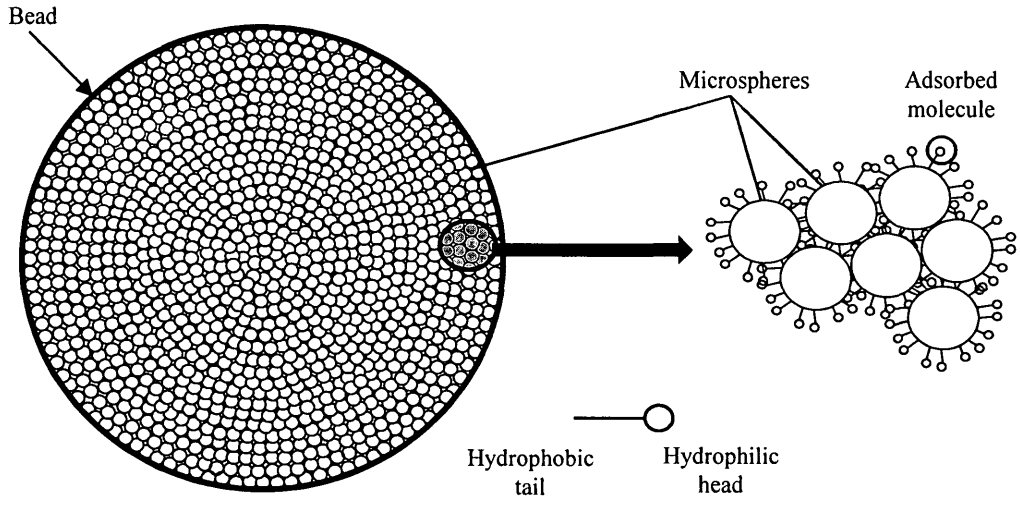

Figure 2.5. Structure of a macroreticular resin (adapted from Sigma Aldrich, 1997).

XAD, a trade name by Rohm and Haas, is a polymeric resin that has been used repeatedly as an adsorbent to collect nitrophenols in air or in water (Herterich and Hermann, 1990; Nishioka and Lewtas, 1992; Ku and Lee, 2000; Morville et al., 2004). XAD is a macroreticular resin (Fig. 2.5), meaning that it is very porous in nature. Each XAD bead is composed of numerous microspheres and both XAD-2^{TM} and XAD-4^{TM} have a structure that is based on a styrene-divinylbenzene polymer that is very porous (Fig 2.6). The hydrophobic portion of the adsorbing molecule will then interact with the hydrophobic divinylbenzene component of the XAD. XAD-4^{TM} resin, having a higher surface area than XAD-2^{TM} (Kennedy, 1973; van Vliet and Weber, 1981), and being

previously chosen by Busca (2010) to collect nitrophenols, as part of her master's thesis, will be the adsorbent used in this research (Table 2.6).

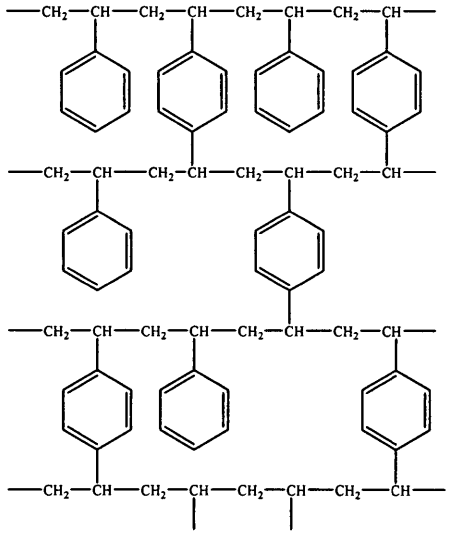

Figure 2.6. Chemical structure of styrene-divinylbenzene copolymer resin (Lane, 1999).

Table 2.6. Characteristics of unground XAD-2™ and XAD-4™ resin (adapted from Kennedy, 1973).

	Average Diameter (μm)	Surface Area ($m^2\ g^{-1}$)	Average Pore Diameter (cm x 10^8)	Skeletal Density ($g\ cm^{-3}$)	Average Diameter after Grinding for 17 h (μm)
Unground XAD-2™	~500[a]	300	90	1.081	-
Unground XAD-4™	760	780	90	1.085	0.75[b]

[a] Average size of XAD resin bead was used
[b] Geometric mean diameter (Gundel and Lane, 1999)

XAD-4™, when purchased, is in the form of small, porous beads that are wetted in a water and salt mixture to prevent bacterial growth. Prior to use, the resin is cleaned

with various solvents and dried. For the adsorbent to be able to stick to a surface, such as a filter or denuder, it is ground to a fine powder with a planetary ball mill. Doing so increases the outer surface area of the resin (Table 2.6). The ground resin then adheres to the filter or denuder surface through London van der Waals forces and electrostatic interactions (Gundel and Lane, 1999).

2.7. Gas-Particle Partitioning

SVOC in the atmosphere can partition between the gas and particle phases. Knowledge of the partitioning of these compounds is important in understanding their total concentrations, atmospheric yields and possible isotopic fractionation between the phases. Junge (1977), proposed that compounds with vapour pressures between 10^{-6} Pa and 10^{-2} Pa were considered to be semi-volatile, and compounds with vapour pressures lower and higher than those limits were considered to be non-volatile and volatile, respectively (Fig. 2.7). This assumption is initially based on the Brunauer, Emmett and Teller (BET) multilayer isotherm (Brunauer et al., 1938) and reduced to the Langmuir isotherm. Contrary to the Langmuir isotherm, which assumes that gases can adsorb onto a particulate to form a monolayer, the BET isotherm assumes that each molecule adsorbed onto a particle can in turn act as an adsorption site for another molecule. The target phenols in this study cover a wide range of vapour pressures and apart from the 4-methylphenol, all lie within the semi-volatile range (Table 2.7).

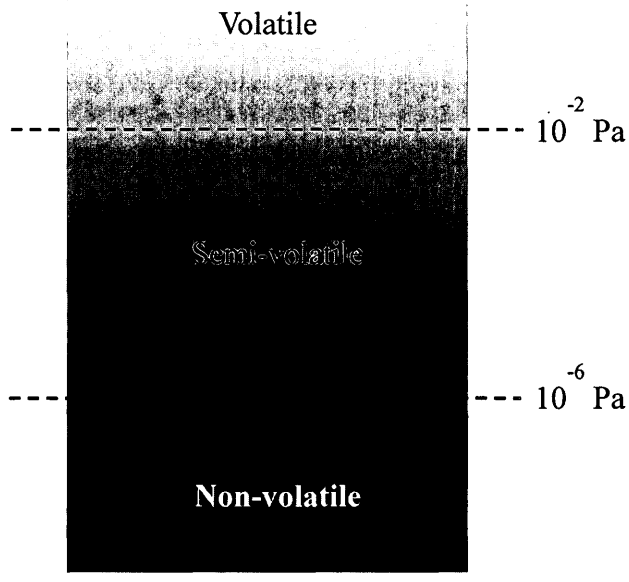

Figure 2.7. Schematic of the classification of volatile, semi-volatile and non-volatile species, as proposed by Junge (1977).

Table 2.7. Summary of vapour pressure data for target phenols.

Compound	Vapour Pressure at 303 K (Pa)
4-me-ph	1×10^{1} (at 294 K)[a]
4-me-2-NP	1.11×10^{1}[b]
4-NP	1.03×10^{-2}[b]
3-me-4-NP	3.13×10^{-3}[b]
2-me-4-NP	8.69×10^{-3}[b]
2,6-dime-4-NP	6.42×10^{-4}[b]

[a] CRC Handbook of Chemistry and Physics (2013)
[b] Gong (private communication)

Several factors have been identified that affect the partitioning of SVOC, including vapour pressure, temperature, relative humidity and polarity. The partitioning coefficient, K_p, in $m^3\ \mu g^{-1}$ can be calculated using Eq. 2.1.

$$K_P = \frac{P/TSP}{G} \qquad \text{Eq. 2.1}$$

Here, P and G are the particle associated and gas concentrations of compound A in ng m^{-3}. TSP is the total suspended particulate material concentration in $\mu g\ m^{-3}$. Therefore, as TSP increases, partitioning into PM is favoured. Depending on whether the particle is a solid or a liquid, gases can adsorb onto the particle or absorb into liquid. It is expected that for particles consisting mainly of minerals, physical adsorption will dominate (Pankow, 1994). However, in an urban atmosphere, where PM is primarily organic in nature, absorption of the gas into the particle dominates (Pankow, 1999). For an ideal liquid, Raoult's law states that the ratio of the partial vapour pressure of each component to its vapour pressure as a pure liquid is approximately equal to its mole fraction (Eq. 2.2). Here, $p_A$and p_A^* are the partial pressure of component A in a solution and the vapour pressure of the pure liquid, respectively. χ_A is the mole fraction of component A.

$$p_A = \chi_A p_A^* \qquad \text{Eq. 2.2}$$

Activity coefficients are often used to account and correct for deviations from ideal behavior. At equilibrium, the activity of the gas phase and absorbing particle phase are equal. Thus by incorporating the activity of the component, Eq. 2.2 becomes Eq. 2.3. Here, ζ_A is the activity of component A.

$$p_A = \zeta_A \chi_A p_A^* \quad \text{Eq. 2.3}$$

The mole fraction, χ_A is the fraction of the number of moles of A absorbed in the organic matter phase of the particle over the total number of moles of all organic compounds in the absorbing phase. If the particulate atmospheric concentration, P_A in units of ng m^{-3}, is known, as well as the molecular weight of the compound, Eq. 2.4 can be used to determine the number of moles of component A (Pankow, 1994).

$$n_A = \frac{P_A}{MW_A 10^9} \quad \text{Eq. 2.4}$$

The total number of moles in the absorbing phase, n_{Tot}, can then be found using Eq. 2.5.

$$n_{Tot} = \frac{f_{om} TSP}{MW_{om} 10^6} \quad \text{Eq. 2.5}$$

Here, f_{om} is the weight fraction that is absorbing in the organic matter (om) phase and MW_{om} is the mean molecular weight of the absorbing om phase. When absorptive properties dominate, such as in an urban setting, Rault's Law (Eq. 2.3), is combined with Eq. 2.1, 2.4 and 2.5, giving Eq. 2.6 (Pankow, 1999).

$$K_P = \frac{f_{om} 760 RT}{MW_{om} \zeta_i p_{L,A}^0 10^6} \quad \text{Eq. 2.6}$$

Here, 760 is used to correct for $p_{L,A}^0$, the vapour pressure of component A, if in units of Torr. R is 8.2 x 10^{-5} m^3 atm mol^{-1} K^{-1} and T is temperature in Kelvin.

2.8. Stable Carbon Isotope Ratio

The application of stable carbon isotope ratios of VOC to gain insight into atmospheric processes in the last decade has become increasingly popular. Carbon has

two stable isotopes, ^{12}C and ^{13}C, with ^{13}C having a natural abundance of 1.1 %. The ratio of the two isotopes in different compounds or isotopologues can vary depending on their source and the chemical processing that it has undergone. These differences tend to be very small and are frequently presented in per mille notation. The stable carbon isotope ratio is often referred to as a delta value ($\delta^{13}C$) and is corrected to a standard value, the Vienna-Peedee Belemnite (V-PDB), $(^{13}C/^{12}C)_{V\text{-}PDB} = 0.0112372$ (Craig, 1957). The delta value is then defined as Eq. 2.7.

$$\delta^{13}C = \frac{(^{13}C/^{12}C)_{sample} - (^{13}C/^{12}C)_{V-PDB}}{(^{13}C/^{12}C)_{V-PDB}} \times 1000‰ \qquad \text{Eq. 2.7}$$

2.9. Kinetic Isotope Effect

The KIE occurs when the rate constant of a reaction is sensitive to the atomic mass of the reacting species. This effect is most pronounced when the isotope replaced is of small atomic mass, such as hydrogen with deuterium. Carbon, on the other hand, will have a much smaller KIE. The KIE for stable carbon isotopes is defined as the rate constant for ^{12}C only containing compounds over the rate constant of the same compound with one ^{13}C (k_{12}/k_{13}). Because of the low natural abundance of ^{13}C, it is assumed that only one of the carbon atoms in the nitrophenol will be replaced with a heavier isotope and the location of ^{13}C in the molecule is random.

Chemical isotope effects are caused by the vibrational motions in a molecule, relating to the zero point energy. When an atom in a compound is replaced with a heavier isotope, the zero point energy is lowered. This in turn lowers the potential energy of the

reacting species as well as the transition state, causing a KIE. The KIE for carbon reactions are very small and are represented in per mille notation, referred to as ε (Eq. 2.8).

$$\varepsilon = \frac{k_{12} - k_{13}}{k_{13}} \times 1000‰ \qquad \text{Eq. 2.8}$$

2.10. Principles of Isotope Ratio Based Processing and Yield Calculations

The concentration of secondary pollutants in ambient air is dependent on the extent of processing of the precursor, which is very difficult to measure. Previously used methods to determine this include measuring the PCA of a species to determine the period of time that the certain species has been exposed to the HO radical. This can be calculated using differences in mixing ratios of VOC such as the change in the benzene and toluene ratio (Parrish et al., 1992; Jobson et al., 1998; Jobson et al., 1999; Kleinman et al., 2003; Parrish et al., 2007). A more recently developed method uses the isotope ratio of an ambient species, the KIE and the isotope ratio source signature to determine the PCA (Rudolph and Czuba, 2000; Rudolph et al., 2003; Thompson, 2003; Stein and Rudolph, 2007; Kornilova, 2012).

The extent of processing is also known as the reaction coordinate, or the fraction of reacted precursor over the initial amount of precursor and is given as Eq. 2.9. Here, F is the reaction coordinate, χ_{amb} is the measured mixing ratio of the precursor and χ_0 is the mixing ratio of the precursor in the absence of chemical processing.

$$F = \frac{\chi_0 - \chi_{amb}}{\chi_0} \qquad \text{Eq. 2.9}$$

By rearranging Eq 2.9, χ_{proc}, the mixing ratio of the amount of precursor that has been processed, can be calculated (Eq. 2.10).

$$\chi_{proc} = \chi_{amb} \frac{F}{1 - F} \qquad \text{Eq. 2.10}$$

In the atmosphere it is difficult to determine the concentration the precursor would have in the absence of processing. In contrast to laboratory studies for ambient samples, F usually is not known; isotope ratio measurements allow for the determination of F. To proceed with calculations to quantify the reaction coordinate, the assumption that the atmosphere is a closed system is made. The following equations do not take the mixing of two different air masses into account. Equations 2.11 and 2.12 are combined to derive Eq. 2.13 (Rudolph and Czuba, 2000).

$$\delta^{13}C_{pre} = \delta^{13}C_0 + k_{12}\varepsilon[HO]t \qquad \text{Eq. 2.11}$$

Here, $\delta^{13}C_{pre}$ is the isotope ratio of the measured ambient precursor and $\delta^{13}C_0$ is the isotope ratio of the source, which has been previously measured (Czapiewski et al., 2002; Rudolph et al., 2002; Rudolph, 2007); [HO]t is the average HO concentration over a time interval and is the PCA.

$$\chi_{amb} = \chi_0 \exp(-k_{12}[HO]t) \qquad \text{Eq. 2.12}$$

In this equation (Eq. 2.13), [HO]t is eliminated, and the reaction coordinate, F, can be determined using the isotope ratio of the ambient precursor and the source

signature alone. In this equation, $\Delta\delta^{13}C$ is the difference in isotope ratios between the ambient precursor and the source.

$$F = 1 - exp\left(-\frac{\Delta\delta^{13}C}{\varepsilon}\right) \quad \text{Eq. 2.13}$$

Equation 2.14 is derived by relating the isotope ratio of the product to that of the precursor. Here, $\delta^{13}C_t^{prod}$ is the isotope ratio of the ambient product. This equation assumes that there is no product that is lost that may create fractionation and is a correct average, even if air mass mixing does occur.

$$F = \frac{\delta^{13}C_0 - \delta^{13}C_t^{pre}}{\delta^{13}C_t^{prod} - \delta^{13}C_t^{pre}} \quad \text{Eq. 2.14}$$

With F now known, the amount of ambient precursor that was processed could be calculated (Eq. 2.14). This, in conjunction with concentration measurements of the secondary products, can be used to derive ambient yields of SOA.

2.11. Isotope Ratio Measurements of Secondary Products

Laboratory studies looking into the isotope ratios of products formed from secondary processes have not been widely studied (Irei, 2008; Fisseha et al., 2009[b]; Irei et al., 2011). Irei (2008) looked at the isotope ratios of compound specific products, specifically nitro-, nitrohydroxy- and hydroxyl aromatic compounds, formed from the photooxidation of aromatic VOC. It was found that the isotope ratios for methylnitrophenols and methylnitrocatechols were similar to the isotope ratio of the sum of all products. Fisseha et al. (2009[b]) looked into the photooxidation of β-pinene as it formed nopinone. A depletion of ^{13}C in nopinone was not observed and showed a similar

isotope ratio as the initial β-pinene. The precursor became depleted in ^{12}C as it reacted but the same trend was not observed with the product. Irei et al. (2011) looked at the change in isotope ratio of particulate organic matter (POM) as it is formed from the photooxidation of toluene. As expected by the KIE, the isotope ratio of the POM is initially lower than that of the precursor, depleted in ^{13}C, and as the reaction proceeds, it becomes more enriched in ^{13}C.

Compound specific isotope ratio measurements of SOA in the atmosphere have also only been studied by a small number of research groups (Fisseha et al., 2009[a]; Li et al., 2010; Moukhtar et al., 2011). Fisseha et al. (2009[a]) measured the isotope ratios of formic acid, acetic acid and oxalic acid, specifically, as well as that of different aerosol fractions. Results were difficult to interpret but were shown to somewhat correlate with ozone mixing ratios, a precursor of the compounds. Li et al. (2010) looked at the isotope ratios of 2-methyltetrols, which are biomarkers, at two separate sampling sites. Observations included differences in isotope ratios between the two sites but without a known cause. Moukhtar et al. (2011) looked at the isotope ratio of 2-methyl-4-nitrophenol in PM at York University. When compared to laboratory studies (Irei, 2008), it was suggested that 2-methyl-4-nitrophenol is likely formed from the photooxidation of toluene but due to the limited number of data points, firm conclusions were not made.

3. Methodology

3.1. Overview

This section describes the methodology used for the sampling, extraction and analysis of ambient phenols. A method, developed by Moukhtar et al. (2011), used to determine concentrations and stable carbon isotope ratios of nitrophenols in PM, has been modified to have a larger range of target compounds as well as to sample both gas and particle phase phenols. A method developed by Gundel and Hering, (1998) and Galarneau, et al., (2006), modified by Busca (2010) and further developed in this work, that uses XAD as an adsorbent for collecting atmospheric phenols will also be presented.

Nitrophenols were sampled using high volume air samples on quartz filters for PM measurements and on XAD-coated quartz filters for gas and particle phase measurements. Filters were extracted using acetonitrile and underwent several filtration and evaporation steps. HPLC and SPE were used as clean up steps and solvent exchange steps, respectively. Derivatization with BSTFA was always done prior to analysis. Concentration measurements were obtained with GC-MS and GC-IRMS was used for isotope ratio measurements.

The GC-IRMS measurements were evaluated and tested using samples prepared from bulk phenols with carbon isotope ratios determined by offline isotope ratio measurement. Offline measurements were done by combusting the individual target compounds under vacuum and then isolating the carbon dioxide gas into another tube under vacuum. The sample was then introduced directly into the IRMS for detection.

3.2. Quartz filter cleaning

Quartz fibre filters (Pallflex Tissuquartz membrane filters – 2500 QAT – PallGelman Sciences) that had dimensions of 20.32 cm x 25.40 cm, were cleaned prior to being used for sampling. This was done by placing four filters on a custom built, equally spaced, four-tier quartz rack. The filters were heated in a muffle furnace (Fisher Scientific Model 550-58) at 1,123 K for 24 hours. After the filters cooled to room temperature in the furnace, they were removed with tweezers and placed in a Pyrex container that was covered with a sheet of Teflon and a plastic lid until sampling or coating with XAD.

3.2.1. XAD Cleaning

Amberlite XAD-4^{TM}, 20-60 mesh (Sigma Aldrich), when purchased, is a water wet product combined with sodium chloride and sodium carbonate to inhibit bacterial growth. The product was cleaned according to a procedure described by Lane (private communication). 500 g of XAD was placed in a beaker and methanol (Reagent grade, Sigma Aldrich) was slowly poured in, while stirring, until the resin was fully immersed and the solvent was a few millimeters above the surface. This slurry was then sonicated for 30 minutes using a Bransonic Ultrasonic Cleaner (Model SS10R-DTH). The XAD-methanol slurry was filtered by suction filtration through a 47 mm Nuclepore membrane filter (Whatman) with a pore size of 0.25 μm or 0.45 μm.

The filtered XAD was transferred to a clean, dry beaker. Dichloromethane (Reagent grade, Sigma Aldrich) was poured into the same beaker in the same manner as

methanol. The XAD slurry was sonicated for 30 minutes and suction filtered again. To remove excess dichloromethane, hexane was mixed with the filtered XAD and was sonicated for 30 minutes more. After filtering the XAD for the final time, the XAD was transferred to two 22.9 cm x 33.0 cm Pyrex containers. The containers were left uncovered in an empty fume hood to dry for a period of two to three weeks at room temperature until there was no longer a hexane odour. The XAD was periodically mixed with a glass stirring rod to aid drying.

3.2.2. Grinding of XAD-4™

Prior to coating, it was necessary for the XAD to be ground to a fine powder. Two agate pots were first cleaned with acetone. Ten agate balls, with diameters of 10 mm, and approximately 10 g of cleaned and dried XAD-4™ were placed into each of the agate pots to fill approximately two thirds to three quarters of the pot. The pots were covered with an agate lid that was equipped with a rubber gasket. The pots were then clamped into a Retsch PM400 Planetary Ball Mill on opposite sides, so as to balance the instrument. The XAD was then ground at 400 rpm for 17 hours or 34 hours. Following grinding, the XAD was transferred to amber jars that had Teflon lids and the agate pots, lids and balls were cleaned with acetone.

3.2.3. XAD-4™ Filter Coating

Typically, 12 quartz filters (20.32 cm x 25.40 cm) were coated at a time. Approximately 13 g or 22 g of ground XAD-4™ was weighed on an analytical balance

and placed into a 1 L beaker. Hexane (Chromasolv Plus, Sigma Aldrich) was added to the beaker and was stirred with a glass stirring rod. Ten glass plates were placed into a thin layer chromatography (TLC) chamber (27.0 cm × 26.5 cm × 7.0 cm) to take up solvent space. The TLC chamber was immersed into a sonic bath and the XAD-hexane slurry was poured into it. 1 L of hexane was used to rinse the beaker and was also poured into the TLC chamber, which was then covered with aluminum foil and was then sonicated for 30 minutes. The concentration of the slurry in the hexane was approximately 6.5 g L^{-1} as recommended by Lane (private communication) or 10.5 g L^{-1}.

Stainless steel mesh was folded in a manner to hold each filter individually when coating. Filters were placed in each of the mesh holders and were immersed into the XAD-hexane slurry ten times. Sonication was turned off during coating, but turned on in between each individual filter coating and the filters were then placed on a rack to dry. Hexane was added when needed due to evaporation. Once each of the filters was dipped, the slurry was sonicated for 30 minutes. The filters were then submersed in the slurry in opposite order ten additional times. The XAD was filtered using suction filtration and Nuclepore membrane filters to recover the hexane. Filters were wrapped in aluminum foil on the rack overnight to dry. The following day, hexane was placed in the TLC chamber with the ten glass plates. Each of the coated filters was then immersed into the hexane ten times to remove any excess XAD and was dried on a rack. Once hexane had fully evaporated, determined by a lack of odour from the filters, they were placed into a Pyrex container that was covered with a Teflon sheet and a plastic lid until used for ambient sampling.

3.3. Filter Sampling

From September 2008 to September 2010, sampling was conducted on the outdoor roof of the fifth floor of the Arboretum Parking Structure at York University. Ambient samples since September 2010 were collected on the roof of the Petrie Science and Engineering Building. High volume air sampling was used for ambient sampling onto filters. The sampling time varied from half a day to four days and after sampling, each filter was individually placed into a mason jar, covered, and stored in a freezer at 253 K until extraction.

3.3.1. Air Sampler Calibration

Air samplers were calibrated monthly or whenever worn brushes were replaced on either of the motors. Two high volume air samplers (TE-6001 from Tisch Environmental Inc.) were equipped with PM2.5 heads but only one air sampler was equipped with a flow recorder for calibration. A calibration curve was constructed using a TE-5028A calibrator (Tisch Environmental Inc.) (Fig. 3.1). The calibrator was secured firmly to the air sampler with the recorder, and a water manometer was attached to the calibrator. The flow rate was varied to obtain five different points and readings from the manometer along with readings from the recorder were taken. Each of these was corrected for ambient temperature and pressure and certified values from Tisch Environmental Inc. were used in calculations. When the calibration curve was constructed, the equation of the line was used to determine which recorder reading was required for a standard flow rate of 1.13 m^3 min^{-1}. The manometer reading at this recorder reading was then used to calibrate the second air sampler.

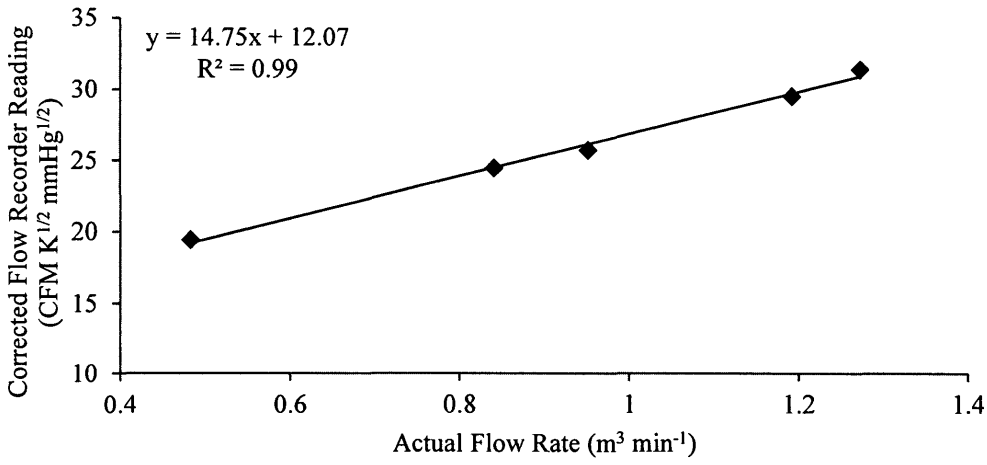

Figure 3.1. Typical calibration curve for PM2.5 high volume air sampler (Calibration curve is from June 27, 2011)

3.3.2. Parallel Sampling

Parallel sampling was done by first calibrating each of the air samplers to ensure that the flow was matched. Samples collected on filters at a standard flow rate of 1.13 $m^3 min^{-1}$ and the sampling time was for a period of one to three days.

3.3.3. Sampling in Series

To collect samples on filters in series, a filter was first placed in the filter holder of the air sampler and a stainless steel piece of mesh, with a grid pattern of approximately 0.5 cm x 0.5 cm, was placed over it. The top filter was then placed on top of the mesh and the filter holder was then secured in place.

3.3.4. Particle Size Cutoff and Face Velocity

When the flow rate of the air sampler was changed, the particle size cut-off of the sampling head and the face velocity was inherently changed as well. The change in particle size was then calculated according to Eq. 3.1.

$$\epsilon = \frac{2u}{w}\left(\frac{C_c \rho D_p^2}{18\mu}\right) \qquad \text{Eq. 3.1}$$

Here, ϵ is the efficiency of the sampler, u is the flow rate of the sampler, w is the width of the impactor jet, C_c is the Cunningham slip correction factor, ρ is the particle density, D_p is the particle diameter and μ is the viscosity of air. The ratio of Eq. 3.1 for an air sampler at a certain flow rate is taken over Eq. 3.1 for the same air sampler at a different flow rate, which results in the elimination of certain variables and Eq. 3.2.

$$D_{p2}^2 = \frac{D_{p1}^2 u_1}{u_2} \qquad \text{Eq. 3.2}$$

The face velocity of the filter takes into account the area of the filter in which air is sampled through, A, and the flow rate of the sampler, u. The face velocity of the filter, μ_{FV}, is then calculated using Eq. 3.3.

$$\mu_{FV} = \frac{u}{A} \qquad \text{Eq. 3.3}$$

3.4. Sample Processing

3.4.1. Standards and Solvents Used

All standards used were purchased from Sigma Aldrich or Supelco and had a purity of 97 % to 99.8 %. Standard solutions were prepared by accurately weighing out approximately 0.01 g of each individual compound (Table 3.1). The standard was transferred quantitatively to a 100 mL volumetric flask and was diluted with acetonitrile (Chromasolv, Sigma Aldrich). The solution was then transferred to an amber jar, capped with a Teflon lid and Parafilm® and stored at 253 K in a freezer. The solvent used from September 2008 to September 2011 for filter extractions, HPLC mobile phase and calibration standards was acetonitrile, Chromasolv® for HPLC and was purchased from Sigma Aldrich. From September 2011 onwards, Pestanal® acetonitrile, for pesticide residue analysis, purchased from Supelco, was used.

Table 3.1. Concentrations of standards solutions of target compounds, internal standards and volumetric standards.

Standard	Abbreviation	Stock Concentration ($ng\ \mu L^{-1}$)
2-methylphenol	2-me-ph	104
4-methylphenol	4-me-ph	101
4-methyl-2-nitrophenol	4-me-2-NP	133
4-nitrophenol	4-NP	101
2-methyl-3-nitrophenol	2-me-3-NP	103
2-methyl-5-nitrophenol	2-me-5-NP	106
3-methyl-4-nitrophenol	3-me-4-NP	103
2-methyl-4-nitrophenol	2-me-4-NP	108
2,6-dimethyl-4-nitrophenol	2,6-dime-4-NP	101
heptadecane	C17	223
octadecane	C18	229
nonadecane	C19	209

3.4.2. Filter Extraction

Filters and standards were brought to room temperature prior to extraction. The filter was placed on a cleaned stainless steel board and cut into eight pieces using a clean pair of tweezers and a scalpel. Approximately 4 μg (40 μL of approximately 100 ng μL^{-1} concentration) of each of the internal standards 2-methylphenol, 2-methyl-3-nitrophenol and 2-methyl-5-nitrophenol, were spiked onto one of the filter pieces. The filter pieces were then folded, being careful not to touch the sampled portion, and placed into an amber jar. Acetonitrile was poured over the filter pieces and a glass stirring rod was used to mix them prior to being covered with a Teflon lined lid. A Bransonic Ultrasonic Cleaner (Model SS10R-DTH) was used to sonicate the filter sample for 15 minutes.

The filter sample was then filtered into a 250 mL round bottom flask through a 20 mL glass syringe (Popper & Sons) equipped with either a 0.2 μm syringe filter (PTFE Chromspec filter, Chromatographic Specialties) when extracting XAD coated filters or a 0.45 μm syringe filter when extracting uncoated filters. The filter pieces were then sonicated with acetonitrile and filtered three additional times. Each time, the extract was added to the same flask. The extract was evaporated from approximately 80 mL to 0.5 mL using a rotary evaporator with the water bath being controlled at 315 K to 317 K. The sample was transferred to a centrifuge tube with a pipette and was subsequently centrifuged for five minutes to ten minutes using a Fisher Scientific Centrific centrifuge (Model 228) to remove fine particles. The sample was then transferred to a 2 mL conical vial with a conical stirring bar. While being mixed, the sample was evaporated under a flow of nitrogen (Grade 5.0, 99.999%, Linde) at approximately 200 mL min^{-1} to a volume

of approximately 220 μL. This was then transferred to a 1 mL vial with a 200 μL insert for HPLC injection. The round bottom flask was rinsed with 5 mL of acetonitrile and was evaporated, centrifuged and blown-down with nitrogen again. This process was repeated for a total of three rinses. Each of the rinses was separated individually by HPLC.

3.4.3. HPLC Sample Clean-up

HPLC was used as a clean-up step to minimize peak overlap for concentration and isotope ratio measurements. The HPLC used was an HP 1050 HPLC equipped with a Supelcosil LC-18 column (Supelco) with dimensions 25 cm x 4.6 mm and 5 μm packing size and a variable wave detector (VWD) that was set to 320 nm. The mobile phase of the HPLC consisted of water and acetonitrile at a constant flow rate of 1 mL min^{-1} (Fig. 3.2). The solvent gradient began with 100 % deionized Milli-Q water (18 mΩ) and linearly decreased to 45 % water and 55 % acetonitrile at ten minutes. At 15 minutes, the mobile phase was 15 % water and 85 % acetonitrile and at 30 minutes the gradient ended with 100 % acetonitrile. During the 30 minute solvent program, the effluent was collected when the target compounds eluted from the column which was between 10 minutes and 17 minutes. This was repeated for a total of four runs and all of the effluents were combined into one flask. Typical HPLC chromatograms for ambient filters and a spiked filter are shown in Fig 3.3.

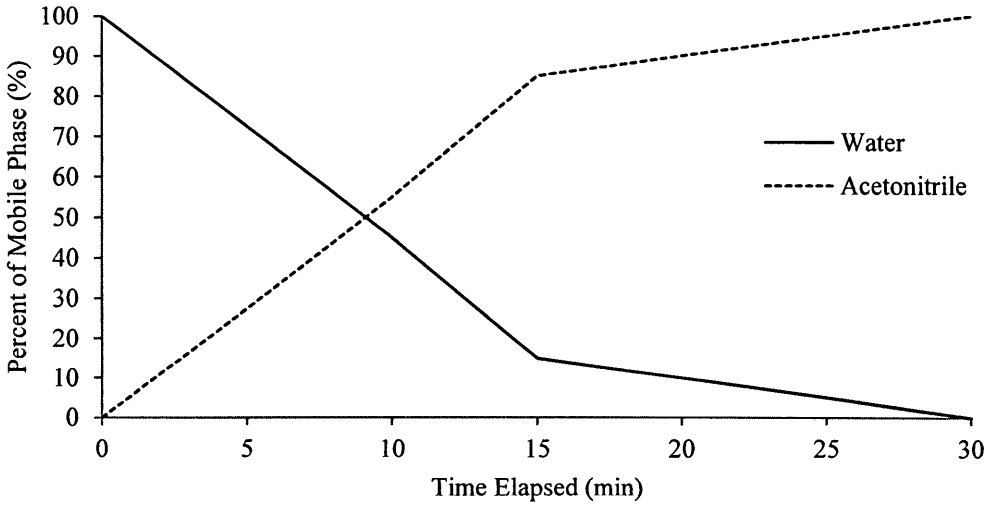

Figure 3.2. Gradient program used for HPLC separation.

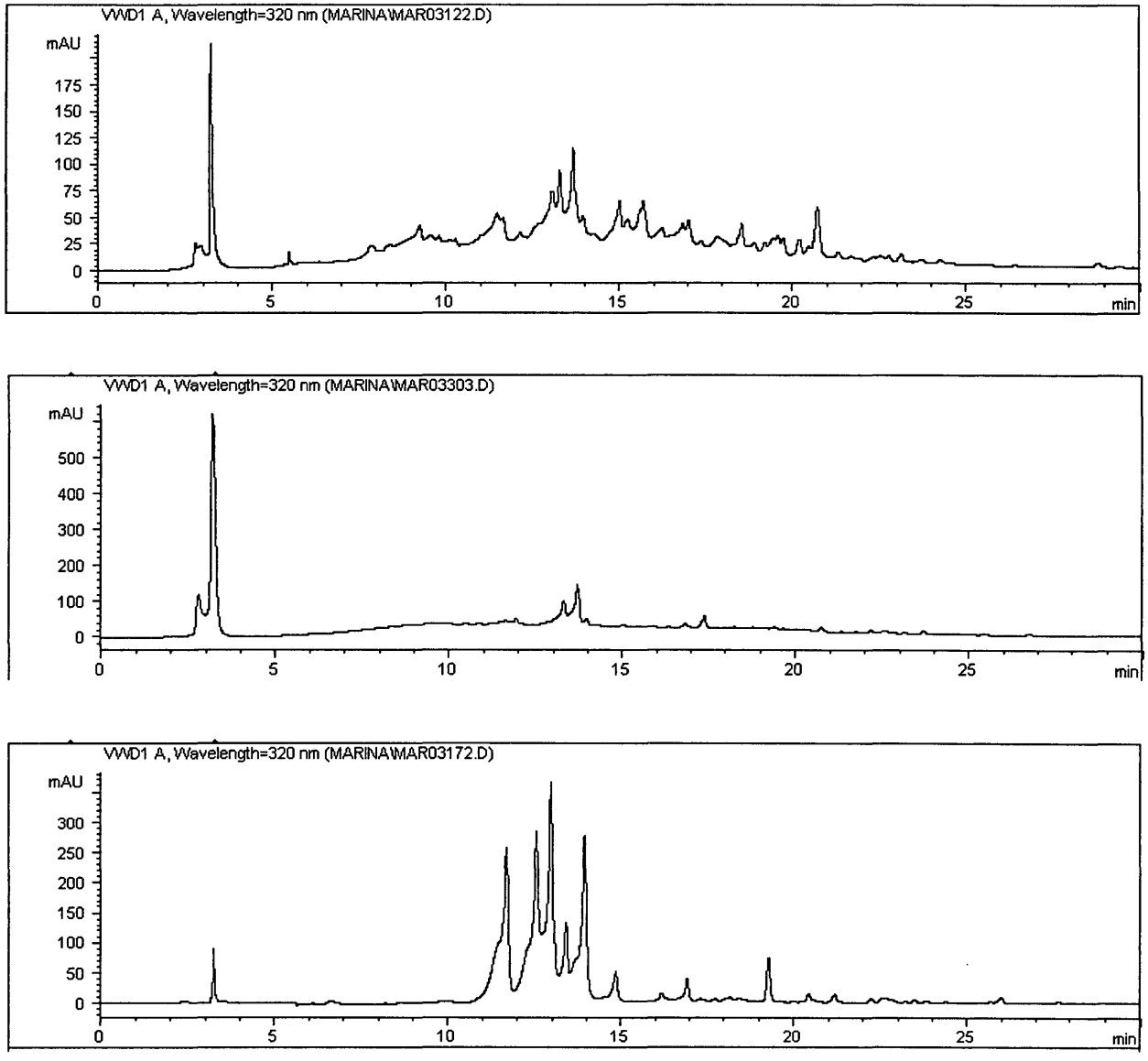

Figure 3.3. Typical chromatogram for an ambient quartz filter (top), an ambient XAD coated filter (middle) and a spiked filter (bottom).

3.4.4. Acetonitrile Evaporation and Solid Phase Extraction

Acetonitrile evaporation and SPE was used as a clean-up step and a solvent exchange step. The effluent collected from the HPLC contained water, acetonitrile and

the target compounds. Acetonitrile was evaporated from the solution at either 278 K for two and a half hours or at room temperature for approximately one hour or until the solution was reduced to approximately half of the initial volume. The solution, now containing water and the target compounds, underwent SPE. An Oasis hydrophilic – lipophilic balanced (HLB) extraction cartridge was first conditioned with 1 mL of acetonitrile, followed by 1 mL of Milli-Q water. The solution was acidified with 30 μL or 3 μL of 0.02 M phosphoric acid to an approximate pH of 2 or 5, respectively, and was pipetted into the SPE cartridge, which eluted into a waste beaker. The empty flask was rinsed with 3 mL of water, and was also passed through the cartridge. Once the solution had fully passed through, approximately 10 mL of acetonitrile was used to desorb the nitrophenols and the solution was collected into a flask.

The solvent collected from the SPE cartridge was evaporated from approximately 10 mL to 0.5 mL. The solution was transferred to a conical vial and the flask was rinsed with 3 mL of acetonitrile and evaporated twice. The solution was added to the same conical vial. The solution was then evaporated under a flow of nitrogen of 200 mL min^{-1} to approximately 80 μL. At this point, 20 μL of a mixture of the volumetric standards heptadecane, octadecane and nonadecane, with a concentration of approximately 220 ng μL^{-1}, was added to the solution. It was then covered and stirred for a few minutes. Half of this solution was pipetted into a vial with an insert, covered with a cap and Parafilm®, and stored in a freezer at 253 K until analysis by GC-IRMS.

3.4.5. Derivatization with BSTFA

To increase the thermal stability of the nitrophenols, they were derivatized prior to injection into GC-MS or GC-IRMS. The derivatizing agent used was BSTFA and reacted according to the reaction presented in Fig. 3.4. To derivatize the solution, 10 μL or 20 μL of BSTFA was added to the mixture with the volumetric standards. The solution was capped with a Teflon seal and was stirred at room temperature for 5 minutes. The entire solution (approximately 40 μL to 50 μL) was then transferred to a 2 mL vial with a 200 μL insert using an Eppendorf pipette.

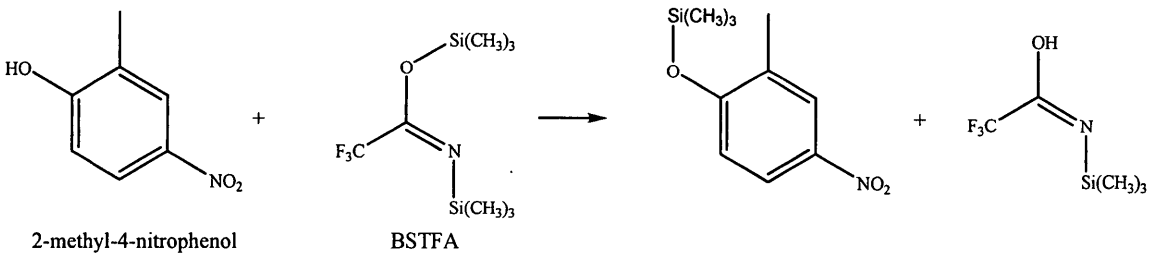

Figure 3.4. Reaction of BSTFA with 2-methyl-4-nitrophenol (adapted from Knapp, 1979).

3.5. Concentration Measurements by GC-MS

GC-MS was used for concentration measurements (Fig. 3.5). The sample was injected via a HP 6890 auto sampler into a HP 5890 GC equipped with a HP 5972 mass spectrometer. After rinsing with solvent five times, 1 μL of sample was injected into the GC through splitless injection. The carrier gas used was high purity helium (Grade 5, 99.999% purity, Linde). The injector temperature was held at 538 K and the detector temperature was held at 553 K.

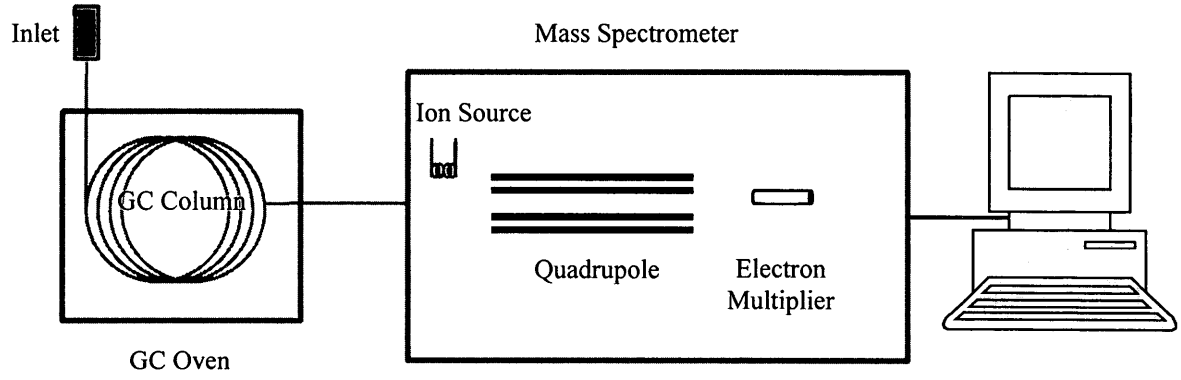

Figure 3.5. Schematic of GC-MS setup.

The initial temperature program used was for the separation of two target compounds, 4-methyl-2-nitrophenol and 2-methyl-4-nitrophenol, and two internal standards, 2-methyl-3-nitrophenol and 2-methyl-5-nitrophenol was 62.5 minutes long and is shown in Fig 3.6. In this program, the initial temperature was held at 373 K for ten minutes. The temperature was ramped at 10 K min^{-1} for eight minutes to 453 K and held for one minute. It was then ramped at 1 K min^{-1} for 25 minutes to 478 K and subsequently ramped at 6 K min^{-1} to 553 K and held for ten minutes. The acquisition mode was scanning mode.

To separate the six target compounds: 4-methylphenol, 4-methyl-2-nitrophenol, 4-nitrophenol, 3-methyl-4-nitrophenol, 2-methyl-4-nitrophenol and 2,6-dimethly-4-nitrophenol compounds, the three internal standards: 2-methylphenol, 2-methyl-3-nitrophenol and 2-methyl-5-nitrophenol and the volumetric standards: heptadecane, octadecane and nonadecane, a 125 minute temperature program was used (Fig. 3.6). This

was a 125 minute program that used selective ion monitoring (SIM) to acquire the data. The initial temperature was held at 373 K for ten minutes. The temperature was then ramped at 1 K min^{-1} to 473 K and held for one minute. It was then finally ramped at 10 K min^{-1} to 553 K and held for six minutes. The columns that were used were either a Rtx-5MS column (60 m x 0.25 mm i.d. x 0.5 μm film thickness) or a DB-5MS or SLB-5MS (60 m x 0.25 mm i.d. x 1 μm film thickness). The masses monitored as well as the times at which they were monitored are listed in Table 3.2.

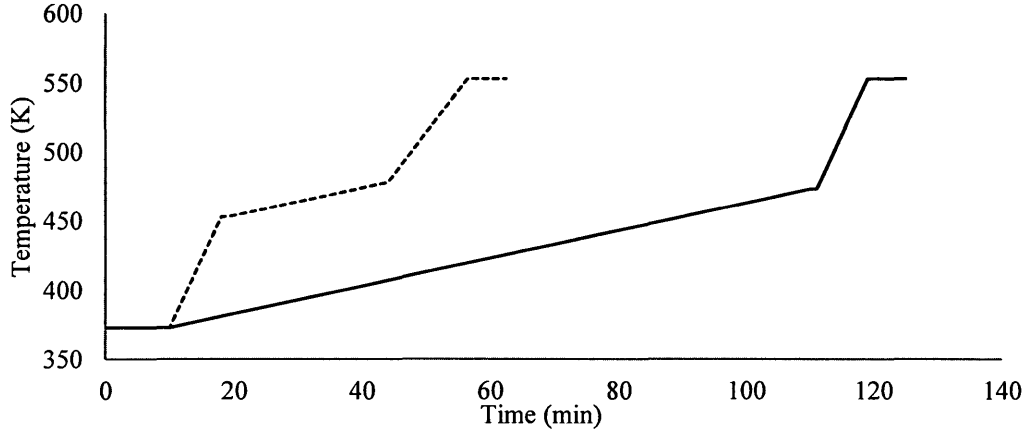

Figure 3.6. Plot of the temperature programs used for GC separation. The dashed line is the GC temperature program used to separate target compounds 4-methyl-2-nitrophenol and 2-methyl-4-nitrophenol and internal standards 2-methyl-3-nitrophenol and 2-methyl-5-nitrophenol and the solid line is the GC temperature program used to separate all six target compounds.

Table 3.2. m/z monitored for all target compounds, internal standards and volumetric standards and the times that they were monitored at using columns with different film thicknesses.

Standard	m/z monitored in SIM	Retention times monitored	
		Rtx-5MS Column (0.5 μm film thickness)	SLB-5MS or DB-5MS Column (1 μm film thickness)
2-me-ph	180, 165	15-30	15-55
4-me-ph	180, 165	15-30	15-55
4-me-2-NP	225, 210, 165	30-70	55-90
4-NP	211, 196, 150	30-70	55-90
2-me-3-NP	225, 208, 165	30-70	55-90
2-me-5-NP	225, 210, 165	30-70	55-90
3-me-4-NP	225, 210, 165	30-70	55-90
2-me-4-NP	225, 210, 165	30-70	55-90
2,6-dime-4-NP	239, 224	70-125	90-125
C17	85	70-125	90-125
C18	85	70-125	90-125
C19	85	70-125	90-125

3.5.1 Quantification of Target Compounds by GC-MS

To quantify target compounds, a calibration of the internal standards and of each target compound was used. Peak areas were determined by summing the peak areas in arbitrary units (AU) of the specific m/z monitored for each compound for both calibration mixtures and ambient samples (Table 3.2). The mass of the target compound in solution was calculated using Eq. 3.4.

$$m_T = \frac{PA_T Cal_{IS}}{Cal_T PA_{IS}} m_{IS}^{Der} \frac{MW_T^{free}}{MW_T^{Der}} \quad \text{Eq. 3.4}$$

Here, m_T is the mass of the target compound in the sample, PA_T and PA_{IS} are the peak areas of the target compound and internal standard, respectively and Cal_T and Cal_{IS} are

the responses of the calibration curves for the target compound and internal standard, respectively. m_{IS}^{Der} is the mass of the derivatized internal standard that was spiked onto the filter, and MW_T^{free} and MW_T^{Der} are the molecular weights of the free target compound and the derivatized target compound, respectively. The blank mass, m_B, is then subtracted from the resulting mass, m_T, and is then divided by the sampling volume, V, to get a final atmospheric concentration, C_T (Eq. 3.5).

$$C_T = \frac{m_T - m_B}{V} \qquad \text{Eq. 3.5}$$

3.6. Analysis by GC-IRMS

All isotope ratio measurements were conducted at Environment Canada in Dr. L. Huang's laboratory using a Micromass Isoprime IRMS (Isomass Scientific, Inc.). Offline measurements, also known as a dual inlet method, were conducted by using the IRMS alone while online measurements or continuous flow measurements were used by coupling a GC and a combustion furnace to the IRMS. For each of these methods, three m/z were monitored for the analysis of $^{12}C^{16}O_2$ and its isotopologues (Table 3.3). All peaks were evaluated based on peak boundaries that have been determined using measurements of standard mixtures. Allison's algorithm (1995), which is similar to the one used by Craig (1957), has been applied to correct the ^{17}O interferences in mass 45. To avoid interference from NO_2, which also contributes to mass 46, average 46/44 ratios from compounds that did not contain nitrogen (heptadecane, octadecane and nonadecane) were used and were very similar to the corrections used by Irei (2008).

Table 3.3. CO_2 isotopologues contributing to monitored m/z 44, 45 and 46.

m/z	Isotopologue Monitored
44	$^{12}C^{16}O^{16}O$
45	$^{13}C^{16}O^{16}O$, $^{12}C^{16}O^{17}O$
46	$^{12}C^{17}O^{17}O$, $^{13}C^{16}O^{17}O$, $^{12}C^{16}O^{18}O$

3.6.1. Offline IRMS Measurements

For offline measurements, 9.53 mm O.D. tubing quartz tubes (Pegasus Industrial Specialties Inc., Canada) were cut into approximately 25 cm pieces and were flame-sealed on one end. The vials were then rinsed with water, distilled water and finally acetone and were subsequently air dried and heated at 313 K under vacuum. Copper oxide (Sigma Aldrich) was sifted through a 50 mesh sieve to remove small pieces. The remaining copper oxide was cleaned three times with acetone and air dried for approximately two hours. The pieces were then heated to 823 K for two hours, cooled and stored in a sealed glass jar.

Approximately 2 g of copper oxide was placed in a cleaned quartz vial with one to three crystals of the target phenol. The vial was attached to the extraction line and placed in a beaker with ice, water and salt while being placed under vacuum to evacuate air in the vial. The vial was then flame-sealed and checked for leaks. The contents of each vial were combusted at 1,123 K for 24 hours in a muffle furnace.

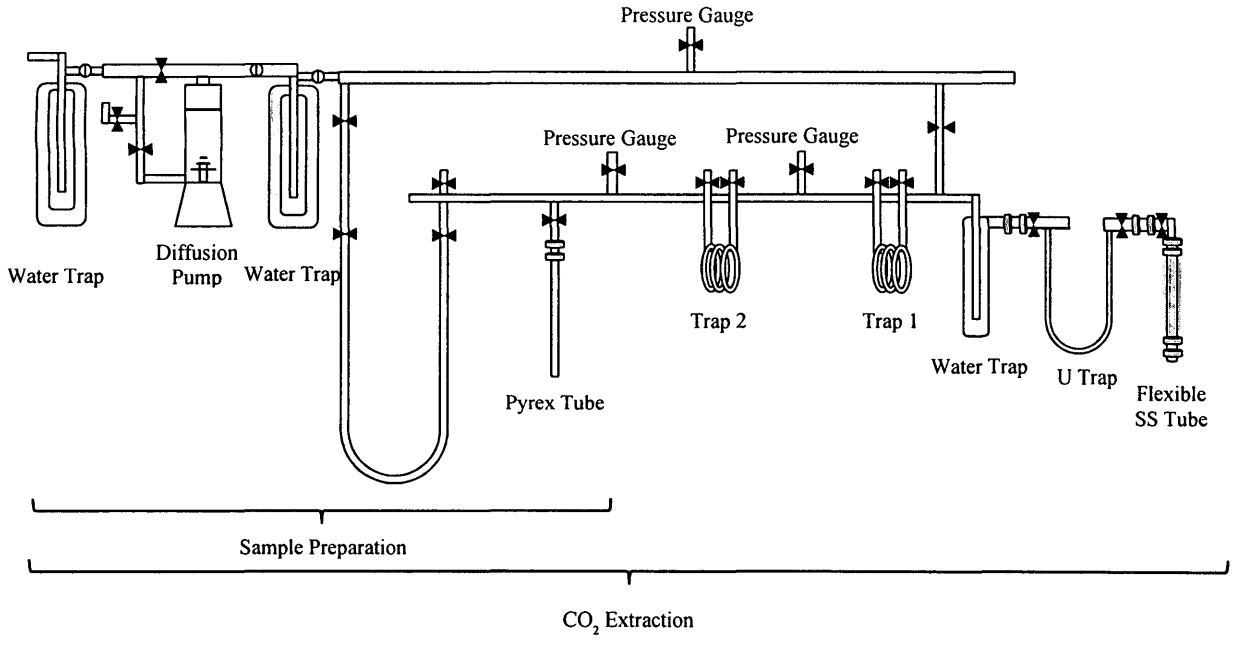

Figure 3.7. Schematic of CO_2 extraction line (courtesy of Dr. L. Huang).

Quartz vials containing the combusted material were attached to a flexible stainless steel tube as shown in the extraction line in Fig 3.7. The entire extraction line was evacuated and all valves were then shut. The quartz tube was broken and water was removed by immersing the water trap in a solution of ethanol and dry ice. Traps 1 and 2 were immersed in liquid nitrogen filled dewars to trap the carbon dioxide stepwise. The carbon dioxide was then transferred and isolated in a 15 cm x 3.2 mm i.d. Pyrex vial (Pegasus Industrial Specialties Inc.) that was immersed in liquid nitrogen. The vial was then sealed with a flame.

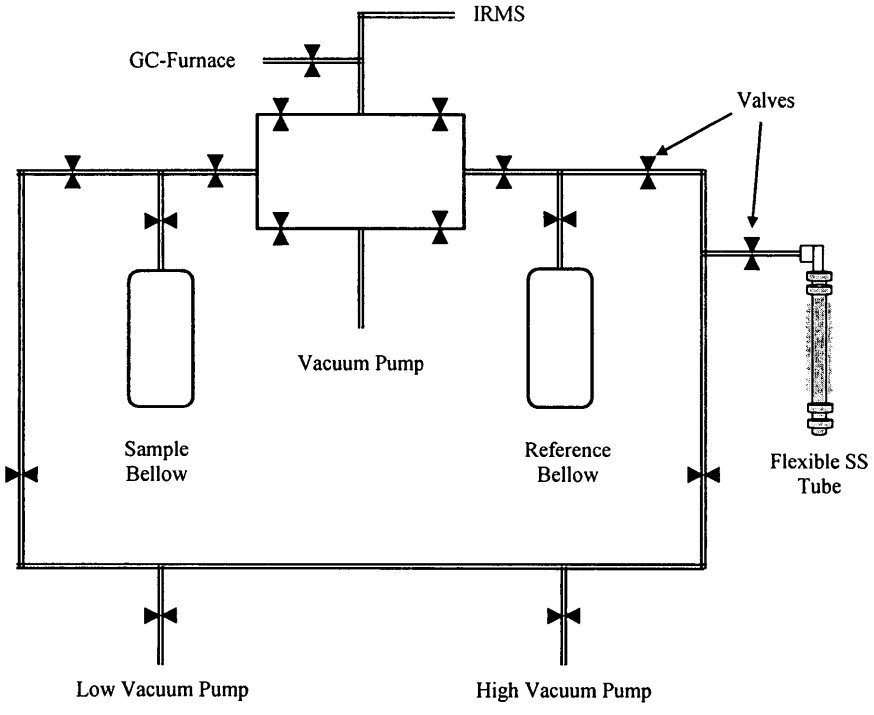

Figure 3.8. Schematic of dual inlet setup for offline analysis.

Offline measurements were conducted using the high precision dual inlet method (McKinney et al., 1950) (Fig. 3.8). In this method, carbon dioxide prepared from a standard is introduced into the reference bellow and carbon dioxide from the combustion of the target compounds is introduced into the sample bellow. The contents of each of the bellows were thoroughly mixed by compressing and expanding them to eliminate the possibility of fractionation within the bellow and each was individually introduced into the IRMS for 20 seconds, alternately, six times. Each individual combustion tube was analyzed in triplicate.

3.6.2. Online IRMS Measurements

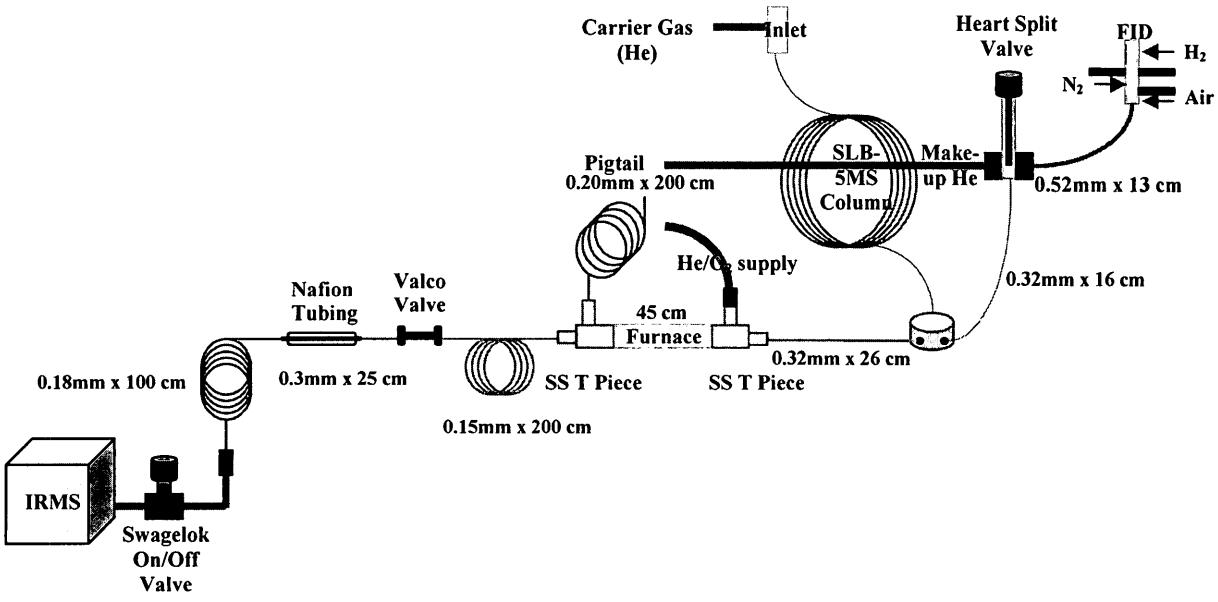

Figure 3.9. Schematic of GC-IRMS setup.

Samples that contained nitrophenols with concentrations greater than 1 ng μL^{-1} were analyzed with GC-IRMS. This setup (Fig. 3.9) included an electronically controlled heart split valve (SGE Analytical Science Pty Ltd.) in the GC oven that directed the column effluent to the flame ionization detector (FID) when the GC column's background was eluting or to the combustion furnace when target compounds were eluting to minimize contamination of the IRMS. The carrier gas used was high purity BIP helium (Linde Canada Ltd.) For isotopic composition measurements, 3 μL of the derivatized sample was injected manually into a SLB-5ms (60 m x 0.25 mm i.d. x 0.5 μm film thickness) column which had a carrier gas flow rate of 1 mL min^{-1}. The temperature

program was 135 minutes long and was slightly longer than the previously used program (Fig. 3.10). The initial temperature of the oven was 373 K and held for ten minutes. It was then ramped at 0.5 K min^{-1} until 423 K, then ramped at 5 K min^{-1} until 473 K and held for one minute. It was finally ramped at 10 K min^{-1} until reaching the final temperature of 553 K and was held for six minutes. A calibration curve of the GC-IRMS was made in a similar way as the GC-MS calibration, only injecting 3 μL of standards to increase the mass of carbon and therefore the signal.

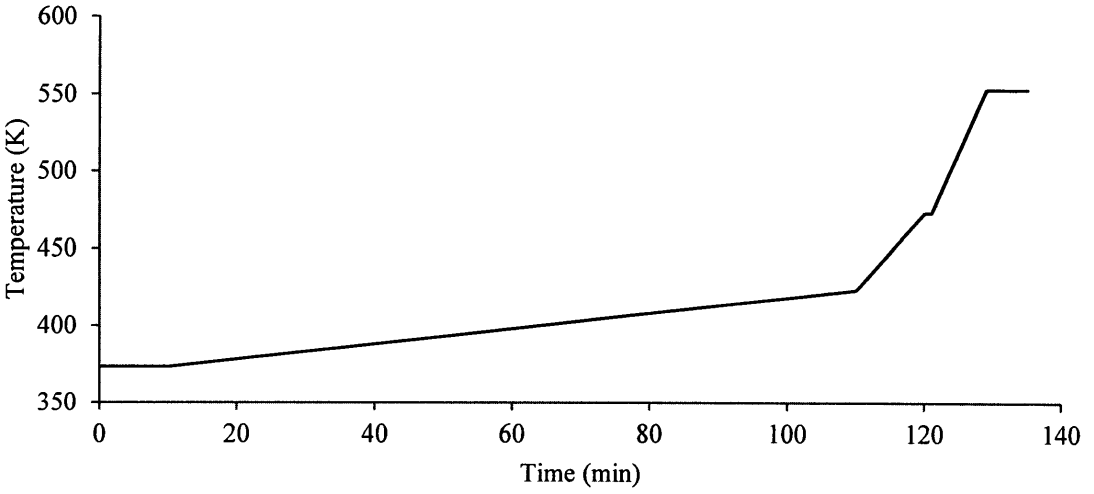

Figure 3.10. Temperature program used for GC-IRMS analysis of nitrophenols.

The GC-combustion furnace interface was similar to that described by Matthews and Hayes (1978) with some modifications as described by Irei (2008). The combustion tube was a gas-tight ceramic tube (Bolt Technical Ceramic Inc.) with dimensions of 0.5 mm i.d. x 6.4 mm o.d. that was cut to approximately 45 cm in length (Fig 3.11). High purity 0.1 mm platinum, copper and nickel wires (Alfa-Aesar) were fed through the

interior of the tube to aid in the combustion process. The wires were pulled through the tube so to leave approximately 7 cm of empty space in the end facing the GC to allow room for the capillary to pass through.

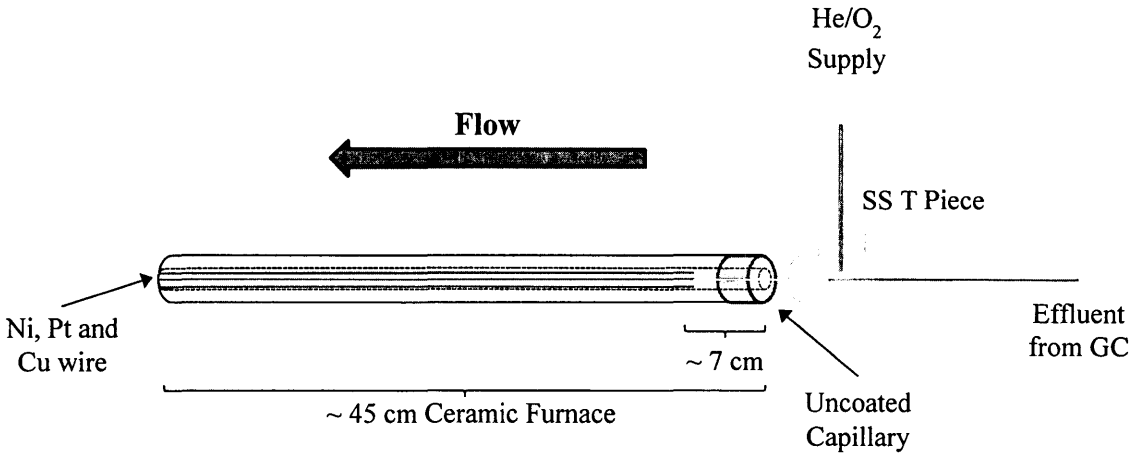

Figure 3.11. Schematic of combustion furnace setup used for GC-IRMS measurements (adapted from Irei, 2008).

The portion of the capillary from the y-piece that was inserted into the furnace was first uncoated. This was done by heating concentrated sulfuric acid in a shallow dish and then immersing the end part of the capillary into it. Approximately 10 cm of the coating was removed and the capillary was trimmed. The uncoated portion of the capillary was inserted approximately 7 cm into the furnace.

A dilute mixture of oxygen in helium was introduced into the furnace to provide enough of an abundance of oxygen to combust the compounds but dilute enough not to damage the IRMS. The temperature of the furnace was held at 1,223 K and was used to combust eluting compounds to carbon dioxide and water. A flow restrictor (pigtail) was

placed at the end of the combustion tube such as to allow a small fraction (10 % to 20 %) of the effluent to enter the IRMS detector. Water was removed by passing through a Nafion permeation dryer prior to proceeding to the IRMS for analysis. For calibration of the isotope ratio measurements, a carbon dioxide reference gas was injected several times directly for 30 second periods into the IRMS during the GC runs (Fig. 3.12) and the carbon isotope ratio of this carbon dioxide is traceable to the internationally accepted V-PDB reference (Huang et al., 2012). Each sample was analyzed in duplicate.

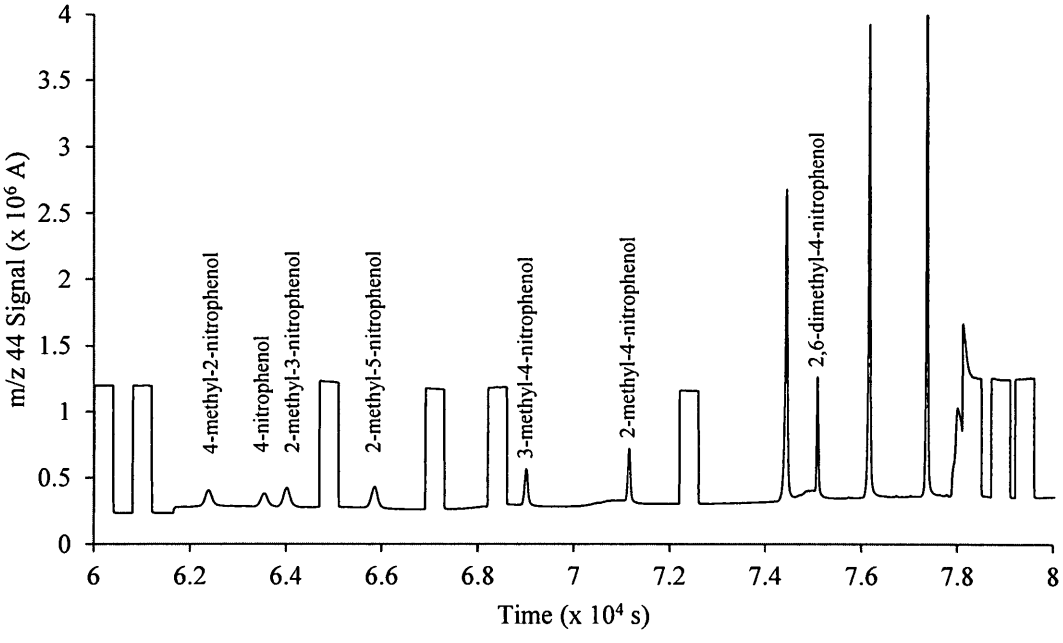

Figure 3.12. Fraction of a sample GC-IRMS chromatogram of a calibration mixture.

The addition of the trimethylsilyl (TMS) contribution from derivatization with BSTFA using Eq. 3.6 was corrected by following a procedure described by Irei et al.

(2013). To correct for the change in carbon isotope ratio due to introducing a TMS group, compounds with known isotope ratios were derivatized and analyzed. The isotope ratio of underivatized phenols was calculated from the isotope ratios of the derivative and the TMS group using mass balance as follows:

$$\delta^{13}C_{free} = \frac{\#C_{deriv}}{\#C_{free}} \times \delta^{13}C_{deriv} - \frac{\#C_{TMS}}{\#C_{free}} \times \delta^{13}C_{TMS} \qquad \text{Eq. 3.6}$$

Here, $\delta^{13}C_{free}$ is the isotope ratio of the underivatized compound, $\#C_{deriv}$, $\#C_{free}$, and $\#C_{TMS}$ is the number of carbons on the derivatized compound, underivatized compound and TMS group, respectively. $\delta^{13}C_{deriv}$ is the isotope ratio of the derivatized compound and $\delta^{13}C_{TMS}$ is the isotope ratio of the TMS group.

4. Results

4.1. Method Validation and Optimization

The procedure, originally developed by Moukhtar et al. (2011), was modified. With the new modifications, several method validation tests were conducted. This section will present the evaluation of sampling, extraction and analysis.

4.1.1. Sampling Method Validation

4.1.1.1. Air Sampling Drift

Air samplers were calibrated monthly or each time that the brushes of the electric motors were replaced. There were two occasions in which air samplers were calibrated three times without replacing brushes. To show to which degree the air samplers drifted between calibrations, the values for the new calibration set to the standard flow rate of 1.13 m^3 min^{-1} were substituted into the first calibration (August 21, 2009 and February 12, 2010) and the flow rates were calculated (Table 4.1).

Several tests were ran in which the flow rates of the air samplers were changed. As a result, face velocities and the particle size cut-off also changed. As the flow rate of the air sampler decreases, the particle size cut-off increases, allowing particles with aerodynamic diameters larger than 2.5 μm to be sampled. Results of these changes are shown in Table 4.2.

Table 4.1. Air sampler drift between calibrations for air sampler motors that were continuously functional.

Calibration Date	Equation of the Line for the Calibration Curve	Flow According to First Calibration (m^3 min^{-1})	Relative Difference (%)
August 21, 2009	24.1x + 0.1	1.13	
September 24, 2009	22.6x + 3.8	1.21	7
November 1, 2009	21.5x + 2.5	1.11	2
February 12, 2010	23. 4x + 1.6	1.13	
March 16, 2010	21.5x + 4.1	1.14	1
May 10, 2010	22.2x + 3.4	1.15	2

Table 4.2. Change in particle size cut-off and face velocity due to varying flow rates of high volume air samplers. Particle size cut-off and face velocity were determined according to the equations in Section 3.3.4.

Flow Rate (m^3 min^{-1})	Particle Size Cut-off (μm)	Face Velocity (cm s^{-1})
1.13	2.5	40.0
0.65	3.3	23.0
0.57	3.5	20.2
0.4	4.2	14.1
0.31	4.8	11.0
0.0167[a]	2.5	20.1

[a] Flow rate of a low-volume air sampler

4.1.1.2. Parallel Sampling

Occasionally, two samples were collected in parallel. To validate this procedure, similar filters (two XAD coated filters or two quartz filters) were used to collect ambient air. Parallel sampling tests were conducted eight times between 2009 and 2012. Sampling time varied from one day to four days. Figure 4.1 shows the ratio of concentrations on air sampler A over those found on air sampler B.

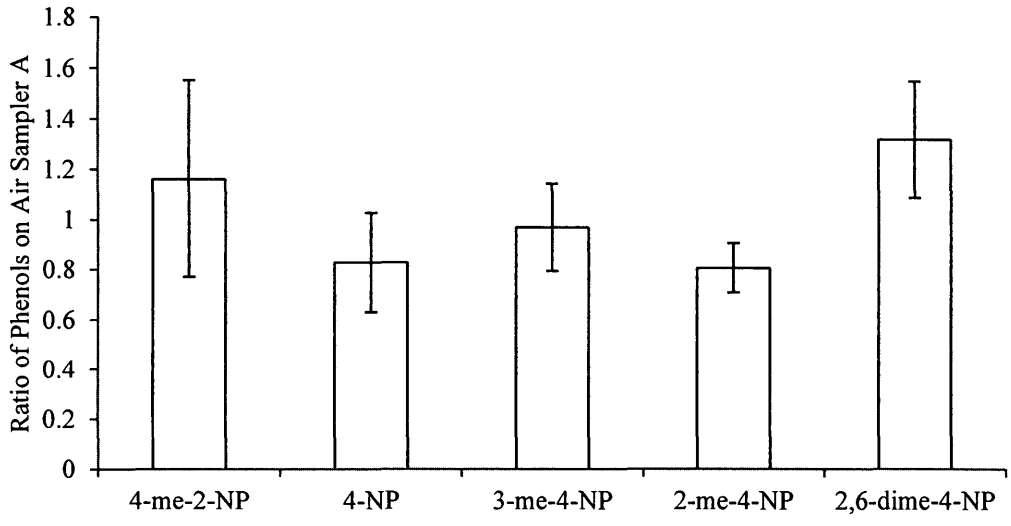

Figure 4.1. The ratio of phenols found on air sampler A over air sampler B for filters (XAD-coated and quartz) that collected ambient air in parallel. Values are averaged over eight parallel sampling tests varying from one day to four days between 2009 and 2012; Error bars represent the error of the mean.

4.1.1.3. Sampling in Series

In most sampling cases, one filter sample was collected at a time. To determine the collection efficiency of each type of filter, one filter was placed over the other with a stainless steel piece of mesh in between. Figures 4.2 and 4.3 illustrate the percentage of mass of select target compounds sampled on the top filter over the total mass found on the top and bottom filters.

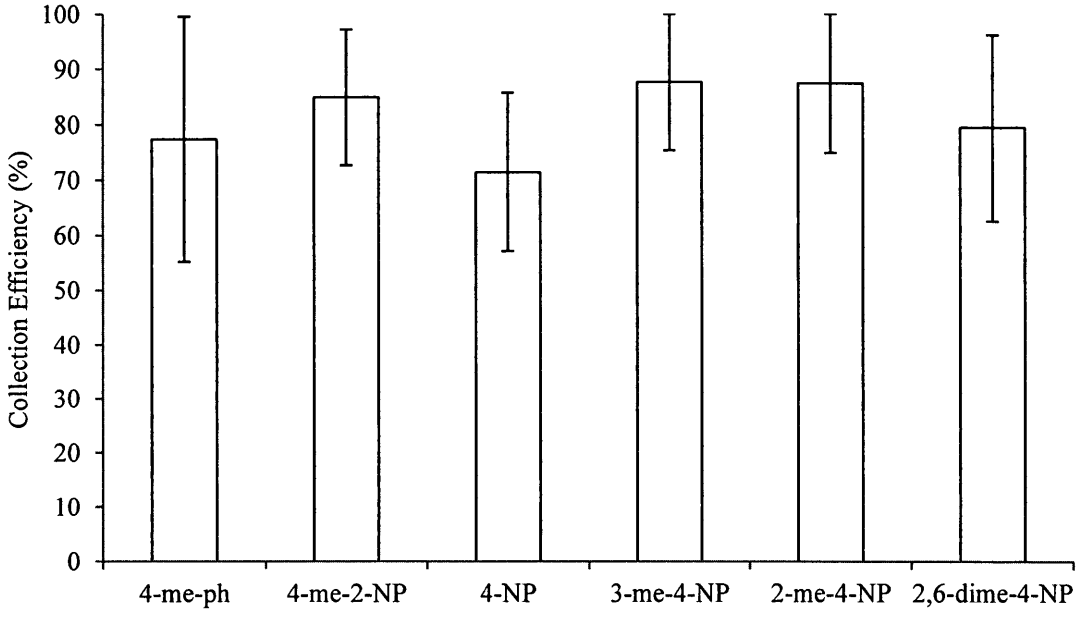

Figure 4.2. Efficiency of quartz filter samples when collected in series based on three tests. The error bars represent the error of the mean; sampling time varied from one day to three days.

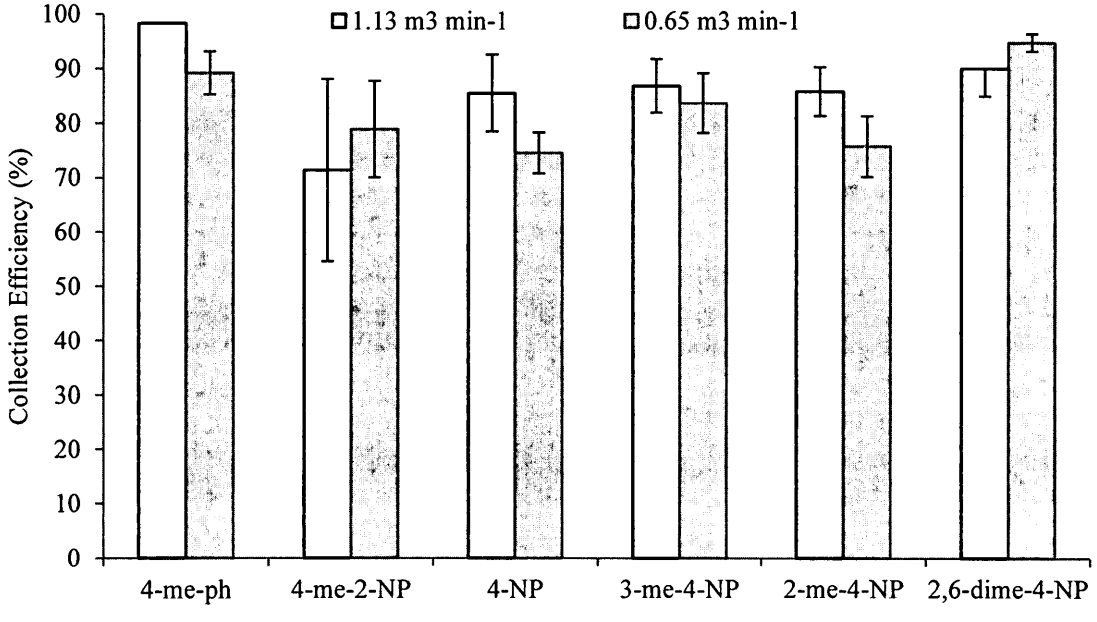

Figure 4.3. Efficiency of XAD-coated filter samples when ambient samples were collected in series following method modifications at varying flow rates (See Section 4.1.2).

4.1.1.4. Sampling Time

Sampling time, particularly when sampling PM, varied from one day to three days. Sampling for three days can increase the amount of artifacts as well as the uncertainty of the measurements. A test was conducted in which quartz filters collected ambient samples in parallel. On one air sampler, one filter collected ambient samples for three days and on the second air sampler, filters collected ambient samples for one day each. The masses on each of the three filters were summed and compared to the mass found on the sample that was collected for three days.

Table 4.3. Experimental data from filter samples that were collected in parallel. Filter A was collected a sample for three consecutive days and Filters B, C and D each collected samples for one day. Samples were collected from July 18 to 20, 2009 at a flow rate of 1.13 m^3 min^{-1}.

	Mass (ng)					Percent Difference[a] (%)
	Filter A	Filter B	Filter C	Filter D	Filter B + C +D	
4-me-ph	10	<DL	<DL	15	15	50
4-me-2-NP	<DL	<DL	<DL	<DL	<DL	NA
4-NP	2997	381	584	2099	3064	2.2
3-me-4-NP	142	72	<DL	87	159	12
2-me-4-NP	926	287	212	379	878	-5.2

[a] The percent difference was calculated by: $\frac{\sum Mass\ on\ Filter\ B,C,D - Mass\ on\ Filter\ A}{Mass\ on\ Filter\ A}\ x\ 100\%$

4.1.1.5. Sampling PM2.5

Typically, both air samplers used were equipped with PM2.5 heads that contain 40 small impactor jets which collect particles that are 2.5 μm and smaller. To investigate the possibility that nitrophenols exist in a particle size range larger than 2.5 μm, one of the air sampler heads was replaced with a PM10 head, containing 16 larger impactor jets.

Results from analysis of samples collected on quartz filter in parallel are compared in Table 4.4.

Table 4.4. Comparison of nitrophenol concentrations when sampling in parallel with an air sampler equipped with a PM2.5 head and a second air sampler equipped with a PM10 head. The flow rate of the samplers was 1.13 m^3 min^{-1} and sampling was conducted from June 22, 2009 to June 24, 2009.

Compound	Concentration (ng m^{-3})	
	PM2.5	PM10
4-me-ph	0.004	0.007
4-me-2-NP	0.004	0.007
4-NP	0.21	0.20
3-me-4-NP	0.02	0.03
2-me-4-NP	0.05	0.06
2,6-dime-4-NP	0.06	0.09

4.1.2. Adjustments to Adsorbent Coating Procedure

Busca (2010) found that the efficiency of the XAD-coated filters was lacking and that there was consistently a 30 % to 40 % breakthrough onto the second filter. It was suggested that this could be improved by increasing the concentration of the slurry or increasing the time that the XAD is ground. The first test conducted was grinding the XAD-4™ according to the procedure described in Section 3.2.2 but increasing the grinding period from 17 hours to 34 hours, 51 hours and 68 hours. XAD samples were taken from the agate pots at each of the time intervals and scanning electron microscope images were acquired (Fig. 4.4.). Scanning electron microscope images were also acquired for filters that were coated with XAD ground for 17 hours and with XAD ground for 34 hours (Fig. 4.5).

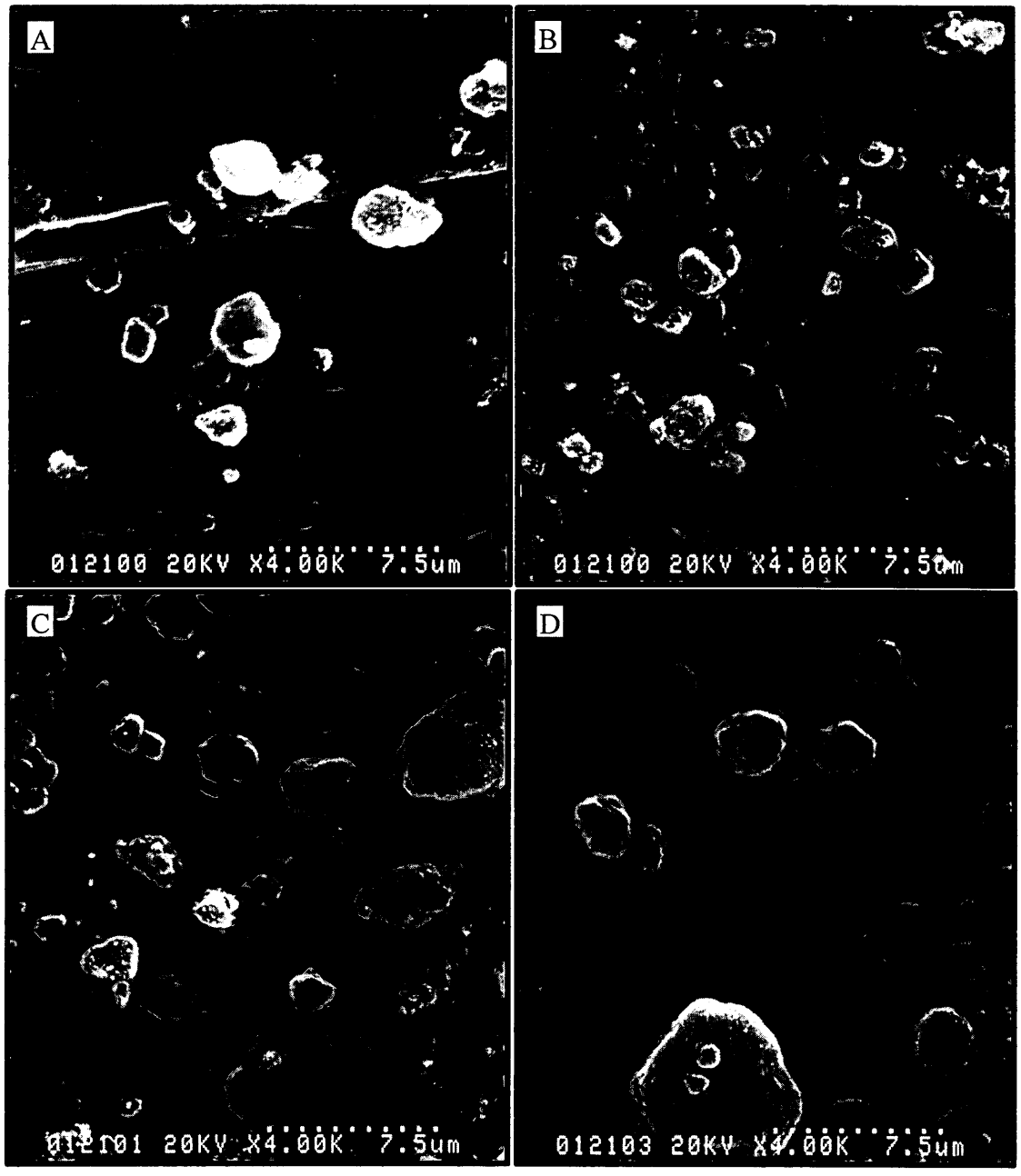

Figure 4.4. Scanning electron microscope images of XAD after being ground for 17 hours (A), 34 hours (B), 51 hours (C) and 68 hours (D). The images are magnified by 4000x and were acquired using a Hitachi S-520 Scanning Electron Microscope at York University. The instrument was operated at 20 kV and had a 10 mm working distance.

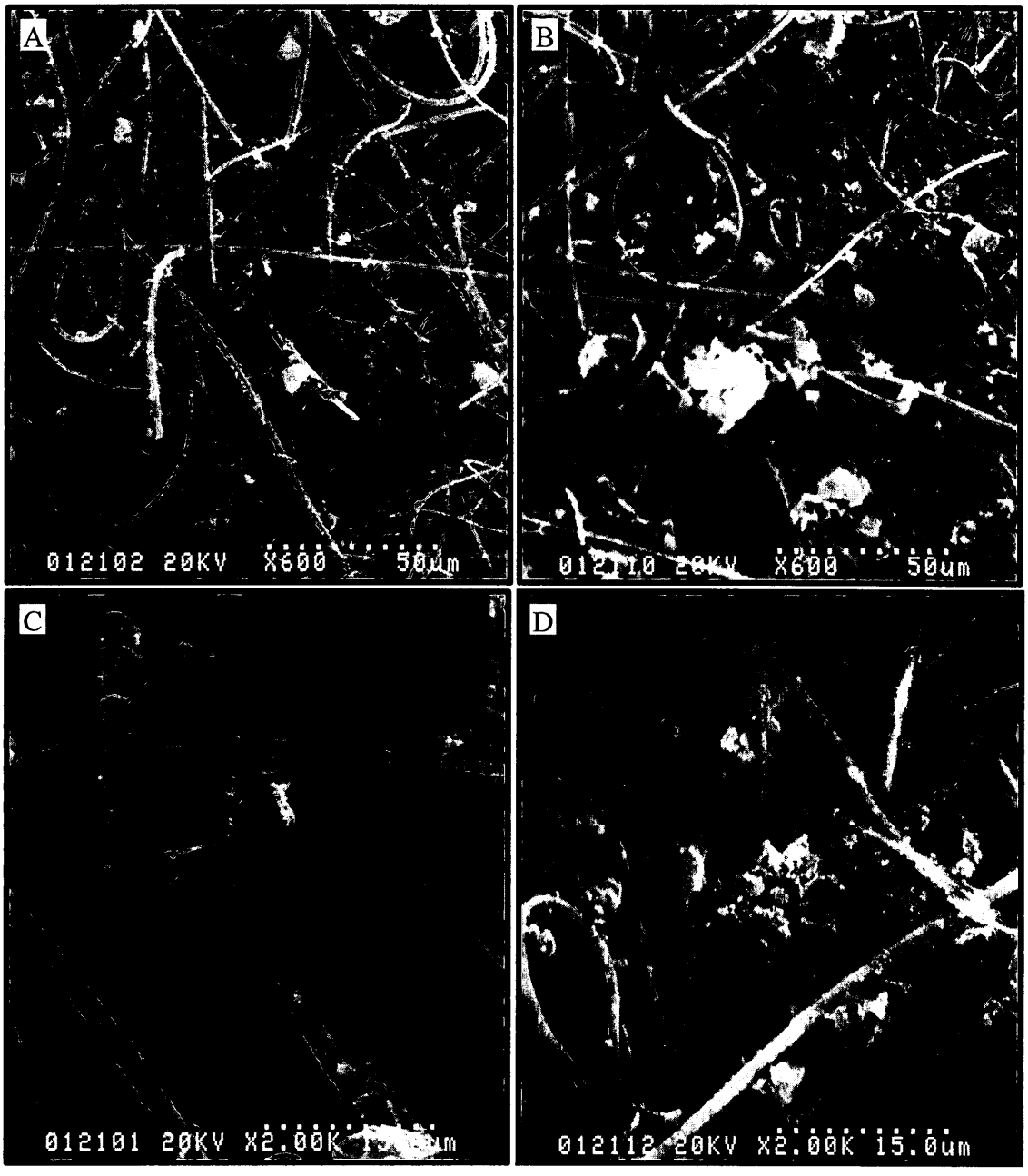

Figure 4.5. Scanning electron microscope images of XAD-coated filters. Images A and C (acquired by Busca, 2010) were coated using XAD particles that were ground for 17 hours and images B and D were coated with XAD particles that were ground for 34 hours. Images A and B are magnified by 600x and images C and D were magnified by 2000x. All images were acquired using a Hitachi S-520 Scanning Electron Microscope at York University. The instrument was operated at 20 kV and had a 10 mm working distance.

To test if having a smaller XAD particle to coat filters at an increased slurry concentration would have an effect on the amount of XAD on the filters, the mass of filters was taken prior to and following the coating procedure (Table 4.5). The modifications made to the procedure significantly increased the mass of XAD on the filter, which inherently improved the efficiency (Section 4.1.1.3). These modifications were applied to all XAD filters from February 2011 onward.

Table 4.5. Masses of 20.32 cm x 25.40 cm quartz fiber filters prior to and following the XAD coating procedure using XAD ground for different periods and different slurry concentrations. Results for filters coated with XAD ground for 17 hours were obtained by Busca (2010).

Filter	XAD Concentration: 6.5 mg mL^{-1} XAD Grinding Period: 17 hours			Filter	XAD Concentration: 10.8 mg mL^{-1} XAD Grinding Period: 34 hours		
	Mass Before Coating (g)	Mass After Coating (g)	Mass of XAD on Filter (g)		Mass Before Coating (g)	Mass After Coating (g)	Mass of XAD on Filter (g)
1	3.30846	3.37880	0.07034	1	3.23948	3.76120	0.43172
2	3.30157	3.35664	0.05507	2	3.23926	3.75808	0.51882
3	3.31647	3.38644	0.06997	3	3.27436	3.78180	0.50744
4	3.27310	3.35241	0.07931	4	3.23144	3.83868	0.60724
5	3.30190	3.35963	0.05773	5	3.25626	3.83278	0.57652
6	3.29303	3.36591	0.07288	6	3.23354	3.85092	0.61738
7	3.206	3.35844	0.15244	7	3.32609	3.96081	0.69991
8	3.169	3.33907	0.17007	8	3.20852	3.94277	0.73425
				9	3.15508	3.92302	0.76874
				10	3.33960	3.98910	0.64950
				11	3.30333	3.97044	0.66711
				12	3.25958	3.98155	0.72157
AVG	3.27	3.36	0.09		3.25	3.88	0.63
SD	± 0.05	± 0.01	± 0.04		± 0.05	± 0.09	± 0.10

AVG is average and SD is standard deviation.

4.1.3. Blank Values, Detection Limits and Artifacts

4.1.3.1. Blanks

Blank values were monitored periodically during the course of this research and are summarized in Tables 4.6 and 4.7. Blank filters underwent the same cleaning, storage, extraction and analysis procedures as ambient samples. Each type of filter, quartz and XAD-coated, were separately analyzed for blanks. XAD blanks prior to and following method modifications did not change significantly and were therefore combined.

Table 4.6. Average and standard deviations of five blank quartz filters. The atmospheric blank concentration was determined by using a high volume sampler volume of 4882 m^3, which is typical for three day PM sample collection.

Compound	Average Mass of Blank (ng)	Standard Deviation of Blank (ng)	High Volume Blank (ng m^{-3})
4-me-ph	2.5	3.3	0.0005
4-me-2-NP	1.6	1.5	0.0003
4-NP	24.7	32.1	0.050
3-me-4-NP	1.9	2.2	0.0004
2-me-4-NP	2.2	2.6	0.0005
2,6-dime-4-NP	0.4	0.6	0.0001

Table 4.7. Average and standard deviation of eight blank XAD-coated filters. The atmospheric blank concentration was determined by using a high volume sampler volume of 1627 m^3, which is typical for 1 day sampling. Blank values were measured by Busca, Hassani and Saccon.

Compound	Average Mass of Blank (ng)	Standard Deviation of Blank (ng)	High Volume Blank (ng m^{-3})
4-me-ph	5.5	2.5	0.003
4-me-2-NP	3.4	1.7	0.002
4-NP	9.4	5.0	0.006
3-me-4-NP	2.8	1.7	0.002
2-me-4-NP	2.5	0.4	0.002
2,6-dime-4-NP	1.8	0.9	0.001

The isotope ratios for filter blanks were not determined since, due to the small blank values, they could not be quantified by GC-IRMS. 3 μL of acetonitrile was injected to test if the GC column or the combustion furnace contributed to blanks and that there were no residual products in either component. A sample chromatogram, shown in Fig. 4.4, confirms the absence of detectable peaks for phenols.

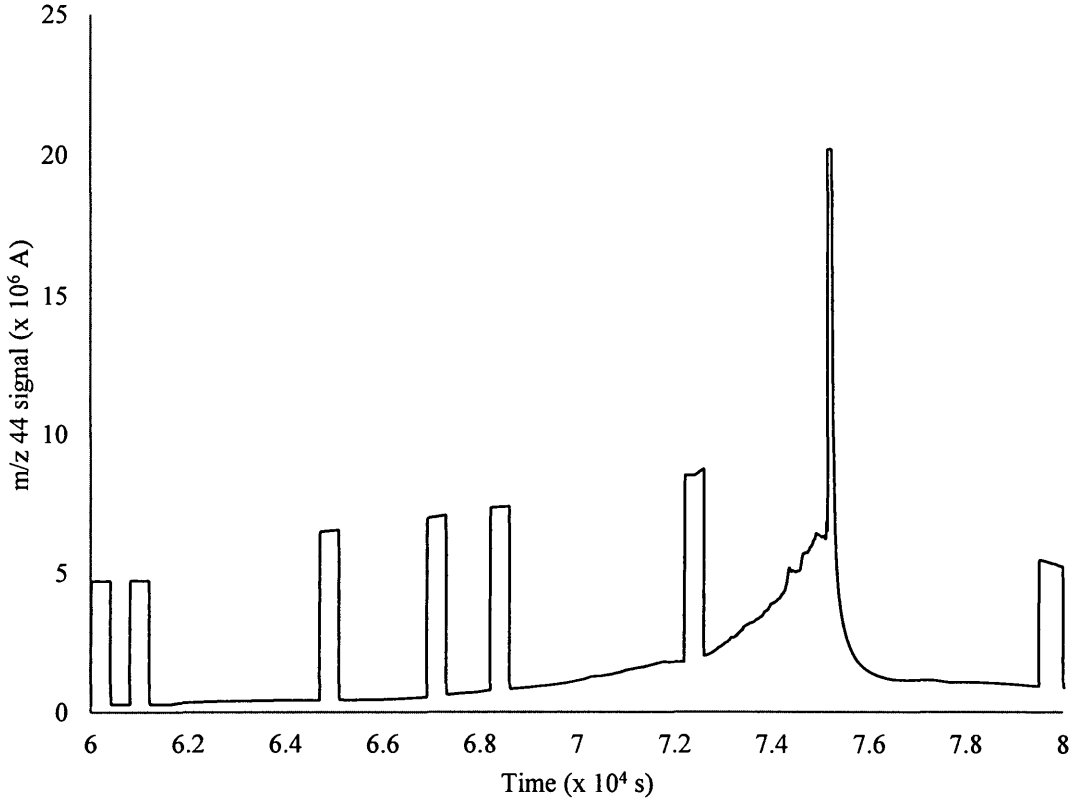

Figure 4.6. Fraction of a m/z 44 GC-IRMS chromatogram of a 3 μL acetonitrile injection.

4.1.3.2. Detection and Quantification Limits

Detection limits (DL) and quantification limits (QL) of samples collected on quartz and XAD-coated filters were found by using three times and ten times, respectively, the standard deviation of the blank value (Section 4.1.3.1). DL and QL were then converted to atmospheric concentrations using a typical sampling time of three days for quartz filters and one day sampling time for XAD-coated filters at a standard flow rate of 1.13 $m^3 min^{-1}$ (Tables 4.8 and 4.9).

Table 4.8. Detection limits and quantification limits for quartz filters. A volume of 4882 m^3 was used to obtain atmospheric concentrations, which is typical of three day sampling.

Compound	DL (ng)	QL (ng)	High Volume DL ($ng\ m^{-3}$)	High Volume QL ($ng\ m^{-3}$)
4-me-ph	9.9	33	0.002	0.007
4-me-2-NP	4.5	15	0.001	0.003
4-NP	96.3	321	0.020	0.066
3-me-4-NP	6.6	22	0.001	0.005
2-me-4-NP	7.8	26	0.002	0.005
2,6-dime-4-NP	1.8	6	0.0004	0.001

Table 4.9. Detection limits and quantification limits for XAD-coated filters. A volume of 1627 m^3 was used to obtain atmospheric concentrations, which is typical of one day sampling.

Compound	DL (ng)	QL (ng)	High Volume DL ($ng\ m^{-3}$)	High Volume QL ($ng\ m^{-3}$)
4-me-ph	7.5	25	0.005	0.015
4-me-2-NP	5.1	17	0.003	0.010
4-NP	15.0	50	0.009	0.031
3-me-4-NP	5.1	17	0.003	0.010
2-me-4-NP	1.2	4	0.001	0.002
2,6-dime-4-NP	2.7	9	0.002	0.006

4.1.3.3. Artifacts

An unknown contamination in processed filter samples began to appear in significant quantities in 2010. This problem could not be resolved until late 2011. All filters that were analyzed during this time were not used for isotope ratio measurements due to the considerable size of the contamination and the uncertainty it would introduce. The contamination was the source of several difficulties in the lab including the degradation of HPLC and GC columns, filaments and the ion source of the mass

spectrometer and resulted in the loss of several samples. This section will present the appearance, testing, unusual behaviour and resolution of this contamination.

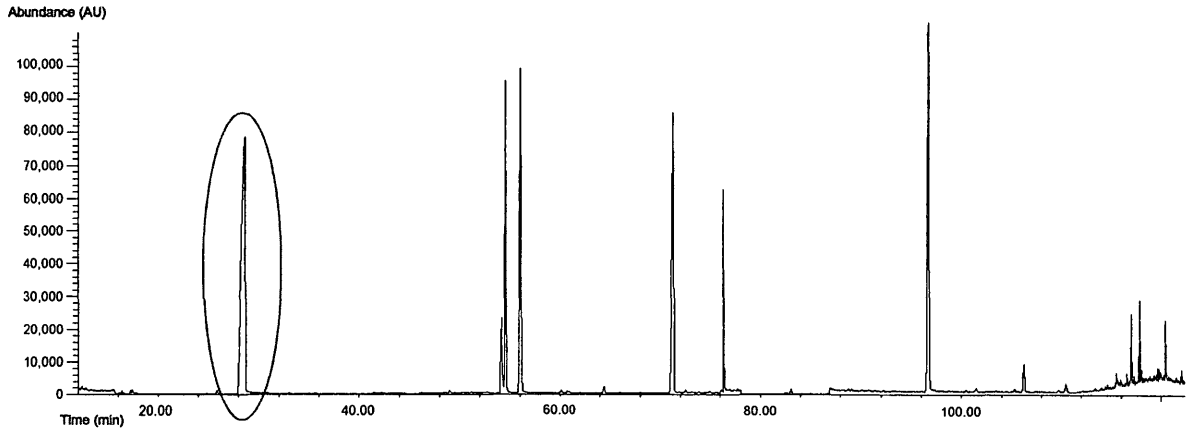

Figure 4.7. SIM chromatogram of an ambient quartz filter. The circled peak is an unknown contaminant present in all samples.

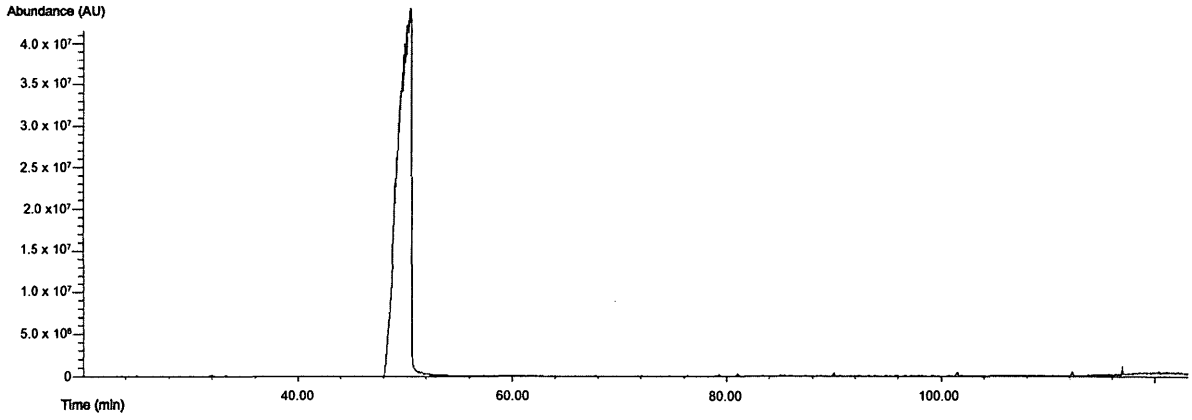

Figure 4.8. SIM chromatogram of an ambient quartz filter following the increase of the contamination.

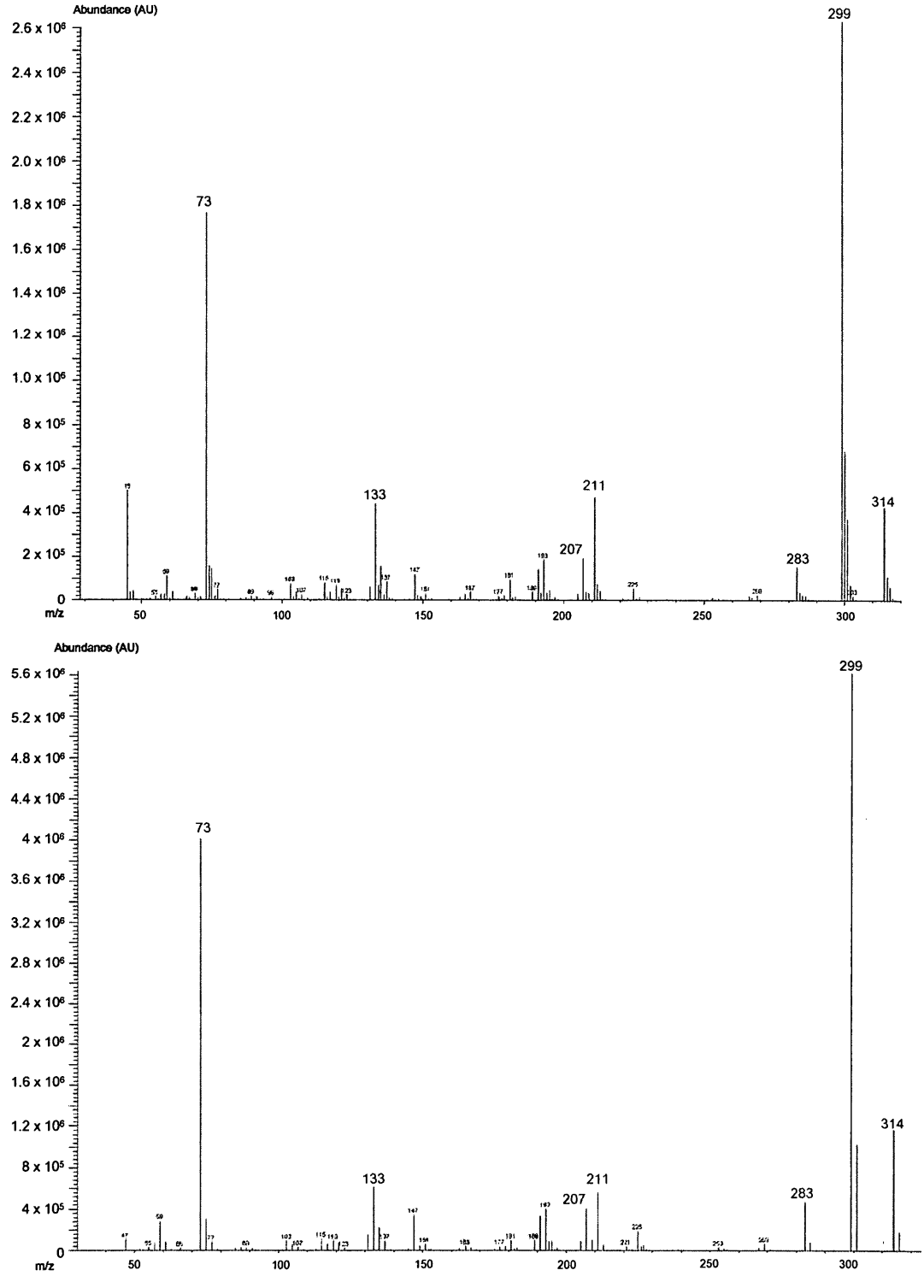

Figure 4.9. Mass spectra of contaminant peak before (top) and after (bottom) significant increase in size.

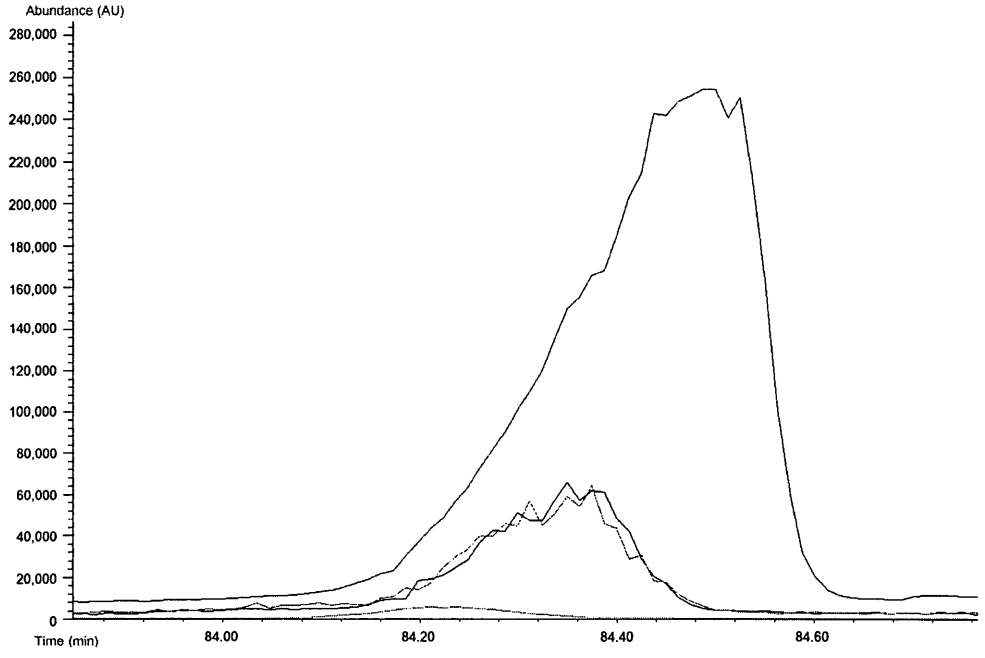

Figure 4.10. Overlaid chromatogram illustrating the degradation of the sensitivity of the MS after repeat runs due to the contamination. The blue, black, pink and green lines represent the first, second, third and fourth runs, respectively.

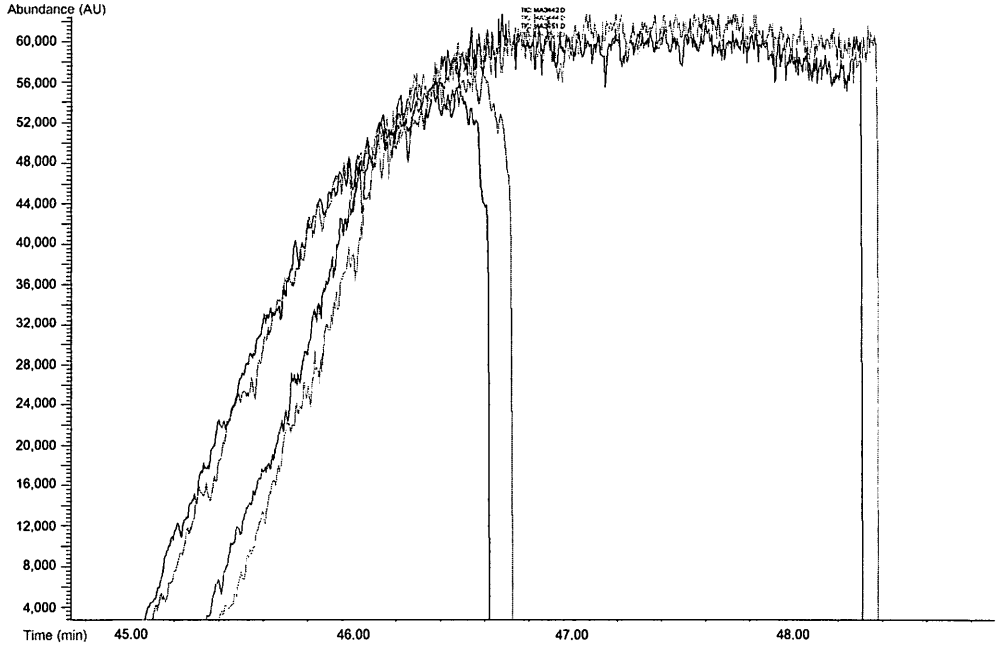

Figure 4.11. Overlaid chromatogram illustrating the growth of the contamination peak over 12 runs. The black, pink, blue, and green lines are the first, third, tenth and twelfth runs.

Once confirming that the contamination had always been present in filter samples, and observing the degradation and uncertainty of the measurements, the next step was to determine the source of the contamination, which could have been ambient air, filters, solvents, derivatizing agents or the HPLC and GC columns used. Table 4.10 presents a summary of tests that were conducted and how the source of the contamination was discovered.

Table 4.10. Summary of tests conducted in determining the contamination source.

Test Conducted	Result
Blank quartz filter extraction	Contaminant present
Blank XAD-coated filter extraction	Contaminant present
Blank quartz filter extraction (filter not baked)	Contaminant present
BSTFA GC-MS injection	No contamination
BSTFA + water GC-MS injection	No contamination
Acetonitrile Chromasolv® GC-MS injection	Contamination sometimes present
Concentrated acetonitrile Chromasolv® GC-MS injection (Evaporated from 100 mL to 50 μL)	No contamination
Acetonitrile extract from SPE cartridge GC-MS injection	Contamination present
Collection of acetonitrile Chromasolv® from HPLC effluent	Contamination present
Split vent line cleaned	No contamination
Gold tip at GC-MS interface cleaned	No contamination
GC injection inlet cleaned	No contamination
Carrier gas hydrocarbon trap replaced	No contamination
Vacuum pump oil replaced	No contamination
Derivatized acetonitrile GC-MS injection	Contamination present
Blank filter extraction with acetonitrile Pestanal®	No contamination
Concentrated and derivatized acetonitrile Pestanal® GC-MS injection (Evaporated from 100 mL to 50 μL)	Contamination present
Acetonitrile Pestanal® sampled from HPLC reservoir (stored in glass decanter)	Contamination present
Blank filter extracted; solution for SPE step acidified to pH 5 instead of pH 2	No contamination

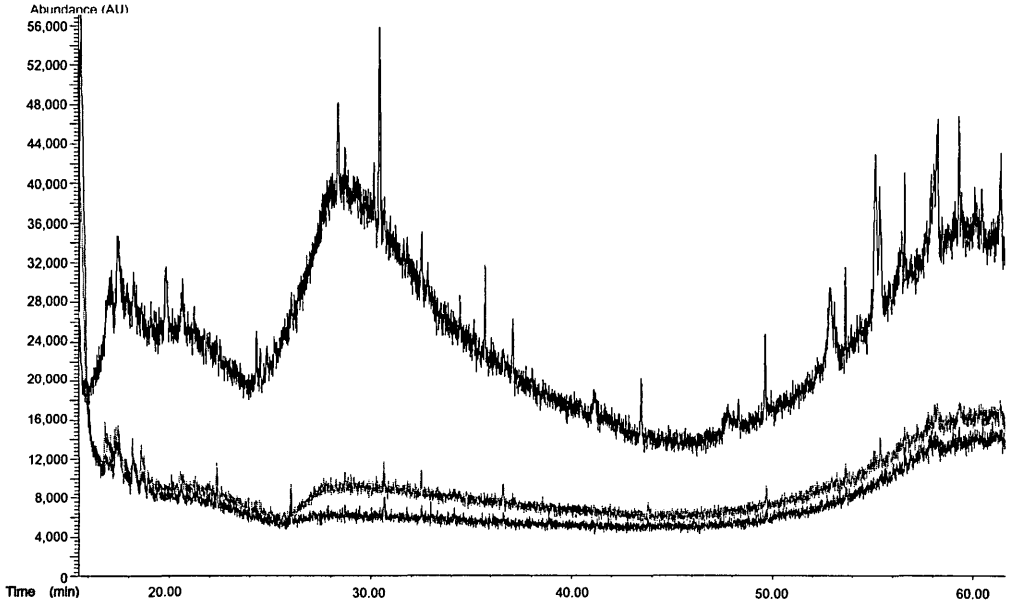

Figure 4.12. Chromatogram illustrating the evolution of the contaminant due to light exposure. The black, pink and blue lines represent the acetonitrile Pestanal® after being exposed to light in a glass decanter in a fume hood after one day, two days and five days, respectively.

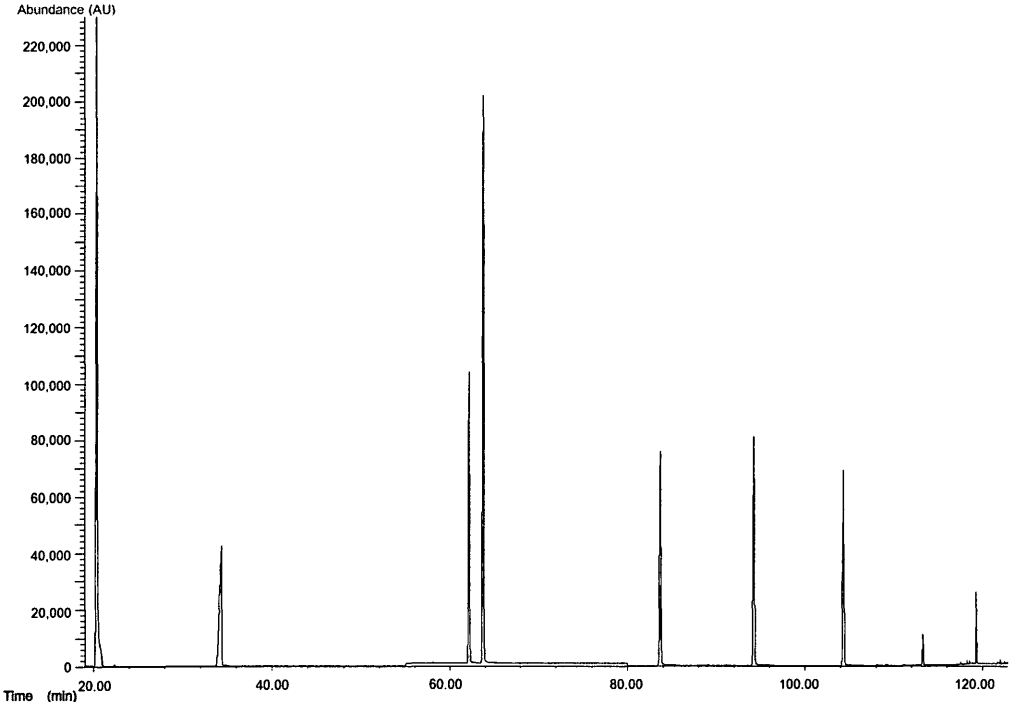

Figure 4.13. Chromatogram of an extracted blank quartz filter spiked with internal standards and volumetric standards. The solution undergoing the SPE extraction step was acidified to pH 5 rather than pH 2.

The contaminant exhibited an unusual behaviour, such that when exposed to light and opened to lab air, its size decreased (Fig. 4.12). This was tested several times and was found to not be due to a decrease in GC-MS sensitivity. The contamination was also found to increase in size with subsequent runs, and was mainly found to be present when BSTFA was also injected. The contaminant source was confirmed early on to be the acetonitrile, which was considered to be of high purity and was previously used in filter extractions for several years. The size of the contaminant was discovered to be dependent on pH used during the SPE extraction step and decreased significantly in size when pH was increased from 2 to 5 (Fig. 4.13). Table 4.11 describes the conditions used prior to and following the resolution of the contaminant problem.

Table 4.11. Extraction procedure conditions prior to contamination and following contaminant resolution.

Parameter	Prior to Contamination	Following Contamination
Solvent Used	Acetonitrile Chromasolv® Plus	Acetonitrile Pestanal®
Origin	USA	Germany
Volume of Bottles	4 L	1 L
Storage time	Indefinite	Minimal
pH before SPE	2	5

4.1.4. Analytical Procedure Validation

4.1.4.1. Recoveries

Internal standards were periodically spiked onto blank filters to determine the efficiency of the extraction procedure. The filters used were cleaned, stored and extracted according to the standard procedure. Table 4.12 summarizes average recoveries of spiked

phenols. The internal standards used were 2-methyl-phenol, which was used as an internal standard for 4-methyl-phenol, and 2-methyl-3-nitrophenol and 2-methyl-5-nitrophenol, which were averaged to correct for recovery of the remaining phenols. The recoveries of each of the standards are also given relative to the internal standard used to correct for them.

Each filter extracted was spiked with two internal standards, 2-methyl-3-nitrophenol and 2-methyl-5-nitrophenol. The average of the recoveries was used for calculations of concentrations and was also used as a diagnostic tool. Figure 4.14 demonstrates the recoveries of the two internal standards for each type of filter used for ambient sampling.

Table 4.12. Averaged recoveries of phenols from blank quartz and XAD-coated filters that were spiked with 4 μg of target compounds and extracted according to the extraction procedure. Recoveries for XAD-coated filter found by Busca (2010) were combined in the averages ± the standard deviation. IS is internal standard.

Compound	Quartz Filters		XAD-coated Filters	
	Recovery (%)	Recovery Relative to IS	Recovery (%)	Recovery Relative to IS
2-me-ph	29 ± 18	1	13 ± 8	1
4-me-ph	27 ± 14	1 ± 0.03	64 ± 53	0.95 ± 0.05
4-me-2-NP	28 ± 8	0.52 ± 0.23	63 ± 26	0.46 ± 0.30
4-NP	34 ± 9	0.84 ± 0.30	70 ± 3	0.75 ± 0.20
2-me-3-NP	34 ±3	0.84 ± 0.11	59 ± 11	0.93 ± 0.06
2-me-5-NP	34 ± 6	1.04 ± 0.05	61 ± 12	1.05 ± 0.06
3-me-4-NP	34 ± 6	1.03 ± 0.26	63 ± 19	0.69 ± 0.02
2-me-4-NP	41 ± 7	1.09 ± 0.28	71 ± 6	0.74 ± 0.22
2,6-dime-4-NP	31 ± 9	0.98 ± 0.20	90 ± 12	0.66 ± 0.34

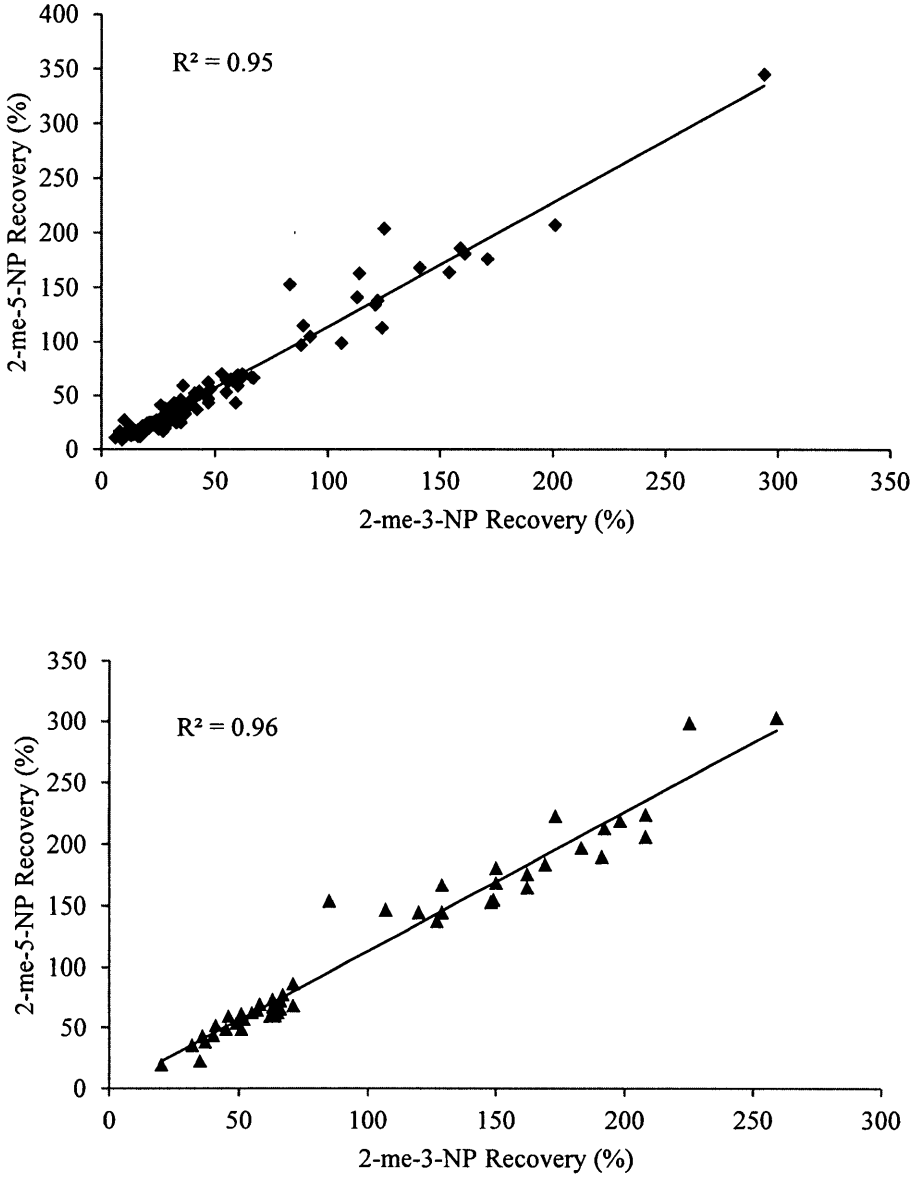

Figure 4.14. Correlation of the recoveries between the two internal standards, 2-methyl-3-nitrophenol and 2-methyl-5-nitrophenol for all PM samples on quartz filters (top) and all gas and PM samples on XAD-coated filters (bottom).

Filters were stored in a freezer between sampling and extraction, as well as the extracts between extraction and GC-IRMS analysis. To examine if there were any losses due to storage, blank filters were spiked with each of the target compounds and internal standards, and were extracted (Table 4.13). The filters were stored for a period of six months.

Table 4.13. Recoveries from blank quartz filter samples that were spiked with 4 μg of internal standards, stored in a glass jar in a freezer at 253 K for six months and extracted and analyzed.

Compound	Recovery (%)
2-me-ph	14 ± 4
4-me-ph	22 ± 8
4-me-2-NP	28 ±13
4-NP	NA
2-me-3-NP	26 ± 5
2-me-5-NP	37 ± 11
3-me-4-NP	34 ± 21
2-me-4-NP	32 ± 17
2,6-dime-4-NP	41 ± 17

4.1.5. Chromatography

4.1.5.1. Retention Times

A nonpolar Supelco LC-18 column was used in HPLC and the VWD was regularly set at 310 nm, a wavelength in which nitrophenols had a strong absorbance but the cresols did not. To identify their retention times, the VWD was set to 280 nm. The nitrophenols were separated using GC for analysis using a 60 m 5 % diphenyl and 95 % dimethylpolysiloxane column. The film thickness used was either 0.5 μm or 1 μm. The retention times for each of the columns and temperature program are listed in Table 4.14.

Table 4.14. Retention times of target compounds, internal standards and volumetric standards for HPLC, GC-MS and GC-IRMS. Retention times for GC measurements slightly changed when small sections of the column were cut for maintenance.

Compound	HPLC	GC-MS			GC-IRMS
		Rtx-5 60 m x 0.25 mm i.d. x 0.5 μm 62.5 min program	Rtx-5 60 m x 0.25 mm i.d. x 0.5 μm 125 min program	SLB-5 / DB-5 60 m x 0.25 mm i.d. x 1 μm 125 min program	DB-5 60 m x 0.25 mm i.d. x 1 μm 135 min program
2-me-ph	12.0[a]	22.5	14.3	28.1	NA
4-me-ph	12.9[a]	23.4	15.7	31.4	NA
4-me-2-NP	15.2	35.6	50.7	74.1	60.2
4-NP	13.8	36.2	51.6	75.2	61.2
2-me-3-NP	13.5	36.2	52.0	75.6	61.6
2-me-5-NP	13.9	36.9	53.5	77.3	63.1
3-me-4-NP	13.0	38.3	57.6	81.5	67.3
2-me-4-NP	13.5	40.6	61.5	86.3	71.8
2,6-dime-4-NP	14.4	47.0	74.8	100.6	85.6
C17	NA	44.7	73.4	97.5	83.6
C18	NA	49.0	83.9	108.3	94.2
C19	NA	52.2	93.9	115.4	104.3

[a] Retention times were found at $\lambda = 280$ nm

4.1.5.2. GC-MS & GC-IRMS Calibration

A calibration curve was created for each of the phenols and volumetric standards by injecting mixtures of standards at varying concentrations, typically 1 ng μL^{-1} to 15 ng μL^{-1}, into the GC-MS. Calibrations were run every month or after the ion source was cleaned. In between calibrations, standard mixtures were injected to monitor changes in sensitivity of the mass spectrometer. Calibration curves using GC-IRMS were created using calibration mixtures with a concentration range of 0.5 ng μL^{-1} to 15 ng μL^{-1}, and injecting 3 μL rather than 1 μL as used in GC-MS. Figures 4.15 and 4.16 show a typical calibration curve for 2-methyl-4-nitrophenol using the two different methods. The

intercepts for each of the calibration curves were set to zero due to the absence of a statistically significant axis intercept. Typical slopes, errors and linear regression coefficients are listed in Table 4.15.

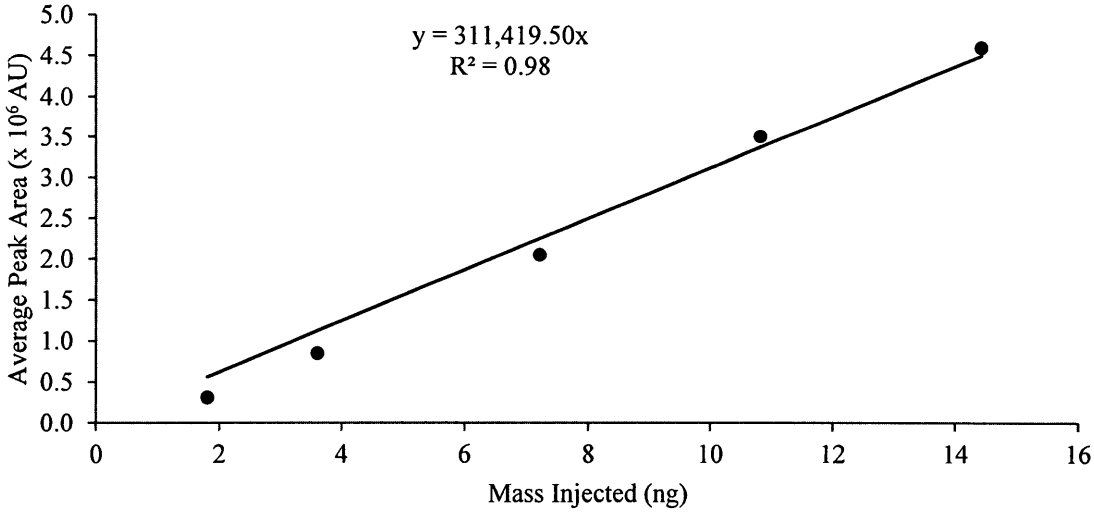

Figure 4.15. GC-MS calibration curve for 2-methyl-4-nitrophenol.

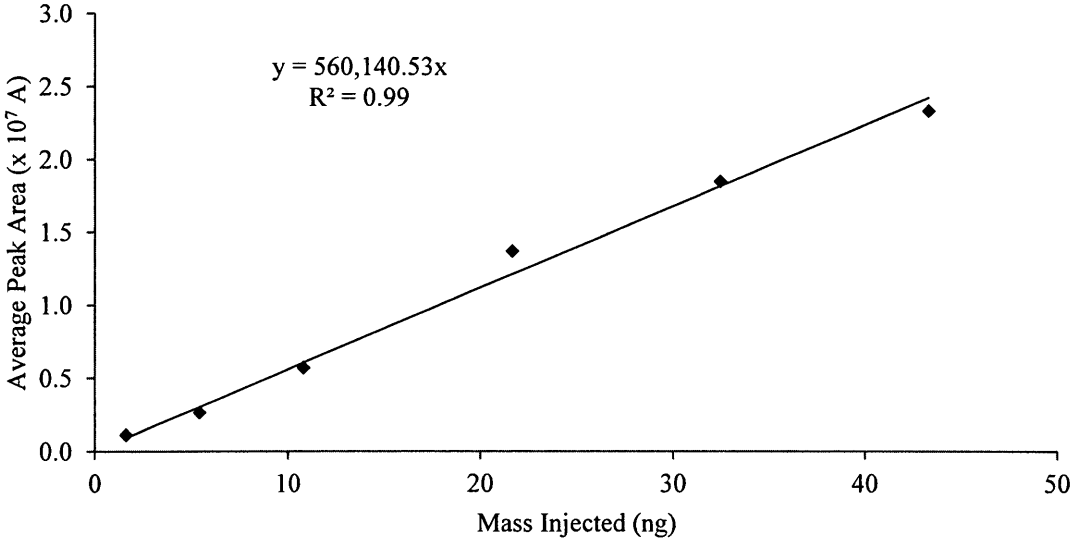

Figure 4.16. GC-IRMS calibration curve of 2-methyl-4-nitrophenol.

Table 4.15. Slopes, errors of the slopes and regression coefficients from typical GC-MS and GC-IRMS calibration curves of target compounds, internal standards and volumetric standards. Units of slopes and errors of slopes are peak area (in arbitrary units) ng^{-1} μL for GC-MS and for GC-IRMS are A ng^{-1} μL.

Compound	GC-MS			GC-IRMS		
	Slope (x 10^5)	Error of Slope (x 10^4)	R^2	Slope (x 10^6)	Error of Slope (x 10^5)	R^2
2-me-ph	6.96	1.4	1	-	-	-
4-me-ph	10.6	4.0	1	-	-	-
4-me-2-NP	3.19	2.1	0.99	0.91	0.43	1
4-NP	4.61	1.6	0.99	0.89	0.50	0.99
2-me-3-NP	1.95	0.6	1	1.20	0.77	1
2-me-5-NP	3.78	1.5	0.99	1.63	0.84	0.99
3-me-4-NP	2.82	1.2	0.99	1.48	0.67	1
2-me-4-NP	3.46	1.3	0.98	1.66	0.71	0.99
2,6-dime-4-NP	2.97	1.3	0.98	2.14	1.0	0.99
C17	1.52	0.5	1	3.40	2.2	0.98
C18	1.50	0.4	1	4.73	3.0	0.99
C19	1.47	0.4	1	5.15	3.3	0.99

4.2. Method Evaluation

This section will give results of method performance tests, specifically the precision and accuracy of the optimized conditions. The precision and accuracy of both concentration and isotope ratio measurements will be presented.

4.2.1. Precision

All samples and calibration mixtures were analyzed by GC-MS in duplicate. To determine the precision of this method, the ratio of the target compound signal to that of the internal standard signal was found for each run. The differences in ratios between the first and second runs, assuming the error was random, were calculated and averaged. The standard deviations of the averages are given in Table 4.16.

Table 4.16. The uncertainty of GC-MS measurements, σ, for each compound relative to both internal standards.

Compound	$\sigma_{2\text{-me-3-NP}}$ (%)	$\sigma_{2\text{-me-5-NP}}$ (%)
4-me-ph	5.3[a]	
4-me-2-NP	4.9	4.9
4-NP	3.9	3.7
3-me-4-NP	3.9	4.2
2-me-4-NP	3.5	3.0
2,6-dime-4-NP	3.9	4.2
C17	3.8	5.2
C18	3.6	3.9
C19	3.8	3.8

[a] σ for 4-me-ph was found relative to 2-me-ph

Like GC-MS measurements, all isotope ratio measurements acquired with GC-IRMS were run in duplicate. Table 4.17 shows the average standard deviation of isotope ratios from repeat calibration standards and ambient samples. The precision of the GC-IRMS was found to be within 0.3 ‰ for each compound. Extracts from two filter samples, X011111A-TOP and X041111A-TOP, were each injected into the GC-IRMS four times to monitor the reproducibility of the method. The results from these tests are shown in Table 4.18.

Table 4.17. Average standard deviations of carbon isotope ratios for phenols determined from repeat runs of calibration standards and ambient samples.

Compound	σ_{avg} (‰)
4-me-2-NP	0.31
4-NP	0.27
2-me-3-NP	0.27
2-me-5-NP	0.19
3-me-4-NP	0.30
2-me-4-NP	0.26
2,6-dime-4-NP	0.31

Table 4.18. Precision of GC-IRMS for two filter extracts that were each analyzed a total of four times.

		Isotope Ratio (‰)				
		4-NP	2-me-3-NP	2-me-5-NP	2-me-4-NP	2,6-dime-4-NP
X011111A-TOP	1	-35.4	-27.1	-27.1	-30.6	-34.8
	2	-35.1	-27.3	-27.0	-31.0	-34.7
	3	-35.5	-26.5	-26.7	-30.5	-35.5
	4	-35.2	-26.7	-27.2	-30.4	-34.7
	AVG	-35.3	-26.9	-27.0	-30.6	-34.9
	SD	0.2	0.4	0.2	0.3	0.4
X041111A-TOP	1	-31.4	-26.3	-27.2	-31.0	
	2	-31.4	-26.6	-27.2	-31.4	
	3	-31.3	-27.0	-27.7	-31.3	
	4	-31.0	-26.5	-27.3	-31.1	
	AVG	-31.3	-26.6	-27.4	-31.2	
	SD	0.2	0.3	0.2	0.2	

4.2.2. Accuracy of Isotope Ratio Measurements

The accuracy of IRMS measurements was determined by using offline and online measurements. Offline measurements, determined according to the procedure described in Section 3.6.1, were compared with online measurements, which were acquired by injecting calibration standards or extracts of filters spiked with standards into the GC-IRMS. The results from these tests are presented in this section.

4.2.2.1. Offline Measurements

Offline measurements for most of the nitrophenols have been previously measured by former group members. Although analysis of the same compound was redone using the same batch of nitrophenols, leakages in the extraction line resulted in

isotope fractionation, and were therefore were not used in this study and only offline values for 4-nitrophenol were determined (Table 4.19). To gain insight into the accuracy of the GC-IRMS and to determine if isotopic fractionation occurs during the analysis procedure, offline values were compared to online values (Table 4.20).

Table 4.19. Summary of offline measurements of 4-nitrophenol. Five sample tubes were each analyzed in triplicate, and averages and standard deviations (SD) are presented.

Sample Tube	Isotope Ratio ± SD (‰)
1	-28.66 ± 0.01
2	-28.65 ± 0.03
3	-28.98 ± 0.15
4	-29.24 ± 0.19
5	-29.09 ± 0.09
AVG	-28.92 ± 0.26

Table 4.20. Accuracy of GC-IRMS; Online values are averaged over ten points for each compound (± denotes error of the mean). Values are for injected masses between 2 ng and 55 ng.

Compound	Offline Value (‰)	Online Value (Calibration Standard) (‰)	Online Value (Spiked Filter) (‰)
4-me-2-NP	-26.9[a]	-27.0 ± 0.1	-
4-NP	-28.9	-28.9 ± 0.1	-28.5 ± 0.4
2-me-3-NP	-26.7[a]	-26.7 ± 0.1	-26.8 ± 0.4
2-me-5-NP	-27.2[a]	-27.3 ± 0.1	-27.3 ± 0.3
3-me-4-NP	-25.7[b]	-25.6 ± 0.1	-25.5 ± 0.2
2-me-4-NP	-27.4[a]	-27.5 ± 0.1	-27.5 ± 0.1
2,6-dime-4-NP	-29.0[b]	-29.0 ± 0.1	-

[a] measured by Moukhtar et al., (2011); [b] measured by Irei, (2008)

4.2.2.2. Isotope Ratio of TMS Group

As discussed in Section 3.4.5, all samples were derivatized with BSTFA prior to analysis, resulting in the addition of a TMS group to the phenol. To determine the isotope ratio of the TMS group, which cannot be determined by offline measurements, 50 ng to 100 ng of derivatized target compounds were injected into the GC-IRMS and the isotope ratio of the TMS group was calculated using the isotope ratio of the phenols, determined by offline measurements (Section 3.6.2). For the seven phenols, the TMS delta was found to be -48.0 ± 0.1 ‰ (Figure 4.17).

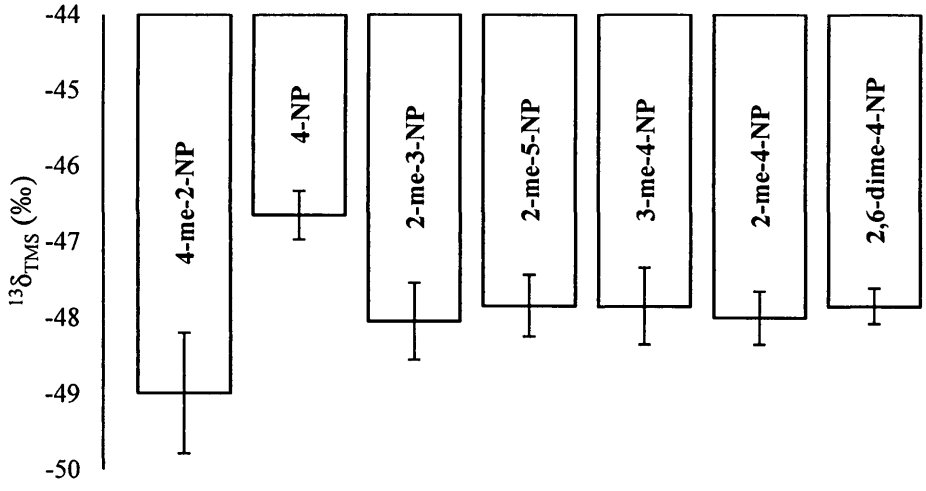

Figure 4.17. Isotopic composition of TMS group found by injecting various derivatized compounds. The error bars represent the standard deviations based on an average of five measurements for each phenol.

To test the minimum amount of mass needed to gain maximum accuracy and precision, various concentrations and volumes of 2-methyl-3-nitrophenol were injected into the IRMS. The results from this test are shown in Fig. 4.18.

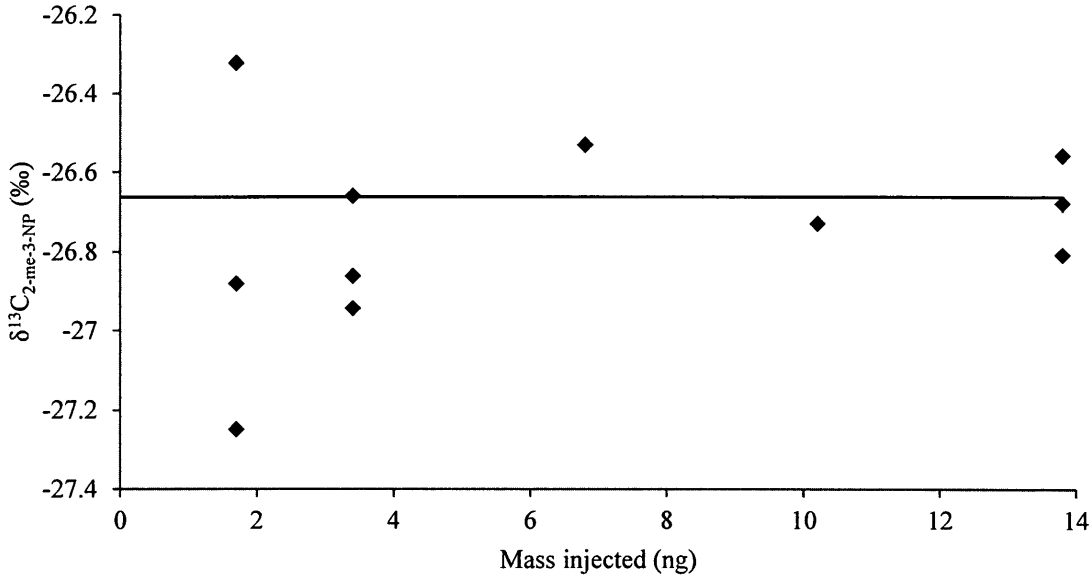

Figure 4.18. Changes in the delta value of 2-methyl-3-nitrophenol as a function of mass injected; the solid line indicates the offline value of 2-methyl-3-nitrophenol (-26.7‰) (Moukhtar et al., 2011). Average delta values and standard deviations for data points at 1.7 ng, 3.4 ng and 13.7 ng, are -26.8 ± 0.5 ‰, -26.8 ± 0.1 ‰ and -26.7 ± 0.1 ‰, respectively.

4.3. Ambient Measurements

The developed sampling, extraction and analysis procedures were applied for ambient concentration and stable carbon isotope ratio measurements are presented in this section. The individual results for each sample along with meteorological conditions and pollution data are listed in the Appendix.

4.3.1. Concentration Measurements

The following section presents a summary of concentration measurements of target compounds in PM2.5 alone (Section 4.3.1.1) and in the gas phase and PM2.5 together (Section 4.3.1.2). Statistical data, box and whisker plots and frequency distributions are shown for each data set.

4.3.1.1. Concentration Measurements of Phenols in PM2.5

Table 4.21. Summary of concentration measurements of phenols found in PM2.5 sampled on quartz filters. The sampling period was from March 2009 to August 2012.

Compound	Number of Samples Found On[a]	Concentration (ng m^{-3})				
		Average	Error of the Mean	Median	Max	Min
4-me-ph	72 / 88	0.13	0.04	0.03	3.47	<DL
4-me-2-NP	81/115	0.06	0.02	0.01	1.69	<DL
4-NP	114/115	0.80	0.14	0.36	11.61	0.02
3-me-4-NP	107/115	0.23	0.06	0.04	5.41	<DL
2-me-4-NP	113/115	0.48	0.10	0.13	6.92	<DL
2,6-dime-4-NP	98/108	0.07	0.01	0.03	1.04	<DL

[a] Concentrations that were >DL

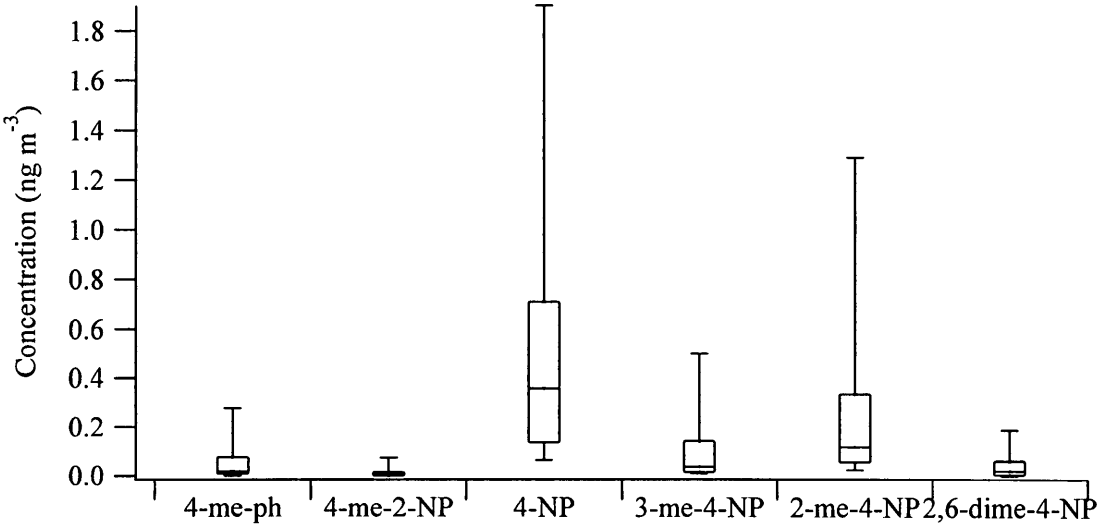

Figure 4.19. Box and whisker plot of concentrations of target phenols in PM2.5; Error bars represent the 90th and 10th percentiles and the upper and lower ends of the box are the 75th and 25th percentiles. The horizontal line represents the median.

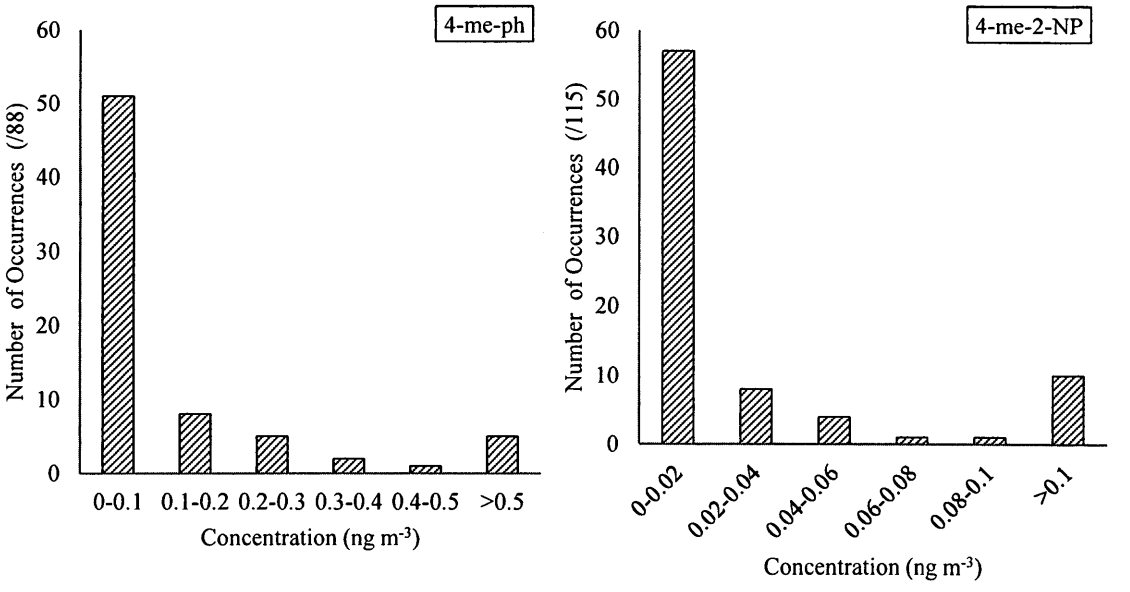

Figure 4.20. Frequency distribution of phenols found in PM2.5.

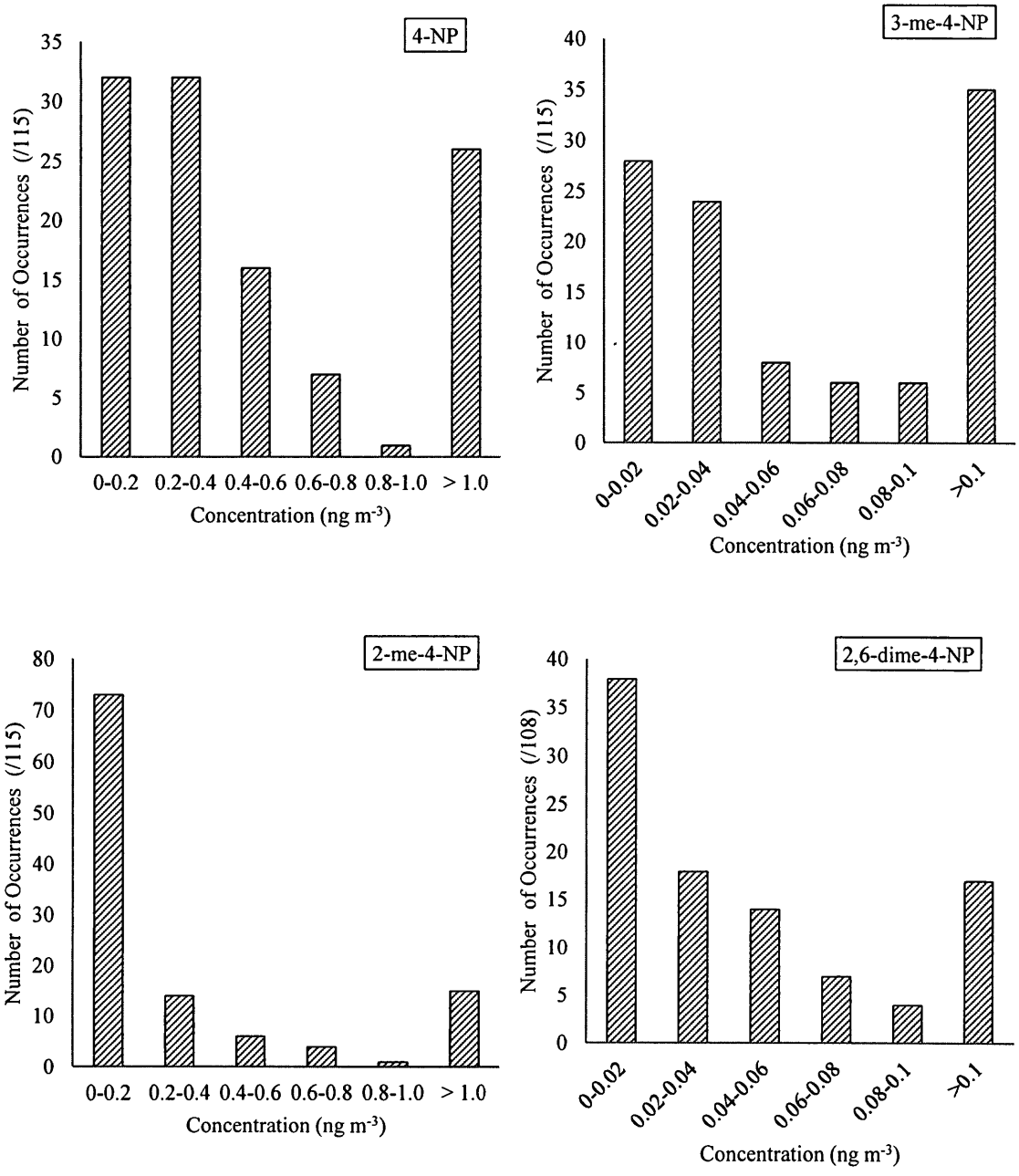

Figure 4.20 (cont'd). Frequency distribution of phenols found in PM2.5.

4.3.1.2. Concentration Measurements of Phenols in the Gas Phase and PM2.5

Table 4.22. Summary of concentration measurements of phenols found in the gas phase and PM2.5 sampled on XAD-coated filters. The sampling period was from February 2011 to August 2012.

Compound	Number of Samples Found On[a]	Concentration (ng m^{-3})				
		Average	Error of the Mean	Median	Max	Min
4-me-ph	11/12	2.59	0.78	2.44	9.01	<DL
4-me-2-NP	29/37	2.78	0.89	0.90	18.85	<DL
4-NP	37/37	6.88	1.10	4.10	18.57	0.61
3-me-4-NP	37/37	1.09	0.23	0.65	4.32	0.11
2-me-4-NP	37/37	3.22	0.46	2.86	8.51	0.19
2,6-dime-4-NP	37/37	1.06	0.22	0.86	5.44	0.05

[a] Concentrations that were >DL

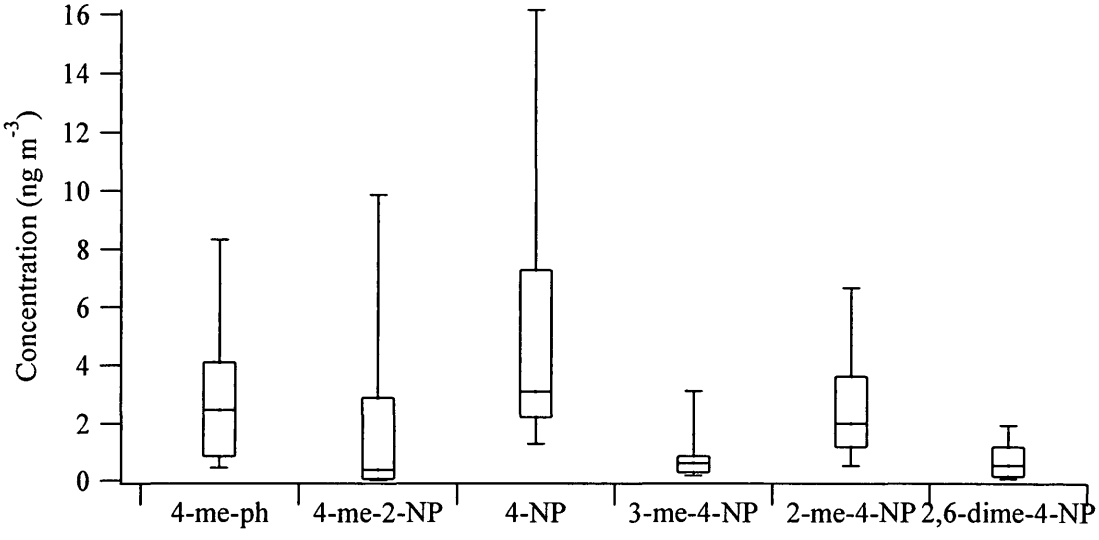

Figure 4.21. Box and whisker plot of concentrations of target phenols in gas phase and PM2.5; Error bars represent the 90th and 10th percentiles and the upper and lower ends of the box are the 75th and 25th percentiles. The horizontal line represents the median.

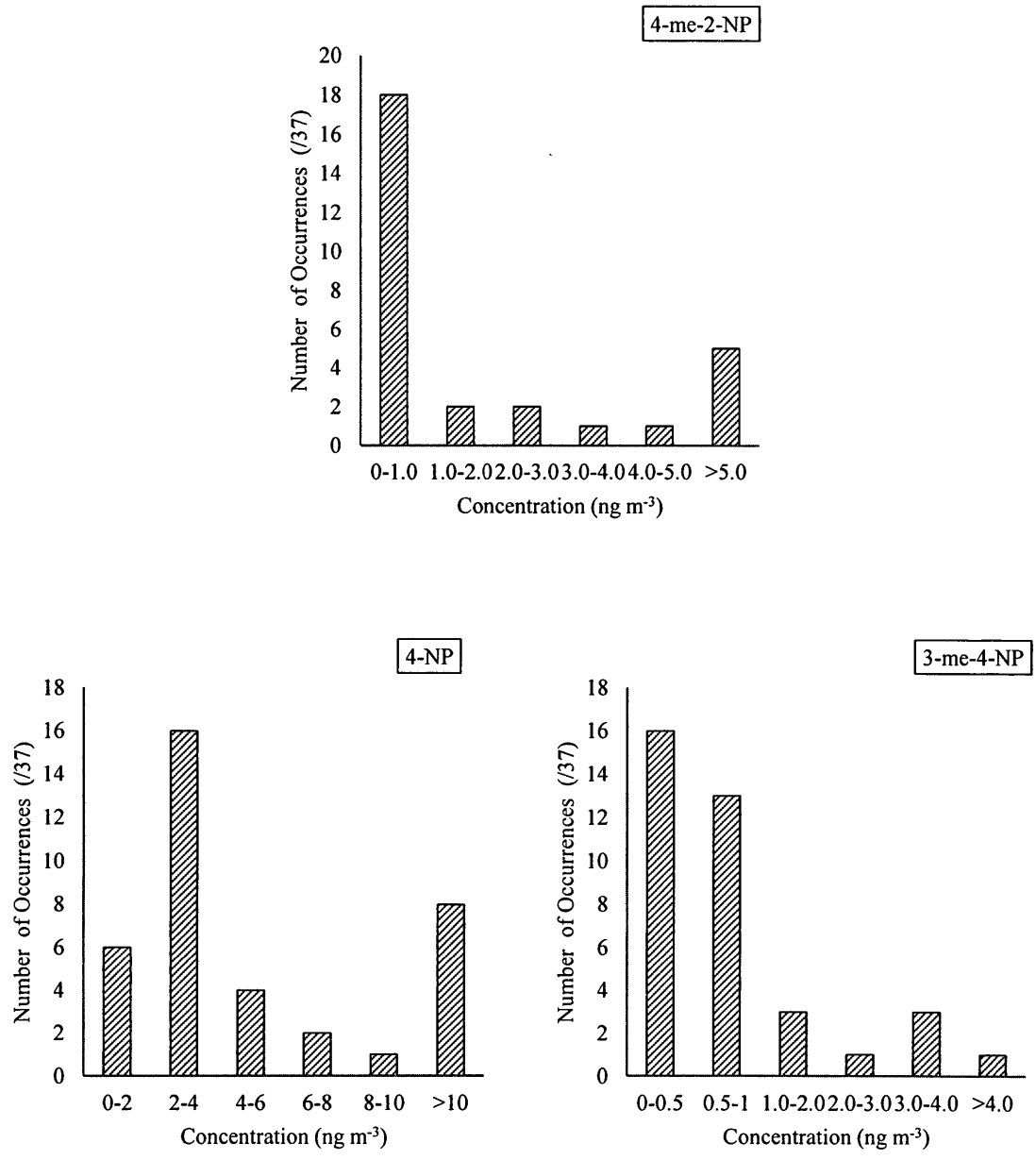

Figure 4.22. Frequency distribution of phenols found in gas phase and PM2.5. 4-me-ph was not shown due to the low number of available data.

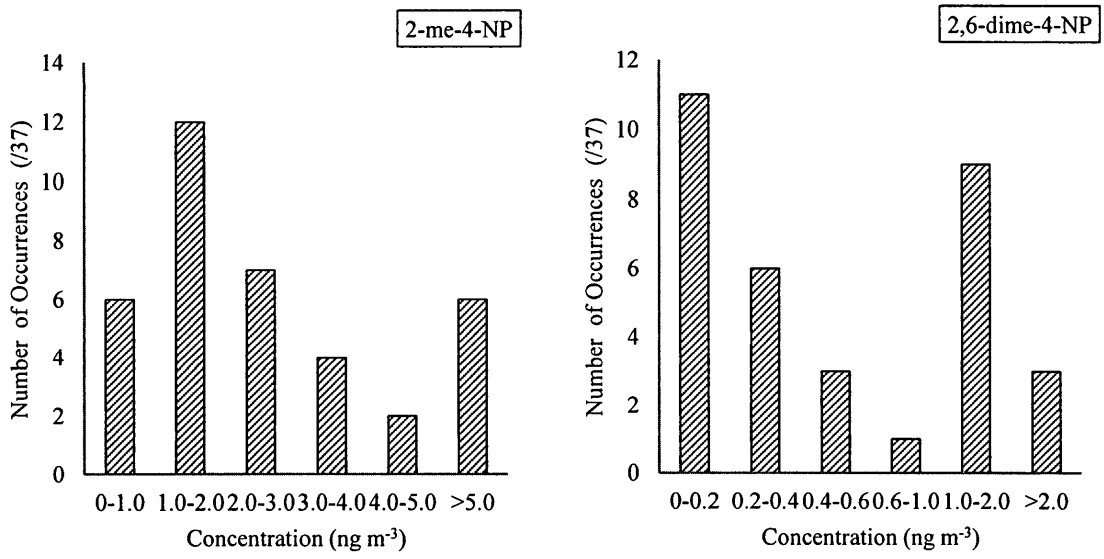

Figure 4.22 (cont'd). Frequency distribution of phenols found in gas phase and PM2.5.

4.3.1.3. Ambient Sampling Tests

Results from sampling air with quartz filters and XAD-coated filters in series and parallel are presented in Fig. 4.23 and results from sampling during the day (8 am to 8 pm) and the night (8 pm to 8 am) are shown in Fig. 4.24.

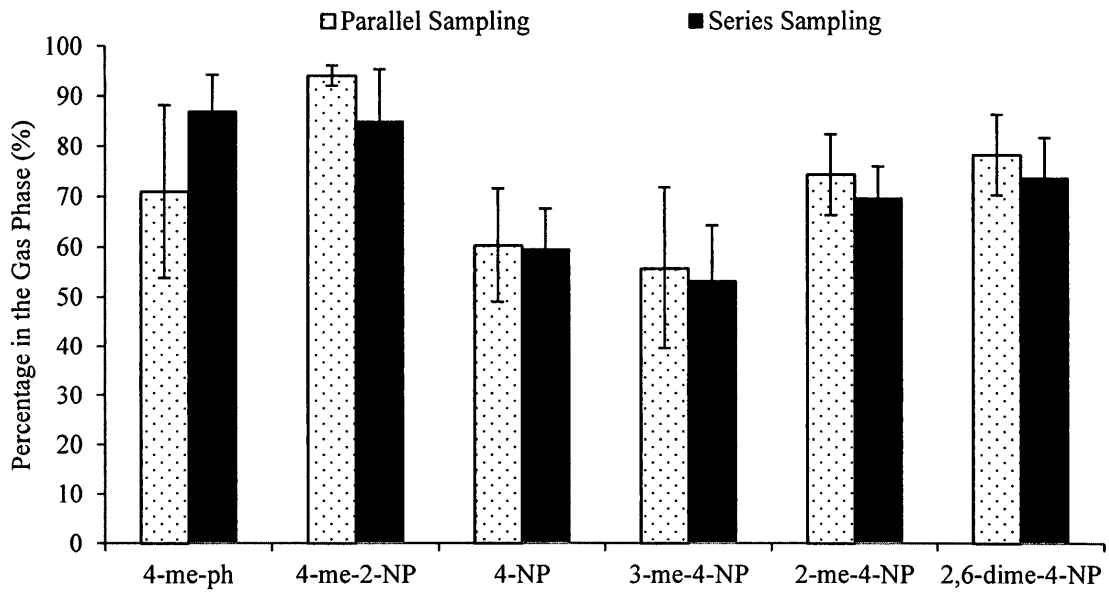

Figure 4.23. Partitioning of nitrophenols in ambient air. Parallel sampling included sampling PM2.5 and gas phase and PM2.5 in parallel and sampling in series included placing a quartz filter over an XAD-coated filter with mesh in between. The error bars represent the error of the mean.

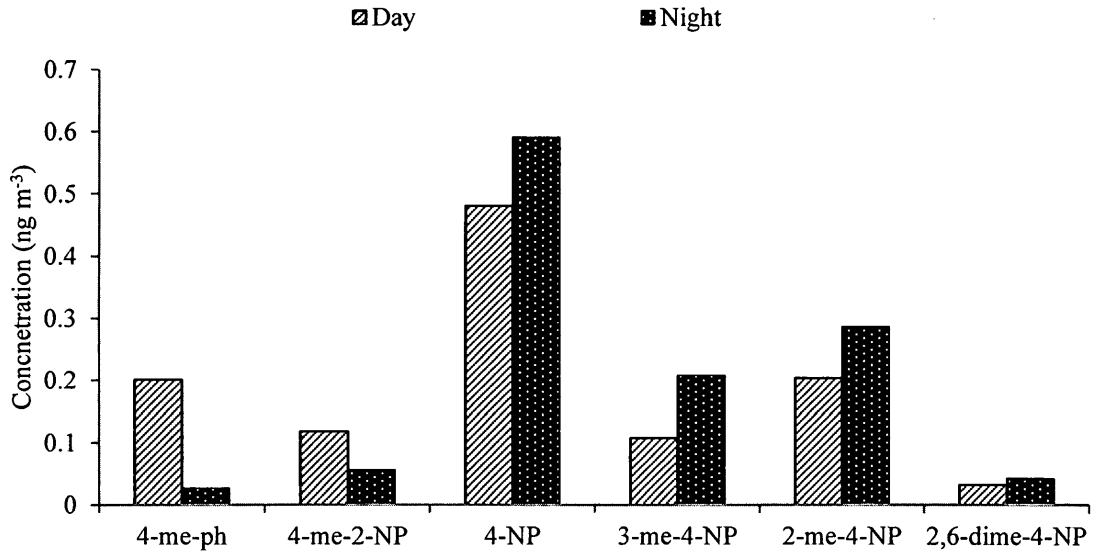

Figure 4.24. Diurnal measurements of ambient phenols in PM2.5. Sampling was done from October 13, 2009 to October 15, 2009 and the sampling period was approximately 12 hours.

4.3.2. Stable Carbon Isotope Ratio Measurements

The following section summarizes isotope ratio measurements of target compounds in PM2.5 alone (Section 4.3.2.1) and in the gas phase and PM together (Section 4.3.2.2). Statistical summaries, box and whisker plots and frequency distributions are shown.

4.3.2.1. Stable Carbon Isotope Ratio Measurements of Phenols in PM2.5

Table 4.23. Summary of isotope ratio measurements of phenols found in PM2.5 sampled on quartz filters. The sampling period was from March 2009 to August 2012.

Compound	Number of Measurements	Isotope Ratio (‰)				
		Average	Error of the Mean	Median	Max	Min
4-me-2-NP	4	-33.8	0.5	-33.8	-32.8	-34.7
4-NP	30	-33.5	0.3	-33.7	-30.4	-36.4
3-me-4-NP	25	-33.0	0.4	-32.5	-28.4	-36.2
2-me-4-NP	38	-33.2	0.3	-33.5	-28.4	-36.0
2,6-dime-4-NP	7	-34.1	0.7	-34.9	-30.6	-35.9

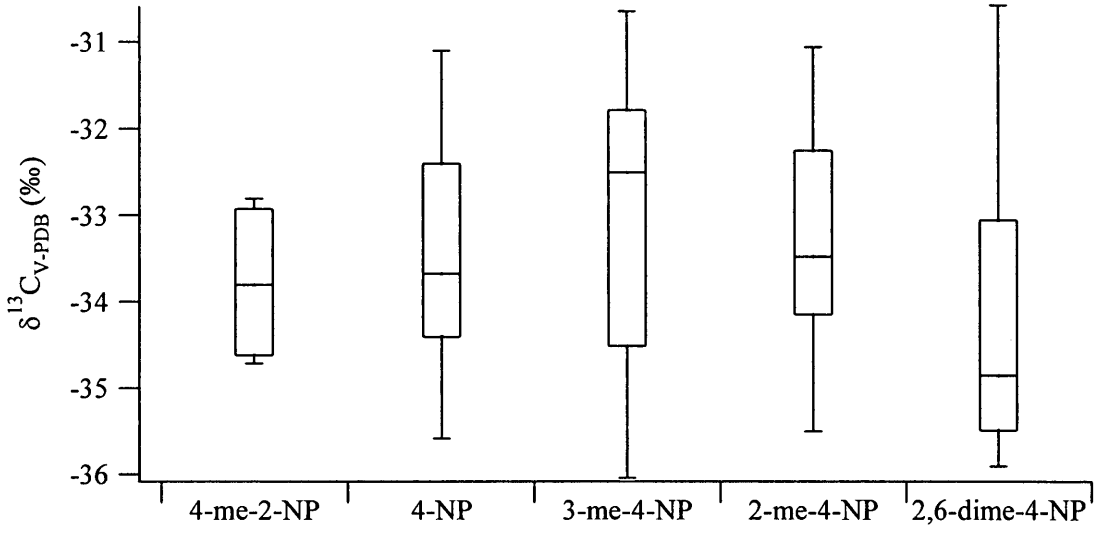

Figure 4.25. Box and whisker plot of stable carbon isotope ratios of target phenols in PM2.5; Error bars represent the 90th and 10th percentiles and the upper and lower ends of the box are the 75th and 25th percentiles. The horizontal line represents the median.

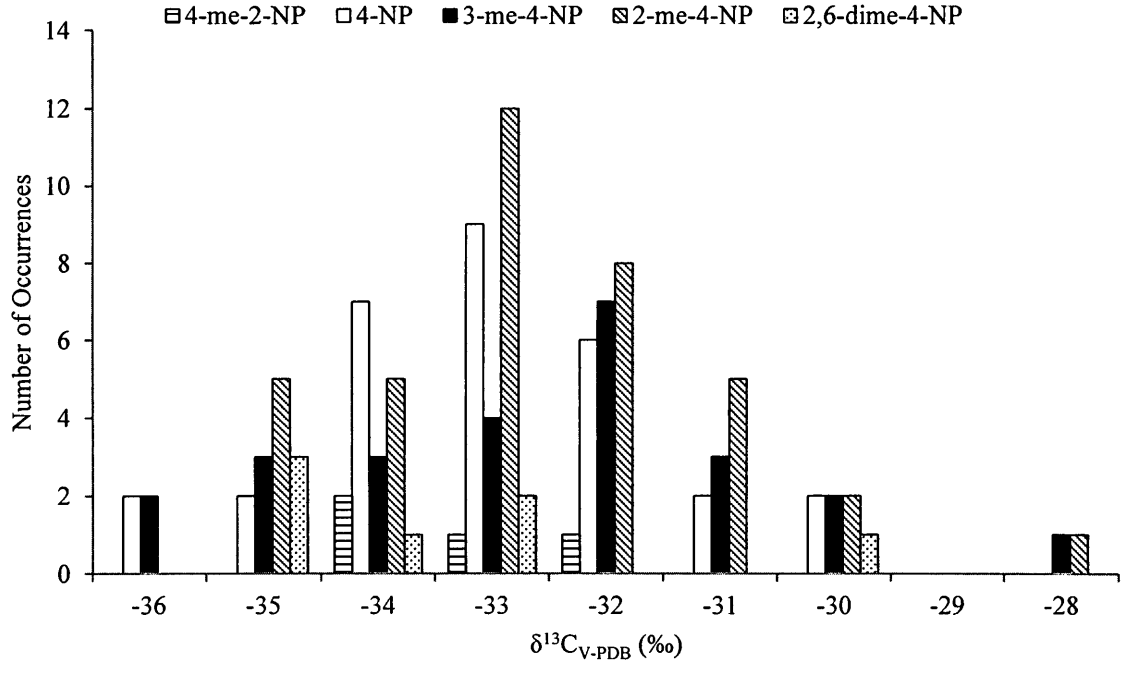

Figure 4.26. Frequency distribution of stable carbon isotope ratios of phenols in PM2.5.

4.3.2.2. Stable Carbon Isotope Ratio Measurements of Phenols in Gas Phase and PM2.5

Table 4.24. Summary of isotope ratio measurements of phenols found in gas phase and PM2.5 sampled on quartz filters. The sampling period was from March 2009 to August 2012.

Compound	Number of Measurements	Isotope Ratio (‰)				
		Average	Error of the Mean	Median	Max	Min
4-me-2-NP	12	-32.8	0.4	-33.2	-30.7	-34.6
4-NP	28	-33.5	0.3	-33.4	-30.7	-36.4
3-me-4-NP	19	-33.1	0.3	-33.1	-30.0	-35.5
2-me-4-NP	30	-32.7	0.3	-32.8	-30.2	-35.5
2,6-dime-4-NP	15	-33.4	0.5	-33.3	-29.4	-37.0

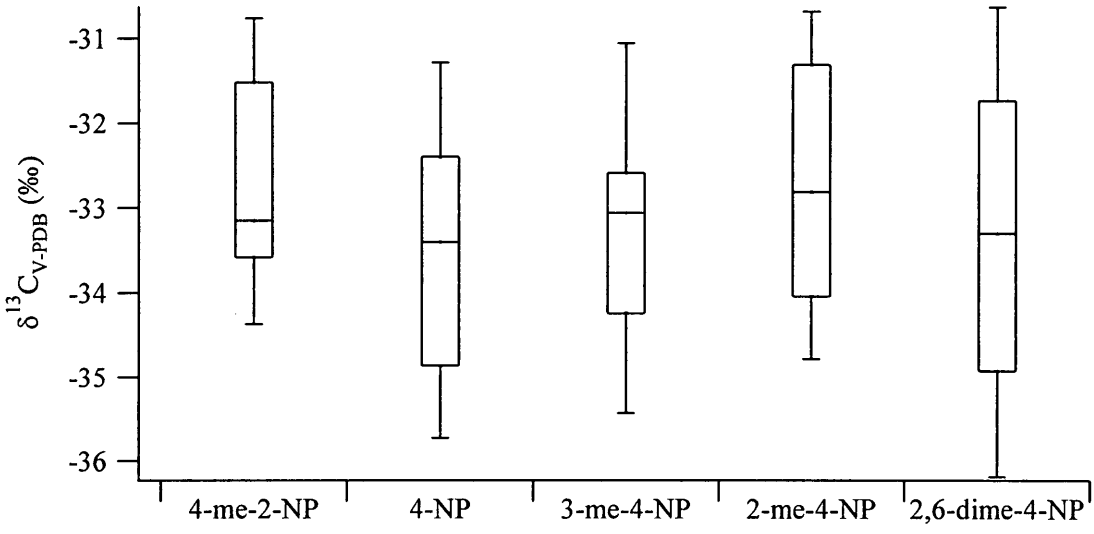

Figure 4.27. Box and whisker plot of stable carbon isotope ratios of target phenols in gas phase and PM2.5; Error bars represent the 90th and 10th percentiles and the upper and lower ends of the box are the 75th and 25th percentiles. The horizontal line represents the median.

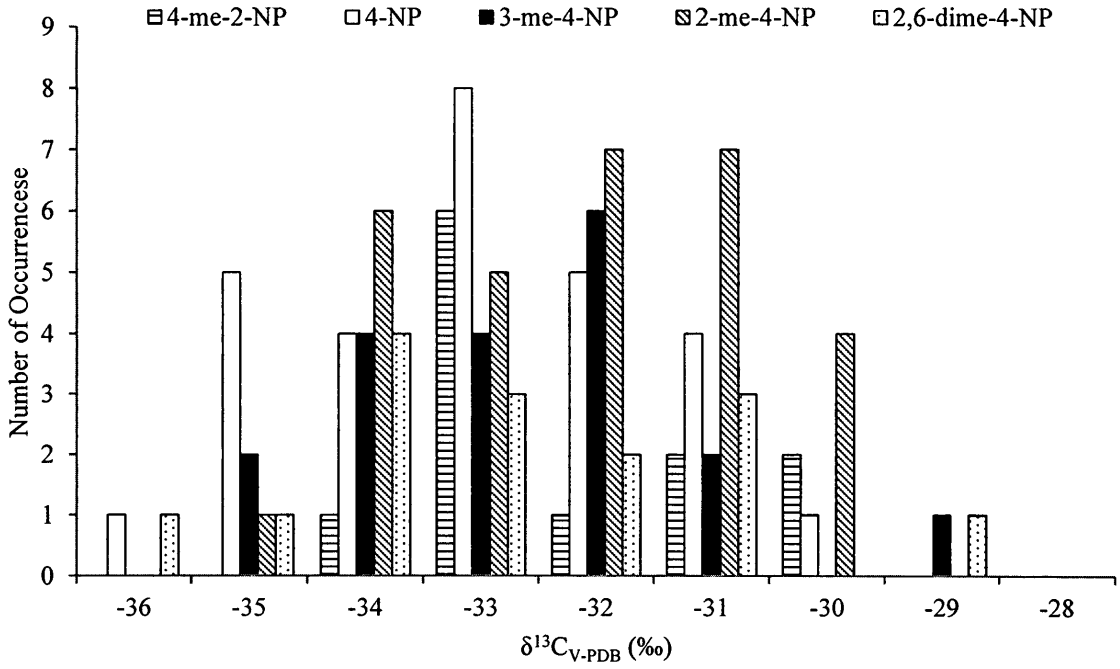

Figure 4.28. Frequency distribution of stable carbon isotope ratios of phenols in gas phase and PM2.5.

5. Discussion

5.1. Performance Criteria

5.1.1. Precision and Accuracy

The overall performance of the complete method is dependent on detection limits, precision and accuracy (Table 5.1). Typically, for most environmental analytical methods, a precision of less than 5 % is acceptable. For concentration measurements, the precision was determined by using data obtained from runs that were performed in duplicate (Table 4.16). The relative precision of the method used for concentration

measurements using GC-MS was less than 5 % for most compounds, indicating that running samples in duplicate is sufficient to acquire a precise measurement.

Table 5.1. Performance summary of the complete extraction and analysis method.

Compound	GC-MS Precision[a] (%)	GC-IRMS Precision (‰)	Method DL for Quartz filters (ng m^{-3})	Method DL for XAD-coated filters (ng m^{-3})
4-me-ph	5.3	NA	0.002	0.005
4-me-2-NP	4.9	0.31	0.001	0.003
4-NP	3.9	0.27	0.020	0.009
3-me-4-NP	4.1	0.30	0.001	0.003
2-me-4-NP	3.3	0.26	0.002	0.001
2,6-dime-4-NP	4.1	0.31	0.0004	0.002

[a] Average precision relative to two internal standards

Table 5.2. Averages, standard deviations and 95 % confidence intervals for filters run in quadruplicate.

Compound	X011111A-TOP		X041111A-TOP	
	Average ± SD (‰)	95 % Confidence Level (‰)	Average ± SD (‰)	95 % Confidence Level (‰)
4-NP	-35.3 ± 0.2	0.3	-31.3 ± 0.2	0.3
2-me-3-NP	-26.9 ± 0.4	0.6	-26.6 ± 0.3	0.6
2-me-5-NP	-27.0 ± 0.2	0.3	-27.4 ± 0.2	0.3
2-me-4-NP	-30.6 ± 0.3	0.5	-31.2 ± 0.2	0.3
2,6-dime-4-NP	-34.9 ± 0.4	0.6	NA	NA

The GC-IRMS isotope ratio measurements had significantly higher precision and were approximately a hundred times as precise as the GC-MS, with a precision of 0.3 ‰. Two ambient filters were analyzed in quadruplicate to further validate the use of duplicate measurements (Table 4.18). The standard deviation for each quantifiable

compound that had a mass of more than 3 ng per 3 μL injection was less than 0.5 ‰, a value that is acceptable for continuous flow GC-IRMS measurements. This was important since the analysis of a sample in quadruplicate would take an entire day due to the lengthy temperature program. It was confirmed that for most compounds, the isotope ratio did lie within 0.5 ‰ of the average value with 95 % certainty (Table 5.2). Other studies using continuous flow GC-IRMS for atmospheric measurements have a similar precision for their compounds of interest (Rudolph et al., 2000; Rice et al., 2001, Czapiewski et al., 2002; Rudolph et al., 2002; Saito et al., 2002; Rudolph et al., 2003; Kornilova, 2012). The precision for offline measurements, which essentially is the IRMS alone, was found to be within 0.2 ‰ (Table 4.19). The variation observed in the isotopic composition between different tubes of combusted 4-nitrophenol may have arisen from difficulties encountered during the extraction procedure using the extraction line. If there was a minor leak in the extraction line, change in isotope ratios due to contamination by atmospheric carbon dioxide could occur.

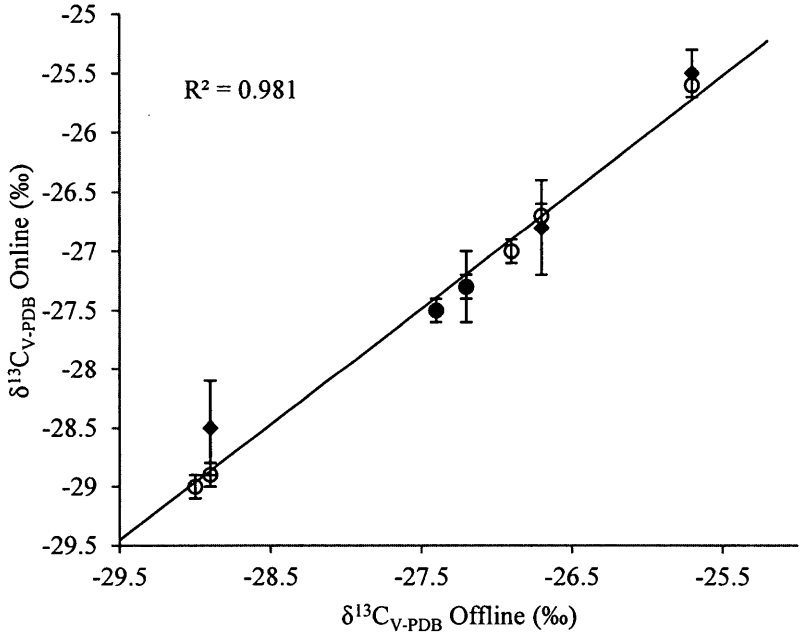

Figure 5.1. Comparison of stable carbon isotope ratios of nitrophenols determined by online and offline methods. The open circles are online values determined from calibration mixtures and the black diamonds are online values determined from spiked filters. The solid line is the line representing the least squares fit. The isotope ratios for 4-methyl-2-nitrophenol and 2,6-dimethyl-4-nitrophenol could not be quantified from the spiked filter. The equation of the line is: $^{13}C_{V\text{-}PDB}$ Online = $\delta^{13}C_{V\text{-}PDB}$ Offline x (0.982 ± 0.045) – (0.50 ± 1.1) ‰.

The accuracy of ambient concentration and isotope ratio measurements could not be determined directly since their values are not known in the atmosphere. However, for GC-IRMS, the accuracy of the measurement was found through the comparison of the isotope composition of standards from offline and online values. Online values determined by two different types of tests were compared to offline values in order to isolate if fractionation was occurring during the analysis procedure, which included injection, separation and combustion or if fractionation was occurring in the extraction

procedure or during storage. The averages from both online methods differed at most by 0.4 ‰ from the offline values and were often within 0.1 ‰ to 0.2 ‰. Figure 5.1 shows the agreement between the offline and online measurements. The intercept of the line is slightly less than -0.5 ‰ with an uncertainty of ±1.1 ‰. When online values are predicted through statistics from a 1:1 line, the average difference between offline and online values was 0.1 ‰. This indicates that there is no significant bias in the measurement and that any bias that may occur is within the uncertainty of the method and that there is no detectable fractionation in the extraction, storage, derivatization, injection, separation or combustion procedure.

Table 5.3. $\delta^{13}C_{TMS}$ ± the standard deviation determined from derivatized nitrophenols with the inclusion of all compounds and exclusion of 4-methyl-2-nitrophenol and/or 4-nitrophenol. The isotope ratio of the TMS group of BSTFA determined by Moukhtar et al. (2011) and Irei et al. (2013) is also shown for comparison.

	$\delta^{13}C_{TMS}$ (‰)
Inclusion of All Compounds	-47.9 ± 0.7
Exclusion of 4-me-2-NP	-47.7 ± 0.5
Exclusion of 4-NP	-48.1 ± 0.4
Exclusion of 4-me-2-NP and 4-NP	-48.0 ± 0.1
Moukhtar et al. (2011)	-45.31 ± 0.51
Irei et al. (2013)	-49.94 ± 0.33

In this research, accurate knowledge of the isotope ratio of the TMS group, which is added to the target compounds through derivatization, is critical. Independent of the target compound that is analyzed, the derived isotope ratio of the TMS group should be identical. It is shown that from Fig. 4.17, the derived isotope ratio is relatively constant for each compound. The points that vary the most from the average in this figure are 4-methyl-2-nitrophenol and 4-nitrophenol. The isotope ratio of the TMS group was found

with the inclusion and exclusion of these values (Table 5.3). It was decided to use the isotope ratio of -48.0 ‰ for the TMS group for two reasons. The first being that 4-methyl-2-nitrophenol often had small concentrations in standard mixtures and due to the temperature program, resulted in a broad peak that had higher uncertainties when integrated. Furthermore, the isotope ratio of 4-nitrophenol as determined from offline measurements had a relatively high uncertainty, which can propagate when determining the isotope ratio of the TMS group. Nevertheless, the difference in isotope ratios determined from different subsets did not differ significantly and are within the uncertainty of the measurement. The isotope ratios of the TMS group determined by Moukhtar et al. (2011) and Irei et al. (2013) are also shown in Table 5.3 for comparison. The delta value of the TMS group in this work is similar but not completely identical to these values. The differences observed are most likely due to using a different batch and supplier of BSTFA.

Depending on the accuracy of the $\delta^{13}C_{TMS}$, the correction of the isotope ratio for the addition of a TMS group to the target compounds can create a systematic bias to the measured isotope ratios of target compounds. Based on the low uncertainty of the $\delta^{13}C_{TMS}$, this effect is assumed to be minimal. Equation 3.6 is used to calculate the isotope ratio of the TMS group, taking into account the isotope ratio of derivatized standards with known delta values. The equation is then rearranged once the TMS delta value is known and if the TMS group is biased by 0.3 ‰, for example, the isotope ratios of the target compounds will in turn be biased by approximately 0.1 ‰, which is within

the uncertainty of the measurement. When the isotope ratio of the TMS group is averaged over the seven compounds, the error of the mean is 0.1 ‰.

5.1.2. Linearity

Table 5.4. Mass range used for calibration of the GC-MS and GC-IRMS. The masses given are the masses injected into the GC for analysis.

Compound	Calibration Mass Range (ng)	
	GC-MS	GC-IRMS
2-me-ph	1.3 - 10.4	NA
4-me-ph	1.3 - 10.1	NA
4-me-2-NP	1.7 - 13.3	2.0 - 53.3
4-NP	1.3 - 10.1	1.5 - 40.3
2-me-3-NP	1.3 - 10.3	1.5 - 41.3
2-me-5-NP	1.3 - 10.6	1.6 - 42.5
3-me-4-NP	1.3 - 10.3	1.5 - 41.3
2-me-4-NP	1.4 - 10.8	1.6 - 43.3
2,6-dime-4-NP	1.3 - 10.1	1.5 - 39.4
C17	2.8 - 22.3	2.3 - 45.6
C18	2.9 - 22.9	2.3 - 31.2
C19	2.6 - 20.9	2.1 - 28.5

NA: Data not available

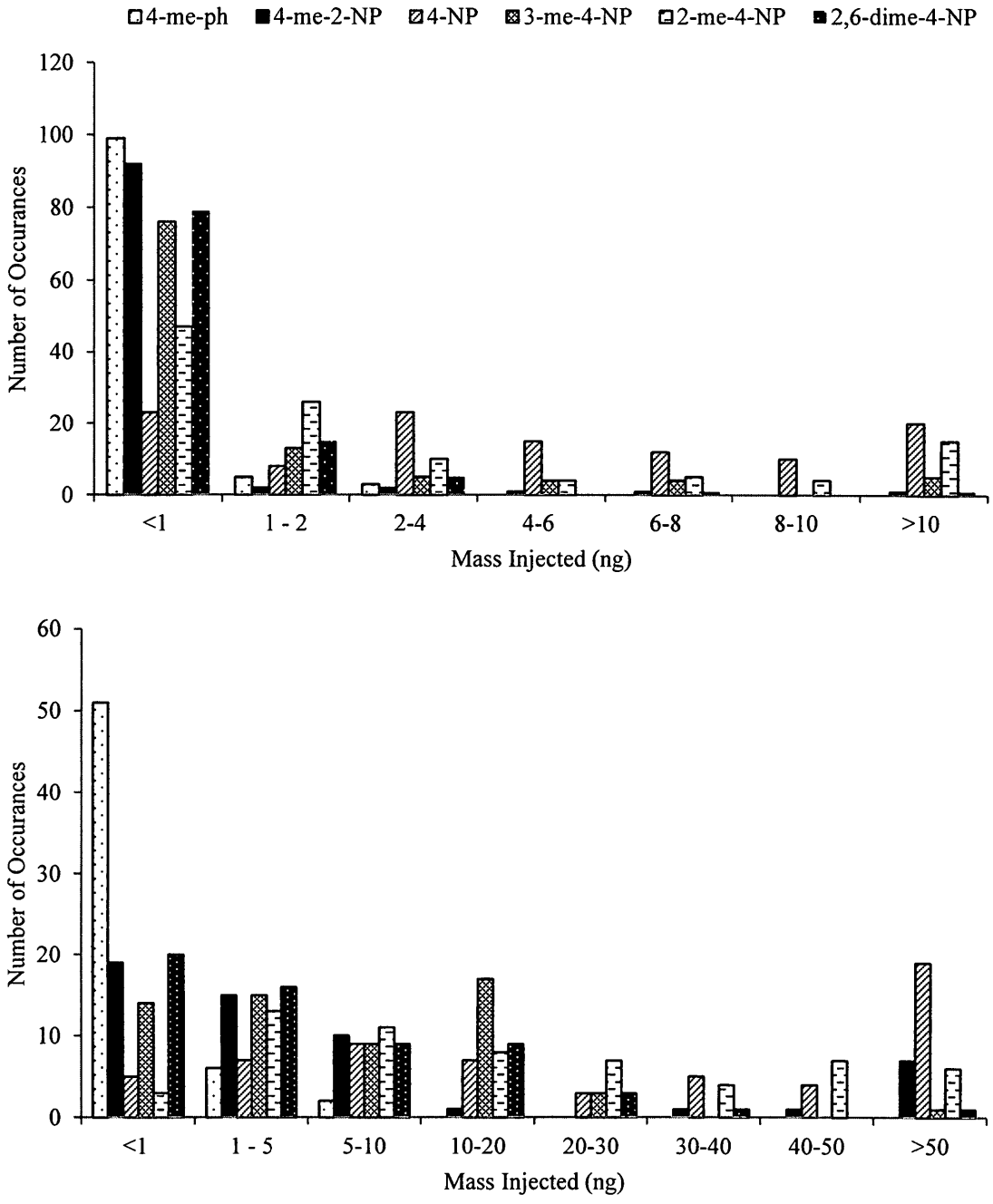

Figure 5.2. Distribution of the masses injected into GC-MS from ambient samples. The top figure represents values from quartz filters and the bottom figure represents values from XAD-coated filters.

The linear regression value (R^2) for the GC-MS was consistently 0.98 to 1 for all compounds. The error of the slope was 3 % for most compounds but was up to 7 % for 4-methyl-2-nitrophenol. The error of the slope was influenced by forcing the intercept through the origin. The percent difference in concentration measurements either including or excluding the intercept was found to be within 10 %. Similar calibration results were observed with the GC-IRMS. The linear regression coefficient (R^2) from calibration curves for each compound was generally between 0.99 and 1. The relative error of the slope was slightly higher for GC-IRMS than for GC-MS but was still less than 10 %. The higher error could have been due to using manual injections for GC-IRMS measurements. Most of the samples that were injected into the GC-MS or GC-IRMS had injection masses that were less than the maximum masses represented in the calibration curve (Table 5.4). Figure 5.2 demonstrates the distribution of masses injected into the GC-MS. The mass range presented represents the masses used in the calibration but is not necessarily representative of the linear range since masses above this were not tested.

5.1.3. Blank Values and Detection Limits

Detection limits for GC-MS instruments, typically determined by the sensitivity of the instrument and detector used, were very low in this method. Normally, the detection limits depend on the ratio of the signal to the size of the statistical fluctuations of the blank signal (Skoog et al., 2007). Typical detection limits for MS that are coupled with GC are from 0.25 pg to 100 pg (Skoog et al., 2007). The detection limits from the GC-MS instrument itself in this research were extremely low. This was because SIM was

used and there was a complete absence of blank peaks in the areas of interest. Detection limits were determined using the fluctuations in the noise of the baseline and were found to be equivalent to a sub nanogram mass on the filter, which is equivalent to less than 10 fg m^{-3} for all target compounds when using standard high volume sampling conditions.

The main contribution to the detection limits observed in this research was introduced from blank values present on the quartz filters themselves as well as the XAD adsorbent (Table 5.1). Quartz filters are made of high purity quartz fibers that are tightly woven to form a thin mat (Watson and Chow, 2001). These filters have been known to adsorb hydrocarbon gases and have contaminations from aluminum and silicon (Chow, 1995). Although quartz filters were baked prior to sampling or coating to remove organic contaminants, their blank values may still be affected due to storage prior to and following sampling. Blank values for quartz filters were generally in the low nanogram range for most of the compounds (Table 4.6). The highest blank observed was for 4-nitrophenol. Initially, the blank for 4-nitrophenol was low but in recent tests has increased due to an unknown contaminant in the laboratory. Nevertheless, 4-nitrophenol is the target compound that has the highest observed ambient concentrations and is therefore least affected by the blank. When the blank values are converted to atmospheric concentrations based on typical three day sampling, blank values are in the sub pg m^{-3} range for most target compounds and in the sub ng m^{-3} range for 4-nitrophenol.

It was more concerning to determine blank values for XAD-coated filters since an adsorbent was introduced to the filter media. When received from the supplier, XAD is wetted in a mixture of water, sodium chloride and sodium carbonate to limit bacterial

growth (Sigma-Aldrich Co., 1998). It was found that without cleaning, XAD-4^{TM} has significant amounts of organic contaminants (Hunt and Pangaro, 1982). Since then, it has been customary to clean the XAD in a variety of solvents, as described in Section 3.2.1. Blank values for XAD-coated filters were found to be higher than blank values from uncoated filters but were in the same order of magnitude (Table 4.7). Blank values were in the pg m^{-3} range, which is well below the range of most of the target compounds in the atmosphere, especially when sampling gas phase and PM together. The detection limits based on mass collected on the filters are slightly higher than those found by Cecinato et al. (2005), which was approximately 0.5 ng for each target phenol on a Teflon filter. However, with a sampling flow rate of 5 L min^{-1} and a sampling time of six hours, this corresponds to an atmospheric detection limit of 0.28 ng m^{-3}, which is significantly higher than the atmospheric detection limits achieved in this work, which correspond to an average detection limit of approximately 0.02 ng m^{-3} for a six hour sampling period.

To detect possible blank contributions from the GC column, combustion furnace or capillaries in the GC-IRMS system, pure acetonitrile was injected. Figure 4.4 confirms that there is no interference for the target phenols. The wide feature towards the end of the chromatogram is due to column bleed caused by the increased ramping of column temperature. When using IRMS to determine isotope ratios, the limit of detection is determined by the desired accuracy and precision of the measurements and not by the smallest mass that can be detected. As the mass of the specific compound decreases, the accuracy and precision both degrade. In this research, determining the minimum mass needed to achieve a both accurate and precise measurement was essential since when

analyzing PM samples especially, concentrations were typically very low. Targeting a very good precision therefore may result in having a very small data set but at the same time, being too generous with the precision will give a large data set with high uncertainties, which will be difficult to interpret. Figure 5.3 shows that by using counting statistics, as the mass injected increases, the standard deviation lessens. It was finally determined that the minimum mass injected should be 3 ng. However, since a 1 μL injection would heavily reduce the number of useful measurements since most samples have less than 3 ng μL^{-1}, it was decided to use 3 μL injections, which would be suitable for samples with a minimum concentration of 1 ng μL^{-1}. There were certain occasions in which the concentrations analyzed were lower than this specification. The consequence was that the target value of the precision of the measurement would be compromised but as shown in Fig. 4.18, even with a 1.7 ng injection, which is equivalent to 0.6 ng μL^{-1}, the precision remained within 0.5 ‰ and had an average online value that differed by only 0.1 ‰ from the offline value.

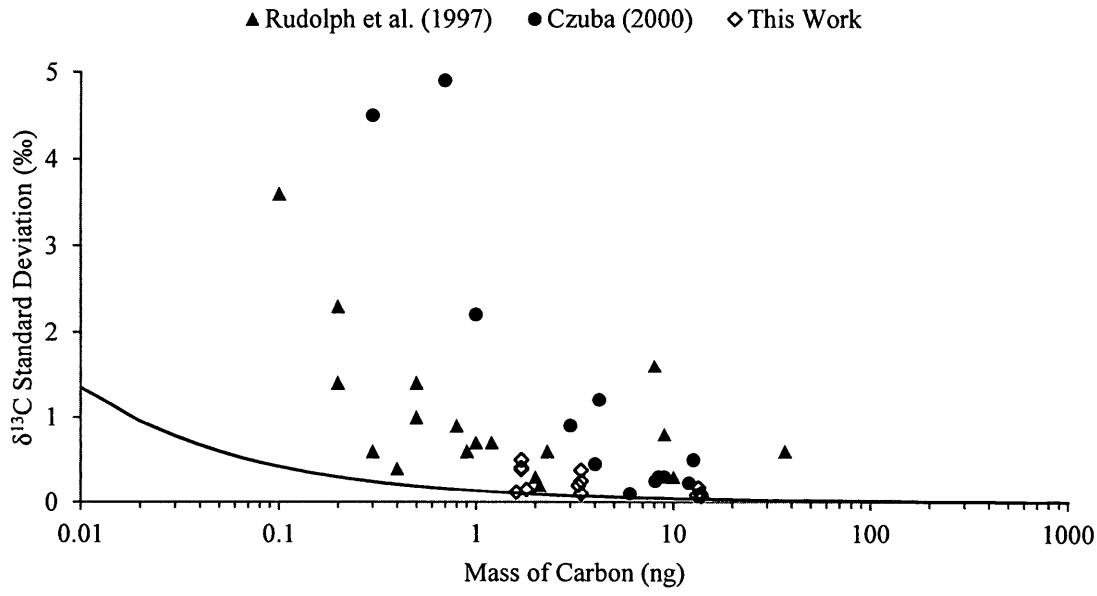

Figure 5.3. Dependence of the standard deviation of isotope ratio on the mass of carbon injected. The solid line represents the standard deviation determined by counting statistics, with 1 in every 2000 ions being detected and 20 % of the mass injected making it to the detector.

5.1.4. Artifacts

An unknown contaminant, present in all samples, began to evolve and intensify in 2010. The contaminant, once evolved, was confirmed to be present in all previous samples as it shared the same mass spectrum (Fig. 4.9). The contaminant had a significant adverse effect on the GC and MS due to its enormous concentration. The sensitivity of the MS also decreased rapidly. It was not unusual for peaks to decrease to 10 % of its size for repeat runs when the contamination was at its worst (Fig. 4.10). This required the ion source in the MS to be cleaned biweekly and for filaments to be replaced more frequently. Each time the ion source was cleaned, the system needed to be

recalibrated, which cost approximately three to four days of lab time. The contamination continuously overshot in each chromatogram and had a peak width in the order of minutes that would increase with each injection (Fig. 4.11). The size of the contaminant also degraded the electron multiplier horn, which is a costly component of the MS. Furthermore, the GC column was damaged and peak shapes began to deteriorate.

There was difficulty in assigning the source of the contaminant due to its unusual and inconsistent behavior. Due to the extensive extraction procedure and multiple instruments used, there were several possible sources. Table 4.10 describes tests that were conducted to aid the discovery of the source. The extraction solvent, acetonitrile, was found to ultimately be the contaminant source but a detectable contaminant was found to only be present when the samples were derivatized with BSTFA. This was perhaps the worst possible scenario since replacing the extraction solvent would require plenty of time and effort, given that the method had already been established.

It was first thought to use a solvent of higher purity, but the acetonitrile used was already of 99.9 % purity, according to the manufacturer, Sigma-Aldrich. Prior to the contaminant becoming problematic, a global acetonitrile shortage occurred. This happened because one of the main acetonitrile producers in the world in China was shutdown prior to the 2008 Olympics in an effort to improve local air quality. Furthermore, production in the United States slowed down due to damage from Hurricane Ike. At the same time, the world was going through an economic crisis. This acerbated the shortage since acetonitrile is a byproduct of acrylonitrile that is used in

fabrics. It is thought that a contamination was introduced into the acetonitrile once production was revived.

It was suggested by the supplier to substitute the currently used acetonitrile Chromasolv®, which was produced in the United States of America, with acetonitrile Pestanal®, which was produced in Germany. Upon arrival, the Pestanal® appeared to not have the contaminant, but with time, it began to appear. Tests conducted upon the new solvent were often inconclusive and exhibited strange results. It was found that the contamination decreased when exposed to light and air (Fig. 4.12). This was not an ideal solution since the contamination was still of considerable size and impacted results.

It was ultimately found that the contaminant was a function of pH. As described in Section 3.4.4, the solution prior to SPE is acidified to a pH of 2. It was found that increasing the pH to 5 rather than 2 substantially decreased the size and impact of the contaminant (Fig. 4.13). It was determined that to minimize the size of the contaminant, the solvent would be permanently substituted with acetonitrile Pestanal® and the solution would be acidified to pH 5 (Table 4.11). Following these modifications, the HPLC column, GC column and quadrupole from the MS needed to be replaced due to the extent of damage from the contaminant. It is not yet known why the contaminant behaved the way it did. Information gathered from results indicates that there is a hydroxyl group present, since it was derivatized with BSTFA and that its formation is pH dependent.

5.2. Method Validation and Characterization

The recoveries of the internal standards were mainly used for diagnostic testing of the extraction procedure and analysis. Initially, the recoveries were used to evaluate concentration measurements, but this increased the uncertainty in the measurements. The recoveries of the compounds were generally low due to the extensive extraction procedure and several steps with possibilities for losses. Recoveries of phenols from quartz filters were generally less than recoveries from XAD-coated filters (Table 4.12). This occurred because of possible loss of sample during injection for the HPLC clean-up step, a problem with the HPLC that was resolved for most XAD-coated filter samples.

The recoveries relative to the internal standard were expected to be one, and for most of the phenols, were generally close to one within the standard deviation of the measurements (Table 4.12). The exception was for 4-methyl-2-nitrophenol, which had a low recovery relative to the internal standard when spiked on both quartz and XAD-coated filters. This could be due to its relatively high vapour pressure and the likelihood of existing mainly in the gas phase (Section 2.7). It is thought that the main loss for 4-methyl-2-nitrophenol could be during the rotary evaporation or the nitrogen blow-down. A possible solution could have been to use a more appropriate internal standard. However, a deuterated version of the compound was not available commercially and would not be suitable for isotope ratio analysis due to the strong possibility that it would not be completely separated from the target compound.

The two internal standards chosen for this research were 2-methyl-3-nitrophenol and 2-methyl-5-nitrophenol. These were chosen due to not being present in the

atmosphere in detectable quantities and that they should theoretically behave similarly to the target compounds since they are isomers (Moukhtar et al., 2011). Generally, the average of the concentration using each internal standard was used to calculate final concentrations. Results shown in Fig. 4.14 validate this procedure. The internal standards should behave similarly to each other and other target compounds in the sample. The recoveries shown in Fig. 4.14 are for all samples and have a linear regression value of 0.95 and 0.96 for quartz filters and XAD-coated filters, respectively. The recoveries shown in this figure are sometimes larger than 100 % due to changes in sensitivity of the instrument. Since derivatized and polluted samples were injected into the GC-MS, the ion source degraded over time. When this occurred, the volumes predicted using volumetric standards would increase drastically due to having a smaller peak. With this seemingly larger volume, that is used to correct the internal standard, the recovery is amplified to values that are greater than 100 %. The recoveries found were used to diagnose changes in the MS sensitivity and differences between both internal standard recoveries. The direct comparison of signals for target substances and internal standards, which was used to determine ambient concentrations, avoids problems resulting from changes in the instrument's sensitivity as long as the change is identical for all measured compounds. This was indeed found to be the case since the average standard deviation of the signal relative to the internal standards was consistent within 5 % (Table 4.16).

There was concern that there could have been losses during the storage of the filters between sampling and extraction. To determine if these losses were occurring, filters that were spiked and stored for six months prior to extraction were compared with

filters that were extracted immediately after spiking (Table 4.13 and Fig. 5.4). As shown in Fig. 5.4, there are no significant losses due to storage, and recoveries are very similar. This was therefore validated that storing the filters in the freezer had no significant losses, except for 2-methyl phenol.

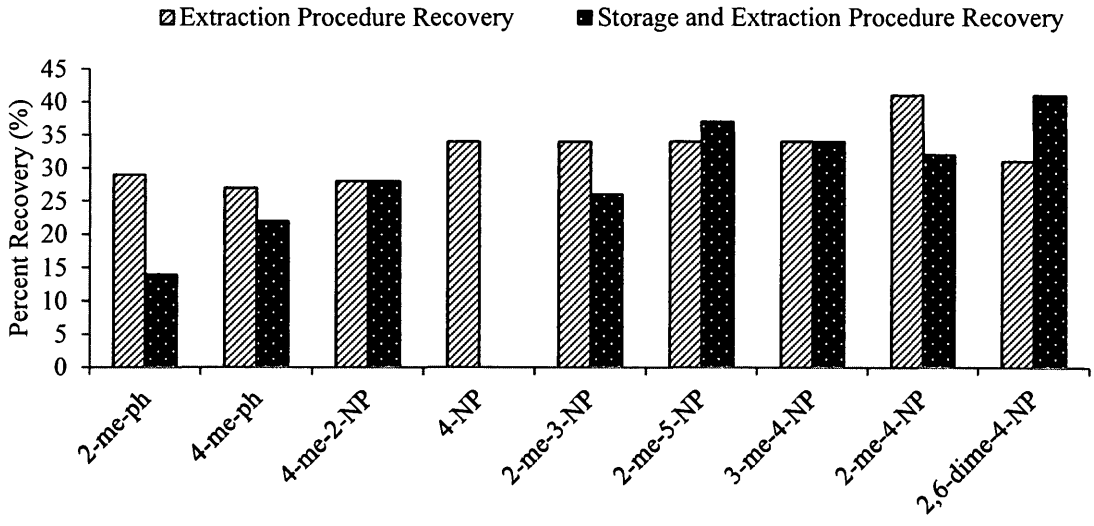

Figure 5.4. Comparison of recoveries from filters that immediately underwent the extraction procedure after spiking and for filters that were spiked, stored for six months and extracted. 4-nitrophenol was not spiked on the filters for storage tests since it was not a target compound at the time.

5.3. Sampling

PM2.5 sampling by high volume air samplers has long been used as a conventional sampling method for ambient air collection. This was chosen as the sampling method for this work due to the goal of conducting isotope ratio measurements of SOA. Given the low concentrations of specific products of the atmospheric oxidation of aromatic VOC found in SOA, a significant air volume was required to be collected.

High volume air samplers, at a standard flow rate of 1.13 m^3 min^{-1}, can sample upwards of 1600 m^3 of air for 24 hour sampling and close to 5000 m^3 of air for three day sampling.

One of the caveats of using the air samplers available at York University was that only motors that used carbon brushes could fit in the sampler housing. This meant that the brushes periodically needed to be replaced. On each occasion, the air samplers were recalibrated. There were two events in which air samplers were calibrated at three instances without the brushes needing to be replaced. Results from these calibrations were compared to establish the extent of drift in air sampler flow rate between calibrations. Results from the calibrations indicated that the flow rate of the samplers were quite stable and drifted at most by 7 % (Table 4.1).

5.3.1. Parallel Sampling

Two air samplers were available for sampling and were quite useful when validating the method. Parallel sampling tests using both quartz and XAD-coated filters were combined in Fig. 4.1 to illustrate the differences between the two air samplers. The differences observed were most likely due to differences in sampling volume; however, if this was the only possible reason for the discrepancies, each target compound should have been affected in the same way, as this would be a systematic error. For the five phenols shown, the average ratio and standard deviation of concentrations between the two air samplers is 1.01 ± 0.22. The largest deviation found was for 4-methyl-2-nitrophenol, which is also the most volatile of the species shown. This compound was often found to have low concentrations and had a recovery that was approximately half of that of the internal standards used. The uncertainty in the air samplers alone is 7 %, due

to drift and when this uncertainty is combined with the uncertainty introduced by measurement uncertainties when comparing parallel sampling, the overall estimated uncertainty is 23 %, in very good agreement with the observed variability.

5.3.2. Sampling Efficiency

The XAD coating procedure, initially designed by Gundel and Herring (1998), was adapted by Busca (2010) to coat large filters for the collection of ambient nitrophenols using high volume air samplers. It was found that using this method, a 30 % to 40 % breakthrough onto the second filter was observed when using two filters in series (Busca, 2010) (Section 4.1.2). It was proposed that possible solutions to reduce the breakthrough could include grinding the XAD-4^{TM} to a smaller mean diameter or to increase the concentration of the XAD-hexane slurry that is used for coating (Busca, 2010). Scanning electron microscope pictures were taken of XAD-4^{TM} that had been ground for 17 hours, the previously used grinding time, 34 hours, 51 hours and 68 hours (Fig. 4.4). It is clear that doubling the initial grinding time of 17 hours to 34 hours decreases the average mean diameter of the particles and increases the number concentration of small particles. It was also found that there is no significant difference when grinding for 51 hours or 68 hours instead of 34 hours and it was therefore determined to grind the XAD for 34 hours.

Table 5.5. Calculated diffusion coefficients of each target compound class as suggested by Fuller et al. (1966).

Compound Class	Calculated Diffusion Coefficient ($cm^2\ s^{-1}$)
Nitrophenols	0.077
Methylnitrophenols	0.071
Dimethylnitrophenols	0.066

Through comparison of scanning electron microscope pictures of filters coated using XAD ground for different time intervals (Fig. 4.5), it is evident that the filters coated with XAD ground for 34 hours have a higher quantity of adsorbent and far less bare spaces. Based on calculated diffusion coefficients (Table 5.5), a quartz fiber filter thickness of 0.432 mm (Pall Life Sciences, 2002) and a face velocity of 40 $cm^2\ s^{-1}$ for a 1.13 $m^3\ min^{-1}$ flow rate, the distance that a gas phase methylnitrophenol molecule diffuses while passing through the filter, on average, is 130 μm, which is considerably larger than the distance between filter fibers and XAD particles. However, even though the sampling efficiency may not be diffusion limited, the XAD adsorbent may not adsorb each gas molecule 100 % of the time and gas molecules could possibly desorb from the adsorbent.

The concentration of the slurry was also increased to maximize the amount of sorbent that would be coated on the filters. A XAD-hexane slurry was created with XAD that had been ground for 34 hours and the slurry concentration was increased from 6.5 mg L^{-1} to 10.5 mg L^{-1}. Filters were weighed prior to and following the coating procedure to determine the mass of XAD that had been coated on the filter (Table 4.5). The average mass of XAD on each filter increased from 0.09 g to 0.63 g. It is expected

that the increase in mass on the filters is due to the decreased particle size and therefore an increased mass on the filters due to electrostatic forces as well as the increase in the XAD concentration in the slurry.

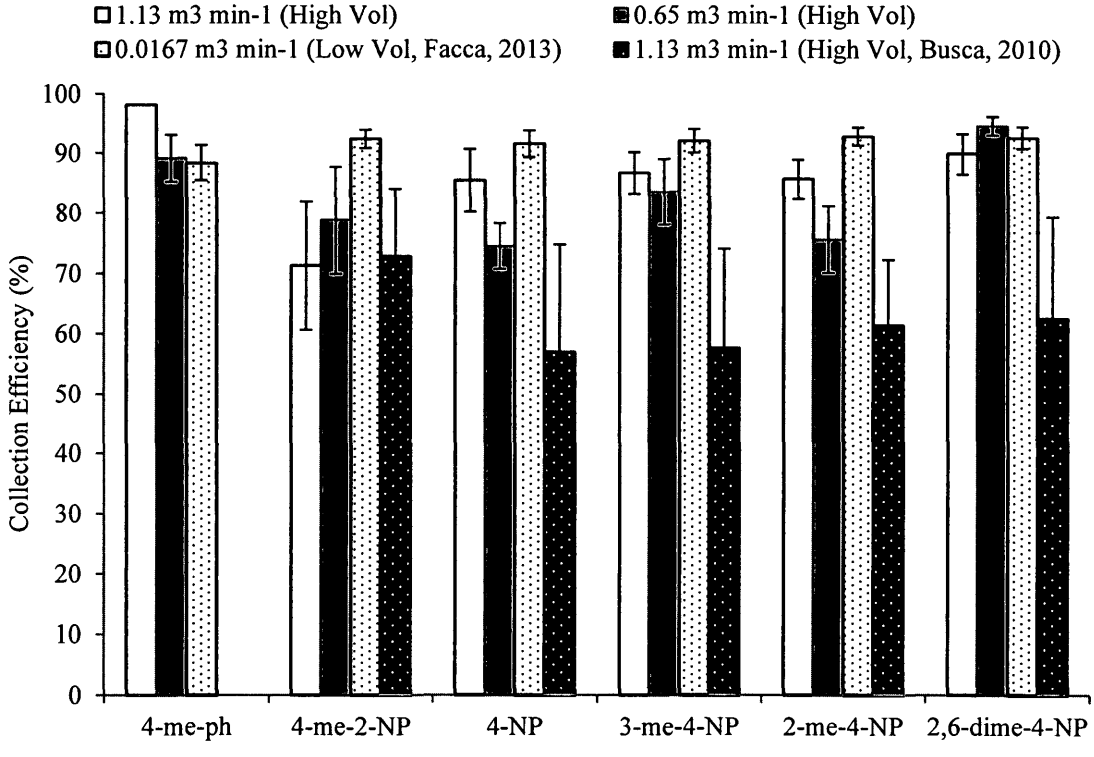

Figure 5.5. Comparison of breakthrough tests for XAD-coated filters conducted in this work with work by Facca (2013) and Busca (2010). Results from Hassani (private communication) were included in averages for high volume samples at a flow rate of 1.13 m^3 min^{-1}.

Collection efficiency tests of XAD-coated filters using high-volume air samplers indicate that the observed breakthrough could be due to incomplete adsorption on XAD. This may explain that a decrease in volume flow rate and face velocity does not improve collection efficiency. However, when comparing results from this work with results from

Facca (2013), collection efficiency is significantly improved for low volume sampling (Fig. 5.5). The face velocity for a 47 mm filter using a low volume sampler at a flow rate of 0.0167 m^3 min^{-1} is 20 cm^2 s^{-1}, similar to the face velocity of a large filter at 0.65 m^3 min^{-1}. Since the low and high volume filters were coated using the same type of procedure and the filter material is identical, the low efficiency of the XAD adsorbent can be ruled out as explanation for the sampling efficiency. A possible reason for the decreased sampling efficiency of the filters using high volume samplers is that the sampling of 47 mm filters includes sampling in a commercially available filter pack, designed to sample filters in series. Unlike sampling 47 mm filters on a low volume sampler, high volume sampling with two filters in series simply used a piece of mesh placed in between the two filters. Although the filters are secured in place, the method is not ideal. There could perhaps be a leak within the assembly, causing a fraction of the flow to bypass the top filter and pass through the bottom filter (Fig. 5.6.).

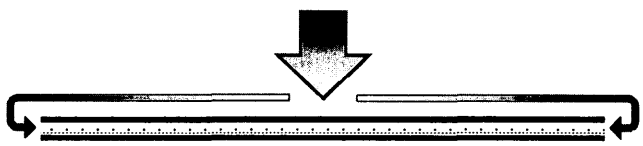

Figure 5.6. Schematic of possible flow pathway when sampling in series on a high volume air sampler. The dark lines represent the filters and the dotted line is the mesh in between the top and bottom filters.

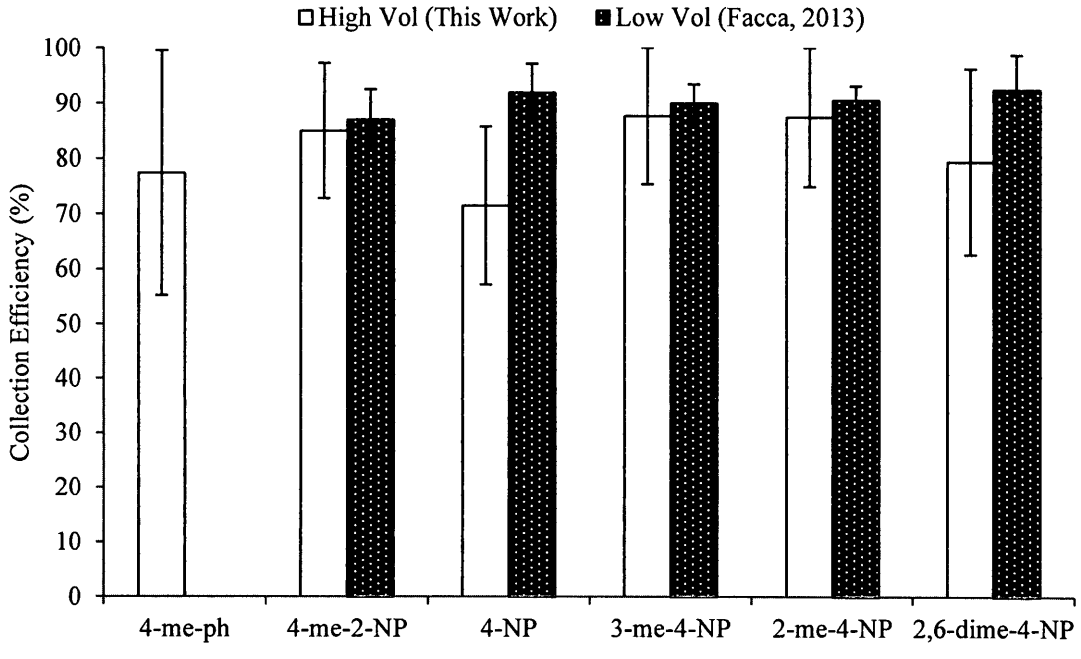

Figure 5.7. Comparison of collection efficiencies for quartz filters conducted in this work using high volume samplers with work by Facca (2013) using low volume samplers.

The efficiency of filters, regardless of sampling flow rate, should retain 99 % of the particles (Chow, 1995). Quartz fiber filters used in this study are said to have an aerosol retention of 99.9 % (Pall Life Sciences, 2002). Quartz filters were found to have an average aerosol retention of all phenols 80 % (Fig. 5.7). Here, the largest uncertainty was observed for 4-methylphenol, which was found to have variable recoveries in the extraction procedure due to its high volatility. When compared with measurements using low volume sampling (Fig 5.7), the collection efficiency seems to generally stay the same or decrease. It is expected that the observed breakthrough could be due to two reasons. The first could be that observed material on the second filter is due to blow-off, occurring

when there is volatization from the particle due to the pressure difference between the two filters (Umlauf, 1999). Though this may be an important loss, the observed breakthrough is unlikely to be caused by blow-off since the second filter is not a SIF and the gas phase may have only have a slight possibility of impaction. The second and more probable reason could be that the method used for sampling quartz filters in series using high volume air samplers could be prone to the same issues when sampling XAD-coated filters in series (Fig. 5.6).

As previously discussed, the mass required for isotope ratio measurements is significantly higher than the mass needed for concentration measurements alone. Nitrophenols have been found in very small concentrations in PM2.5 (Section 4.3.1.1.) and require large sampling volumes to have the possibility of these measurements. There was concern that a three day sampling period would increase the amount of artifacts, both positive and negative. Results from an experiment conducted to validate the lengthy sampling time is presented in Table 4.3. The largest percent difference was seen with 4-methylphenol. However, the difference in masses was 5 ng, which is small and therefore has a larger uncertainty associated with it. When combining measurements together and using them in comparison, the uncertainty of each value is propagated and the measurements are subjected to an uncertainty of 23 %. The differences for the remaining phenols are small and the results suggest that there is no significant bias when having sampling times substantially longer than three days compared to sampling for 24 hours.

To identify possible contribution from PM larger than 2.5 μm, one of the air sampler heads was replaced with a head that samples particles with aerodynamic diameters up to 10 μm. Results shown in Section 4.1.1.5 and Table 4.4 indicate that the differences in concentrations are in the pg m^{-3} range. This is consistent with theory, such that SOA will primarily exist in the particle size range of 2.5 μm and under and particles with larger diameters consist of particles derived from mechanical processes and consist of dust, sea spray and plant particles (Finlayson-Pitts and Pitts, 2000).

5.4. Overall Uncertainty

The overall uncertainties of the measurements are summarized in Table 5.6. The precision, linearity, difference in recoveries of internal standards and sampling efficiency of each filter type has been taken into consideration and were calculated using propagation of error. The uncertainty of the isotope ratio measurement took into account the precision and accuracy of the measurement. All uncertainties presented are averaged over all of the target compounds.

Table 5.6. Relative overall uncertainty of measurements for different sampling methods used.

Sampling Method	Overall Uncertainty (%)
PM Concentration	23
Gas + PM Concentration	24
Isotope Ratio	0.05

It was observed that any isotopic fractionation that may have occurred during the sampling, extraction and analysis procedure was within the uncertainty of the

measurement of 0.5 ‰. Information presented in Section 4.2.1. and discussed in Section 5.1.1. show that isotopic fractionation does not occur to a detectable extent during the extraction and analysis procedure. Each filter was spiked with two internal standards prior to extraction and as a result, their isotope ratios were monitored. Figure 5.8 shows the isotope ratio of 2-methyl-3-nitrophenol that was spiked on each ambient filter. At most, it differed by 0.6 ‰ from the offline value and the standard deviation was 0.2 ‰.

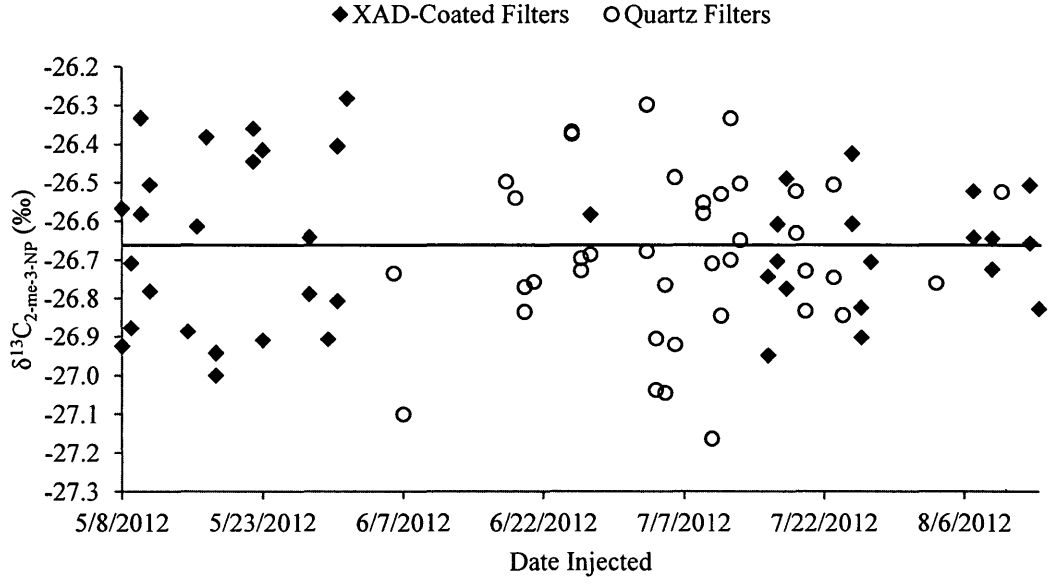

Figure 5.8. Isotope ratio of 2-methyl-3-nitrophenol that was spiked on each ambient filter prior to extraction. The solid line is the offline value of 2-methyl-3-nitrophenol. The average and standard deviation of the spiked internal standard is -26.66 ‰ ± 0.19 ‰.

5.5. Overview of Ambient Measurements

Ambient concentration measurements of nitrophenols have been studied before in the atmosphere by a small number of research groups (Section 2.5). Figures 5.9 and 5.10

show how concentrations found in this work compare to what was found elsewhere. Nishioka and Lewtas (1992) sampled in Boise, Idaho, which is a high altitude metropolitan area. Cecinato et al. (2005) and Morville et al. (2004) sampled in Rome, Italy and Strasboug, France, respectively, both of which are urban locations. Moukhtar et al. (2011) and Busca (2010) both sampled at York University. Herterich and Hermann (1990) sampled in a remote site in Garmisch-Partenkirchen, Germany. Lüttke and Levesen (1997) sampled at Great Dun Fell, which is a rural environment. It appears that the York University area is only lightly polluted in nitrophenols in both PM and gas phase and has concentrations that are considerably lower than what has been found in other studies. Studies shown are representative of both urban and rural areas and there appears to be no clear-cut distinction in concentrations between sampling sites. Cecinato et al. (2005), who sampled in an urban environment in 2003 seems to have the highest nitrophenol concentrations in PM, but has low concentrations when sampling gas phase alone (Fig. 5.10).

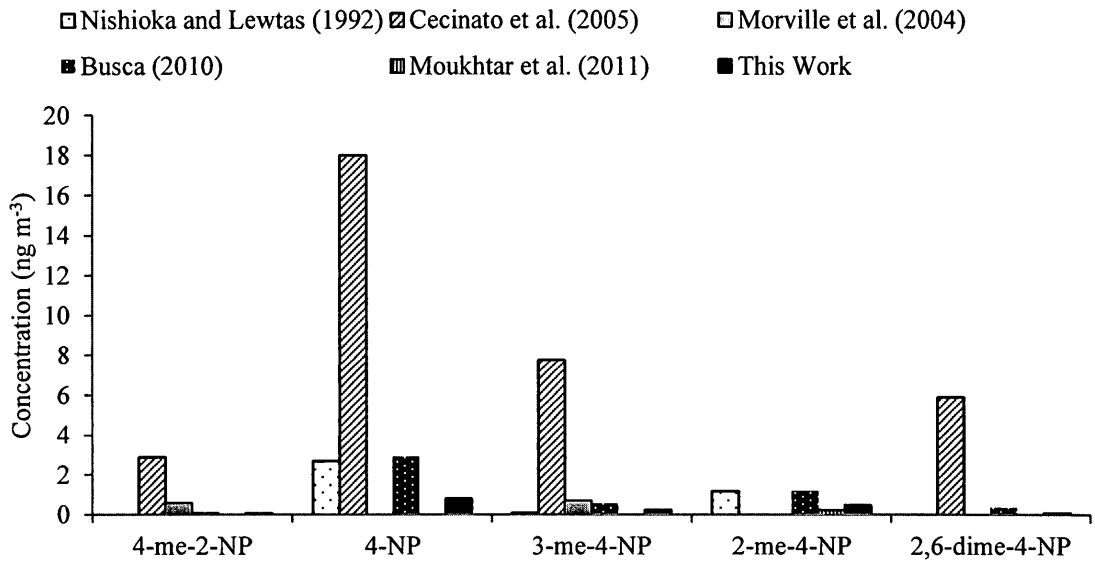

Figure 5.9. Comparison of nitrophenol concentrations in ambient PM from this work with literature. Data from Morville et al. (2004) and Busca (2010) are concentrations of nitrophenols in the gas phase and PM combined.

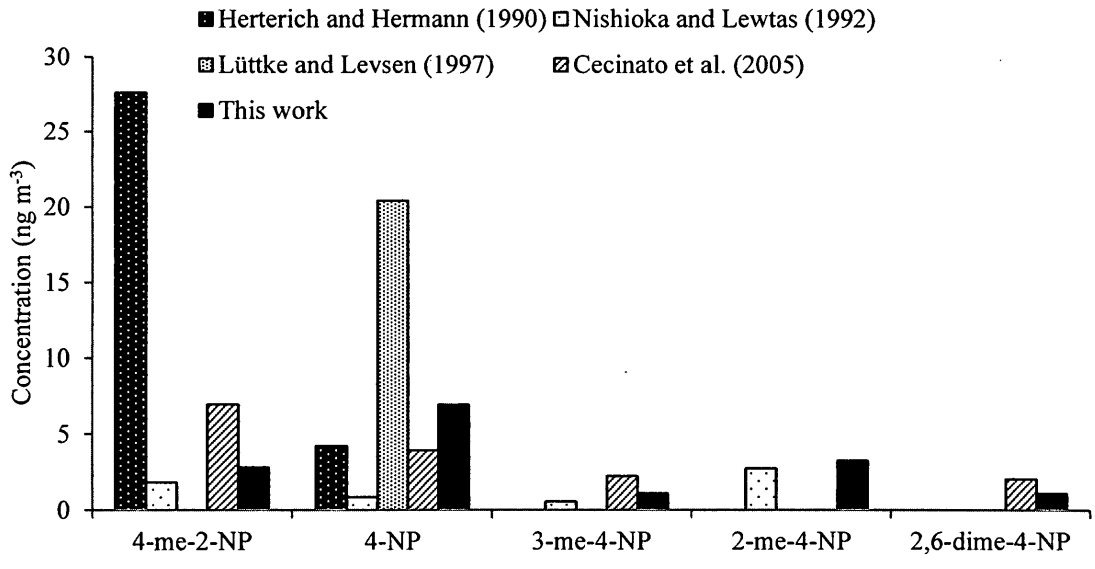

Figure 5.10. Comparison of nitrophenol concentrations in the gas phase from this work (gas phase + PM) with literature.

Extensive laboratory studies looking into the products formed from the photooxidation of VOC have been conducted; however, only two studies were conducted in which the formation yields of nitrophenols were quantitatively reported (Forstner et al., 1997; Irei, 2008). Using these yields, atmospheric concentrations were predicted using precursor mixing ratios and carbon isotope ratios measured at York University by Kornilova (2012) (Table 5.7). The predicted concentrations are drastically higher than the average concentrations observed and in all cases, the predicted concentrations are orders of magnitude higher.

Table 5.7. Predicted nitrophenol atmospheric concentrations based on yields found from laboratory studies. Initial precursor mixing ratios used were based on using the average PCA and average ambient mixing ratio of the precursor to find the amount of precursor processed in the Toronto area (Eq. 2.12). Precursor data were provided by Kornilova (2012).

Compound	Laboratory Yield (%)	Predicted Atmospheric Concentration ($ng\ m^{-3}$)	Average Atmospheric Concentration in PM ($ng\ m^{-3}$)	Average Atmospheric Concentration in Gas +PM ($ng\ m^{-3}$)
4-me-2-NP	4.4[a]	98[a]	0.06	2.78
3-me-4-NP	6.8[a], 0.096[b]	152[a], 2[b]	0.23	1.09
2-me-4-NP	10[a], 16.3[b]	224[a], 364[b]	0.48	3.22
2,6-dime-4-NP	3.3[a]	48[a]	0.07	1.06

[a] Forstner et al., 1997; [b] Irei, 2008

5.6. Gas and Particle Phase Phenols

The following section will compare differences in concentrations and isotopic compositions of nitrophenols in ambient air. Although previous studies, discussed in Section 2.5, show that differences in concentrations between the gas phase and PM exist, differences in isotope ratios have not been looked into.

5.6.1. Ambient Concentration Measurements of Gas and Particle Phase Phenols

One of the most obvious correlations that was expected would have been a decrease in nitrophenol concentrations in PM with increasing temperature coupled with an increase in gas phase concentrations. The data in Fig. 5.11 somewhat follow this expectation, but surprisingly the total concentrations (Fig. 5.12) also show a decrease in concentration with increasing temperature.

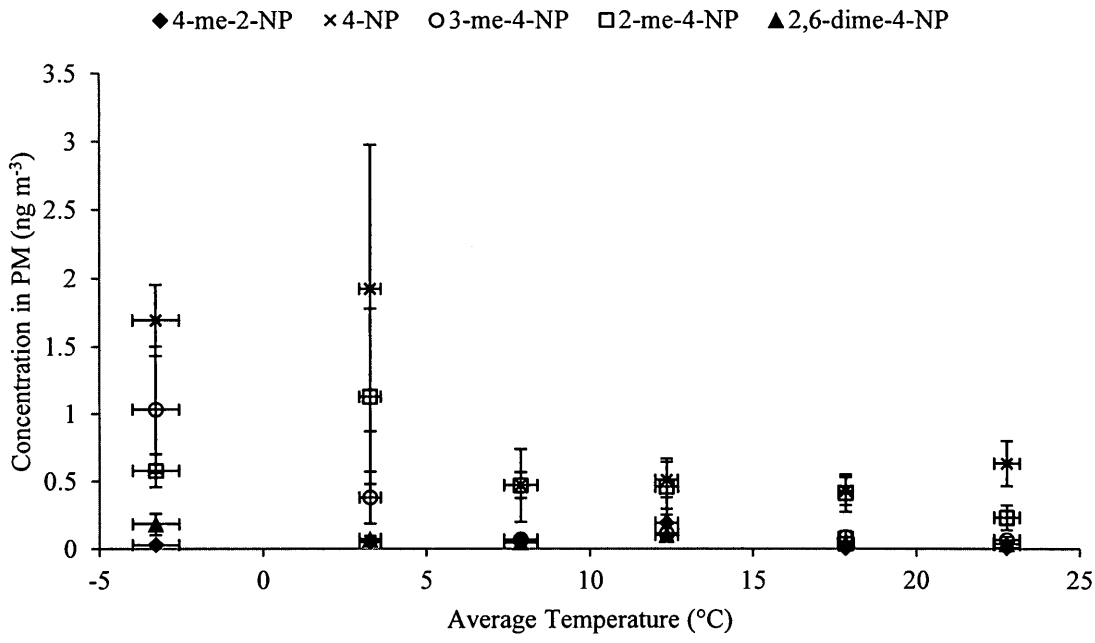

Figure 5.11. Dependence of nitrophenol concentrations in PM with temperature. Each point represents the average concentrations and temperatures over the following ranges: < 0 ^{0}C, 0 ^{0}C to 5 ^{0}C, 5 ^{0}C to 10 ^{0}C, 10 ^{0}C to 15 ^{0}C, 15 ^{0}C to 20 ^{0}C and > 20 ^{0}C. The error bars in each direction are the errors of the means.

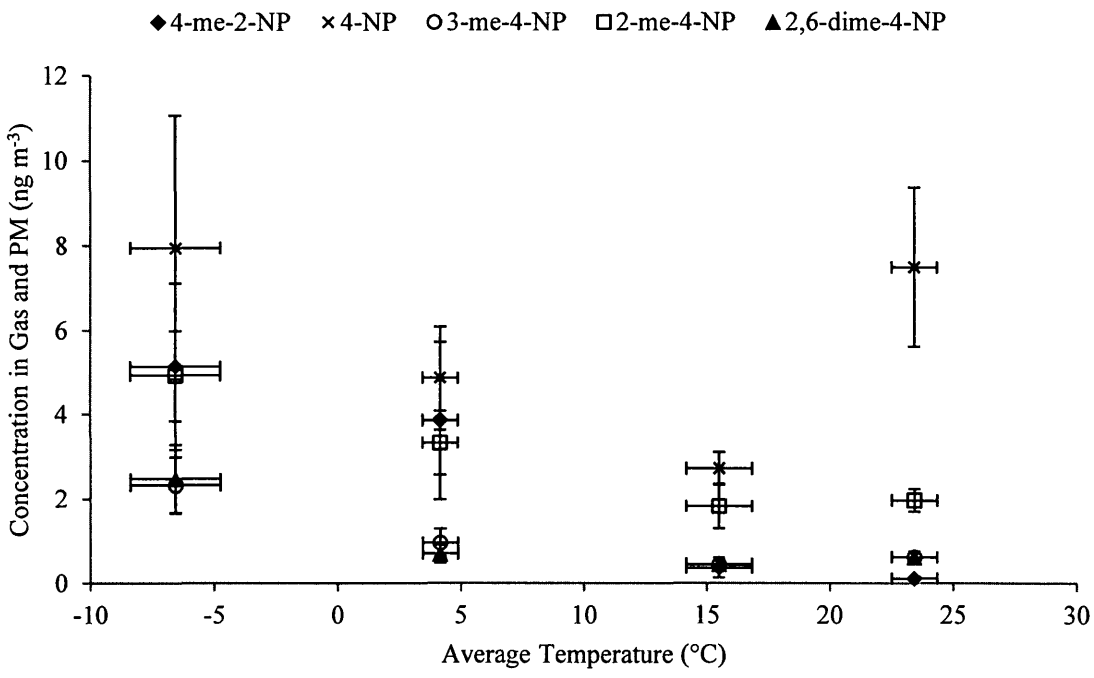

Figure 5.12. Dependence of nitrophenols in gas phase and PM with temperature. Each point represents the average concentrations and temperatures over the following ranges: < 0 ^{0}C, 0 ^{0}C to 10 ^{0}C, 10 ^{0}C to 20 ^{0}C and > 20 ^{0}C. The error bars in each direction are the errors of the means.

The highest nitrophenol levels in the gas phase and PM, apart from 4-nitrophenol, were observed when the temperatures were lowest (Fig. 5.12). This can perhaps be due to the decreased boundary layer height in the winter and dilution in the summer. With a decreased boundary layer height, pollutants are more concentrated and there is limited mixing. Another possibility is that there can be losses of nitrophenols due to photochemistry and removal by HO at a rate that is similar to that of the precursor reaction. If the nitrophenols favour PM, this loss will be slower.

Concentrations of phenols in both phases were found to increase with increasing NO_2 mixing ratio (Fig. 5.13). This could be due to two reasons. If phenols are primary emissions, their concentrations should be correlated with NO_2 levels; however, if phenols are formed through secondary processes, their concentrations should also be correlated with NO_2 since NO_2 is a precursor in the formation mechanism. Furthermore, emissions of toluene are also expected to be correlated with NO_x emissions. With the given information and limited data set, it is not possible to confirm whether phenols are primary emissions from concentration measurements alone.

A correlation was also observed between target compound concentrations in both phases with PM2.5 levels (Fig. 5.14). As PM2.5 levels increased, concentrations of phenols in PM2.5 increased, which is expected since as the particulate loading in the atmosphere increases, there is more material for the phenols to partition on. Concentrations of phenols in both phases were also highest when PM2.5 loading was highest. This could be an indicator for increased photochemistry and pollution.

Possible relationships between the wind trajectory and phenol concentrations were also investigated. From Fig. 5.15, it is observed that the highest phenol concentrations in each phase are seen when the wind originates from the Southwest where the 400 and 401 highways intersect and where there is possible influence from downtown Toronto and the city center of Detroit that is located further downwind.

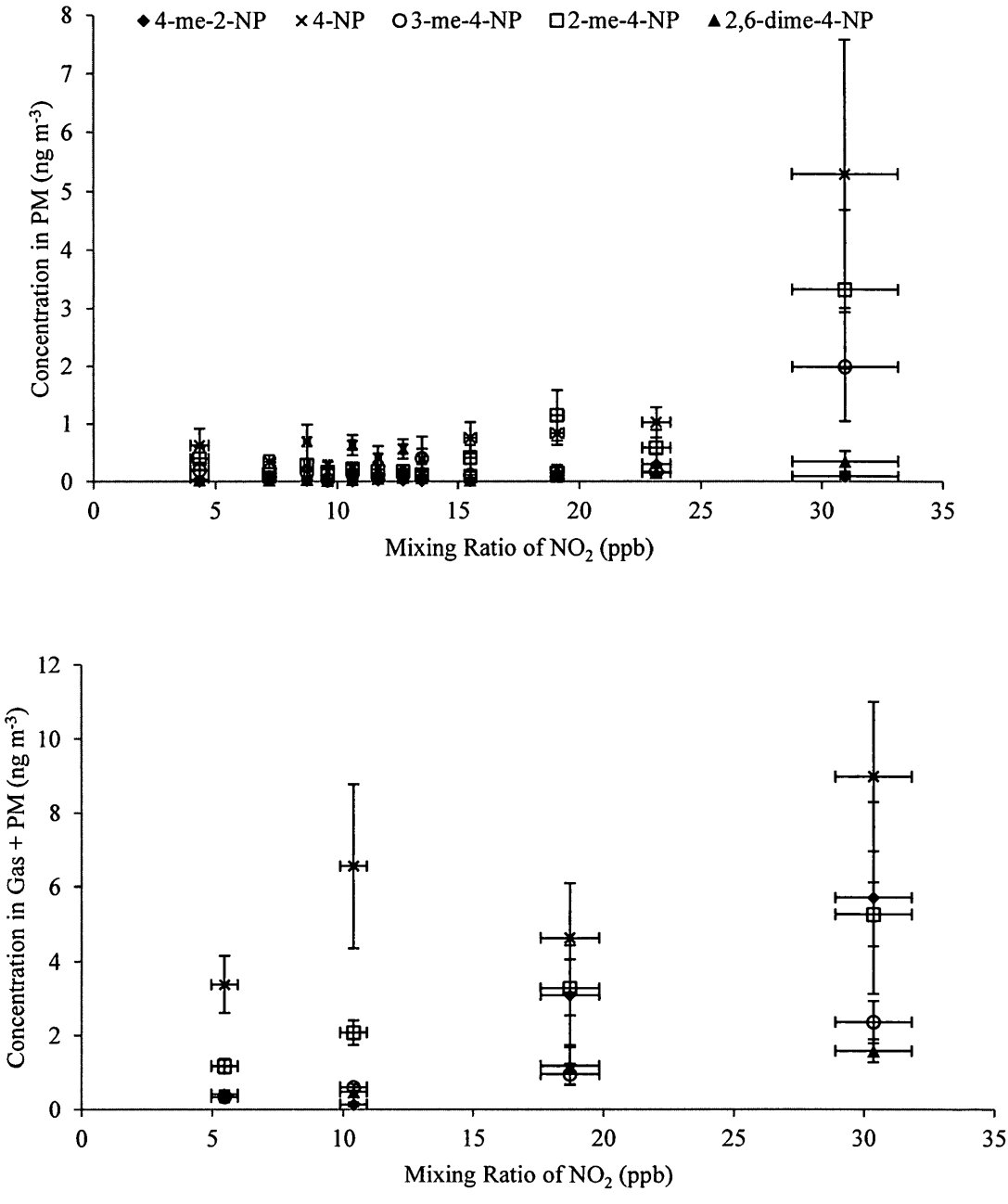

Figure 5.13. Plot of dependence of phenol concentrations in PM alone (top) and in gas phase and PM (bottom) with NO_2 mixing ratios. NO_2 mixing ratios were averaged during daylight hours between 8 am and 5 pm, local time. Data was sorted in order of increasing NO_2 mixing ratios and each point is an average of ten points. The error bars in each direction are the errors of the means.

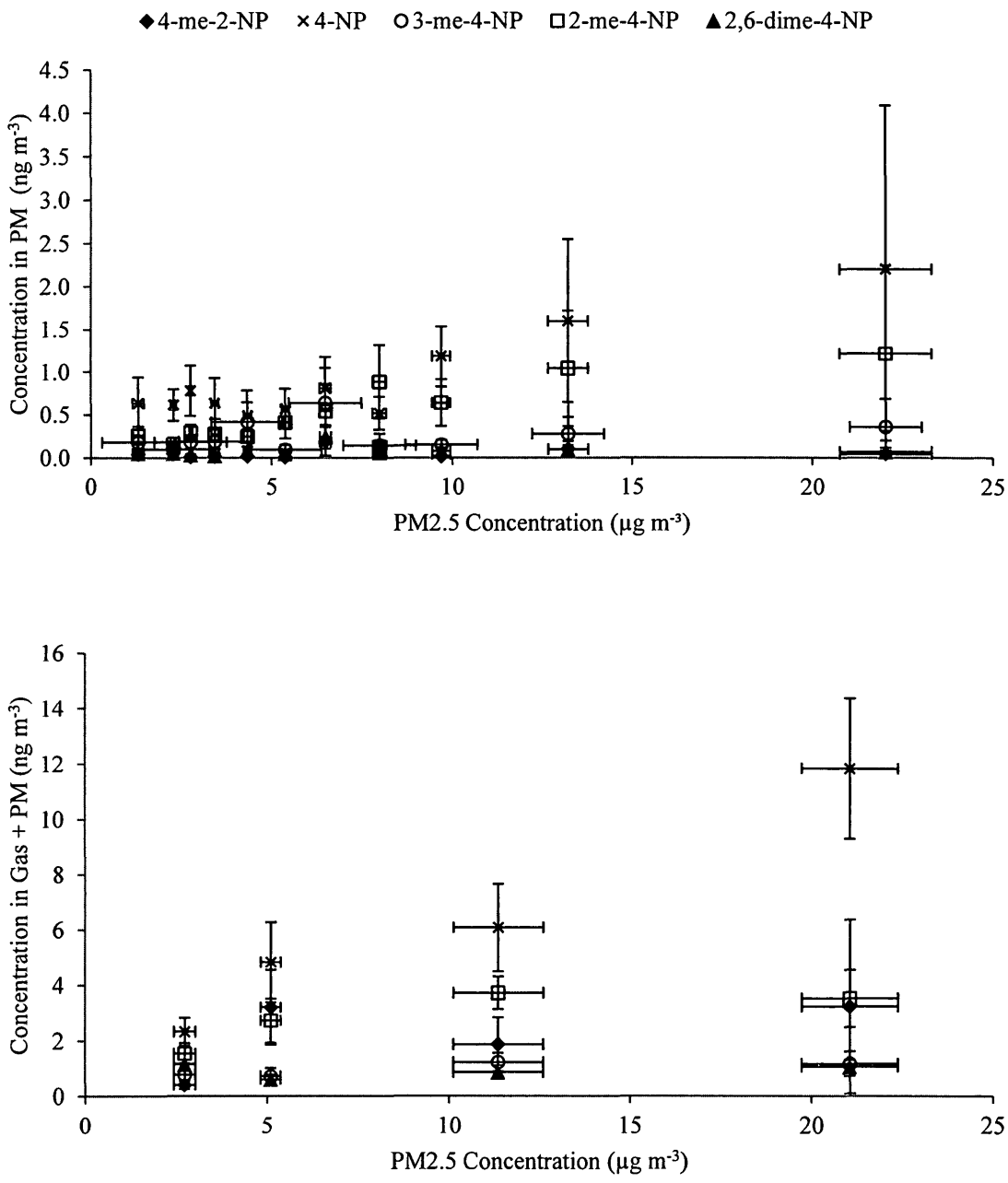

Figure 5.14. Plot of dependence of phenol concentrations in PM alone (top) and in gas phase and PM (bottom) with PM2.5 concentrations. Data was sorted in order of increasing PM2.5 concentrations and each point is an average of ten points. The error bars in each direction are the errors of the means.

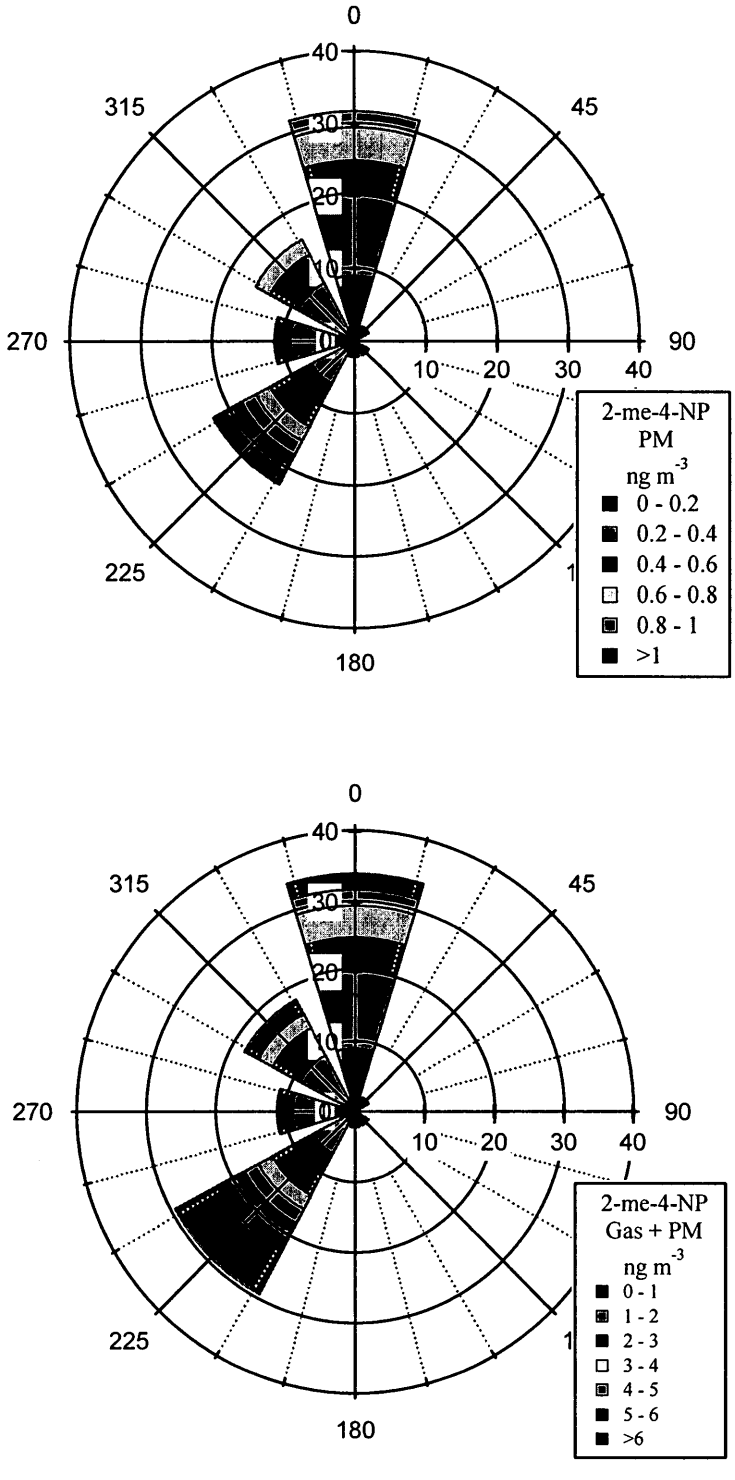

Figure 5.15. Wind rose plot of 2-methyl-4-nitrophenol concentrations found in PM (top) and gas phase and PM (bottom).

Sampling nitrophenols in PM alone and in the gas phase and PM together using high volume air samplers can give a preliminary estimate on the relative concentrations in each separate phase. Average concentrations over all filter samples collected are shown in Table 5.8. Data shown was not collected in parallel. Each compound, independent of vapour pressure, is present predominantly in the gas phase. Given the range in vapour pressure, it was expected to observe a dependence in the partitioning. This data set shows a significantly larger portion in the gas phase than what is shown in Table 5.9 for filters that collected samples in parallel. The discrepancies are most likely explained by the small set of points collected in parallel in Table 5.9.

Table 5.8. Average concentrations and errors of the means of ambient nitrophenols in PM and gas phase and PM.

Compound	Vapour Pressure at 303 K (Pa)	Concentration (ng m^{-3})		Ratio of Averages PM/(Gas + PM)
		PM	Gas + PM	
4-me-ph	1×10^{1} (at 294 K)[a]	0.13 ± 0.04	2.59 ± 0.78	0.05
4-me-2-NP	1.11×10^{1}[b]	0.06 ± 0.02	2.78 ± 0.89	0.02
4-NP	1.03×10^{-2}[b]	0.80 ± 0.14	6.88 ± 1.10	0.12
3-me-4-NP	3.13×10^{-3}[b]	0.23 ± 0.06	1.09 ± 0.23	0.21
2-me-4-NP	8.69×10^{-3}[b]	0.48 ± 0.10	3.22 ± 0.46	0.15
2,6-dime-4-NP	6.42×10^{-4}[b]	0.07 ± 0.01	1.06 ± 0.22	0.07

[a] CRC Handbook of Chemistry and Physics (2013)
[b] Gong (private communication)

Table 5.9 shows that the partitioning of the phenols can vary largely with temperature. For all phenol species, the partitioning of phenols is enhanced towards the gas phase at higher temperatures; however, the data set size is limited.

Table 5.9. Average percentage of phenols found in PM for filter samples that were collected in parallel, ± the error of the mean. The number in brackets indicates the number of samples used in the averages.

Compound	Average of Concentration in PM / Concentration in Gas + PM	
	Average Temperature: 1.9 °C	Average Temperature: 24.5 °C
4-me-2-NP	0.01, 0.03 (2)	0.04 (1)
4-NP	0.71 ± 0.07 (5)	0.12 ± 0.06 (3)
3-me-4-NP	0.91 ± 0.19 (5)	0.01 (1)
2-me-4-NP	0.64 ± 0.26 (5)	0.20 ± 0.12 (3)
2,6-dime-4-NP	0.32 ± 0.08 (5)	0.12 (1)

For PM and gas phase and PM samples that were collected in parallel, the concentrations correlated very well with each other (Fig. 5.16). This indicates that there is an equilibrium between the gas and particle phase for each target compound. While a point for 4-nitrophenol at low PM concentration with a gas phase concentration of approximately 18 ng m^{-3} seems to be an outlier, it was confirmed that it is not statistically significant in the complete data set and an experimental problem could not be identified. Nevertheless, for each of the compounds, as the concentration in PM increases, the concentration in the gas phase and PM increases linearly.

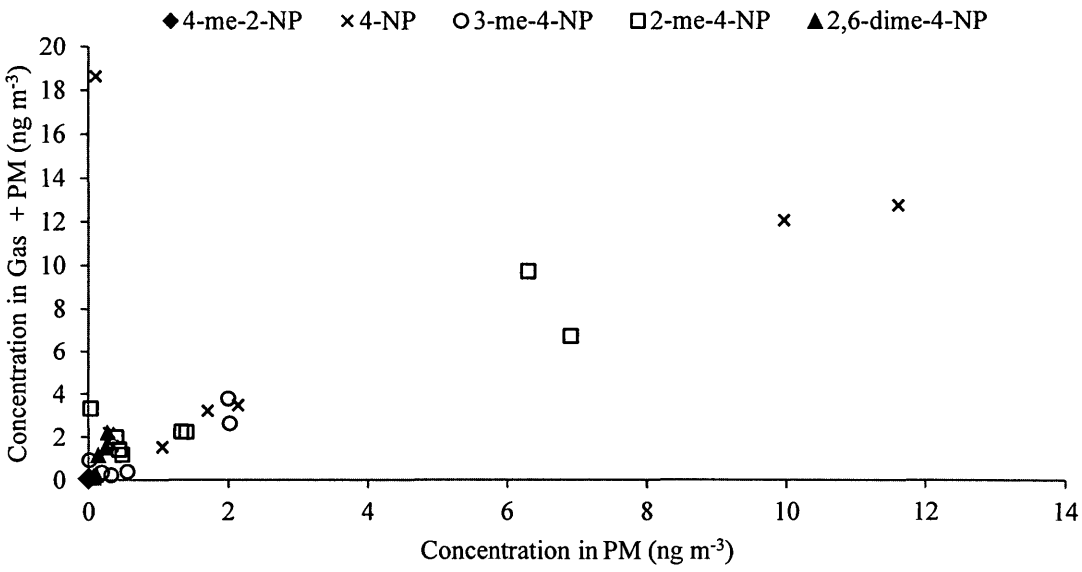

Figure 5.16. Correlation between gas phase and PM and PM nitrophenol concentrations for samples that were collected in parallel. The slope of this plot is 0.76 with an intercept of 2.1.

The average partitioning of the nitrophenols in each phase was determined through two different methods in this work, parallel and series sampling using high volume air samplers, and one different method by using denuder sampling with a low volume air sampler (Facca, 2013). For each of the phenols, it was seen that the majority, regardless of the method used, were found in the gas phase (Fig. 5.17). There are some discrepancies between the methods, most likely due to concentrations found using high volume samplers not being corrected for filter efficiency.

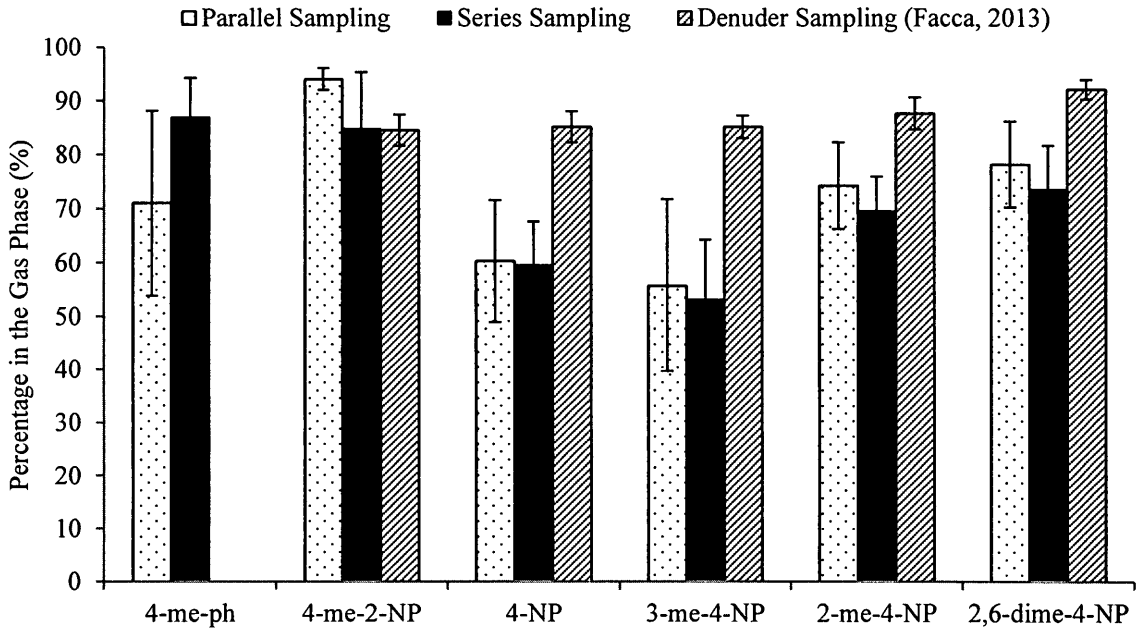

Figure 5.17. Average percentage of nitrophenols found in the gas phases as determined by different sampling methods.

Table 5.10. Calculated partitioning coeffecients (K_p) for target compounds for samples that were collected in parallel.

Compound	K_p (m^3 μg^{-1})	
	This Work	Facca (2013)
4-me-2-NP	0.053	0.045
4-NP	0.033	0.022
3-me-4-NP	0.035	0.034
2-me-4-NP	0.041	0.044
2,6-dime-4-NP	0.040	0.022

Partitioning coefficients for each of the target compounds were calculated using Eq. 2.1. Averages of partitioning coefficients for samples that collected the gas phase and PM and PM in parallel are shown in Table 5.10 and are compared to calculated values

from Facca (2013). The values agree with those found by Facca (2013), which used a different sampling system to collect and separate the target phenols.

5.6.2. Ambient Isotope Ratio Measurements of Gas and Particle Phase Phenols

As previously stated, all isotope ratio measurements were biased to samples that had a minimum mass of 3 ng per 3 μL injection. This possible bias was small when analyzing 4-nitrophenol and 2-methyl-4-nitrophenol from XAD-coated filter samples, since there were only ten and two samples, respectively, that had too low concentrations for isotope ratio analysis. However, this was critical for all other target compounds and samples, particularly PM samples alone. To confirm whether or not there was indeed a bias, a box and whisker plot was created (Fig. 5.18) to see if the isotope ratio was dependent on ambient concentrations of phenols. The plot shown is for 2-methyl-4-nitrophenol, but other target compounds presented the same trend. The average concentrations in each of the bins are relatively close to each other and no significant differences or biases are observed.

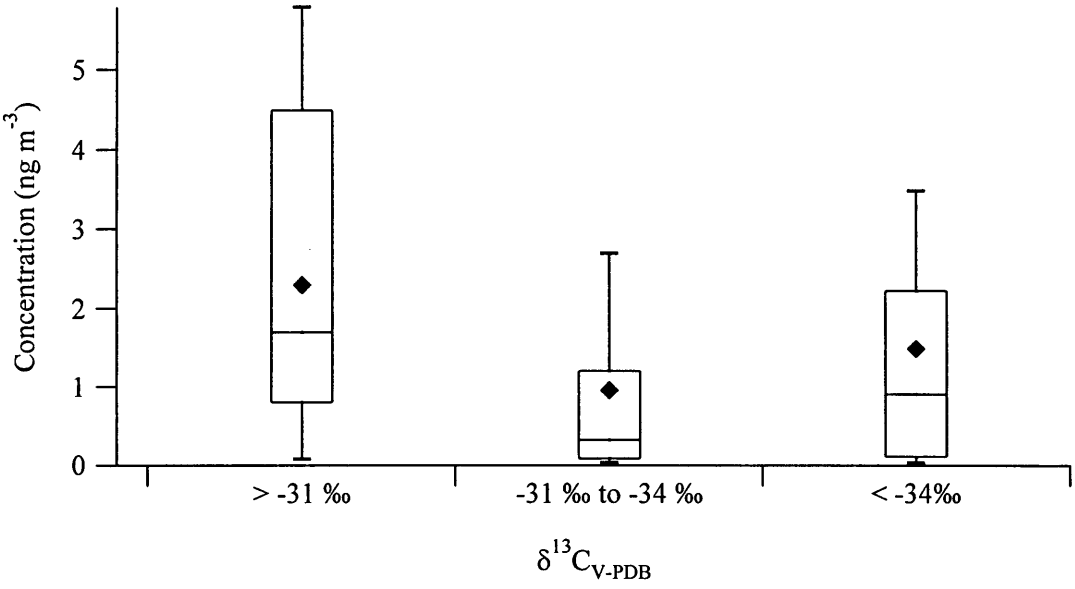

Figure 5.18. Box and whisker plot of stable carbon isotope ratios and concentrations of 2-methyl-4-nitrophenol in gas phase and PM and in PM; Error bars represent the 90th and 10th percentiles and the upper and lower ends of the box are the 75th and 25th percentiles. The horizontal line represents the median and the black diamond is the mean concentration in each category. The number of data points in each bin is 7, 53 and 20, respectively and the errors of the means are 0.8 ng m^{-3}, 0.2 ng m^{-3} and 0.4 ng m^{-3}, respectively and 0.1 ‰, 0.1 ‰ and 0.2 ‰, respectively.

Dependences between points from the ratios and differences of isotopic composition in each phase were not observed with wind direction, pollutant levels (NO_2, O_3 and PM2.5) or average temperatures. Figures 5.19 and 5.20 show the relationships between average temperature and NO_2 mixing ratios, respectively, with isotope ratios. There appears to be no systematic correlation with either of the parameters. This could be because of the limited data set size and the resulting uncertainty of the averaged values; however, even within the uncertainty, strong systematic dependencies can be ruled out.

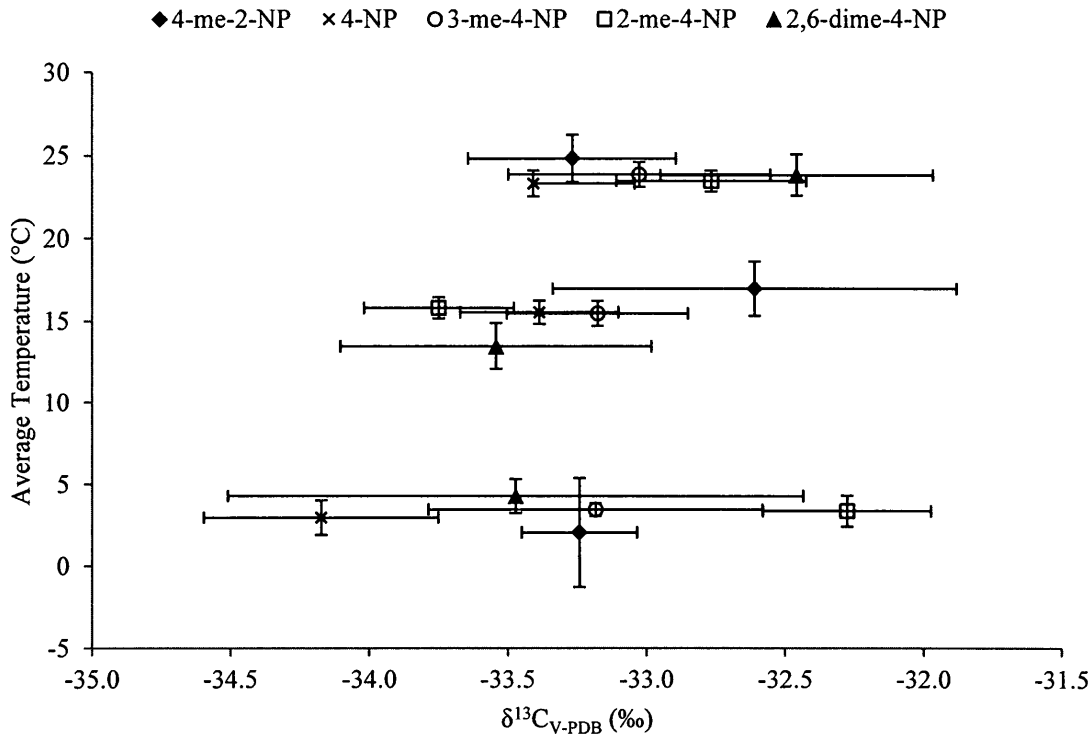

Figure 5.19. Plot showing the relationship of the average daily temperature with isotope ratios. Points shown were sorted in order of increasing temperature and each point is an average of points that have temperatures in the following ranges: < 10 ^{0}C, 10 ^{0}C to 20 ^{0}C and > 20 ^{0}C. The error bars in each direction are the errors of the means.

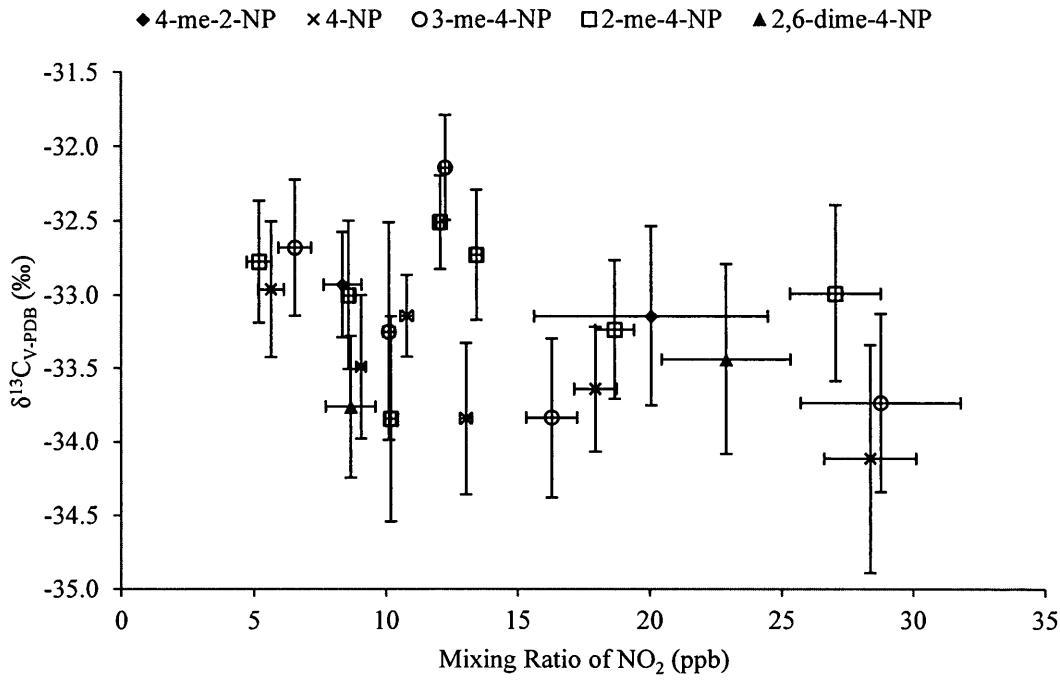

Figure 5.20. Plot showing the relationship of NO_2 mixing ratios with isotope ratios. NO_2 mixing ratios were averaged during daytime hours from 8 am to 5 pm, local time. Points were sorted in order of increasing NO_2 mixing ratios and each point is an average of ten points. The error bars in each direction are the errors of the means.

The isotope ratios of 3-methyl-4-nitrophenol and 2-methyl-4-nitrophenol were plotted to investigate if a correlation existed between isomers (Fig. 5.21). There appears to be strong evidence that the isotope ratios are indeed correlated as many of the points lie along the 1:1 line. Reasons for this dependence could be due to the co-variation in the isotope ratios of sources, including formation in the atmosphere. Another possibility is removal from the atmosphere by reactions with similar rate constants and KIE.

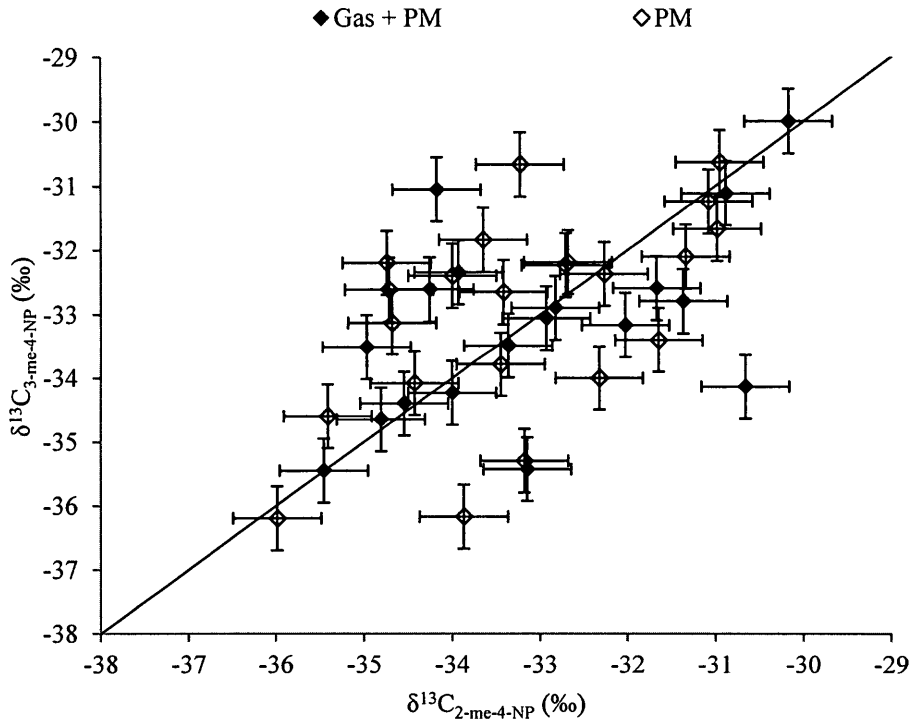

Figure 5.21. Correlation of isotope ratios between isomers 3-methyl-4-nitrophenol and 2-methyl-4-nitrophenol for filter samples that were collected in parallel. The error bars represent the uncertainty of the measurement of 0.5 ‰ and the solid line is a 1:1 line.

Figure 5.22 shows the difference in isotope ratios of 2-methyl-4-nitrophenol and 3-methyl-4-nitrophenol. As the isotope ratio of 2-methyl-4-nitrophenol increases, the difference in delta values between the two isomers increases. Based on the structures of the two isomers, 3-methyl-4-nitrophenol should be more reactive since all three functional groups direct reaction at carbon number six. If this isomer is indeed more reactive, then the trend observed in Fig. 5.22 is consistent with this finding. As 2-methyl-4-nitrophenol ages, 3-methyl-4-nitrophenol begins to react further with the HO radical

and fractionation, causing an enrichment in ^{13}C. Another possible reason for the small, but systematic dependence seen in Figure 5.22 could be a small difference in KIE for loss reactions. The small deviation from a 1:1 correlation in isotope ratios between the two isomers is likely the result of atmospheric loss reactions with similar, but not completely identical rate constants and KIE.

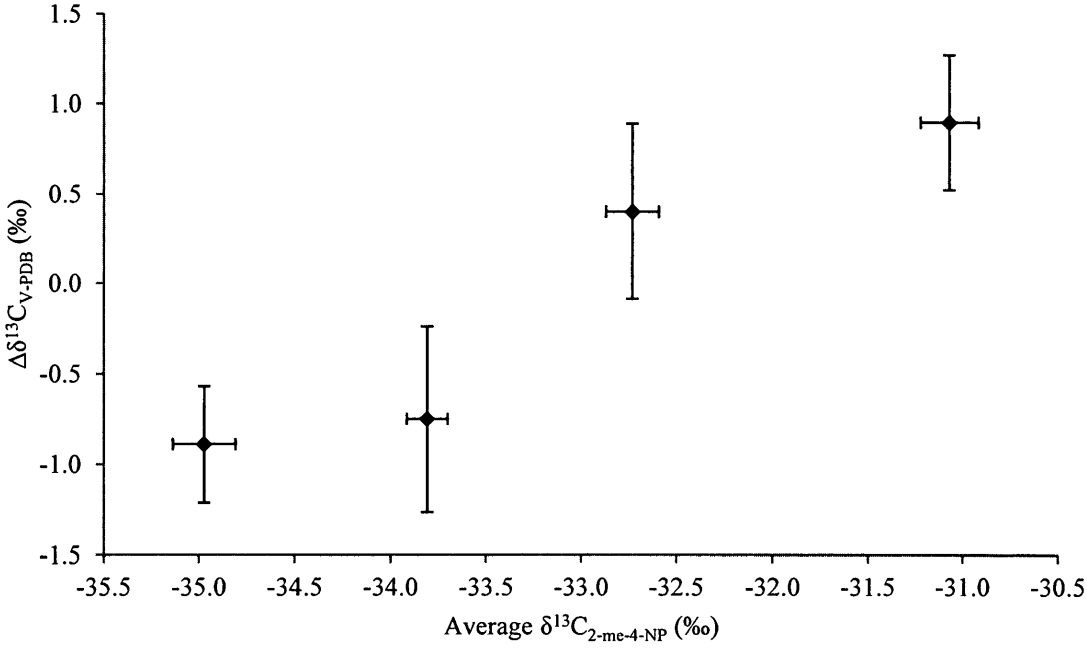

Figure 5.22. Plot of the difference in isotope ratios of 2-methyl-4-nitrophenol and 3-methyl-4-nitrophenol ($\Delta\delta^{13}C_{V\text{-}PDB} = \delta^{13}C_{2\text{-}me\text{-}4\text{-}NP} - \delta^{13}C_{3\text{-}me\text{-}4\text{-}NP}$) in relation to the isotope ratio of 2-methyl-4-nitrophenol. 2-methyl-4-nitrophenol isotope ratio data was sorted and each point represents an average over ten points. The error bars in each direction represent the errors of the means.

5.6.3. Difference in Isotope Ratios of Phenols between Phases

The frequency distributions of the isotope ratios for each of the target compounds in each of the phases are shown in Fig. 4.26 and Fig. 4.28. Each of these distributions peak at approximately -33 ‰ and are relatively symmetrical. The normalized frequency distribution of the isotopic composition of 2-methyl-4-nitrophenol in each phase is shown in Fig. 5.23. On average, there appeared to be little significant differences in the distribution and the highest percentage of isotope ratios in each phase were clustered around -34 ‰ to -31 ‰.

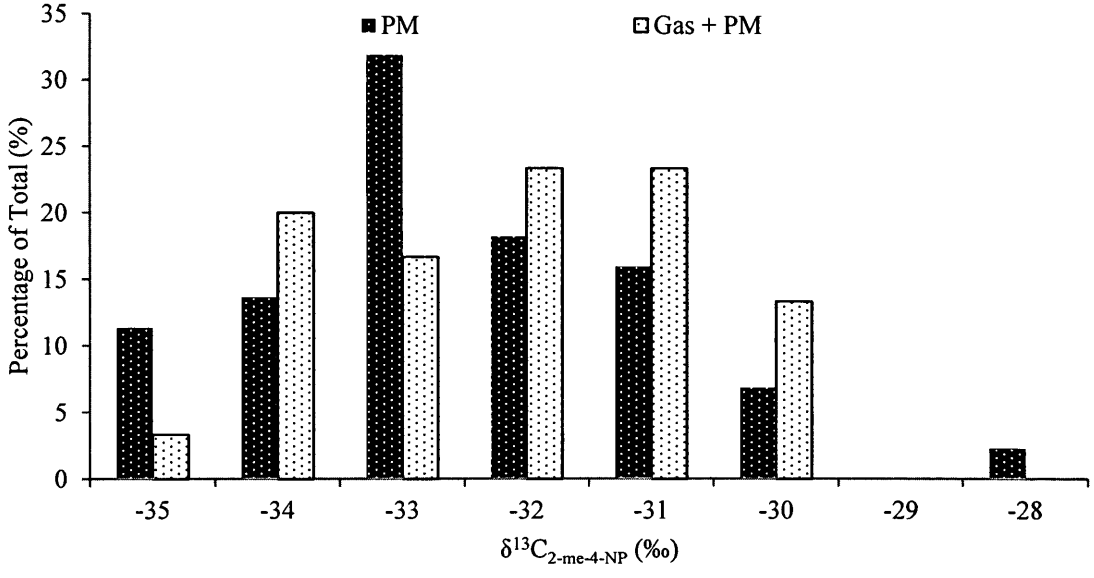

Figure 5.23. Frequency distribution of the isotopic composition of 2-methyl-4-nitrophenol in PM and in gas + PM. 44 samples were used for PM and 30 samples were used for gas + PM.

Parallel sampling of PM and gas phase and PM together using quartz and XAD-coated filters was conducted to see if there are in fact differences between the two phases. Table 5.11 shows results from samples that were collected in parallel. Differences for 4-nitrophenol and 2-methyl-4-nitrophenol are not observed by looking at the average isotopic composition. However, for 3-methyl-4-nitrophenol, there are certain clear differences that are observed, although there are only two points. Possible reasons for these differences are discussed in Section 5.7.

Table 5.11. Summary of averages and errors of the means of isotope ratios of target phenols from samples that were collected in parallel.

Compound	Number of Samples	PM (‰)	Gas Phase and PM (‰)
4-NP	7	-33.3 ± 0.3	-33.4 ± 0.4
3-me-4-NP	2	-32.6, -32.2	-34.4, -35.5
2-me-4-NP	8	-32.6 ± 0.5	-32.2 ± 0.7

Isotope effects can occur when compounds partition between phases. These isotope effects are known as equilibrium isotope effects (Kaye, 1992). Differences in carbon isotope ratios of the same compound between phases due to these effects are usually small and within the uncertainty of the measurement. However, quantifiable differences in isotopic composition between phases can still exist but can be due to gas phase losses of products or if there is an injection of fresh emissions, the formation of freshly formed products. The condition is that exchange between the two phases is slower than the processes causing isotope ratio changes in one of the phases. The average isotope ratios of target compounds found in PM and in the gas phase and PM together are

shown in Fig. 5.24. It should be noted that isotope ratios of target compounds in PM are biased towards filter samples that have higher concentrations. It appears that especially for 4-methyl-2-nitrophenol and 2,6-dimethyl-4-nitrophenol, there is a difference in isotope ratio between the phases. However, the data set is especially limited for these compounds in PM with a sample set size of four and seven, respectively.

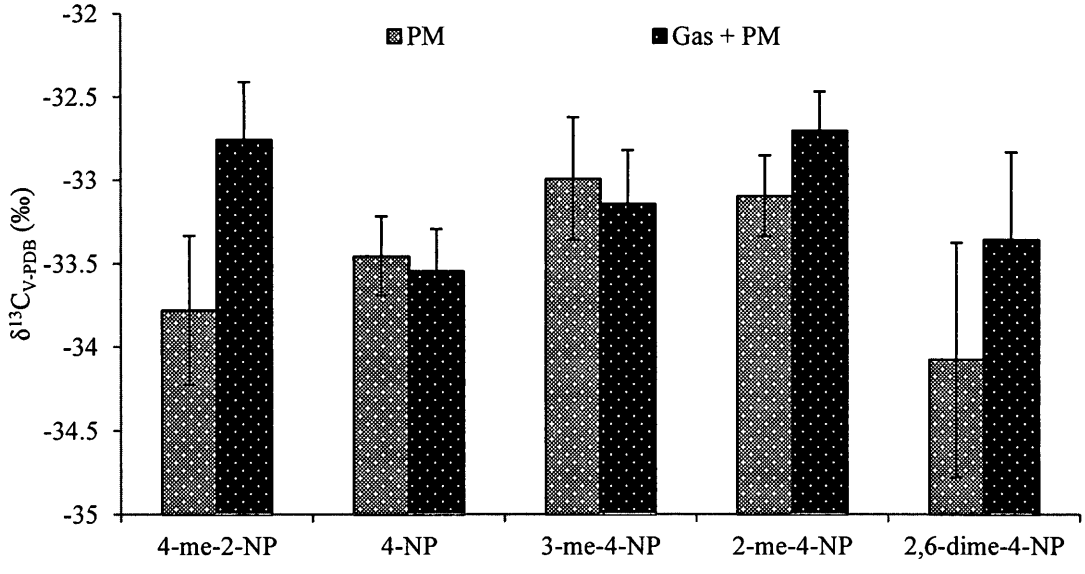

Figure 5.24. Comparison of the average isotope ratios of nitrophenols found in PM alone and in gas phase and PM. The error bars represent the error of the mean.

Given the presented information, the data set presented may be too limited to be able to quantify differences in isotopic composition between the gas phase and PM. When looking at averages for samples in parallel (Table 5.11) as well as averages over all samples (Fig. 5.24), isotopic compositions of the same compounds but in different phases seem to be relatively similar.

5.7. Atmospheric Processing

5.7.1. Photochemical Age

The main basis for choosing nitrophenols as target compounds in this study was that the phenols, specifically 2-methyl-4-nitrophenol, had an isotope ratio that was similar to the isotope ratio of the sum of all products that are formed specifically from the photooxidation of toluene (Fig. 5.25). Having this property enables the ability to determine the extent of processing of toluene, as well as the PCA, based on the isotope ratio of products. The PCA of the product can be calculated by rearranging and combining Eq. 2.11 and 2.12. Using mass balance, the PCA is determined using Eq. 5.1. In this equation, k_{12} is equivalent to k_{HO} for practical purposes since the impact of any isotope effect will be far less than the uncertainty of rate constant measurements.

$$\delta^{13}C_{prod} = \frac{\delta^{13}C_o - \exp(-k_{HO}[HO]t)(\delta^{13}C_o + k_{12}\varepsilon[HO]t)}{1 - \exp(-k_{HO}[HO]t)} \qquad \text{Eq. 5.1}$$

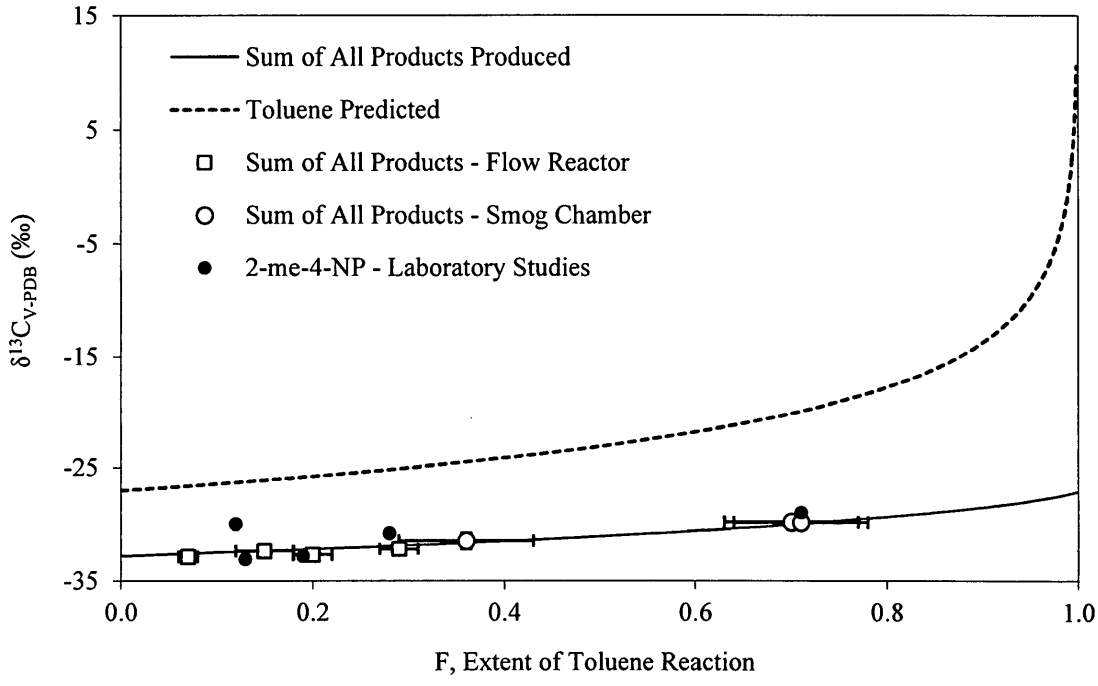

Figure 5.25. Plot of the change in $\delta^{13}C_{V\text{-}PDB}$ of toluene and the sum of all products formed as a function of the extent of the toluene reaction, F (adapted from Irei, 2011).

Each of the variables are known for Eq. 5.1, apart from [HO]t, the PCA. This equation was used to calculate the PCA for each product based on the product's isotope ratio and the precursor's source signature isotope ratio (Fig. 5.26). The isotope ratio for products formed from m-xylene seemed to be most sensitive at a low PCA when compared to benzene and toluene. Reaction products from benzene, the least reactive precursor of the three, was found to be least sensitive to a change in isotope ratio due to a change in PCA. Nevertheless, the isotope ratios of the products' PCA is less sensitive than that of the precursor. When PCA increases, the sensitivity of the dependence of

isotope ratios of the product on PCA decreases. In this case, mixing with an aged air mass will not greatly impact isotopic composition.

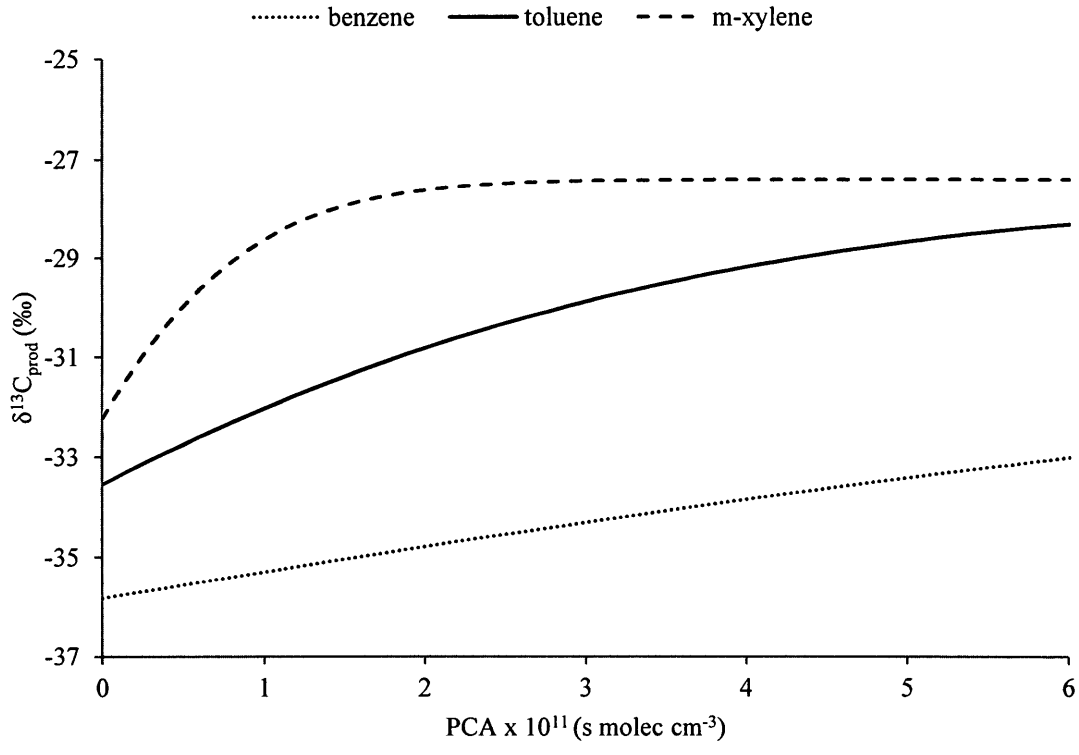

Figure 5.26. PCA calculated using the isotope ratio of the product for specific precursor-product pairs. The rate constants, KIE and source signatures are listed in Section 2.

Determining the PCA of a species using a product's isotopic composition can be valuable in gaining insight into chemical processing in the atmosphere; however, there are several considerations that need to be taken into account. It should be noted that since nitrophenols in ambient air in the Toronto area have been found to be predominantly in the gas phase (Fig. 5.17), the plot shown in Fig. 5.26 may not be accurate since gas phase losses and their isotopic fractionation are not taken into account. Although there is only

limited knowledge of the rate constants and isotope effects for losses of nitrophenols (Section 2.4), the main loss is expected to be through reaction with the HO radical. This reaction occurs through the electrophilic addition of the HO radical to the ring greater than 80 % of the time (Bejan et al., 2007). Since an HO radical is being added to the ring, fractionation can occur. The KIE for this reaction, however, has not yet been studied. Other sources of error could be which source signature is used. The standard deviations of the source signatures used were often in the order of 1 ‰ (Rudolph et al., 2002). At a low PCA, when the product is not very processed, this difference will not have a large effect on the PCA determined; however, if the product is more aged, the slopes of the lines in Fig. 5.26 begin to plateau and a small difference in delta value can result in a large uncertainty in PCA.

Table 5.12. PCA determined for precursors and products that were sampled in parallel. The error is determined from the standard deviation of the source signature.

Filter Name	PCA x 10^{11} (s molec cm^{-3})		
	Toluene[a]	3-me-4-NP	2-me-4-NP
X131109A	0.2 ± 0.3	0.8 ± 0.4	-0.3 ± 0.4
Q261009A	0.9 ± 0.3	NA	1.6 ± 0.5
Q271009A	1.8 ± 0.3	NA	-1.2 ± 0.3
Q281009A	1.8 ± 0.3	-0.7 ± 0.3	-1.2 ± 0.3

[a] Kornilova (2012)

Table 5.12 shows an overview of the PCA determined from precursors and products. Box and whisker plots are also shown for the PCA of the products in Fig. 5.27. Ideally, the PCA determined from the products should match that from the precursor if the product has an isotopic composition that is similar to the isotope ratio of the sum of all products formed. Apart from p,m-xylene and 2,6-dimethyl-4-nitrophenol, the PCA for

all the precursor-product pairs are within the same order of magnitude of each other (Table 5.13). The large discrepancy for 2,6-dimethyl-4-nitrophenol could be due to several reasons. Primarily, p,m-xylene could not be chromatographically separated and the PCA shown is for both compounds combined. The source signature of p,m-xylene can vary by ± 0.5 ‰, which can change the average PCA of 2,6-dimethyl-4-nitrophenol from -0.3 x 10^{11} s molec cm^{-3} to -0.07 x 10^{11} s molec cm^{-3}. Nevertheless, they are still negative values. This points out the significance of fractionation due to possible loss processes of secondary or intermediate products. Lastly, laboratory studies were not conducted and it is therefore not known if 2,6-dimethyl-4-nitrophenol has an isotope ratio that is representative of the sum of all products. This same reasoning applies to benzene and 4-nitrophenol. Nevertheless, it is observed that all of the phenols studied have a PCA that is biased since a fair amount are negative values, which cannot exist.

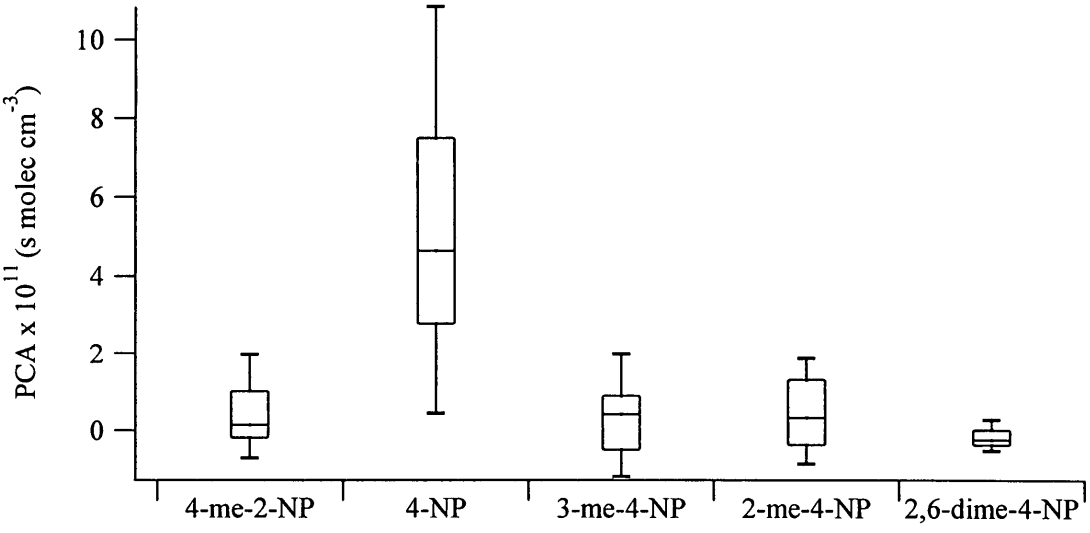

Figure 5.27. Box and whisker plots for the PCA of the target compounds. Error bars represent the 90th and 10th percentiles and the upper and lower ends of the box are the 75th and 25th percentiles. The horizontal line represents the median.

Table 5.13. Averages and errors of the mean of PCA for nitrophenols and their precursors calculated using the isotope hydrocarbon clock (Eq. 5.1). The number of data points used is shown in brackets.

Precursor	Average PCA[a] x 10^{11} (s molec cm^{-3})	Product	Average PCA x 10^{11} (s molec cm^{-3})
toluene	0.7 ± 0.1 (73)	4-me-2-NP	0.4 ± 0.2 (16)
		3-me-4-NP	0.4 ± 0.2 (46)
		2-me-4-NP	0.5 ± 0.1 (74)
benzene	2.2 ± 0.6 (43)	4-NP	5.2 ± 0.5 (63)
p,m-xylene	0.4 ± 0.1 (56)	2,6-dime-4-NP	-0.2 ± 0.1 (22)

[a] Kornilova (2012)

Tables 5.12 and 5.13 show PCA data for precursor and product pairs. Although there are only four samples total and one collecting both phases of products, the PCA determined are similar for half of the samples (X131109A and Q261009A). Negative PCA values are observed for both Q271009A and Q281009A. The only significant difference in weather and pollution data for these two days was that there was precipitation. This suggests that the PCA determined from product isotope ratios is biased. An overall trend is observed from Table 5.13 and Fig. 5.26. The products formed from the most reactive precursors show a PCA that is small and as reactivity of the precursors decrease the PCA increases with p,m-xylene being the most reactive and benzene being the least reactive. Figure 5.27 shows a box and whisker plot of the PCA of the product nitrophenols. The most aged phenol is 4-nitrophenol, perhaps due to the low reactivity of the benzene precursor and the relatively low rate constant for the loss process (Section 2.4) (Grosjean, 1991). The PCA of two isomers, 3-methyl-4-nitrophenol and 2-methyl-4-nitrophenol, were compared in Fig. 5.28. A correlation between the two isomers, within the uncertainty, exists and indicates that the photochemical history is similar; however, there is a substantial number of negative PCAs and the correlation between the PCAs does not follow a 1:1 dependence as expected from the simple concept of a methylnitrophenol isotope ratio that is identical to the isotope ratio of the sum of all products. It is unlikely that the nitrophenols are emitted from primary sources since their isotopic composition is depleted in ^{13}C. Since combustion temperatures are high from transportation sources, a kinetic isotope effect would not be observed.

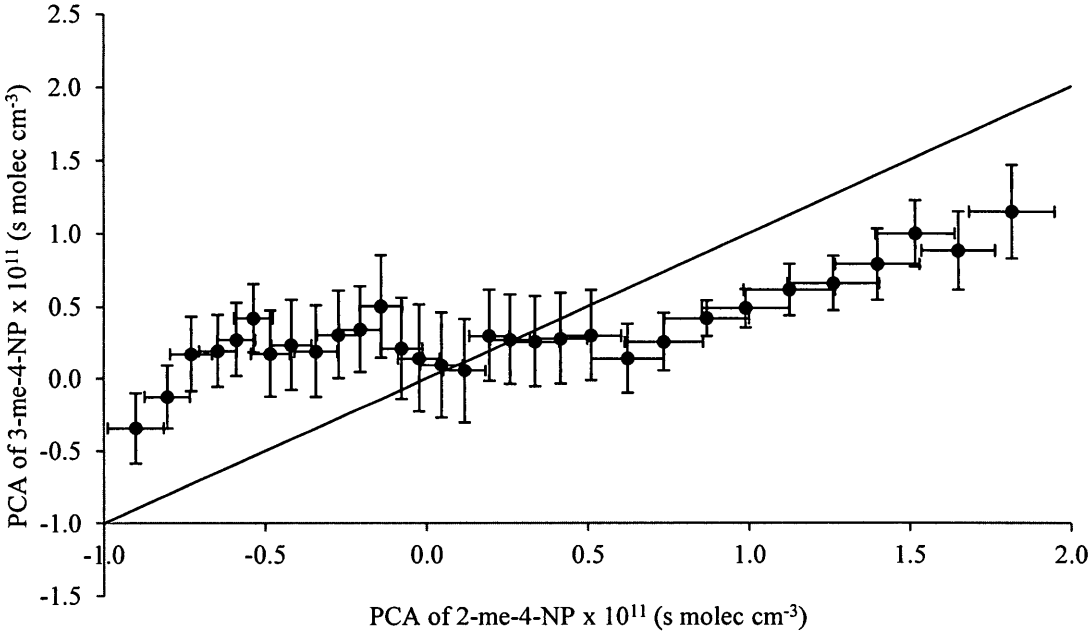

Figure 5.28. Plot of the relationship in PCA of 3-methyl-4-nitrophenol and 2-methyl-4-nitrophenol. 2-methyl-4-nitrophenol PCA were sorted and each point is a running average of 10 points. The error bars in each direction are the errors of the means; the solid line is a 1:1 line.

5.7.2. PCA with Adjustments from Possible Additional Fractionation

Previously, the only fractionation that was taken into account for the formation of nitrophenols (Section 2.1) was for the initial precursor reaction with HO. However, given the considerable number of negative PCA found using product isotope ratios, it was thought that further fractionation could be occurring. For methylnitrophenol formation, the cresol intermediate goes through an HO addition step 92 % of the time (Atkinson et al., 1980). This can induce fractionation, which can further deplete the products formed in ^{13}C. Moreover, loss reactions for nitrophenols also can influence the isotope ratios.

This complex dependence between processing and isotope ratio can be described by a reaction scheme that considers rate constants as well as KIEs. Table 5.14 shows the parameters used for the determination of PCA of products. Results using the parameters listed in Table 5.14 are shown in Fig. 5.29.

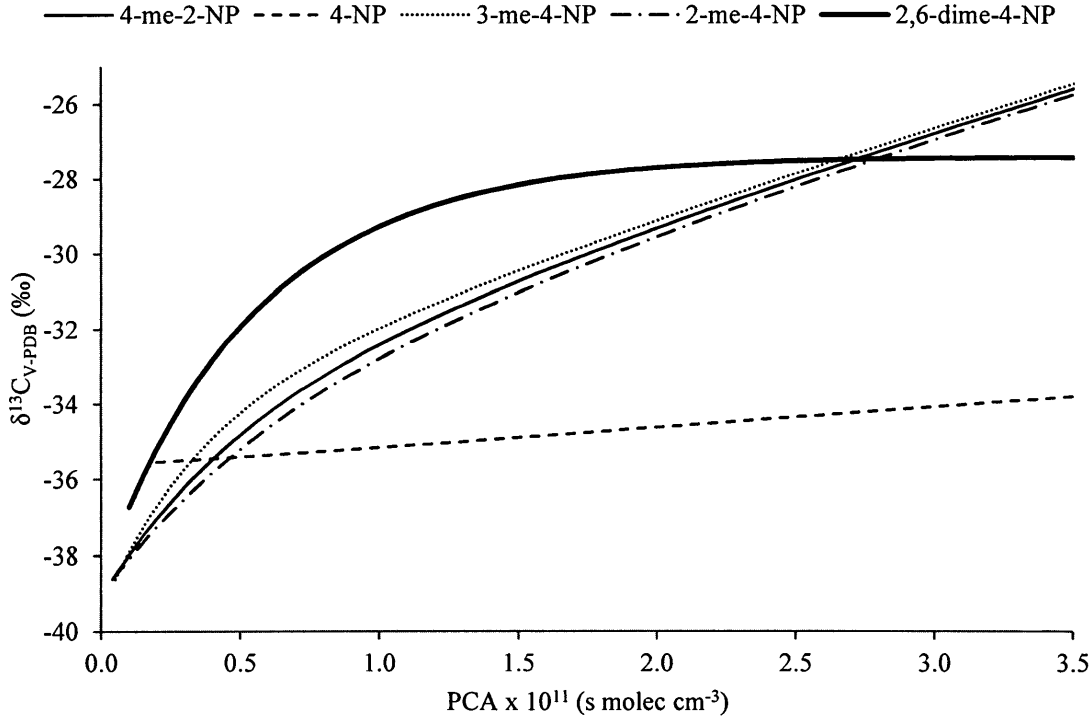

Figure 5.29. Plot of the carbon isotope ratios as a function of PCA for target compounds using parameters in Table 5.14.

Table 5.14. Parameters used to determine the PCA of products. Units of k (rate constant) are in cm^3 molec $^{-1}$ s^{-1}. Since 80 % of the phenols are in the gas phase, the rate constant for the product loss was adjusted to 80 % of the value.

Precursor			Intermediate			Product (Gas + PM)		
	k^a	5.63×10^{-12}		k^a	5.0×10^{-11}		k^g	2.87×10^{-12}
toluene	$\varepsilon_{HO}{}^b$ (‰)	5.95	4-me-ph	$\varepsilon_{HO}{}^d$ (‰)	5.47	4-me-2-NP	$\varepsilon_{HO}{}^h$ (‰)	5.95
	$\delta^{13}C_0{}^c$ (‰)	-27.6						
	k^a	1.39×10^{-12}		k^a	2.70×10^{-11}		k^i	3.40×10^{-13}
benzene	$\varepsilon_{HO}{}^b$ (‰)	7.83	phenol	$\varepsilon_{HO}{}^e$ (‰)	0	4-NP	$\varepsilon_{HO}{}^j$ (‰)	5.36
	$\delta^{13}C_0{}^c$ (‰)	-27.98						
	k^a	5.63×10^{-12}		k^a	6.8×10^{-11}		k^k	2.72×10^{-12}
toluene	$\varepsilon_{HO}{}^b$ (‰)	5.95	3-me-ph	$\varepsilon_{HO}{}^d$ (‰)	5.47	3-me-4-NP	$\varepsilon_{HO}{}^h$ (‰)	5.95
	$\delta^{13}C_0{}^c$ (‰)	-27.6						
	k^a	5.63×10^{-12}		k^a	4.1×10^{-11}		k^l	2.87×10^{-12}
toluene	$\varepsilon_{HO}{}^b$ (‰)	5.95	2-me-ph	$\varepsilon_{HO}{}^d$ (‰)	5.47	2-me-4-NP	$\varepsilon_{HO}{}^h$ (‰)	5.95
	$\delta^{13}C_0{}^c$ (‰)	-27.6						
	k^a	2.31×10^{-11}		k^f	6.59×10^{-11}		k^m	0
m-xylene	$\varepsilon_{HO}{}^b$ (‰)	4.83	2,6-dime-ph	$\varepsilon_{HO}{}^d$ (‰)	4.83	2,6-dime-4-NP	$\varepsilon_{HO}{}^m$ (‰)	0
	$\delta^{13}C_0{}^c$ (‰)	-27.4						

[a] Calvert et al., 2002
[b] Anderson, 2005
[c] Rudolph et al., 2002
[d] Proceeds through addition pathway 92 % of time (5.95x0.92) (Atkinson et al., 1980)
[e] Reaction occurs via HO abstraction (Atkinson et al., 1992)
[f] Atkinson and Aschmann, 1990
[g] Bejan et al., 2007
[h] Assumed to have same ε as toluene
[i] Grosjean, 1991
[j] Loss reaction proceeds mostly by addition pathway (Grosjean, 1991); Assumed to be 90 % of ε of toluene (0.9x5.95)
[k] Rate constant assumed to the average of the rate constant of 3-me-2-NP (3.69×10^{12} cm^3 $molec^{-1}$ s^{-1}) and 4-me-2-NP
[l] Same rate constant as 4-me-2-NP
[m] Assumed to have no loss reaction

The parameters listed in Table 5.14 have a large uncertainty since many assumptions had to be made due to the lack of data measured in laboratory experiments. The KIE of many of the species were based on assumptions. For example, the KIE for the reaction of methylnitrophenols is not known with the HO radical, but since the loss reaction will most likely proceed through an HO addition to the ring, the KIE was assumed to be a percentage of that of the KIE of toluene determined by the probability of a reaction at a carbon atom. Furthermore, the rate constants for some of the products are not known. Based on the structure of the molecule, the rate constants were estimated relative to known rate constants. 3-methyl-4-nitrophenol was assumed to be more reactive than 3-methyl-2-nitrophenol and less reactive than 4-methyl-2-nitrophenol because of the location of the substituents on the ring. 3-methyl-4-nitrophenol has the methyl, nitro and hydroxyl group directing reaction at carbon six. One of the most uncertain assumptions that was made was that there are no loss reactions for 2,6-dimethyl-4-nitrophenol. This is because the nitro and hydroxyl groups direct reactions towards positions that already have substituents on them. Furthermore, it was assumed that nitrophenols in PM do not undergo reactions that result in isotope fractionation since the HO reaction should occur only in the gas phase and consequently, the rate constant for the loss rate of the phenols in the gas phase and PM was adjusted to 80 % of its theoretical value. It was also assumed that nitrophenols in the gas phase are in isotopic equilibrium with nitrophenols in PM.

From Fig. 5.29, it is seen that the isomers formed by photooxidation of toluene show a very similar predicted dependence between PCA and isotope ratio while the

dependencies for 4-nitrophenol and 2,6-dimethyl-4-nitrophenol differ substantially. These two compounds are formed from the least reactive and most reactive species, respectively. The isotope ratio of 2,6-dimethyl-4-nitrophenol changes rapidly at low PCA and quickly comes to a plateau. 4-nitrophenol on the other hand was found to have an isotope ratio that is much less sensitive to a change in PCA. In fact, a small uncertainty in its isotope ratio could present a large uncertainty in PCA.

The following set of equations (Eq. 5.2, 5.3, 5.4 and 5.5) are the differential equations used to determine the isotope ratio of the product at varying PCAs. A look-up table was created for each of the target compounds and is shown in Appendix G.

$$\delta^{13}C_{prod} = \left(\frac{^{13}C}{^{12}C}\right)prod - 1 \times 1000\ ‰ \qquad \text{Eq. 5.2}$$

Here, $^{12}C_{prod/int/pre}$ and $^{13}C_{prod/int/pre}$ are the concentrations of each of the ^{12}C and ^{13}C isotopologues of the product, intermediate and precursor, respectively.

$$d^{12}C_{prod} = -^{12}C_{prod}[HO]dt + {}^{12}C_{int}[HO]dt \qquad \text{Eq. 5.3a}$$

$$d^{13}C_{prod} = -^{13}C_{prod}[HO]dt + {}^{13}C_{int}[HO]dt \qquad \text{Eq. 5.3b}$$

$$d^{12}C_{int} = -^{12}C_{int}[HO]dt + {}^{12}C_{pre}[HO]dt \qquad \text{Eq. 5.4a}$$

$$d^{13}C_{int} = -^{13}C_{int}[HO]dt + {}^{13}C_{pre}[HO]dt \qquad \text{Eq. 5.4b}$$

$$d^{12}C_{pre} = -^{12}C_{pre}[HO]dt \qquad \text{Eq. 5.5a}$$

$$d^{12}C_{pre} = -^{12}C_{pre}[HO]dt \qquad \text{Eq. 5.5b}$$

Here, $^{12}C_{prod/int/pre}$ and $^{13}C_{prod/int/pre}$ are the concentrations of the ^{12}C and ^{13}C isotopologues of the product, intermediate and precursor, respectively and [HO] is the hydroxyl radical concentration.

A box and whisker plot of PCAs is shown in Fig. 5.30. The PCAs were determined using a revised look-up table of isotope ratios as a function of PCAs calculated from Eq. 5.2, 5.3 and 5.4 and using values listed in Table 5.14. Although a similar pattern is shown as in Fig. 5.27, the absence of a significant number of negative values gives a more realistic representation in Fig. 5.30.

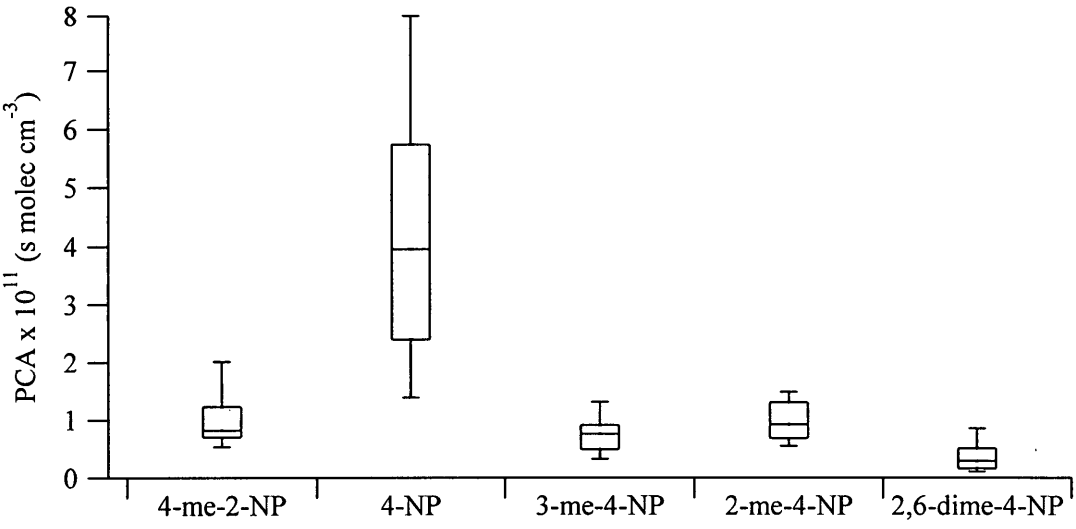

Figure 5.30. Box and whisker plots for the PCA of the target compounds using Eq. 5.2, 5.3. 5.4 and 5.5. Error bars represent the 90th and 10th percentiles and the upper and lower ends of the box are the 75th and 25th percentiles. The horizontal line represents the median.

Table 5.15. Averages and errors of the mean of PCA for nitrophenols and their precursors calculated using the isotope hydrocarbon clock and parameters listed in Table 5.14. The number of data points used is shown in brackets.

Precursor	Average PCA[a] x 10^{11} (s molec cm^{-3})	Product	Average PCA x 10^{11} (s molec cm^{-3})
toluene	0.7 ± 0.1 (73)	4-me-2-NP	0.8 ± 0.1 (16)
		3-me-4-NP	0.8 ± 0.1 (46)
		2-me-4-NP	0.9 ± 0.1 (74)
benzene	2.2 ± 0.6 (43)	4-NP	4.3 ± 0.3 (63)
p,m-xylene	0.4 ± 0.1 (56)	2,6-dime-4-NP	0.3 ± 0.1 (22)

[a] Kornilova (2012)

Table 5.15 shows a comparison of PCA determined from precursors by Kornilova (2012) with values determined from reaction products using the values in Table 5.14. The values shown are significantly more consistent than those derived from the simplified concept applied in Section 5.7.1. For toluene and the methylnitrophenols as well as for xylene and 2,6-dimethyl-4-nitrophenol, the PCAs are consistent within their estimated uncertainty. PCAs derived from products of VOC oxidation show a similar dependence of reactivity of the reactant as found for PCAs derived from precursor isotope ratio as observed by Kornilova (2012). This is most likely due to similar reasons, namely that for precursor VOC with lower reactivity contributions from air masses with aged VOC will have more weight. The discrepancy between benzene and 4-nitrophenol has narrowed but is still present. It is unlikely that this is due to the uncertainty in the KIE for 4-nitrophenol

loss. Changing the KIE for the loss reaction of 4-nitrophenol does not effectively change the PCA and while using a KIE similar to that of benzene rather than toluene, which is a KIE that is approximately 2 ‰ greater, lowers the average PCA of 4-nitrophenol only to 4.1 x 10^{11} s molec cm^{-3} and introducing a KIE for the intermediate step would increase the PCA of 4-nitrophenol. The reason for this difference could be due to the uncertainty of the source. A decrease in the source isotope ratio by 1 ‰ decreases the PCA by approximately 60 % for a product isotope ratio of -34 ‰ and by approximately 30 % for a product isotope ratio of -32 ‰. If the source signature was increased to -27 ‰, the average 4-nitrophenol PCA would be lowered to 2.7 x 10^{11} s molec cm^{-3} with an error of the mean of 0.4 x 10^{11} s molec cm^{-3}.

Figure 5.31 is a modification of Fig. 5.28, which includes adjustments from additional fractionation. For values of low PCA (less than 0.8 x 10^{11} s molec cm^{-3}), the PCAs of the isomers fit the expectation and lie on the 1:1 line. At larger PCA, all PCA lie below the 1:1 line, indicating that there may be something that is not fully understood regarding the processing of these compounds. The rate constant estimated for the loss reaction of 2-methyl-4-nitrophenol was thought to be lower than assumed in Table 5.14 and was therefore adjusted to 50 % of its value and compared in Fig. 5.32. The data is fitted better to the line and the discrepancies observed are most likely within the uncertainty of the measurement.

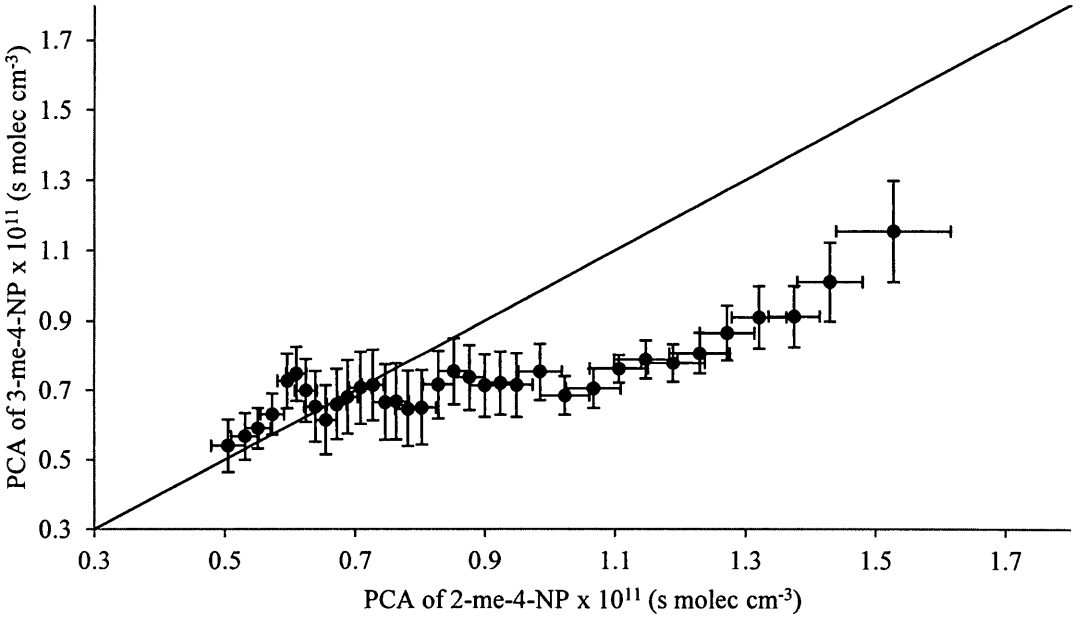

Figure 5.31. Plot of the relationship in PCA of 3-methyl-4-nitrophenol and 2-methyl-4-nitrophenol with adjustments of from possible additional fractionation. Here, the loss rate constant of 2-methyl-4-nitrophenol is assumed to be the same as that of 4-methyl-2-nitrophenol. 2-methyl-4-nitrophenol PCA were sorted and each point is a running average of 10 points. The error bars are the errors of the means. The solid line is a 1:1 line.

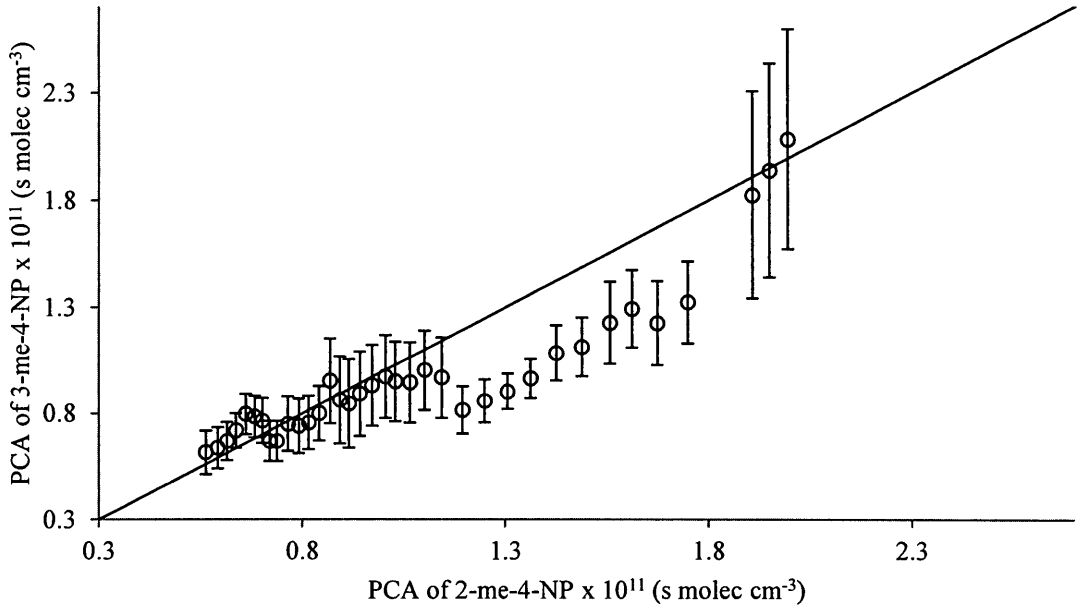

Figure 5.32. Plot of the relationship in PCA of 3-methyl-4-nitrophenol and 2-methyl-4-nitrophenol with adjustments of from possible additional fractionation. Here, the loss rate constant for 2-methyl-4-nitrophenol is assumed to be half of that of 4-methyl-2-nitrophenol. 2-methyl-4-nitrophenol PCA were sorted and each point is a running average of 10 points. The error bars are the errors of the means. The solid line is a 1:1 line.

5.7.3. Determination of the Reaction Coordinate and Ambient Yields

The PCA of a species in combination with ambient concentration measurements can be applied to determine ambient yields (Section 2.10). It was shown in Section 5.7.2 that although methylnitrophenols have been shown in laboratory studies to have an isotope ratio that is similar to the isotope ratio of the sum of all products (Fig. 5.25), their isotopic composition cannot necessarily be traced back to the precursor and the possibility of additional fractionation needs to be considered. Figure 5.33 shows how the reaction coordinate, F, changes with PCA for different compounds. The reaction

coordinate is calculated using principles described in Section 2.10. Specifically, Eq. 2.13 and 2.14 will be used. Since these equations only take the fractionation from the precursor only into account, the yields found are the upper limits.

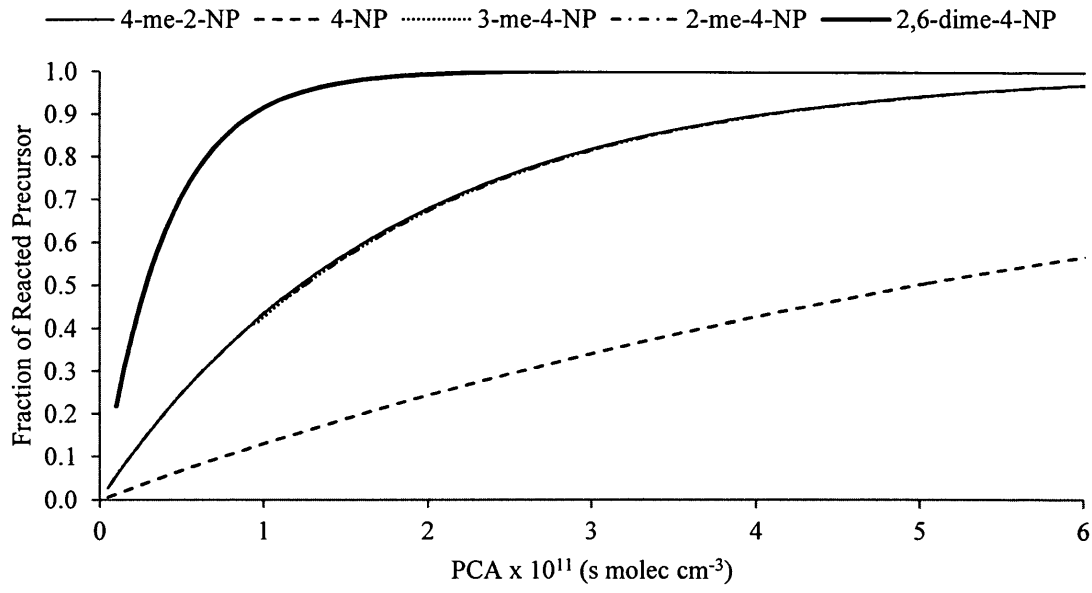

Figure 5.33. Plot of the fraction of precursor reacted (F) as a function of PCA.

Table 5.16. Parameters used for calculating the reaction coordinate, F.

Precursor	$\delta^{13}C_0^{pre} \pm$ SD (‰)[a]	$\varepsilon \pm$ SD (‰)[b]
toluene	-27.6 ± 0.6	5.95 ± 0.28
benzene	-28.0 ± 1.1	7.83 ± 0.42
p,m-xylene	-27.4 ± 0.5	4.83 ± 0.05

[a] Rudolph et al., 2002; [b] Anderson, 2005

Table 5.17. Parameters for the calculation of F (extent of processing) and the comparison of calculated F values using Eq. 2.13 and Eq. 2.14 for parallel sampling and for F determined from the PCA (Fig. 5.32). Each of the ambient precursor and product isotope ratios have uncertainties of ± 0.3 ‰ and the uncertainty for each F value is ± 0.1. SD is the standard deviation of the measurement.

Filter Name	$\delta^{13}C_t^{pre}$ (‰)[b]	$\delta^{13}C_t^{2me4NP}$ (‰)	$\delta^{13}C_t^{3me4NP}$ (‰)	F (Eq. 2.13)	F (Eq. 2.14)		F (PCA)	
					2-me-4-NP	3-me-4-NP	2-me-4-NP	3-me-4-NP
X131109A	-26.7	-33.9	-32.3	0.14	0.12	0.16	0.34	0.40
Q261009A	-24.3	-31.3	-	0.43	0.48	-	0.69	-
Q271009A	-21.1	-35.5	-	0.67	0.45	-	0.25	-
Q281009A	-21.3	-35.4	-34.6	0.65	0.45	0.47	0.27	0.25

[a] Rudolph et al., 2002; [b] Kornilova, 2012; [c] Anderson, 2005

There were four occasions in which parallel sampling was conducted for both products and precursors. Precursor sampling and analysis was done by Kornilova (2012) at the Dufferin St. location of Environment Canada and product sampling was done at York University. F was calculated on these four occasions using both Eq. 2.13 and 2.14 and parameters listed in Table 5.16 with results compared in Table 5.17. As previously mentioned, only one of the four samples collected both gas and PM. When comparing the F values found through calculations using Eq. 2.13 and Eq. 2.14, they agreed very well. The processing was found to be minimal as both product and precursor were found to be freshly emitted or freshly formed and had F values of approximately 0.1. There were some differences when comparing two of the PM samples with the precursors, but can be considered to be within the uncertainty of the F calculation. The F values found using the PCA did not agree and was significantly different for specific compounds.

The sampling location of the precursors at Environment Canada is approximately 3 km east of the sampling location of the products at York University. Environment Canada is located on Dufferin St. and the sampling site at York University is approximately 500 m from the closest major street, Steeles Ave. West. Both streets can accommodate the passage of thousands of cars per hour. If there is a sampling bias due to the domination of fresh emissions due to sampling site location, it would be expected that reaction coordinates calculated from precursor data would be smaller than those calculated from product data. This is not the case that is observed in Table 5.17 and cannot explain the discrepancies.

Table 5.18. Calculated F values based on averaged isotopic composition of nitrophenols (gas phase + PM) and comparison to predicted F values from reactants. SEM is the standard error of the mean. The uncertainty for each F value is ± 0.1.

Precursor	Product	$\delta^{13}C_t^{pre}$ ± SEM (‰)[b]	$\delta^{13}C_t^{prod}$ ± SEM (‰)	F (Eq. 2.13)	F (Eq. 2.14)	F (PCA)
toluene	4-me-2-NP	-24.8 ± 0.4	-32.8 ± 0.4	0.38	0.35	0.40
	3-me-4-NP		-33.1 ± 0.3		0.34	0.38
	2-me-4-NP		-32.7 ± 0.3		0.35	0.43
benzene	4-NP	-25.0 ± 0.5	-33.5 ± 0.3	0.32	0.35	0.43
p,m-xylene	2,6-dime-4-NP	-24.1 ± 0.8	-33.4 ± 0.5	0.50	0.36	0.50

[a] Rudolph et al., 2002; [b] Kornilova, 2012; [c] Anderson, 2005

The isotope ratios of ambient precursors (Kornilova, 2012) and products were averaged to study the extent of VOC processing in Toronto (Table 5.18). When comparing the F values calculated from precursors (Eq. 2.13) with those from products

(Eq. 2.14), the results are very similar for the toluene and benzene precursor-product pairs. The result for m-xylene differs from its product's F value but is similar to the F value derived from PCA. This is expected to be due to the fractionation of the intermediate, 2,6-dimethylphenol. The F values calculated from the PCA also agree with all product and precursor pairs, within the uncertainty of ± 0.1.

The ambient yields of the target compounds were finally calculated by using concentration measurements in conjunction with isotope ratio measurements (Table 5.19). With known precursor mixing ratios and isotope ratios from Kornilova (2012), the amount of precursor processed could be calculated. Yields calculated using F values from Eq. 2.14, considered to be the upper limit of the yields and the PCA derived yields are quite similar. It should be noted that the yields found from laboratory studies are the yields in PM and gas phase yields are unknown. Nevertheless, in all cases, the ambient yields are significantly lower, and often, orders of magnitudes lower than the predicted yields. The lower yields could possibly be due to significantly lower ambient NO_x mixing ratios, which are in the ppb range when compared to laboratory studies which use ppm levels.

Table 5.19. Ambient yields of target compounds. Precursor mixing ratios and product average concentrations and isotope ratios are ± the standard errors of the means; ambient yields are ± the uncertainty of the yield. The ambient yields in each phase was found using the reaction coordinate, F, calculated from both Eq. 2.14 and using the PCA.

Product	Laboratory Yield (%)	Precursor	Average Precursor Mixing Ratio (ppbv)	Gas + PM			PM		
				Avg. Conc. (ng m^{-3})	Ambient Yield (%)		Avg. Conc. (ng m^{-3})	Ambient Yield (%)	
					Eq. 2.14	PCA		Eq. 2.14	PCA
4-me-2-NP	4.4[a]	toluene	0.70 ± 0.06	2.78 ± 0.89	0.12 ± 0.03	0.12 ± 0.03	0.06 ± 0.02	0.003 ± 0.002	0.002 ± 0.001
3-me-4-NP	6.8[a], 0.096[b]			1.09 ± 0.23	0.05 ± 0.01	0.05 ± 0.01	0.23 ± 0.06	0.010 ± 0.004	0.007 ± 0.002
2-me-4-NP	10[a], 16.3[b]			3.22 ± 0.46	0.14 ± 0.04	0.14 ± 0.04	0.48 ± 0.10	0.02 ± 0.01	0.012 ± 0.002
4-NP	-	benzene	0.13 ± 0.01	6.88 ± 1.10	1.73 ± 0.05	1.23 ± 0.24	0.80 ± 0.14	0.20 ± 0.10	0.12 ± 0.03
2,6-dime-4-NP	3.3[a]	m-xylene	0.17 ± 0.02[c]	1.06 ± 0.22	0.16 ± 0.01	0.09 ± 0.02	0.07 ± 0.02	0.010 ± 0.003	0.009 ± 0.003

[a] Forstner et al., 1997; [b] Irei, 2008; [c] mixing ratio of p,m-xylene

6. Conclusion

A method has been developed for the analysis of nitrophenols in the gas phase and PM. This method, originally developed by Moukhtar et al. (2011), was modified to analyze a larger group of target compounds. Furthermore, a method to collect gas and particle phase nitrophenols for concentration measurements on SIFs (Busca, 2010) was adapted to allow isotope ratio measurements. The goal of this was to gain insight into the chemical processing of SOA in the atmosphere, a topic that there is little known about. Gas phase and PM samples were collected using XAD-coated filters and PM samples alone were collected using quartz filters.

The method developed was found to be a precise and accurate method with a precision of 5 % with a detection limit in the pg m^{-3} range for concentration measurements by GC-MS. For atmospheric conditions exceeding nitrophenol concentrations of 0.1 ng m^{-3}, a precision of 0.3 ‰ for isotope ratio measurements by GC-IRMS was achieved. Several method evaluation tests, including sampling test, storage tests, and recovery tests have validated the use of the method. The extensive extraction procedure used gave an overall recovery of phenols between 50 % and 70 % but was consistent over all target compounds. From the tests, it was concluded that the determination of isotope ratios had a bias of 0.1 ‰ or less.

An artifact, confirmed to be from the solvent used, acetonitrile, contaminated samples between 2010 and 2011. The contamination was found to mainly be present when the derivatizing agent, BSTFA, was used and was also found to be pH dependent.

Modifications to the procedure, including increasing the pH prior to the SPE step from 2 to 5 and substituting the previously used acetonitrile Chromasolv® with acetonitrile Pestanal®, significantly decreased the size and impact of the contamination. Filters that were contaminated with this artifact were not used for isotope ratio analysis.

Modifications to the filter coating procedure with an XAD resin improved the filter efficiency from approximately 60 % to approximately 80 % or better. Overall, concentration measurements were made for a total of 162 ambient samples, 115 of which were PM samples and 47 were gas phase and PM samples. Of these, 86 samples were successfully used for isotope ratio analysis; 44 of which were PM samples and 42 were gas phase and PM samples. These samples allowed for the characterization of nitrophenols in a suburban region of a major metropolitan area. Concentration measurements were found to be in the sub to low ng m^{-3} range. The isotope ratio of the nitrophenols in this area showed that they are formed predominantly from secondary processes, in agreement with what is proposed in laboratory studies.

The collection of both PM samples alone and gas phase and PM samples together allowed gaining additional insight into the partitioning of the nitrophenols in ambient air. Consistent with results from samples collected using denuders and low volume filter packs (Facca, 2013), the majority of nitrophenols (greater than 80 %) were confirmed to be in the gas phase in the Toronto area. A high correlation between gas phase and particle phase nitrophenols was observed. This was most likely due to mixing and an equilibrium existing between the two phases. Nitrophenols in both phases seemed to have the same

effect with temperature, having lowest concentrations at highest temperatures, but for different reasons. The partitioning of nitrophenols in PM into the gas phase explained this for PM phenols but the decrease in gas phase concentration was perhaps due to the increased boundary layer height and in turn, the dilution of nitrophenols during the summer.

Expectedly so, nitrophenol concentrations increased with increasing NO_2 and PM2.5 concentrations. The correlation with NO_2 is most likely due to the collocation of emissions with alkylbenzenes, which are both precursors for nitrophenol formation.

Measured ambient isotope ratios of nitrophenols were compared with predictions from a simple model based on the assumption that the nitrophenol isotope ratios represent the average isotope ratios of all reaction products. From the comparison it was concluded that this simple model cannot explain the lower end measured isotope ratios. A more detailed model considering isotope fractionation of the reactions of intermediates in the reaction sequence and isotope fractionation for loss reactions of nitrophenols gave a much better agreement. PCA determined using the more detailed model showed good agreement with PCA derived from ambient isotope ratio measurement of the precursor VOC.

Ambient yields, calculated using the reaction coordinate found from isotope ratios and PCA, were found to be significantly lower, often orders of magnitude lower, than predicted from laboratory studies. This shows that laboratory studies cannot necessarily be quantitatively extrapolated to the atmosphere.

This research project achieved the goal of gaining a deeper understanding of the chemical processing of SOA in the atmosphere. The combination of concentration and isotope ratio measurements allows one to know if the species is a primary emission or a secondary product, how long the species has been processed in the atmosphere and what its ambient yield is. This information could not be determined from using concentration measurements alone. This method allows for the possibility to investigate other secondary products, provided that they are formed specifically from one precursor.

Extensive studies should be conducted such as the simultaneous sampling of precursors, intermediates and products in both phases for concentration and isotope ratio measurements. Increasing the sample set size of both PM and gas phase and PM measurements should be done to have a better comparison of possible differences in isotope composition between phases due to isotope effects. Laboratory studies looking into the fractionation and KIE of different multi-step reaction mechanism should be conducted to reduce the uncertainty of the PCA that are calculated.

References

Allison, C.E., Francey, R.J., Meijer, H.A.J.: Recommendations for the reporting of stable isotope measurements of carbon and oxygen in CO_2 gas, in: Reference and intercomparison materials for stable isotopes of light elements, Int. At. Energy Agency, Vienna, 155-162, 1995.

Anderson, R.S.: Carbon kinetic isotope effects in the gas-phase reactions of nonmethane hydrocarbons with hydroxyl radicals and chlorine atoms, Ph.D. thesis, York University, Toronto, ON, 2005.

Andino, J.M., Smith, J.N., Flagan, R.C., Goddard, W.A., III, Seinfeld, J.H.: Mechanism of atmospheric photooxidation of aromatics: a theoretical study, J. Phys. Chem., 100, 10967-10980, 1996.

Atkinson, R.: Gas-phase tropospheric chemistry of organic compounds, J. Phys. Chem. Ref. Data, 2, 1-216, 1994.

Atkinson, R.: Atmospheric chemistry of VOCs and NO_x, Atmos. Environ., 34, 2063-2101, 2000.

Atkinson, R. and Aschmann, S.M.: Rate constants for the gas-phase reactions of the OH radical with the cresols and dimethylphenols at 296 ± 2 K, Int. J. Chem. Kinet., 22, 59-67, 1990.

Atkinson, R., Carter, W.P.L., Darnall, K.R., Winer, A.M., Pitts, J.N. Jr.: A smog chamber and modeling study of the gas phase NO_x-air photooxidation of toluene and the cresols, Int. J. Chem. Kinet., 12, 779-836, 1980.

Atkinson, R., Aschmann, S.M., Arey, J.: Reactions of OH and NO_3 radicals with phenol, cresols, and 2-nitrophenol at 296 ± 2 K, Envion. Sci. & Technol., 26, 1397-1403, 1992.

Bejan, I., Barnes, I., Olariu, R., Zhou, S., Wiesen, P., Benter, T.: Investigations on the gas-phase photolysis and OH radical kinetics of methyl-2-nitrophenols, Phys. Chem. Chem. Phys., 9, 5686-5692, 2007.

Bennett, J.: Flow reactor studies of aromatic hydrocarbon photo-oxidation products using on-line gas/particle separation and MS-MS analysis, Ph.D. thesis, York University, Toronto, ON, 2010.

Bolzacchini, E., Bruschi, M., Hjorth, J., Meinardi, S., Orlandi, M., Rindone, B., Rosenbohm, E.: Gas-phase reaction of phenol with NO_3, Envion. Sci & Technol., 35, 1791-1797, 2001.

Bruce, R.M., Santodonato, J., Neal, M.W.: Summary review of the health effects associated with phenol, Toxicol. Ind. Health., 3, 535-568, 1987.

Brunauer, S., Emmett, P.H., Teller, E.: Adsorption of gases in multimolecular layers, J. Amer. Chem. Soc., 60, 309-319, 1938.

Busca, R.: Method development for the sampling and analysis of atmospheric nitrophenols, M.S. thesis, York University, Toronto, ON, 2010.

Calvert, J.G., Atkinson, R., Becker, K.H., Kamens, R.M., Seinfeld, J.H., Wallington, T.J., Yarwood, G.: The mechanisms of atmospheric oxidation of aromatic hydrocarbons, Oxford University Press, New York, United States of America, 2002.

Carter, W.P.L.: A detailed mechanism for the gas-phase atmospheric reactions of organic compounds, Atmos. Environ., 24A, 481-518, 1990.

Cecinato, A., Di Palo, V., Pomata, D., Scianò, M., Possanzini, M.: Measurement of phase-distributed nitrophenols in Rome ambient air, Chemosphere, 59, 679-683, 2005.

Chow, J.: Measurement methods to determine compliance with ambient air quality standards for suspended particles, J. Air Waste. Manage., 45, 320-382, 1995.

Craig, H.: Isotopic standards for carbon and oxygen and correction factors for mass-spectrometric analysis of carbon dioxide, Geochem. Cosmo. Acta, 12, 133-149, 1957.

CRC Handbook of Chemistry and Physics, 93rd edition, CRC Press, Boca Raton, FL 2013.

Czapiewski, K., Czuba, E., Huang, L., Ernst, D., Norman, A.L., Koppmann, R., Rudolph, J.: 2002. Isotopic composition of non-methane hydrocarbons in emissions from biomass burning, J. Atmos. Chem., 43, 45-60, 2002.

Czuba, E.: Development of a technique to study stable carbon isotope composition of NMHCs in ambient air, M.S. thesis, York University, Toronto, ON, 2000.

Derwent, R.G., Davies, T.J., Delaney, M., Dollard, G.J., Field, R.A., Dumitrean, P., Nason, P.D., Jones, B.M.R., Pepler, S.A.: Analysis and interpretation of the continuous hourly monitoring data for C_2-C_8 hydrocarbons at 12 United Kingdom sites during 1996, Atmos. Environ., 34, 297-312, 2000.

Dockery, D.W., Pope, A., Xu, X., Spengler, J.D., Ware, J.H., Fay, M.E., Ferris, B.G. Jr., Speizer, F.E.: An association between air pollution and mortality in six U.S. cities, New Engl. J. Med., 329, 1753-1759, 1993.

Environment Canada: Historical Weather Data, Toronto North York Site, http://climate.weather.gc.ca, Accessed August 30, 2012[a].

Environment Canada: Volatile Organic Compounds, Main Emission Sources, http://www.ec.gc.ca/air/default.asp?lang=En&n=D130165D-1, Date modified: May 23, 2012[b].

Facca, C.: Method development of a denuder based technique for the determination of the partitioning of nitrophenols, M.S. thesis, York University, Toronto, ON, 2013.

Finlayson-Pitts, B.J. and Pitts, J.N., Jr.: Chemistry of the upper and lower atmosphere, Academic Press, California, United States of America, 2000.

Fisseha, R., Saurer, M., Jäggi, M., Siegwolf, R.T.W., Dommen, J., Szidat, S., Samburova, V., Baltensperger, U.: Determination of primary and secondary sources of organic acids and carbonaceous aerosols using stable carbon isotopes, Atmos. Environ., 43, 431-437, 2009[a].

Fisseha, R., Spahn, H., Wegener, R., Hohaus, T., Brasse, G., Wissel, H., Tillmann, R., Wahner, A., Koppmann, R., Kiendler-Scharr, A.: Stable carbon isotope composition of secondary organic aerosol from β-pinene oxidation, J. Geophys. Res., 114, D02304, 2009[b].

Forstner, H., Flagan, R. & Seinfeld, J.: Secondary organic aerosol from the photooxidation of atomatic hydrocarbons: molecular composition, Environ. Sci. & Technol., 31, 1345-1358, 1997.

Fuller, E.D., Schettler, P.D., Giddings, J.C.: A new method for prediction of binary gas-phase diffusion coefficients: Ind. Eng. Chem, 58, 19-27, 1966.

Galarneau, E., Harner, T., Shoeib, M., Kozma, M., Lane, D.: A preliminary investigation of sorbent-impregnated filters (SIFs) as an alternative to polyurethane foam (PUF) for sampling gas-phase semivolatile organic compounds in air, Atmos. Environ., 40, 5734-5740, 2006.

Goldstein, A. and Shaw, S.: Isotopes of volatile organic compounds: an emerging approach for studying atmospheric budgets and chemistry, Chem. Rev., 103, 5025-5048, 2003.

Gong, X.: private communication.

Grosjean, D.: Atmospheric reactions of ortho cresol: gas phase and aerosol products, Atmos. Environ., 18, 1641-1652, 1984.

Grosjean, D.: Atmospheric fate of toxic aromatic compounds, Sci. Total Environ., 100, 367-414, 1991.

Gundel, L. and Herring, S.V.: Absorbing filter media for denuder-filter sampling of total organic carbon in airborne particles, Record of invention WIB 1457, Lawrence Berkeley National Laboratory, United States of America, 1998.

Gundel, L. and Lane, D.: Sorbent-coated diffusion denuders for direct measurement of gas-particle partitioning by semi-volatile organic compounds, in: Lane, D.: Gas and particle phase measurements of atmospheric organic compounds, Gordon and Breach Science Publishers, Canada, 287-332, 1999.

Guo, H., Wang, T., Louie, P.K.K.: Source apportionment of ambient non-methane hydrocarbons in Hong Kong: Application of a principal component analysis/absolute principal component scores (PCA/APCS) receptor model, Environ. Pollut., 129, 489-498, 2004.

Hagerman, L.M., Aneja, V.P., Lonneman, W.A.: Charcterization of non-methane hydrocarbons in the rural southeast United States, Atmos. Environ., 31, 4017-4038, 1997.

Hamilton, J.F., Webb, P.J., Lewis, A.C., Reviejo, M.M.: Quantifying small molecules in secondary organic aerosol formed during the photo-oxidation of toluene with hydroxyl radicals, Atmos. Environ., 39, 7263-7275, 2005.

Hassani, Y.: Private communication.

Henze, D.K., Seinfeld, J.H., Ng, N.L., Kroll, J.H., Fu, T.-M., Jacob, D.J., Heald, C.L.: Global modeling of secondary organic aerosol formation from aromatic hydrocarbons: high- vs. low-yield pathways, Atmos. Chem. Phys., 8, 2405-2421, 2008.

Herterich. R. and Herrmann, R.: Comparing the distribution of nitrated phenols in the atmosphere of two German hill sites, Environ. Technol., 11, 961-972, 1990.

Huang, L., Chivulescu, A., Ernst, D., Zhang, W., Lee, Y.S.: Maintaining consistent traceability in high precision isotope measurements of CO_2: verifying atmospheric trends of $\delta^{13}C$, Atmos. Meas. Tech. Discuss., 5, 4003-4040, 2012.

Hunt, G. and Pangaro, N.: Potential contamination from the use of synthetic adsorbents in air sampling procedures, Anal. Chem., 54, 369-372, 1982.

Irei, S.: Laboratory studies of stable carbon isotope ratio of secondary particulate organic matter, Ph.D. thesis, York University, Toronto, ON, 2008.

Irei, S., Rudolph, J., Huang, L., Auld, J., Hastie, D.: Stable carbon isotope ratio of secondary particulate organic matter formed by photooxidation of toluene in indoor smog chamber, Atmos. Environ., 45, 856-862, 2011.

Irei, S., Rudolph, J., Huang, L.: Compound-specific stable carbon isotope ratios of phenols and nitrophenols derivatized with N,O-bis(trimethylsilyl)trifluoroacetamide, Anal. Chim. Acta, 786, 95-102, 2013.

Jang, M. and Kamens, R.M.: Characterization of secondary aerosol from the photooxidation of toluene in the presence of NO_x and 1-propene, Environ. Sci. & Technol., 35, 3626-3639, 2001.

Jobson, B.T., Parrish, D.D., Goldan, P., Kuster, W., Fehsenfeld, F.C., Blake, D.R., Blake, N.J., Niki, H.: Spatial and temporal variability of nonmethane hydrocarbon mixing ratios and their relation to photochemical lifetime, J. Geophys. Res., 103, 13,557-13,567, 1998.

Jobson, B.T., McKeen, S.A., Parrish, D.D., Fehsenfeld, F.C., Blake, D.R., Goldstein, A.H., Schauffler, S.M., Elkins, J.W.: Trace gas mixing ratio variability versus lifetime in the troposphere and stratosphere: Observations, J. Geophys. Res., 104, 16,091-16,113, 1999.

Junge, C.E.: Basic considerations about trace constituents in the atmosphere as related to the fate of global pollutants, Adv. Environ. Sci. Tech., 8, 7-25, 1977.

Kaye, J.A.: Isotope effects in gas-phase chemical reactions and photodissociation processes: Overview, in: Kaye, J.A.: Isotope effects in gas-phase chemistry, American Chemical Society, United States of America, 1-14, 1992.

Kennedy, D.C.: Macroreticular Polymeric Adsorbents, Ind. Eng. Chem. Prod. Res. Dev., 12, 56-61, 1973.

Kleinman, L.I., Daum, P.H., Lee, Y.N., Nunnermacker, L.J., Springston, S.R., Weinstein-Lloyd, J., Hyde, P., Doskey, P., Rudolph, J., Fast, J., Berkowit, C.: Photochemical age determinations in the Phoenix metropolitan area, J. Geophys. Res., 108, 4096, 2003.

Knapp, D.R.: Handbook of analytical derivatization reactions, John Wiley & Sons, New York, 1979.

Kornilova, A.: Stable carbon isotope composition of ambient VOC and its use in the determination of photochemical ages of air masses, Ph.D. thesis, York University, Toronto, ON, 2012.

Kornilova, A., Saccon, M., O'Brien, J.M., Huang, L., Rudolph, J.: Stable carbon isotope ratios and the photochemical age of atmospheric volatile organic compounds, Atmos. Ocean, 1-7, 2013.

Ku, Y. and Lee, K.C.: Removal of phenols from aqueous solution by XAD-4 resin, J. Hazard. Mater., 80, 59-68, 2000.

Lane, D.: Gas and particle phase measurements of atmospheric organic compounds, Gordon and Breach Science Publishers, Canada, 1999.

Lane, D.: private communication.

Lawrimore, J.H., Das, M., Aneja, V.P.: Vertical sampling and analysis of nonmethane hydrocarbons for ozone control in urban North Carolina, J. Geophys. Res., 100, 22,785-22,793, 1995.

Legreid, G., Reimann, S., Steinbacher, J., Staehelin, J., Young, D., Stemmler, K.: Measurements of OVOCs and NMHCs in a Swiss highway tunnel for estimation of road transport emissions, Environ. Sci. & Technol., 41, 7060-7066, 2007.

Li, Q., Wang, W., Zhang, H., Wang, J., Wang, B., Li, L., Li, H., Wang, B., Zhan, J., Wu, M., Bi, X.: Development of a compound-specific carbon isotope analysis of 2-methyltetrols, biomarkers for secondary organic aerosols from atmospheric isoprene, Anal. Chem., 82, 6767-6769, 2010.

Lüttke, J. and Levsen, K.: Phase partitioning of phenol and nitrophenols in clouds, Atmos. Environ. 31, 2649-2655, 1997.

Matthews, D. and Hayes, J.: Isotope-ratio-monitoring gas chromatography-mass spectrometry, Anal. Chem., 50, 1465-1473, 1978.

McKinney, C.R., McCrea, J.M., Epstein, S., Allen, H.A., Urey, H.C.: Improvements in mass spectrometers for the measurement of small differences in isotope abundance ratios, Rev. Sci. Instrum., 21, 724-730, 1950.

Morville, S., Scheyer, A., Mirabel, P., Millet, M.: A multiresidue method of the analysis of phenols and nitrophenols in the atmosphere, J. Environ. Monitor., 6, 963-966, 2004.

Moukhtar, S., Saccon, M., Kornilova, A., Irei, S., Huang, L., Rudolph, J.: Method for determination of stable carbon isotope ratio of methylnitrophenols in atmospheric particulate matter, Atmos. Meas. Tech., 4, 2453-2464, 2011.

Nishioka, M.G. and Lewtas, J.: Quantification of nitro- and hydroxylated nitro-aromatic/polycyclic aromatic hydrocarbons in selected ambient air daytime winter samples, Atmos. Environ., 26A, 2077-2087, 1992.

Nojima, K., Kawaguchi, A., Ohya, T., Kanno, S., Hirobe, M.: Studies on photochemical reaction of air pollutants. X.[1)] Identification of nitrophenols in suspended particulates, Chem. Pharm. Bull. 31, 1047-1051, 1983.

Ontario Ministry of the Environment: Historical Pollutant Data, Toronto North Site, http://www.airqualityontario.com/history/station.php?stationid=34020, Accessed August 30, 2012.

Pall Life Sciences: Pallflex® Filters, Emfab™, Fiberfilm™ and Tissuquartz™ filters, Product Data Sheet, Pall Life Sciences, Ann Arbor, United States of America, 2002.

Palm, W.U., Behnke, W., Zetzsch, C.: Are light-induced reactions of nitrophenols an efficient sink in atmospheric droplets?, in: Becker, K.H. and Angeletti, G.: Chemical mechanisms of atmospheric processes, Air Pollution Research Report 67, EUR 18765, European Communities, Luxembourg, 377-382, 1999.

Pankow, J.F.: An absorption model of gas/particle partitioning of organic compounds in the atmosphere, Atmos. Environ., 28, 185-188, 1994.

Pankow, J.F.: Fundamentals and mechanisms of gas/particle partitioning in the atmosphere, in: Lane, D.: Gas and particle phase measurements of atmospheric organic compounds, Gordon and Breach Science Publishers, Canada, 287-332, 1999.

Pankow, J.F., Luo, W., Bender, D.A., Isabelle, L.M., Hollingsworth, J.S., Chen, C., Asher, W.E., Zogorski, J.S.: Concentrations and co-occurrence correlations of 88 volatile organic compounds (VOCs) in the ambient air of 13 semi-rural to urban locations in the United States, Atmos. Environ., 37, 5023-5046, 2003.

Parrish, D.D., Hahn, C.J., Williams, E.J., Norton, R.B., Fehsenfeld, F.C., Singh, H.B., Shetter, J.D., Gandrud, B.W., Ridley, B.A.: Indications of photochemical histories of Pacific air masses from measurements of atmospheric trace species at Point Area, California, J. Geophys. Res., 97, 15,883-15,901, 1992.

Parrish, D.D., Stohl, A., Forster, C., Atlas, E.L., Blake, D.R., Goldan, P.D., Kuster, W.C., de Gouw, J.A.: Effects of mixing on evolution of hydrocarbon ratios in the troposphere, J. Geophys. Res., 112, D10S34, 2007.

Piccot, S.D., Watson, J.J., Jones, J.W.: A global inventory of volatile organic compound emissions from anthropogenic sources, J. Geophys. Res., 97, 9897-9912, 1992.

Pope, C.A. 3rd, Thun, M.J., Namboodiri, M.M., Dockery, D.W., Evans, J.S., Speizer, F.E., Heath, C.W., Jr.: Particulate air pollution as a predictor of mortality in a prospective study of U.S. adults, Am. J. Resp. Crit. Care., 151, 669-674, 1995.

Rice, A.L., Gotoh, A.A., Ajie, H.O., Tyler, S.C.: High-precision continuous-flow measurement of $\delta^{13}C$ and δD of atmospheric CH_4, Anal. Chem., 73, 4104-4110, 2001.

Rippen, G., Zietz, E., Frank, R., Knacker, T., Klöpffer, W.: Do airborne nitrophenols contribute to forest decline?, Environ. Technol. Lett., 8, 475-482, 1987.

Rohm and Haas Co.: Amberlite™ XAD-4 industrial grade polymeric adsorbent, Technical Bulletin, Rohm and Haas Co., Philadelphia, United States of America, 2001.

Rudolph, J.: Gas Chromatography-Isotope Ratio Mass Spectrometry, in: Koppmann, R.: Volatile organic compounds in the atmosphere, Blackwell Publishing Ltd, United Kingdom, 388-466, 2007.

Rudolph, J. and Czuba, E.: On the use of isotopic composition measurements of volatile organic compounds to determine the "photochemical age" of an air mass, Geophys. Res. Lett., 27, 3865-3868, 2000.

Rudolph, J., Lowe, D.C., Martin, R.J., Clarkson, T.S.: A novel method for compound specific determination of $\delta^{13}C$ in volatile organic compounds at ppt levels in ambient air, Geophys. Res. Lett., 24, 659-662, 1997.

Rudolph, J., Czuba, E., and Huang, L.: The stable carbon isotope fractionation for reactions of selected hydrocarbons with OH-radicals and its relevance for atmospheric observations in an urban atmosphere, J. Geophys. Res., 10, 29329-29346, 2000.

Rudolph, J., Czuba, E., Norman, A.L., Huang, L., Ernst, D.: Stable carbon isotope composition of nonmethane hydrocarbons in emissions from transportation related sources and atmospheric observations in an urban atmosphere, Atmos. Environ., 36, 1173-1181, 2002.

Rudolph, J., Anderson, R.S., Czapiewski, K.V., Czuba, E., Ernst, D., Gillespie, T., Huang, L., Rigby, C., Thompson, A.E.: The stable carbon isotope ratio of biogenic emissions of isoprene and the potential use of stable isotope ratio measurements to study photochemical processing of isoprene in the atmosphere, J. Atmos. Chem., 44, 39-55, 2003.

Saito, T., Tsunogai, U., Kawamura, K., Nakatsuka, T., Yoshida, N.: Stable carbon isotopic compositions of light hydrocarbons over the western North Pacific and implication for their photochemical ages, J. Geophys. Res., 107, ACH 2/1 – ACH 2/9, 2002.

Sato, K., Hatakeyama, S., Imamura, T.: Secondary organic aerosol formation during the photooxidation of toluene: NO_x dependence of chemical composition, J. Phys. Chem. A, 111, 9796-9808, 2007.

Seinfeld, J.H. and Pandis, S.N.: Atmospheric chemistry and physics - from air pollution to climate change, 2nd Edition, John Wiley & Sons, Inc., United States of America, 2006.

Shafer, W.E. and Schönherr, J.: Accumulation and transport of phenol, 2-nitrophenol and 4-nitrophenol in plant cuticles, Ecotox. Environ. Safe., 10, 239-252, 1985.

Shea, P.J., Weber, J.B., Overcash, M.R.: Biological activities of 2,4-dinitrophenol in plant-soil systems, Residue Rev., 87, 1-41, 1983.

Sigma-Aldrich Co.: Amberlite XAD-2 polymeric adsorbent, Product Specification, Sigma-Aldrich Co., Missouri, United States of America, 1997.

Sigma-Aldrich Co.: Amberlite XAD polymeric resins, Product Information, Sigma-Aldrich Co., Missouri, United States of America, 1998.

Skoog, D.A., Holler, J.F., Crouch, S.R.: Principles of Instrumental Analysis, 6th Edition, Thomson Brooks/Cole, United States of America, 2007.

Stein, O. and Rudolph, J.: Modeling and interpretation of stable carbon isotope ratios of ethane in global chemical transport models, J. Geophys. Res., 112, D14308, 2007.

Thompson, A.: Stable carbon isotope ratios of nonmethane hydrocarbons and halocarbons in the atmosphere, Ph.D. thesis, York University, Toronto, ON, 2003.

Tremp, J., Mattrel, P., Fingler, S., Giger, W.: Phenols and nitrophenols as tropospheric pollutants: emissions from automobile exhausts and phase transfer in the atmosphere, Water Air Soil Poll, 68, 113-123, 1993.

Tsunogai, U., Yoshida, N., Gamo, T.: Carbon isotopic compositions of C_2-C_5 hydrocarbons and methyl chloride in urban, coastal and maritime atmospheres over the western North Pacific, J. Geophys. Res-Atmos., 104, 16033-16039, 1999.

Umlauf, G.: Measuring gas/particle fractions of trace organic compounds in ambient air. Evaluation of electrostatic precipitation, impaction and concentional filtration for separating particles, in: Lane, D.: Gas and particle phase measurements of atmospheric organic compounds, Gordon and Breach Science Publishers, Canada, 287-332, 1999.

van Vliet, B.M., Weber, W.J. Jr.: Comparative performance of synthetic adsorbents and activated carbon for specific compound removal from wastewaters, Water Pollut. Control, 53, 1585-1598, 1981.

Watson, J.G. and Chow, J.C.: Ambient Air Sampling, in: Baron, P.A. and Willeke, K.: Aerosol measurement: principles, techniques and applications, 2nd Ed., Wiley Interscience, United States of America, 2001.

Appendix

Appendix A: Filter Sampling Times, Flow Rates and Sampling Volumes

Filter	Sampling Start		Sampling End		Approx. Sampling Time	Flow Rate (m^3 min^{-1})	Total Volume Sampled (m^3)
	Date	Time	Date	Time			
Q120309B	12-Mar-09	1:30 PM	16-Mar-09	3:10 PM	4 days	1.13	6621.8
Q160409B	16-Apr-09	11:35 AM	19-Apr-09	2:00 PM	3 days	1.13	4881.6
Q240409B	24-Apr-09	10:30 AM	27-Apr-09	7:35 AM	3 days	1.13	4683.9
Q270409B	27-Apr-09	7:40 AM	30-Apr-09	9:25 AM	3 days	1.13	5000.3
Q190509A	15-May-09	11:00 AM	19-May-09	7:10 AM	4 days	1.13	3096.2
Q190509B	15-May-09	11:00 AM	19-May-09	7:10 AM	4 days	1.13	3096.2
Q040609A	4-Jun-09	11:30 AM	7-Jun-09	9:30 AM	3 days	1.13	4746
Q040609B	4-Jun-09	11:30 AM	7-Jun-09	9:30 AM	3 days	1.13	4746
Q190609A	19-Jun-09	9:10 AM	22-Jun-09	10:10 AM	3 days	1.13	4949.4
Q190609B	19-Jun-09	9:10 AM	22-Jun-09	10:10 AM	3 days	1.13	4949.4
Q220609APM10	22-Jun-09	11:35 AM	24-Jun-09	11:20 AM	2 days	1.13	3237.4
Q220609BPM2.5	22-Jun-09	11:35 AM	24-Jun-09	11:20 AM	2 days	1.13	3237.4
Q290609B-TOP	29-Jun-09	8:35 AM	1-Jul-09	9:30 AM	2 days	1.13	3322.2
Q290609B-BOTTOM	29-Jun-09	8:35 AM	1-Jul-09	9:30 AM	2 days	1.13	3322.2
Q030709A-TOP	3-Jul-09	9:55 AM	3-Jul-09	4:00 PM	6 hours	1.13	372.9
Q060709A-TOP	6-Jul-09	9:15 AM	9-Jul-09	9:35 AM	3 days	1.13	4904.2
Q060709A-BOTTOM	6-Jul-09	9:15 AM	9-Jul-09	9:35 AM	3 days	1.13	4904.2
Q130709A	13-Jul-09	2:05 PM	15-Jul-09	2:05 PM	3 days	1.13	3254.4

Filter	Sampling Start		Sampling End		Approx. Sampling Time	Flow Rate (m^3 min^{-1})	Total Volume Sampled (m^3)
	Date	Time	Date	Time			
Q150709A	15-Jul-09	2:10 PM	18-Jul-09	1:20 PM	3 days	1.13	4825.1
Q180709A	18-Jul-09	1:20 PM	21-Jul-09	2:35 PM	3 days	1.13	4966.4
Q180709B	18-Jul-09	1:20 PM	19-Jul-09	3:20 PM	1 day	1.13	4966.4
Q190709B	19-Jul-09	3:20 PM	20-Jul-09	3:15 PM	1 day	1.13	1627.2
Q200709B	20-Jul-09	3:15 PM	21-Jul-09	2:35 PM	1 day	1.13	1582
Q270709A	27-Jul-09	9:50 AM	29-Jul-09	1:30 PM	2 days	1.13	3503
Q290709A	29-Jul-09	2:35 PM	1-Aug-09	5:00 PM	2 days	1.13	3298.8
Q050809A	5-Aug-09	10:55 AM	7-Aug-09	9:15 AM	2 days	1.13	3141.4
Q130809B	13-Aug-09	9:00 AM	17-Aug-13	9:50 AM	4 days	1.13	6508.8
Q180809A	18-Aug-09	9:40 AM	21-Aug-09	10:30 AM	3 days	1.13	4938.1
Q210809A	21-Aug-09	10:50 AM	24-Aug-09	10:30 AM	3 days	1.13	4859
Q240809A	24-Aug-09	10:40 AM	26-Aug-09	1:50 PM	2 days	1.13	3469.1
Q280809A	28-Aug-09	10:21 AM	31-Aug-09	9:40 AM	3 days	1.13	4836.4
Q310809A	31-Aug-09	9:45 AM	2-Sep-09	11:45 AM	2 days	1.13	3390
Q040909A	4-Sep-09	9:30 AM	5-Sep-09	1:30 PM	1 day	1.13	1898.4
Q150909A	15-Sep-09	9:05 AM	18-Sep-09	8:05 AM	3 days	1.13	4813.8
Q180909A	18-Sep-09	8:10 AM	21-Sep-09	10:00 AM	3 days	1.13	5005.9
Q210909B	21-Sep-09	2:10 PM	24-Sep-09	10:10 AM	3 days	1.13	4610.4
Q240909A-TOP	24-Sep-09	10:35 AM	28-Sep-09	10:45 AM	4 days	0.57	3260.1
Q280909A	28-Sep-09	10:50 AM	1-Oct-09	2:50 PM	3 days	1.13	5152.8
Q011009A	1-Oct-09	2:55 PM	5-Oct-09	2:55 PM	4 days	1.13	6508.8
Q051009B	5-Oct-09	3:07 PM	9-Oct-09	1:05 PM	4 days	1.13	6373.2
Q131009B	13-Oct-09	8:15 AM	16-Oct-09	8:00 AM	3 days	1.13	4864.7
Q131009A-AM	13-Oct-09	8:15 AM	13-Oct-09	7:55 PM	12 hours	1.13	791
Q131009A-PM	13-Oct-09	8:00 PM	14-Oct-09	8:00 AM	12 hours	1.13	791
Q141009A-AM	14-Oct-09	8:05 AM	14-Oct-09	8:00 PM	12 hours	1.13	808
Q151009A-AM	15-Oct-09	8:15 AM	15-Oct-09	7:50 PM	12 hours	1.13	785.3

Filter	Sampling Start		Sampling End		Approx. Sampling Time	Flow Rate (m^3 min^{-1})	Total Volume Sampled (m^3)
	Date	Time	Date	Time			
Q151009A-PM	15-Oct-09	7:55 PM	16-Oct-09	8:00 AM	12 hours	1.13	819.3
Q191009A	19-Oct-09	1:35 PM	23-Oct-09	10:30 AM	4 days	1.13	6305.4
Q261009A	26-Oct-09	8:15 AM	27-Oct-09	8:05 AM	1 day	1.13	1615.9
Q271009A	27-Oct-09	11:00 AM	28-Oct-09	7:50 AM	1 day	1.13	1412.5
Q281009A	28-Oct-09	7:55 AM	29-Oct-09	4:50 AM	1 day	1.13	1406.9
Q291009A	29-Oct-09	7:30 AM	30-Oct-09	7:45 AM	1 day	1.13	1423.8
Q051109A	5-Nov-09	8:15 AM	5-Nov-09	11:45 PM	15 hours	1.13	1050.9
Q061109A	6-Nov-09	8:00 AM	7-Nov-09	8:40 AM	1 day	1.13	1672.4
Q071109A	7-Nov-09	8:45 AM	8-Nov-09	7:20 AM	1 day	1.13	1531.2
Q161109A	16-Nov-09	2:20 PM	20-Nov-09	11:20 AM	4 days	1.13	6305.4
Q231109A	23-Nov-09	8:45 AM	26-Nov-09	9:45 AM	3 days	1.13	4949.4
Q271109A	27-Nov-09	7:50 AM	30-Nov-09	7:40 AM	3 days	1.13	4870.3
Q101209A	10-Dec-09	4:20 PM	13-Dec-09	12:20 PM	3 days	1.13	4610.4
Q050110A	5-Jan-10	8:55 AM	6-Jan-10	8:00 AM	1 day	1.13	1565.1
Q060110A	6-Jan-10	8:05 AM	7-Jan-10	8:55 AM	1 day	1.13	1615.9
Q070110A	7-Jan-10	9:00 AM	8-Jan-10	8:00 AM	1 day	1.13	1559.4
Q240210A	24-Feb-10	1:15 PM	25-Feb-10	2:55 PM	1 day	1.13	1740.2
Q240210B	24-Feb-10	1:15 PM	25-Feb-10	2:55 PM	1 day	1.13	1740.2
Q020310B-TOP	2-Mar-10	2:50 PM	3-Mar-10	2:20 PM	1 day	1.13	1593.3
Q020310B-BOTTOM	2-Mar-10	2:50 PM	3-Mar-10	2:20 PM	1 day	1.13	1593.3
Q190310B	19-Mar-10	1:10 PM	22-Mar-09	1:45 PM	1 day	1.13	1666.8
Q310310A-TOP	31-Mar-10	3:50 PM	1-Apr-10	3:45 PM	1 day	1.13	1621.6
Q190410A	19-Apr-10	11:50 AM	20-Apr-10	11:20 AM	1 day	1.13	1593.3
Q210410A	21-Apr-10	1:50 PM	22-Apr-10	11:40 AM	1 day	1.13	1480.3
Q290410B	29-Apr-10	7:50 AM	30-Apr-10	7:50 AM	1 day	1.13	1627.2
Q050510A	5-May-10	8:05 AM	6-May-10	7:55 AM	1 day	1.13	1615.9

Filter	Sampling Start		Sampling End		Approx. Sampling Time	Flow Rate (m^3 min^{-1})	Total Volume Sampled (m^3)
	Date	Time	Date	Time			
Q060510A	6-May-10	8:00 AM	7-May-10	7:40 AM	1 day	1.13	1604.6
Q280510A	28-May-10	8:00 AM	31-May-10	8:00 AM	3 days	1.13	4881.6
Q310510A	31-May-10	8:05 AM	2-Jun-10	7:55 AM	2 days	1.13	3243.1
Q040610A	4-Jun-10	9:15 AM	7-Jun-10	7:20 AM	3 days	1.13	4763
Q070610A	7-Jun-10	7:35 AM	10-Jun-10	7:45 AM	3 days	1.13	4882.9
Q070610B	7-Jun-10	7:35 AM	10-Jun-10	7:45 AM	3 days	1.13	4882.9
Q110610A	11-Jun-10	7:50 AM	14-Jun-10	7:00 AM	3 days	1.13	4825.1
Q250710A	25-Jul-10	9:35 AM	28-Jul-10	9:35 AM	3 days	1.13	4881.6
Q090810A	9-Aug-10	8:00 AM	10-Aug-10	7:30 AM	1 day	1.13	1593.3
Q100810A	10-Aug-10	7:35 AM	12-Aug-10	7:15 AM	2 days	1.13	3237.5
Q160810A	16-Aug-10	8:20 AM	19-Aug-10	7:50 AM	3 days	1.13	4847.7
Q270810A	27-Aug-10	7:40 AM	30-Aug-10	7:50 AM	3 days	1.13	4892.9
Q300810A	30-Aug-10	7:55 AM	2-Sep-10	7:35 AM	3 days	1.13	4859
Q130910A	13-Sep-10	7:55 AM	16-Sep-10	7:50 AM	3 days	1.13	4876
Q200910A	20-Sep-10	8:45 AM	21-Sep-10	8:00 AM	1 day	1.13	1576.4
Q210910A	21-Sep-10	8:05 AM	22-Sep-10	8:10 AM	1 day	1.13	1632.9
Q291010A	29-Oct-10	7:05 AM	1-Nov-10	7:15 AM	3 days	1.13	4892.9
Q040211A-TOP	4-Feb-11	1:10 PM	7-Feb-11	8:40 AM	3 days	0.57	2288.3
Q230211A-TOP	23-Feb-11	8:00 AM	23-Feb-11	7:00 PM	11 hours	0.57	237.3
Q250211A-TOP	25-Feb-11	1:10 PM	26-Feb-11	11:55 AM	1 day	0.31	423
Q090911A	9-Sep-11	7:30 AM	12-Sep-11	7:30 AM	3 days	1.13	4881.6
Q181111B	18-Nov-11	7:25 AM	19-Nov-11	8:50 AM	1 day	0.57	847.5
Q071211B	7-Dec-11	7:20 AM	8-Dec-11	7:10 AM	1 day	0.57	808
Q121211B	12-Dec-11	7:05 AM	13-Dec-11	7:15 AM	1 day	0.57	808
Q131211B	13-Dec-11	7:35 AM	14-Dec-11	7:15 AM	1 day	0.57	808
Q161211B	16-Dec-11	7:20 AM	17-Dec-11	8:15 AM	1 day	0.57	844.7
Q140512A	14-May-12	12:30 PM	15-May-12	5:05 PM	1 day	1.13	1937.9

Filter	Sampling Start		Sampling End		Approx. Sampling Time	Flow Rate (m^3 min^{-1})	Total Volume Sampled (m^3)
	Date	Time	Date	Time			
Q230512A	23-May-12	12:10 PM	24-May-12	12:45 PM	1 day	1.13	1655.5
Q300512A	30-May-12	1:50 PM	31-May-12	2:20 PM	1 day	1.13	1661.1
Q040612A	4-Jun-12	11:05 AM	5-Jun-12	11:05 AM	1 day	1.13	1627.2
Q040612B	4-Jun-12	11:05 AM	5-Jun-12	11:05 AM	1 day	1.13	1627.2
Q060612A	6-Jun-12	2:47 PM	7-Jun-12	2:56 PM	1 day	1.13	2189.9
Q060612B	6-Jun-12	2:47 PM	7-Jun-12	2:56 PM	1 day	1.13	2189.9
Q130612A	13-Jun-12	1:48 PM	14-Jun-12	3:11 PM	1 day	1.13	1721
Q180612A	18-Jun-12	11:08 AM	19-Jun-12	9:22 AM	1 day	1.13	1507.4
Q190612B	19-Jun-12	9:30 AM	20-Jun-12	9:35 AM	1 day	1.13	1632.9
Q250612A	25-Jun-12	10:25 AM	26-Jun-12	10:30 AM	1 day	1.13	1632.9
Q050712A	5-Jul-12	10:00 AM	6-Jul-12	10:00 AM	1 day	1.13	1627.2
Q110712A	11-Jul-12	10:30 AM	12-Jul-12	10:30 AM	1 day	1.13	1627.2
Q120712A	12-Jul-12	10:30 AM	13-Jul-12	10:30 AM	1 day	1.13	1627.2
Q240712A	24-Jul-12	9:35 AM	25-Jul-12	9:35 AM	1 day	1.13	1627.2
Q070812A-TOP	7-Aug-12	9:15 AM	8-Aug-12	7:10 AM	1 day	1.13	1486
X300709B[a]	30-Jul-09	3:15 PM	1-Aug-09	5:50 PM	2 days	1.13	3429.6
X050809B[a]	5-Aug-09	10:55 AM	7-Aug-09	9:15 AM	2 days	1.13	3141.4
X070809A[a]	7-Aug-09	9:20 AM	10-Aug-09	9:05 AM	3 days	1.13	4864.7
X070809B[a]	7-Aug-09	9:20 AM	10-Aug-09	9:05 AM	3 days	1.13	4864.7
X100809A[a]	10-Aug-09	9:10 AM	13-Aug-09	8:00 AM	3 days	1.13	4802.5
X130809A[a]	13-Aug-09	8:05 AM	17-Aug-09	9:50 AM	4 days	1.13	6627.5
X210809B[a]	21-Aug-09	10:35 AM	24-Aug-09	10:15 AM	3 days	1.13	4859
X280809B[a]	28-Aug-09	10:20 AM	31-Aug-09	9:40 AM	3 days	1.13	4836.4
X280909B[a]	28-Sep-09	10:50 AM	1-Oct-09	2:50 PM	3 days	1.13	5152.8
X131109A[a]	13-Nov-09	11:30 AM	16-Nov-09	12:15 PM	3 days	1.13	5068.1
X030211A	3-Feb-11	11:55 AM	4-Feb-11	1:00 PM	1 day	0.57	850.3
X030211B	3-Feb-11	11:55 AM	4-Feb-11	1:00 PM	1 day	0.57	850.3

Filter	Sampling Start		Sampling End		Approx. Sampling Time	Flow Rate (m^3 min^{-1})	Total Volume Sampled (m^3)
	Date	Time	Date	Time			
X040211A-BOTTOM	4-Feb-11	1:01 PM	7-Feb-11	8:40 AM	3 days	0.57	2288.3
X040211B-TOP	4-Feb-11	1:01 PM	7-Feb-11	8:40 AM	3 days	0.57	2288.3
X040211B-BOTTOM	4-Feb-11	1:01 PM	7-Feb-11	8:40 AM	3 days	0.57	2288.3
X230211A-BOTTOM	23-Feb-11	8:00 AM	23-Feb-11	3:00 PM	7 hours	0.57	237.3
X250211A-BOTTOM	25-Feb-11	1:10 PM	26-Feb-11	11:55 AM	1 day	0.31	423
X030311A-TOP	3-Mar-11	7:30 AM	4-Mar-11	7:25 AM	1 day	0.31	444.7
X030311A-BOTTOM	3-Mar-11	7:30 AM	4-Mar-11	7:25 AM	1 day	0.31	444.7
X250311A-TOP	25-Mar-11	7:15 AM	25-Mar-11	2:10 PM	7 hours	0.4	165.2
X250311A-BOTTOM	25-Mar-11	7:15 AM	25-Mar-11	2:10 PM	7 hours	0.4	165.2
X070411A-TOP	7-Apr-11	8:00 AM	8-Apr-11	7:15 AM	1 day	0.57	788.2
X070411A-BOTTOM	7-Apr-11	8:00 AM	8-Apr-11	7:15 AM	1 day	0.57	788.2
X051011A-TOP	5-Oct-11	7:45 AM	6-Oct-11	7:25 AM	1 day	0.65	923
X051011A-BOTTOM	5-Oct-11	7:45 AM	6-Oct-11	7:25 AM	1 day	0.65	923
X061011A-TOP	6-Oct-11	7:30 AM	7-Oct-11	7:30 AM	1 day	0.65	936
X061011A-BOTTOM	6-Oct-11	7:30 AM	7-Oct-11	7:30 AM	1 day	0.65	936
X211011A-TOP	21-Oct-11	8:40 AM	22-Oct-11	9:55 AM	1 day	1.13	1712
X211011A-BOTTOM	21-Oct-11	8:40 AM	22-Oct-11	9:55 AM	1 day	1.13	1712

Filter	Sampling Start		Sampling End		Approx. Sampling Time	Flow Rate (m^3 min^{-1})	Total Volume Sampled (m^3)
	Date	Time	Date	Time			
X281011A-TOP	28-Oct-11	10:40 AM	29-Oct-11	8:30 AM	1 day	1.13	1480.3
X281011A-BOTTOM	28-Oct-11	10:40 AM	29-Oct-11	8:30 AM	1 day	1.13	1480.3
X01111A-TOP	1-Nov-11	7:40 AM	2-Nov-11	7:30 AM	1 day	0.65	808
X01111A-BOTTOM	1-Nov-11	7:40 AM	2-Nov-11	7:30 AM	1 day	0.65	808
X041111A-TOP	4-Nov-11	7:30 AM	5-Nov-11	8:35 AM	1 day	0.65	978.25
X041111A-BOTTOM	4-Nov-11	7:30 AM	5-Nov-11	8:35 AM	1 day	0.65	978.25
X08111A-TOP	8-Nov-11	7:10 AM	8-Nov-11	5:45 AM	11 hours	1.13	711.9
X08111A-BOTTOM	8-Nov-11	7:10 AM	8-Nov-11	5:45 AM	11 hours	1.13	711.9
X18111A-TOP	18-Nov-11	7:25 AM	19-Nov-11	8:50 AM	1 day	0.65	975
X18111A-BOTTOM	18-Nov-11	7:25 AM	19-Nov-11	8:50 AM	1 day	0.65	975
X071211A-TOP	7-Dec-11	7:20 AM	8-Dec-11	7:10 AM	1 day	0.65	929.5
X071211A-BOTTOM	7-Dec-11	7:20 AM	8-Dec-11	7:10 AM	1 day	0.65	929.5
X121211A-TOP	12-Dec-11	7:05 AM	13-Dec-11	7:15 AM	1 day	0.65	942.5
X121211A-BOTTOM	12-Dec-11	7:05 AM	13-Dec-11	7:15 AM	1 day	0.65	942.5
X131211A-TOP	13-Dec-11	7:35 AM	14-Dec-11	7:15 AM	1 day	0.65	923
X131211A-BOTTOM	13-Dec-11	7:35 AM	14-Dec-11	7:15 AM	1 day	0.65	923
X161211A-TOP	16-Dec-11	7:20 AM	17-Dec-11	8:15 AM	1 day	0.65	971.75
X161211A-BOTTOM	16-Dec-11	7:20 AM	17-Dec-11	8:15 AM	1 day	0.65	971.75

Filter	Sampling Start		Sampling End		Approx. Sampling Time	Flow Rate (m^3 min^{-1})	Total Volume Sampled (m^3)
	Date	Time	Date	Time			
X190612A	19-Jun-12	9:30 AM	20-Jun-12	9:35 AM	1 day	1.13	1632.9
X200612A	20-Jun-12	9:42 AM	21-Jun-12	9:42 AM	1 day	1.13	1627.2
X020812A	2-Aug-12	11:00 AM	3-Aug-12	9:30 AM	1 day	1.13	1525.5
X040812A	4-Aug-12	7:55 AM	5-Aug-12	9:55 AM	1 day	1.13	1762.8
X050812A	5-Aug-12	10:00 AM	6-Aug-12	7:00 AM	1 day	1.13	1423.8
X060812A	6-Aug-12	7:05 AM	7-Aug-12	9:15 AM	1 day	1.13	1774.1
X070812A-BOTTOM	7-Aug-12	9:15 AM	8-Aug-12	7:10 AM	1 day	1.13	1486
X090812A-TOP	9-Aug-12	9:30 AM	10-Aug-12	9:15 AM	1 day	1.13	1779.8
X090812A-BOTTOM	9-Aug-12	9:30 AM	10-Aug-12	9:15 AM	1 day	1.13	1779.8
X110812A-TOP	11-Aug-12	7:10 AM	12-Aug-12	8:05 AM	1 day	1.13	1689.4
X110812A-BOTTOM	11-Aug-12	7:10 AM	12-Aug-12	8:05 AM	1 day	1.13	1689.4
X120812A-TOP	12-Aug-12	8:10 AM	13-Aug-12	9:35 AM	1 day	1.13	1723.3
X120812A-BOTTOM	12-Aug-12	8:10 AM	13-Aug-12	9:35 AM	1 day	1.13	1723.3

[a] Sampled, extracted and analyzed by Busca (2010)

Filters are named according to the following code: ABbCcDdE where:

A is either Q (quartz filter) or X (XAD-coated filter)
Bb is the day
Cc is the month
Dd is the year
E is the air sampler (A or B)

Appendix B: Atmospheric Concentrations and Recoveries

Filter	Atmospheric Concentration (ng m^{-3})						Recovery (%)		
	4-me-ph	4-me-2-NP	4-NP	3-me-4-NP	2-me-4-NP	2,6-dime-4-NP	2-me-ph	2-me-3-NP	2-me-5-NP
Q120309B	0.04	0.01	1.55	0.23	0.32	0.03	24	47	47
Q160409B	0.01	0.01	0.55	0.07	0.14	0.05	NA	41	52
Q240409B	0.01	0.01	0.37	0.04	0.10	0.05	NA	15	17
Q270409B	0.01	0.01	0.30	0.03	0.07	0.02	NA	13	13
Q190509A	<DL	0.01	0.30	0.03	0.07	0.11	NA	19	21
Q190509B	0.01	0.01	0.50	0.06	0.19	0.19	NA	13	16
Q040609A	<DL	<DL	0.13	0.02	0.03	0.04	NA	35	25
Q040609B	0.01	0.01	0.36	0.03	0.06	0.06	NA	24	27
Q190609A	<DL	0.00	0.10	0.01	0.03	0.14	NA	18	20
Q190609B	<DL	0.00	0.13	0.02	0.04	0.05	NA	20	24
Q220609APM10	0.01	0.01	0.20	0.03	0.06	0.09	NA	15	16
Q220609BPM2.5	<DL	0.00	0.21	0.02	0.05	0.06	NA	59	43
Q290609B-TOP	0.01	0.01	0.04	0.02	0.03	0.05	NA	14	14
Q290609B-BOTTOM	<DL	<DL	0.04	<DL	<DL	<DL	NA	9	9
Q030709A-TOP	0.04	0.04	1.32	0.11	0.15	0.04	NA	39	41
Q060709A-TOP	0.23	<DL	3.07	1.41	1.82	<DL	NA	12	19
Q060709A-BOTTOM	0.00	<DL	<DL	<DL	<DL	<DL	NA	13	13
Q130709A	0.02	0.04	0.08	0.04	0.09	NA	NA	31	30
Q150709A	0.38	0.01	0.18	0.01	0.52	0.02	1	32	34
Q180709A	<DL	<DL	0.61	0.03	0.19	NA	NA	27	29
Q180709B	<DL	<DL	0.23	0.05	0.12	NA	NA	28	33
Q190709B	<DL	<DL	0.36	<DL	0.13	NA	NA	35	46
Q200709B	0.01	<DL	1.29	0.06	0.23	NA	NA	22	25

Filter	Atmospheric Concentration (ng m^{-3})						Recovery (%)		
	4-me-ph	4-me-2-NP	4-NP	3-me-4-NP	2-me-4-NP	2,6-dime-4-NP	2-me-ph	2-me-3-NP	2-me-5-NP
Q270709A	0.10	0.03	2.19	0.31	1.16	0.23	21	28	28
Q290709A	0.23	0.03	2.80	0.50	2.00	<DL	NA	32	43
Q050809A	0.05	<DL	0.30	<DL	0.48	NA	NA	26	28
Q130809B	<DL	<DL	0.35	<DL	0.40	NA	NA	28	32
Q180809A	0.01	<DL	0.08	0.01	0.03	0.01	NA	32	35
Q210809A	<DL	<DL	0.04	0.01	0.01	0.00	NA	26	25
Q240809A	0.01	0.00	0.12	0.02	0.02	0.01	NA	47	62
Q280809A	0.01	0.01	0.06	0.01	0.02	0.00	NA	30	37
Q310809A	<DL	0.01	0.26	0.03	0.08	0.02	NA	26	41
Q040909A	0.02	0.01	0.62	0.33	1.27	0.22	NA	21	25
Q150909A	0.03	<DL	0.36	0.05	0.10	0.01	13	16	12
Q180909A	0.00	<DL	0.23	0.02	0.05	0.00	NA	23	24
Q210909B	0.02	0.01	0.71	0.05	0.10	0.01	NA	10	27
Q240909A-TOP	<DL	0.00	0.11	0.03	0.08	0.03	NA	56	63
Q280909A	0.01	0.01	0.26	0.03	0.07	0.01	NA	29	24
Q011009A	0.01	<DL	0.02	0.41	0.10	0.20	NA	34	36
Q051009B	<DL	<DL	0.10	0.02	0.03	0.00	NA	24	23
Q131009B	0.01	0.01	0.35	0.07	0.14	0.01	NA	26	28
Q131009A-AM	0.33	0.21	0.57	0.09	0.20	0.04	NA	36	38
Q131009A-PM	0.05	0.11	0.25	0.16	0.24	0.09	NA	18	22
Q141009A-AM	0.27	0.14	0.43	0.12	0.19	<DL	NA	42	50
Q151009A-AM	<DL	<DL	0.44	0.11	0.22	0.05	NA	30	27
Q151009A-PM	<DL	<DL	0.93	0.26	0.34	<DL	NA	8	17
Q191009A	0.01	0.07	1.66	0.09	0.18	0.05	NA	6	11
Q261009A	0.13	0.08	0.51	0.07	0.18	0.03	NA	12	15
Q271009A	0.07	0.93	2.11	0.37	1.05	0.42	NA	31	32
Q281009A	0.48	1.38	1.71	0.61	3.50	0.25	NA	25	22
Q291009A	0.64	1.69	1.58	0.67	3.23	0.96	NA	26	23

Filter	Atmospheric Concentration (ng m^{-3})						Recovery (%)		
	4-me-ph	4-me-2-NP	4-NP	3-me-4-NP	2-me-4-NP	2,6-dime-4-NP	2-me-ph	2-me-3-NP	2-me-5-NP
Q051109A	0.27	0.18	0.07	0.10	0.21	0.05	NA	39	45
Q061109A	0.02	0.02	0.06	0.11	0.14	0.05	NA	48	56
Q071109A	0.01	0.04	0.51	0.14	0.24	0.06	NA	60	69
Q161109A	<DL	0.01	0.29	0.03	0.04	0.02	NA	36	59
Q231109A	0.02	0.01	0.28	0.03	0.08	0.01	10	16	18
Q271109A	0.02	0.02	0.03	<DL	0.02	<DL	NA	43	54
Q101209A	0.01	0.01	0.57	0.14	0.16	0.02	NA	33	35
Q050110A	0.02	0.04	0.04	0.08	0.09	0.05	NA	55	64
Q060110A	0.02	0.01	0.73	0.17	0.22	0.04	18	28	23
Q070110A	0.11	0.02	1.84	0.50	0.65	0.10	2	27	17
Q240210A	0.73	0.02	2.00	0.60	0.69	0.09	4	17	12
Q240210B	0.08	0.02	2.85	0.70	0.82	0.08	14	25	19
Q020310B-TOP	0.07	0.01	1.73	0.30	0.38	0.14	19	33	25
Q020310B-BOTTOM	0.14	0.01	1.19	0.18	0.23	0.10	19	28	20
Q190310B	0.13	<DL	1.26	0.19	0.33	0.07	25	60	59
Q310310A-TOP	NA	0.02	0.67	0.10	1.80	0.11	0	53	70
Q190410A	0.10	0.01	0.32	0.07	0.42	0.06	4	92	105
Q210410A	0.24	0.05	0.57	0.16	0.28	0.06	35	47	47
Q290410B	0.08	0.00	0.48	0.06	0.15	0.05	17	30	31
Q050510A	0.07	0.01	0.32	0.10	3.24	0.04	5	26	29
Q060510A	NA	0.01	0.12	<DL	0.14	0.02	0	13	21
Q280510A	0.03	0.01	0.51	0.04	0.08	<DL	9	29	25
Q310510A	0.04	0.01	0.26	0.02	0.07	<DL	10	30	29
Q040610A	0.01	<DL	0.08	0.01	0.06	0.00	6	35	39
Q070610A	NA	0.03	0.30	0.03	0.71	0.03	0	28	38
Q070610B	0.08	0.01	0.13	0.01	0.03	0.02	12	30	29
Q110610A	0.01	0.00	0.11	0.01	0.19	0.01	25	43	51

Filter	Atmospheric Concentration (ng m^{-3})						Recovery (%)		
	4-me-ph	4-me-2-NP	4-NP	3-me-4-NP	2-me-4-NP	2,6-dime-4-NP	2-me-ph	2-me-3-NP	2-me-5-NP
Q250710A	0.02	<DL	0.28	0.02	0.05	0.04	14	37	33
Q090810A	0.01	<DL	0.11	0.03	0.15	0.01	18	37	40
Q100810A	0.02	0.00	0.25	0.03	0.06	0.01	18	39	44
Q160810A	0.02	0.01	0.40	0.04	0.27	0.02	8	29	33
Q270810A	NA	<DL	0.22	0.02	0.09	0.02	0	40	47
Q300810A	0.02	0.01	0.13	0.02	0.08	0.03	16	20	18
Q130910A	0.01	<DL	0.06	0.04	0.07	0.02	27	17	19
Q200910A	NA	0.01	0.06	0.09	0.08	0.02	0	88	97
Q210910A	NA	<DL	0.11	<DL	0.05	0.01	0	66	67
Q291010A	NA	<DL	0.07	0.02	0.04	0.01	0	23	23
Q040211A-TOP	0.06	0.02	1.60	0.40	0.47	0.07	11	62	67
Q230211A-TOP	0.16	0.18	2.58	5.41	1.10	1.04	30	62	70
Q250211A-TOP	NA	0.04	1.79	3.76	0.53	0.42	0	57	65
Q090911A	0.08	<DL	0.39	0.05	0.17	0.01	1	42	37
Q071011A	0.73	0.29	2.01	0.15	0.62	0.01	1	72	83
Q181111B	1.03	<DL	1.71	0.19	1.33	0.08	1	294	345
Q071211B	0.10	<DL	2.15	0.58	1.40	0.11	37	171	176
Q121211B	NA	<DL	9.98	2.03	6.92	0.25	0	125	204
Q131211B	3.47	0.24	11.61	2.00	6.31	0.28	2	83	153
Q161211B	0.03	0.05	1.05	0.32	0.43	0.08	130	201	207
Q140512A	NA	0.02	0.66	0.04	2.32	0.02	1	89	115
Q230512A	NA	0.00	0.40	0.03	0.06	0.01	NA	55	53
Q300512A	NA	0.00	0.15	0.01	0.02	0.00	NA	113	141
Q040612A	NA	<DL	0.14	0.01	0.02	0.00	NA	106	99
Q040612B	NA	<DL	0.16	0.01	0.02	0.00	NA	47	43
Q060612A	NA	<DL	0.29	0.02	0.04	0.01	NA	59	62
Q060612B	NA	0.01	0.40	0.01	0.03	0.00	NA	67	66
Q130612A	NA	0.01	0.69	0.01	0.06	<DL	NA	124	113

Filter	Atmospheric Concentration (ng m^{-3})						Recovery (%)		
	4-me-ph	4-me-2-NP	4-NP	3-me-4-NP	2-me-4-NP	2,6-dime-4-NP	2-me-ph	2-me-3-NP	2-me-5-NP
Q180612A	NA	<DL	0.38	0.02	0.07	0.01	NA	141	168
Q190612B	NA	0.01	0.47	0.02	0.06	0.01	NA	114	163
Q200612B	NA	0.00	0.26	0.01	0.05	0.01	NA	48	67
Q250612A	NA	0.00	0.19	0.01	0.03	0.00	NA	122	138
Q050712A	NA	0.00	1.08	0.03	0.08	0.01	NA	121	134
Q110712A	NA	0.01	0.54	0.03	0.07	0.01	NA	159	186
Q120712A	NA	0.01	0.55	0.03	0.10	0.02	NA	161	181
Q240712A	NA	0.00	0.24	0.02	0.04	0.01	NA	154	164
Q070812A-TOP	NA	0.01	0.47	0.10	0.07	0.01	NA	206	234
X300709B[a]	NA	<DL	3.70	1.10	2.30	0.18	NA	77	50
X050809B[a]	NA	<DL	2.20	0.75	1.20	0.09	NA	46	50
X070809A[a]	NA	<DL	2.20	0.75	1.20	0.09	NA	26	35
X070809B[a]	NA	<DL	2.20	0.75	1.90	0.24	NA	36	41
X100809A[a]	NA	<DL	2.40	0.71	1.80	0.13	NA	30	39
X130809A[a]	NA	0.04	1.60	0.58	2.00	0.13	NA	26	31
X210809B[a]	NA	0.02	2.10	0.49	2.40	1.00	NA	46	59
X280809B[a]	NA	0.12	2.90	0.32	0.76	0.29	NA	51	55
X280909B[a]	NA	0.04	0.87	0.18	0.45	0.30	NA	36	38
X131109A[a]	NA	0.07	2.60	0.46	1.20	0.62	NA	32	42
X030211A	2.44	9.38	6.19	1.67	6.55	1.58	1	36	43
X030211B	9.01	11.87	17.19	3.05	7.86	1.62	2	57	65
X040211A-BOTTOM	0.55	12.20	7.51	1.56	3.24	1.35	46	63	74
X040211B-TOP	2.51	6.49	17.98	3.78	7.07	2.59	1	67	78
X040211B-BOTTOM	0.58	18.39	3.53	0.68	2.86	0.26	42	51	62
X230211A-BOTTOM	0.38	1.38	2.11	2.15	1.57	2.39	26	58	70

Filter	Atmospheric Concentration (ng m^{-3})						Recovery (%)		
	4-me-ph	4-me-2-NP	4-NP	3-me-4-NP	2-me-4-NP	2,6-dime-4-NP	2-me-ph	2-me-3-NP	2-me-5-NP
X250211A-BOTTOM	2.24	1.02	2.25	2.94	1.18	1.17	2	40	44
X030311A-TOP	0.87	1.08	2.93	4.32	1.82	2.68	14	66	73
X030311A-BOTTOM	<DL	0.20	0.82	1.34	0.27	0.31	6	40	44
X250311A-TOP	<DL	<DL	0.61	0.83	4.37	5.44	1	37	39
X250311A-BOTTOM	<DL	<DL	<DL	<DL	0.79	0.97	24	45	49
X070411A-TOP	4.08	3.60	4.10	0.55	3.32	0.48	2	49	54
X070411A-BOTTOM	<DL	2.84	8.19	6.69	1.94	2.33	3	35	23
X051011A-TOP	NA	0.53	2.66	0.26	3.46	0.18	0	55	63
X051011A-BOTTOM	0.03	0.13	0.75	0.05	0.32	0.01	21	52	57
X061011A-TOP	2.03	2.15	4.08	0.65	3.78	1.19	3	65	63
X061011A-BOTTOM	0.08	1.01	1.45	0.22	1.15	0.03	24	71	69
X211011A-TOP	2.66	0.94	1.25	0.17	1.74	0.05	0	51	49
X211011A-BOTTOM	0.05	0.11	0.30	0.02	0.18	<DL	27	64	60
X281011A-TOP	NA	0.87	3.68	0.78	2.43	0.56	0	66	66
X281011A-BOTTOM	0.04	0.25	2.24	0.18	0.47	0.02	24	62	60
X01111A-TOP	NA	9.86	11.07	1.48	5.79	1.52	1	32	36
X01111A-BOTTOM	NA	1.05	3.12	0.34	0.80	0.02	24	63	68
X041111A-TOP	NA	<DL	2.27	0.29	2.19	0.13	1	183	197

Filter	Atmospheric Concentration (ng m^{-3})						Recovery (%)		
	4-me-ph	4-me-2-NP	4-NP	3-me-4-NP	2-me-4-NP	2,6-dime-4-NP	2-me-ph	2-me-3-NP	2-me-5-NP
X041111A-BOTTOM	0.02	0.25	1.00	0.04	0.22	0.01	52	162	176
X08111A-TOP	NA	<DL	4.81	0.73	4.49	0.86	1	71	87
X08111A-BOTTOM	0.06	2.20	2.65	0.36	1.70	0.26	1	20	20
X18111A-TOP	0.89	4.40	2.84	0.31	1.96	0.16	9	208	206
X18111A-BOTTOM	0.26	0.14	0.52	<DL	0.35	0.01	3	259	303
X071211A-TOP	0.57	2.08	3.07	0.35	0.19	0.21	40	191	190
X071211A-BOTTOM	0.13	<DL	1.00	<DL	0.20	0.01	3	169	184
X121211A-TOP	NA	0.08	10.61	2.29	5.81	1.20	1	150	181
X121211A-BOTTOM	3.65	0.25	10.79	2.36	6.63	0.23	2	85	154
X131211A-TOP	5.54	18.85	11.34	3.32	8.51	1.75	3	148	153
X131211A-BOTTOM	0.28	8.05	4.61	1.03	2.33	0.03	7	162	165
X161211A-TOP	0.45	1.25	1.30	0.20	1.19	0.09	75	208	224
X161211A-BOTTOM	0.02	<DL	0.14	<DL	0.42	0.01	38	173	223
X190612A	NA	0.07	18.57	0.94	3.33	1.17	NA	129	145
X200612A	NA	0.05	15.42	0.83	2.86	1.33	NA	46	60
X020812A	NA	0.34	15.90	0.81	2.88	0.92	NA	120	145
X040812A	NA	0.02	8.34	0.50	1.52	0.87	NA	225	299
X050812A	NA	0.15	5.29	0.30	1.01	0.37	NA	127	138
X060812A	NA	0.18	6.04	0.41	1.02	0.63	NA	198	219
X070812A-BOTTOM	NA	0.01	0.57	0.16	0.12	0.01	NA	107	147

Filter	Atmospheric Concentration (ng m^{-3})						Recovery (%)		
	4-me-ph	4-me-2-NP	4-NP	3-me-4-NP	2-me-4-NP	2,6-dime-4-NP	2-me-ph	2-me-3-NP	2-me-5-NP
X090812A-TOP	NA	0.18	1.72	0.11	0.55	0.27	NA	41	52
X110812A-TOP	NA	0.35	3.26	0.20	0.62	0.59	NA	192	213
X110812A-BOTTOM	NA	0.04	0.26	0.03	0.25	0.22	NA	150	169
X120812A-TOP	NA	0.40	3.09	0.20	0.54	0.15	NA	149	155
X120812A-BOTTOM	NA	0.21	0.11	0.01	0.04	0.02	NA	129	167

[a] Sampled, extracted and analyzed by Busca (2010)

Filters are named according to the following code: ABbCcDdE where:

A is either Q (quartz filter) or X (XAD-coated filter)
Bb is the day
Cc is the month
Dd is the year
E is the air sampler (A or B)

Appendix C: Solution Concentrations for GC-MS and GC-IRMS Analysis

Filter	Solution Concentration (ng μL^{-1})					
	4-me-ph	4-me-2-NP	4-NP	3-me-4-NP	2-me-4-NP	2,6-dime-4-NP
Q120309B	0.6	0.04	45.1	6.6	9.3	0.8
Q160409B	0.4	0.6	23.7	2.9	6.2	2.3
Q240409B	0.1	0.1	3.7	0.4	0.9	0.5
Q270409B	0.1	0.1	3	0.3	0.7	0.2
Q190509A	0.1	0.2	4.3	0.4	1.1	1.6
Q190509B	0.1	0.1	5.1	0.6	2	1.9
Q040609A	0.1	0.1	4.3	0.6	1	1.2
Q040909B	0.1	0.1	7	0.6	1.3	1.1
Q190609A	0.1	0.1	2	0.2	0.6	2.7
Q190609B	0.1	0.1	2.5	0.3	0.7	1
Q220609APM10	0.1	0.1	1.6	0.2	0.5	0.7
Q220609BPM2.5	0.1	0.1	4.6	0.4	0.2	1.4
Q290609B-TOP	0	0	0.2	0.1	0.1	0.2
Q290609B-BOTTOM	0	0	0.1	0	0	0
Q030709A-TOP	0.2	0.2	6.6	0.6	0.7	0.2
Q130709A	0.1	0.3	0.6	0.3	0.7	NA
Q150709A	0	0	0.5	0	1.3	0
Q180709A	0	<DL	6.2	0.3	1.9	NA
Q180709B	<DL	<DL	0.9	0.2	0.7	NA
Q190709B	<DL	<DL	0.8	<DL	0.3	NA
Q200709B	0	<DL	2.5	0.1	0.5	NA
Q270709A	1.3	0.1	51.8	4.6	18.1	7.2
Q290709A	2.7	0.4	33.1	5.9	23.7	<DL
Q050809A	0.3	<DL	1.8	<DL	2.9	NA
Q130809B	<DL	<DL	3.5	<DL	4	NA

Filter	Solution Concentration (ng μL^{-1})					
	4-me-ph	4-me-2-NP	4-NP	3-me-4-NP	2-me-4-NP	2,6-dime-4-NP
Q180809A	0.1	<DL	1.1	0.1	0.4	0.1
Q210809A	0.1	<DL	0.9	0.1	0.2	0
Q240809A	0.1	0.1	2.5	0.4	0.4	0.1
Q280809A	0.1	0.2	0.7	0.1	0.2	0
Q310809A	0.1	0.1	4.4	0.5	1.3	0.4
Q040909A	0.1	0	3.5	1.8	7.1	1.3
Q150909A	0.3	0	3.8	0.5	1	0.1
Q180909A	0.1	0.1	6.9	0.5	1.6	0.1
Q210909B	0.1	0.1	6.8	0.4	0.9	0.1
Q240909A-TOP	0.1	0.1	3.1	0.8	2.2	0.9
Q280909A	0.2	0.2	5.8	0.7	1.5	0.3
Q011009A	0	0.1	1.3	0.3	0.6	0
Q051009B	0.1	<DL	4	0.6	1	0.2
Q131009B	0.2	0.2	6.5	1.3	2.6	0.2
Q131009A-AM	1.7	1.1	3	0.5	1	0.3
Q131009A-PM	0	0.1	0.2	0.1	0.2	0.1
Q141009A-AM	0	0	0.1	0	0	0
Q151009A-AM	<DL	0	0.7	0.2	0.4	0.1
Q151009A-PM	0	0	0.7	0.2	0.3	0
Q191009A	0.1	0.8	17.3	1	1.9	0.6
Q261009A	0.3	0.2	1.2	0.2	0.4	0.1
Q271009A	0.3	3.9	8.7	1.5	4.3	1.9
Q281009A	1.8	5.2	6	2.3	12.3	0.9
Q291009A	2.4	6.4	6	2.5	12.3	3.7
Q051109A	1.5	1.1	0.4	0.6	1.3	0.4
Q061109A	0	0	0	0	0.1	0
Q071109A	0	0	0.4	0.1	0.2	0.1
Q161109A	0.1	0.3	6.7	0.6	0.9	0.5

Filter	Solution Concentration (ng μL^{-1})					
	4-me-ph	4-me-2-NP	4-NP	3-me-4-NP	2-me-4-NP	2,6-dime-4-NP
Q231109A	0.1	0	2	0.2	0.6	0
Q271109A	0	0	0	0	0	0
Q101209A	0.4	0.5	31.4	7.6	8.7	1.4
Q050110A	3.3	10.9	9.7	18.5	21.5	12.4
Q060110A	0.1	0	3.2	0.7	0.9	0.2
Q070110A	0.2	0.3	23.6	6.5	8.3	1.5
Q240210A	0.6	2.4	35.9	26.3	27.6	0.6
Q240210B	0.3	0.1	16.6	4.1	4.8	0.5
Q020310B-TOP	0.2	0.1	8	1.4	1.7	0.6
Q020310B-BOTTOM	0.5	0	5.2	0.8	1	0.4
Q190310B	0.4	<DL	9.9	1.5	2.6	0.6
Q310310A-TOP	0.8	<DL	4.1	<DL	14.6	0.6
Q190410A	0.1	0.2	8.3	1.7	10.8	1.6
Q210410A	0.4	0.2	2.5	0.7	1.2	0.3
Q290410B	0.5	0	5.8	0.7	1.8	0.7
Q050510A	0.1	0.1	2.8	0.9	28.6	0.4
Q060510A	0	0	0.6	0	0.7	0.1
Q280510A	0	0	0.4	0	0.1	<DL
Q310510A	0	0	0.2	0	0.1	<DL
Q040610A	0.1	0	3.1	0.5	2.5	0.2
Q070610A	1.7	0.8	8.4	0.8	20.2	0.8
Q070610B	0.5	0.1	2.1	0.2	0.4	0.3
Q110610A	0.2	0.2	4.5	0.6	7.7	0.3
Q250710A	0.2	<DL	8	0.5	1.6	1.2
Q090810A	0.1	0	4.1	1.3	5.7	0.3
Q100810A	0.2	0.1	5.1	0.6	1.3	0.2
Q160810A	0.3	0.4	15.8	1.5	10.9	0.7
Q270810A	0.2	0.1	5.7	0.6	2.3	0.6

Filter	Solution Concentration (ng μL^{-1})					
	4-me-ph	4-me-2-NP	4-NP	3-me-4-NP	2-me-4-NP	2,6-dime-4-NP
Q300810A	0.2	0.1	1.5	0.2	1	0.4
Q130910A	0.1	0	0.5	0.3	0.6	0.2
Q200910A	0.1	0.1	0.8	1.2	1.1	0.3
Q210910A	0.1	0	1	0	0.5	1
Q291010A	0	0	0.5	0.1	0.3	0.1
Q040211A-TOP	0.2	0.3	27.6	6.9	8.1	1.3
Q230211A-TOP	0.2	0.6	8.7	18.2	3.7	3.5
Q250211A-TOP	0.1	0.2	8.9	18.6	2.6	2.1
Q090911A	0.1	0	14.7	1.7	6.5	0.5
Q181111B	0	0	14.3	1.6	11.1	0.6
Q071211B	0.1	0	10.4	2.7	6.8	0.5
Q121211B	0.1	0	50.1	10.2	34.7	1.2
Q131211B	0.2	0.7	34.1	5.9	18.5	0.8
Q161211B	0.1	0.2	3.9	1.2	1.6	0.3
Q140512A	0.3	0.3	14.2	0.8	49.9	0.5
Q230512A	0.2	0	4.1	0.3	0.6	0.1
Q300512A	0.1	0	2.9	0.2	0.4	0.1
Q040612A	0	0	1.6	0.2	0.3	0
Q040612B	0	0	0.8	0.1	0.1	0
Q060612A	0.1	0	3.2	0.2	0.4	0.1
Q060612B	0.2	0.1	7.4	0.2	0.6	0.1
Q130612A	0.2	0.1	11.2	0.1	1	0
Q180612A	0	0	3	0.2	0.5	0.1
Q190612B	0.1	0.2	7.9	0.3	0.9	0.1
Q250612A	0	0	2.6	0.2	0.4	0.1
Q050712A	0.1	0	15.4	0.4	1.2	0.1
Q110712A	0.1	0.1	8.9	0.6	1.2	0.1
Q120712A	0.1	0.1	6.3	0.4	1.1	0.2

Filter	Solution Concentration (ng μL^{-1})					
	4-me-ph	4-me-2-NP	4-NP	3-me-4-NP	2-me-4-NP	2,6-dime-4-NP
Q240712A	0.1	0	3	0.2	0.5	0.1
Q070812A-TOP	0.4	0.4	17.9	3.9	2.8	0.4
X300709B[a]	0.33	<DL	67	21	42	3.2
X050809B[a]	0.17	<DL	15	5.2	8.1	0.61
X070809A[a]	0.18	<DL	31	10.3	26	3.3
X070809B[a]	0.18	<DL	45	15	40	4.4
X100809A[a]	0.14	<DL	36	10.6	27	1.9
X130809A[a]	0.24	1.12	41	15	53	3.5
X210809B[a]	2.8	0.44	54	12.8	62	26
X280809B[a]	2.6	2.3	49	9.9	25	17
X280909B[a]	1.08	2.3	56	6.2	15	5.6
X131109A[a]	0.24	1.5	59	10.5	28	14
X030211A	0.5	71.4	47.2	12.8	49.8	12.1
X030211B	2.9	114.2	165.4	29.4	75.3	15.6
X040211A-BOTTOM	5.1	168.3	103.5	21.4	44.7	20.3
X040211B-TOP	0.8	151	418.1	88	164.4	57.4
X040211B-BOTTOM	6.8	289.3	55.5	10.7	44.8	4.5
X230211A-BOTTOM	0.5	4.4	6.7	6.8	5	8.3
X250211A-BOTTOM	0.3	2.2	4.9	6.4	2.6	4.1
X030311A-TOP	0.7	4.2	11.5	16.9	7.1	11.5
X030311A-BOTTOM	0.1	0.7	3	4.9	1	1.3
X250311A-TOP	0	0	0.2	0.2	1.1	1.6
X250311A-BOTTOM	0	0	0	0	0.3	0.4
X070411A-TOP	0.4	7.5	8.4	1.2	6.9	1.2
X070411A-BOTTOM	0	0	0.1	0.1	0	0
X051011A-TOP	0	0.9	4.6	0.5	6.1	0.3
X051011A-BOTTOM	0.1	0.5	2.4	0.2	1	0
X061011A-TOP	0.3	6.9	12.8	2.1	12.1	4.3

Filter	Solution Concentration (ng μL^{-1})					
	4-me-ph	4-me-2-NP	4-NP	3-me-4-NP	2-me-4-NP	2,6-dime-4-NP
X061011A-BOTTOM	0.1	4.6	6.5	1	5.2	0.2
X211011A-TOP	0.1	6.4	8.4	1.2	11.8	0.4
X211011A-BOTTOM	0.2	1.3	3.3	0.3	1.9	0
X281011A-TOP	0	12.7	52.9	11.4	35.4	9.1
X281011A-BOTTOM	0.2	3.3	28.8	2.4	6.1	0.3
X01111A-TOP	0.3	31.6	34.9	4.8	18.6	5.4
X01111A-BOTTOM	0.2	5.7	16.8	1.9	4.3	0.1
X041111A-TOP	0	0	20.4	2.7	20	1.3
X041111A-BOTTOM	0.1	1.6	6.1	0.3	1.4	0.1
X08111A-TOP	0	0	9.8	1.5	9.3	2
X08111A-BOTTOM	0	0.1	0.1	0	0.1	0
X18111A-TOP	1.3	142.9	91	10.1	63.8	6
X18111A-BOTTOM	0	0	4	0	2.8	0.1
X071211A-TOP	0.6	9.9	14.4	1.7	9.3	1.1
X071211A-BOTTOM	0	0	5.2	0	1	0.1
X121211A-TOP	0.3	0.5	58.6	12.9	32.47	7.5
X121211A-BOTTOM	0.2	0.8	33.2	7.5	20.9	0.8
X131211A-TOP	0.4	55.2	32.7	9.7	24.9	5.7
X131211A-BOTTOM	0.1	47.7	26.8	6.1	13.8	0.2
X161211A-TOP	0.9	7	7.1	1.1	6.6	0.6
X161211A-BOTTOM	0	0	0.9	0	2.5	0
X190612A	0.2	0.9	230.8	11.7	41.4	14.5
X200612A	0.4	0.7	191.9	10.3	35.6	16.5
X020812A	0.5	4.3	202.5	10.3	36.7	11.7
X040812A	0.7	0.7	314.7	18.8	57.3	32.6
X050812A	0.6	2.2	78.8	4.4	15.1	5.6
X060812A	0.9	7.2	238.6	16	40.2	24.7
X070812A-BOTTOM	0.1	0.3	15.7	4.3	3.3	0.4

Filter	Solution Concentration (ng μL^{-1})					
	4-me-ph	4-me-2-NP	4-NP	3-me-4-NP	2-me-4-NP	2,6-dime-4-NP
X090812A-TOP	0.1	1.4	14.1	0.9	4.5	2.2
X110812A-TOP	0.9	9.5	90.1	5.6	17.1	16.4
X110812A-BOTTOM	0.1	1.1	7.6	0.7	7.3	6.2
X120812A-TOP	1.2	9.1	69.7	4.4	12.1	3.4
X120812A-BOTTOM	0.2	6	3.1	0.2	1.3	0.4

[a] Sampled, extracted and analyzed by Busca (2010)

Filters are named according to the following code: ABbCcDdE where:

A is either Q (quartz filter) or X (XAD-coated filter)
Bb is the day
Cc is the month
Dd is the year
E is the air sampler (A or B)

Appendix D: Stable Carbon Isotope Ratios of Ambient Nitrophenols

Filter	Stable Carbon Isotope Ratio (‰)						
	4-me-2-NP	4-NP	3-me-4-NP	2-me-4-NP	2,6-dime-4-NP	2-me-3-NP	2-me-5-NP
Q120309B	-	-36.2	-	-34.1	-	-27.1	-27.4
Q240409B	-	-34.3	-33.8	-33.4	-	-26.5	-27.4
Q270409B	-	-33.9	-32.4	-34.0	-	-26.8	-27.4
Q190509B	-	-	-	-33.5	-		-26.8
Q040609A	-	-33.7	-36.2	-36.0	-	-26.5	-27.2
Q040609B	-	-33.7	-36.0	-35.5	-	-26.9	-27.3
Q190609A	-	-32.4	-32.2	-32.7	-35.5	-26.6	-27.5
Q190609B	-	-32.4	-32.2	-32.7	-35.9	-26.6	-27.4
Q220609APM10	-	-34.3	-36.2	-33.9	-	-27.0	-26.9
Q220609BPM2.5	-	-	-35.5	-33.9	-	-26.8	-27.2
Q180709A	-	-34.6	-	-32.3	-	-26.7	-27.2
Q180709B + Q190709B + Q200709B	-	-	-31.2	-31.1	-	-26.8	-27.2
Q270709A	-	-32.5	-	-32.7	-	-26.5	-27.1
Q050809A	-	-	-	-33.6	-	-26.8	-27.1
Q130809B	-	-34.5	-	-33.7	-	-26.8	-27.1
Q180809A + Q210809A	-	-31.5	-31.7	-31.0	-	-26.8	-27.0
Q240809A	-	-35.1	-	-31.7	-	-26.5	-27.1
Q280809A	-	-	-	-33.7	-	-26.6	-27.2
Q310809A	-	-33.6	-31.8	-33.6	-	-26.3	-26.6
Q040909A	-	-34.4	-32.2	-34.7	-	-26.4	-27.3
Q210909B	-	-34.3	-	-33.8	-	-26.7	-27.1
Q240909A-TOP	-	-34.4	-34.1	-34.4	-	-26.7	-27.4

Filter	Stable Carbon Isotope Ratio (‰)						
	4-me-2-NP	4-NP	3-me-4-NP	2-me-4-NP	2,6-dime-4-NP	2-me-3-NP	2-me-5-NP
Q051009B	-	-32.6	-33.1	-34.7	-	-26.4	-27.0
Q131009B	-	-32.2	-30.7	-33.2	-	-26.7	-27.0
Q131009A-AM + Q141009A-AM + Q151009A-AM	-	-	-	-33.0	-	-26.6	-27.1
Q131009A-PM + Q151009A-PM	-	-30.4	-28.4	-28.4	-	-26.5	-27.2
Q191009A	-	-32.3	-32.6	-34.7	-33.5	-26.3	-26.9
Q261009A	-	-33.4	-	-31.3	-	-26.7	-27.3
Q271009A	-34.3	-30.4	-	-35.5	-35.1	-26.5	-27.1
Q281009A	-34.7	-33.7	-34.6	-35.4	-33.1	-26.7	-27.3
Q051109A	-32.8	-	-34.0	-32.3	-34.9	-26.8	-27.2
Q061109A	-	-33.6	-33.4	-31.6	-	-26.7	-27.5
Q161109A	-	-36.4	-32.1	-31.3	-	-27.2	-27.1
Q050110A	-33.3	-35.7	-	-33.6	-	-26.9	-27.1
Q090911A	-	-33.8	-	-35.7	-	-26.7	-27.0
Q071011A	-	-	-35.3	-33.2	-	-27.0	-26.7
Q181111B	-	-32.5	-	-30.3	-	-26.6	-26.8
Q071211B	-	-33.5	-	-31.2	-	-27.1	-27.6
Q121211B	-	-33.4	-	-34.2	-	-26.7	-27.5
Q131211B	-	-33.8	-32.7	-33.4	-	-26.6	-27.1
Q161211B	-	-33.2	-	-31.8	-	-26.6	-27.0
Q140512A	-	-33.2	-34.5	-	-	-26.7	-27.1
Q130612A	-	-	-30.9	-	-	-26.5	-27.1
Q190612B	-	-	-	-32.0	-		-26.9
Q050712A	-	-31.1	-30.6	-30.9	-	-26.8	-27.4
Q070812A-TOP	-	-	-32.4	-32.3	-30.6	-26.5	-27.3
X300709B[a]	-	-34.6	-32.6	-31.7	-	-26.8	-27.0

Filter	Stable Carbon Isotope Ratio (‰)						
	4-me-2-NP	4-NP	3-me-4-NP	2-me-4-NP	2,6-dime-4-NP	2-me-3-NP	2-me-5-NP
X050809B[a]	-	-32.3	-31.1	-30.9	-	-26.7	-27.1
X070809A[a]	-31.4	-33.6	-32.6	-34.3	-34.9	-26.6	-27.1
X070809B[a]	-30.7	-33.2	-32.8	-34.6	-35.7	-26.7	-27.3
X100809A[a]	-33.6	-34.8	-33.5	-35.0	-	-26.9	-27.4
X130809A[a]	-	-	-30.0	-30.2	-	-26.7	-27.1
X210809B[a]	-	-33.0	-33.2	-32.0	-31.7	-26.9	-27.6
X280809B[a]	-	-32.3	-31.1	-34.2	-	-26.8	-27.3
X280909B[a]	-	-33.0	-34.6	-34.8	-	-26.6	-27.2
X131109A[a]	-	-	-32.3	-33.9	-	-26.5	-27.5
X051011A-TOP	-	-36.0	-	-33.0	-	-26.9	-27.6
X051011A-BOTTOM	-	-35.3	-	-32.9	-	-26.6	-27.2
X061011A-TOP	-	-36.4	-	-31.7	-37.0	-26.9	-27.0
X061011A-BOTTOM	-	-37.0	-	-31.9	-	-26.7	-27.0
X211011A-TOP	-33.1	-35.7	-	-32.6	-	-26.3	-27.2
X211011A-BOTTOM	-	-34.7	-	-32.9	-	-26.6	-27.6
X281011A-TOP	-	-35.5	-	-33.5	-29.4	-26.8	-27.5
X281011A-BOTTOM	-	-35.3	-	-33.7	-	-26.5	-27.0
X01111A-TOP	-	-35.3	-	-30.6	-34.9	-26.9	-27.0
X01111A-BOTTOM	-	-35.1	-	-30.1	-	-26.4	-27.0
X041111A-TOP	-	-31.3	-	-31.2	-	-26.6	-27.3
X08111A-TOP	-	-31.6	-34.1	-30.7	-31.4	-26.9	-27.2
X08111A-BOTTOM	-	-32.0	-	-30.5	-	-27.0	-27.6
X18111A-TOP	-	-31.8	-	-31.2	-	-26.4	-27.3
X18111A-BOTTOM	-	-30.7	-	-31.5	-	-26.4	-27.2
X071211A-TOP	-	-34.9	-	-31.3	-	-26.9	-27.0
X071211A-BOTTOM	-	-34.4	-	-31.6	-	-26.4	-27.3
X121211A-TOP	-	-33.8	-35.4	-33.1	-33.8	-26.8	-26.8
X121211A-BOTTOM	-	-34.5	-	-33.7	-	-26.6	-27.2

Filter	Stable Carbon Isotope Ratio (‰)						
	4-me-2-NP	4-NP	3-me-4-NP	2-me-4-NP	2,6-dime-4-NP	2-me-3-NP	2-me-5-NP
X131211A-TOP	-33.8	-33.7	-34.4	-34.5	-34.4	-26.9	-27.1
X131211A-BOTTOM	-34.2	-34.2	-33.3	-34.4	-	-26.8	-26.9
X161211A-TOP	-	-33.1	-	-31.2	-	-26.4	-27.4
X161211A-BOTTOM	-	-33.9	-	-31.5	-	-26.3	-27.2
X190612A	-34.6	-34.3	-35.5	-35.5	-	-26.4	-27.3
X200612A	-33.2	-35.0	-34.2	-34.0	-33.3	-26.6	-27.1
X020812A	-31.8	-32.7	-33.1	-32.9	-31.5	-26.5	-27.3
X040812A	-33.5	-33.6	-32.9	-32.8	-32.4	-26.6	-27.2
X050812A	-	-32.7	-32.8	-31.4	-34.4	-26.6	-27.1
X060812A	-32.9	-31.2	-	-32.2	-33.3	-26.7	-27.1
X090812A-TOP	-31.0	-33.2	-33.5	-33.4	-32.2	-26.7	-27.0
X090812A-BOTTOM	-	-	-33.9	-33.8	-	-26.5	-27.3
X110812A-TOP	-33.5	-30.7	-	-32.8	-	-26.8	-27.1

[a] Sampled and extracted by Busca (2010)

Filters are named according to the following code: ABbCcDdE where:

A is either Q (quartz filter) or X (XAD-coated filter)
Bb is the day
Cc is the month
Dd is the year
E is the air sampler (A or B)

Appendix E: Photochemical Ages Calculated Without Intermediate Fractionation

Filter	PCA x 10^{11} (s molec cm^{-3})				
	4-me-2-NP	4-NP	3-me-4-NP	2-me-4-NP	2,6-dime-4-NP
Q120309B		-0.73		-0.42	
Q240409B		3.08	-0.20	0.02	
Q270409B		3.83	0.74	-0.33	
Q190509B					
Q040609A		4.46	-1.57	-1.46	
Q040609B		4.32	-1.47	-1.21	
Q190609A		7.61	0.86	0.52	-0.50
Q190609B		7.73	0.90	0.54	-0.55
Q220609APM10		3.11	-1.56	-0.25	
Q220609BPM2.5			-1.22	-0.28	
Q180709A		2.33		0.85	
Q180709B + Q190709B + Q200709B			1.66	1.80	
Q270709A		7.23		0.50	
Q050809A				-0.06	
Q130809B		2.57		-0.13	
Q180809A + Q210809A		10.31	1.30	1.89	
Q240809A		1.45		1.28	
Q280809A				-0.11	
Q310809A		4.56	1.16	-0.11	
Q040909A		2.77	0.89	-0.77	
Q210909B		2.99		-0.23	
Q240909A-TOP		2.82	-0.38	-0.59	
Q051009B		7.13	0.23	-0.73	
Q131009B		8.28	2.18	0.17	
Q131009A-AM + Q141009A-AM + Q151009A-AM				0.33	
Q131009A-PM + Q151009A-PM		15.06	5.63	5.69	
Q191009A		7.81	0.58	-0.75	-0.22
Q261009A		5.17		1.63	
Q271009A	-0.53	15.51		-1.20	-0.44
Q281009A	-0.76	4.38	-0.69	-1.15	-0.14

Filter	PCA x 10^{11} (s molec cm^{-3})				
	4-me-2-NP	4-NP	3-me-4-NP	2-me-4-NP	2,6-dime-4-NP
Q051109A	0.45		-0.33	0.80	-0.41
Q061109A		4.61	0.05	1.32	
Q161109A		-1.10	0.96	1.57	
Q050110A	0.14	0.33		-0.05	
Q090911A		4.14		-1.30	
Q071011A			-1.09	0.20	
Q181111B		7.49		2.52	
Q071211B		4.86		1.68	
Q121211B		4.94		-0.47	
Q131211B		4.16	0.56	0.04	
Q161211B		5.43		1.17	
Q140512A		5.62	-0.61		
Q130612A			1.92		
Q190612B				1.00	
Q050712A		12.12	2.21	1.91	
Q070812A-TOP			0.76	0.84	0.33
X210809B[a]		6.05	0.21	1.02	0.10
X280809B[a]		7.88	1.82	-0.43	
X280909B[a]		6.03	-0.72	-0.81	
X131109A[a]			0.78	-0.28	
X051011A-TOP		-0.28		0.34	
X061011A-TOP		-1.03		1.27	-0.29
X211011A-TOP	0.28	0.25		0.60	
X281011A-TOP		0.65		-0.04	0.68
X01111A-TOP		1.01		2.21	-0.36
X041111A-TOP		11.21		1.70	
X08111A-TOP		10.22	-0.41	2.18	0.17
X18111A-TOP		9.51		1.66	
X071211A-TOP		1.83		1.57	
X121211A-TOP		4.10	-1.16	0.22	-0.25
X131211A-TOP	-0.23	4.28	-0.57	-0.66	-0.35
X161211A-TOP		5.71		1.70	
X190612A	-0.69	3.06	-1.17	-1.18	
X200612A	0.15	1.53	-0.47	-0.33	-0.18
X020812A	1.22	6.69	0.28	0.37	0.13
X040812A	-0.02	4.64	0.39	0.44	0.00
X050812A		6.90	0.46	1.55	-0.35
X060812A	0.40	11.48		0.90	-0.18
X090812A-TOP	1.90	5.60	-0.01	0.08	0.00
X110812A-TOP	-0.02	13.84		0.46	

[a] Sampled and extracted by Busca (2010)

Appendix F: Photochemical Ages Calculated With Intermediate Fractionation

Filter	PCA x 10^{11} (s molec cm^{-3})				
	4-me-2-NP	4-NP	3-me-4-NP	2-me-4-NP	2,6-dime-4-NP
Q120309B				0.67	
Q240409B		2.40	0.56	0.81	
Q270409B		3.13	0.83	0.68	
Q190509B				0.79	
Q040609A		3.48	0.22	0.35	
Q040609B		3.48	0.24	0.43	
Q190609A		5.88	0.88	0.96	0.12
Q190609B		5.88	0.88	0.96	0.09
Q220609APM10		2.40	0.22	0.71	
Q220609BPM2.5			0.30	0.71	
Q180709A		1.88		1.06	
Q180709B + Q190709B + Q200709B			1.15	1.37	
Q270709A		5.69		0.96	
Q050809A		0.00		0.77	
Q130809B		2.05		0.75	
Q180809A + Q210809A		7.63	1.01	1.39	
Q240809A		0.95		1.21	
Q280809A				0.74	
Q310809A		3.65	0.98	0.77	
Q040909A		2.23	0.88	0.56	
Q210909B		2.40		0.73	
Q240909A-TOP		2.23	0.49	0.61	
Q051009B		5.50	0.68	0.56	
Q131009B		6.25	1.30	0.85	
Q131009A-AM + Q141009A-AM + Q151009A-AM				0.89	
Q131009A-PM + Q151009A-PM			2.06	2.21	
Q191009A		6.08	0.79	0.56	0.29
Q261009A		4.03		1.31	
Q271009A	0.56	9.89		0.43	0.15
Q281009A	0.49	3.48	0.42	0.44	0.33
Q051109A	0.86		0.50	1.06	0.16

Filter	PCA x 10^{11} (s molec cm^{-3})				
	4-me-2-NP	4-NP	3-me-4-NP	2-me-4-NP	2,6-dime-4-NP
Q061109A		3.65	0.62	1.23	
Q161109A			0.91	1.31	
Q050110A	0.75			0.77	
Q090911A		3.30		0.40	
Q071011A			0.33	0.85	
Q181111B		5.68		1.60	
Q071211B		3.85		1.34	
Q121211B		4.03		0.65	
Q131211B		3.30	0.76	0.81	
Q161211B		4.39		1.18	
Q140512A		4.39	0.43		
Q130612A			1.24		
Q190612B				1.13	
Q050712A		8.43	1.33	1.42	
Q070812A-TOP			0.83	1.05	0.69
X210809B[a]		1.88	0.785	1.21	
X280809B[a]		6.08	1.18	1.43	
X280909B[a]	1.2	3.65	0.785	0.63	0.16
X131109A[a]	1.41	4.38	0.74	0.578	0.095
X051011A-TOP	0.69	1.5	0.6	0.5	
X061011A-TOP			1.52	1.63	
X211011A-TOP		4.75	0.655	1.13	0.51
X281011A-TOP		6.08	1.18	0.65	
X01111A-TOP		4.75	0.42	0.54	
X041111A-TOP			0.86	0.708	
X08111A-TOP				0.89	
X18111A-TOP				1.21	0.24
X071211A-TOP	0.79			0.985	
X121211A-TOP		0.125		0.79	0.97
X131211A-TOP		0.55		1.51	0.16
X161211A-TOP		8.03		1.34	
X190612A		7.43	0.495	1.48	0.555
X200612A		7.04		1.34	
X020812A		1.33		1.31	
X040812A		3.3	0.315	0.87	0.26
X050812A	0.65	3.48	0.45	0.595	0.205
X060812A		4.58		1.34	
X090812A-TOP	0.51	2.4	0.3	0.43	
X110812A-TOP	0.77	1.13	0.47	0.68	0.31

[a] Sampled and extracted by Busca (2010)

Appendix G: Look-Up Table for Photochemical Ages of Products in the Gas Phase and PM Calculated with Intermediate Fractionation

4-me-2-NP		4-NP		3-me-4-NP		2-me-4-NP		2,6-dime-4-NP	
$\delta^{13}C_{V\text{-}PDB}$ (‰)	PCA x 10^{11} (s molec cm^{-3})	$\delta^{13}C_{V\text{-}PDB}$ (‰)	PCA x 10^{11} (s molec cm^{-3})	$\delta^{13}C_{V\text{-}PDB}$ (‰)	PCA x 10^{11} (s molec cm^{-3})	$\delta^{13}C_{V\text{-}PDB}$ (‰)	PCA x 10^{11} (s molec cm^{-3})	$\delta^{13}C_{V\text{-}PDB}$ (‰)	PCA x 10^{11} (s molec cm^{-3})
-38.6	0.06	-35.5	0.20	-38.6	0.05	-38.6	0.06	-36.7	0.03
-38.3	0.09	-35.5	0.30	-38.3	0.08	-38.3	0.09	-36.5	0.05
-38.0	0.12	-35.4	0.40	-37.9	0.10	-38.1	0.12	-36.3	0.06
-37.7	0.15	-35.4	0.50	-37.6	0.13	-37.8	0.15	-36.1	0.08
-37.4	0.18	-35.3	0.60	-37.3	0.15	-37.6	0.18	-35.9	0.09
-37.1	0.21	-35.3	0.70	-37.0	0.18	-37.3	0.21	-35.7	0.11
-36.8	0.24	-35.2	0.80	-36.7	0.20	-37.1	0.24	-35.5	0.12
-36.6	0.27	-35.2	0.90	-36.4	0.23	-36.8	0.27	-35.3	0.14
-36.3	0.30	-35.1	1.00	-36.2	0.25	-36.6	0.30	-35.1	0.15
-36.1	0.33	-35.1	1.10	-35.9	0.28	-36.4	0.33	-34.9	0.17
-35.8	0.36	-35.0	1.20	-35.7	0.30	-36.2	0.36	-34.8	0.18
-35.6	0.39	-35.0	1.30	-35.5	0.33	-36.0	0.39	-34.6	0.20
-35.4	0.42	-34.9	1.40	-35.3	0.35	-35.8	0.42	-34.4	0.21
-35.2	0.45	-34.9	1.50	-35.1	0.38	-35.6	0.45	-34.3	0.23
-35.0	0.48	-34.8	1.60	-34.9	0.40	-35.4	0.48	-34.1	0.24
-34.8	0.51	-34.8	1.70	-34.7	0.43	-35.2	0.51	-33.9	0.26
-34.6	0.54	-34.7	1.80	-34.6	0.45	-35.0	0.54	-33.8	0.27
-34.5	0.57	-34.7	1.90	-34.4	0.48	-34.9	0.57	-33.6	0.29
-34.3	0.60	-34.6	2.00	-34.2	0.50	-34.7	0.60	-33.5	0.30
-34.1	0.63	-34.6	2.10	-34.1	0.53	-34.5	0.63	-33.3	0.32
-34.0	0.66	-34.5	2.20	-33.9	0.55	-34.4	0.66	-33.2	0.33
-33.8	0.69	-34.4	2.30	-33.8	0.58	-34.2	0.69	-33.0	0.35

4-me-2-NP		4-NP		3-me-4-NP		2-me-4-NP		2,6-dime-4-NP	
$\delta^{13}C_{V\text{-}PDB}$ (‰)	PCA x 10^{11} (s molec cm^{-3})	$\delta^{13}C_{V\text{-}PDB}$ (‰)	PCA x 10^{11} (s molec cm^{-3})	$\delta^{13}C_{V\text{-}PDB}$ (‰)	PCA x 10^{11} (s molec cm^{-3})	$\delta^{13}C_{V\text{-}PDB}$ (‰)	PCA x 10^{11} (s molec cm^{-3})	$\delta^{13}C_{V\text{-}PDB}$ (‰)	PCA x 10^{11} (s molec cm^{-3})
-33.7	0.72	-34.4	2.40	-33.7	0.60	-34.1	0.72	-32.9	0.36
-33.5	0.75	-34.3	2.50	-33.5	0.63	-33.9	0.75	-32.8	0.38
-33.4	0.78	-34.3	2.60	-33.4	0.65	-33.8	0.78	-32.6	0.39
-33.2	0.81	-34.2	2.70	-33.3	0.68	-33.6	0.81	-32.5	0.41
-33.1	0.84	-34.2	2.80	-33.2	0.70	-33.5	0.84	-32.4	0.42
-33.0	0.87	-34.1	2.90	-33.1	0.73	-33.3	0.87	-32.3	0.44
-32.8	0.90	-34.1	3.00	-32.9	0.75	-33.2	0.90	-32.2	0.45
-32.7	0.93	-34.0	3.10	-32.8	0.78	-33.1	0.93	-32.0	0.47
-32.6	0.96	-34.0	3.20	-32.7	0.80	-33.0	0.96	-31.9	0.48
-32.5	0.99	-33.9	3.30	-32.6	0.83	-32.8	0.99	-31.8	0.50
-32.4	1.02	-33.8	3.40	-32.5	0.85	-32.7	1.02	-31.7	0.51
-32.2	1.05	-33.8	3.50	-32.4	0.88	-32.6	1.05	-31.6	0.53
-32.1	1.08	-33.7	3.60	-32.3	0.90	-32.5	1.08	-31.5	0.54
-32.0	1.11	-33.7	3.70	-32.2	0.93	-32.3	1.11	-31.4	0.56
-31.9	1.14	-33.6	3.80	-32.1	0.95	-32.2	1.14	-31.3	0.57
-31.8	1.17	-33.6	3.90	-32.1	0.98	-32.1	1.17	-31.2	0.59
-31.7	1.20	-33.5	4.00	-32.0	1.00	-32.0	1.20	-31.1	0.60
-31.6	1.23	-33.5	4.10	-31.9	1.03	-31.9	1.23	-31.0	0.62
-31.5	1.26	-33.4	4.20	-31.8	1.05	-31.8	1.26	-30.9	0.63
-31.4	1.29	-33.4	4.30	-31.7	1.08	-31.7	1.29	-30.9	0.65
-31.3	1.32	-33.3	4.40	-31.6	1.10	-31.6	1.32	-30.8	0.66
-31.2	1.35	-33.3	4.50	-31.6	1.13	-31.5	1.35	-30.7	0.68
-31.1	1.38	-33.2	4.60	-31.5	1.15	-31.4	1.38	-30.6	0.69
-31.0	1.41	-33.2	4.70	-31.4	1.18	-31.3	1.41	-30.5	0.71
-30.9	1.44	-33.1	4.80	-31.3	1.20	-31.2	1.44	-30.5	0.72
-30.8	1.47	-33.0	4.90	-31.2	1.23	-31.1	1.47	-30.4	0.74

4-me-2-NP		4-NP		3-me-4-NP		2-me-4-NP		2,6-dime-4-NP	
$\delta^{13}C_{V\text{-}PDB}$ (‰)	PCA x 10^{11} (s molec cm^{-3})	$\delta^{13}C_{V\text{-}PDB}$ (‰)	PCA x 10^{11} (s molec cm^{-3})	$\delta^{13}C_{V\text{-}PDB}$ (‰)	PCA x 10^{11} (s molec cm^{-3})	$\delta^{13}C_{V\text{-}PDB}$ (‰)	PCA x 10^{11} (s molec cm^{-3})	$\delta^{13}C_{V\text{-}PDB}$ (‰)	PCA x 10^{11} (s molec cm^{-3})
-30.7	1.50	-33.0	5.00	-31.2	1.25	-31.0	1.50	-30.3	0.75
-30.6	1.53	-32.9	5.10	-31.1	1.28	-30.9	1.53	-30.2	0.77
-30.5	1.56	-32.9	5.20	-31.0	1.30	-30.8	1.56	-30.2	0.78
-30.5	1.59	-32.8	5.30	-30.9	1.33	-30.7	1.59	-30.1	0.80
-30.4	1.62	-32.8	5.40	-30.9	1.35	-30.6	1.62	-30.0	0.81
-30.3	1.65	-32.7	5.50	-30.8	1.38	-30.5	1.65	-30.0	0.83
-30.2	1.68	-32.7	5.60	-30.7	1.40	-30.4	1.68	-29.9	0.84
-30.1	1.71	-32.6	5.70	-30.7	1.43	-30.4	1.71	-29.8	0.86
-30.0	1.74	-32.6	5.80	-30.6	1.45	-30.3	1.74	-29.8	0.87
-29.9	1.77	-32.5	5.90	-30.5	1.48	-30.2	1.77	-29.7	0.89
-29.9	1.80	-32.5	6.00	-30.4	1.50	-30.1	1.80	-29.7	0.90
-29.8	1.83	-32.4	6.10	-30.4	1.53	-30.0	1.83	-29.6	0.92
-29.7	1.86	-32.4	6.20	-30.3	1.55	-29.9	1.86	-29.6	0.93
-29.6	1.89	-32.3	6.30	-30.2	1.58	-29.8	1.89	-29.5	0.95
-29.5	1.92	-32.3	6.40	-30.2	1.60	-29.8	1.92	-29.4	0.96
-29.4	1.95	-32.2	6.50	-30.1	1.63	-29.7	1.95	-29.4	0.98
-29.4	1.98	-32.2	6.60	-30.0	1.65	-29.6	1.98	-29.3	0.99
-29.3	2.01	-32.1	6.70	-30.0	1.68	-29.5	2.01	-29.3	1.01
-29.2	2.04	-32.1	6.80	-29.9	1.70	-29.4	2.04	-29.2	1.02
-29.1	2.07	-32.0	6.90	-29.8	1.73	-29.3	2.07	-29.2	1.04
-29.0	2.10	-32.0	7.00	-29.8	1.75	-29.3	2.10	-29.2	1.05
-29.0	2.13	-31.9	7.10	-29.7	1.78	-29.2	2.13	-29.1	1.07
-28.9	2.16	-31.9	7.20	-29.6	1.80	-29.1	2.16	-29.1	1.08
-28.8	2.19	-31.8	7.30	-29.6	1.83	-29.0	2.19	-29.0	1.10
-28.7	2.22	-31.8	7.40	-29.5	1.85	-28.9	2.22	-29.0	1.11

Appendix H: Meteorological Data for Sampling Dates

Filter	Average Temp. (^{0}C)[a]	Max Temp. (^{0}C)[a]	Min Temp. (^{0}C)[a]	Wind Direction (^{0})[b]	Max Wind Speed (km h^{-1})[a]	Total Rain (mm)[a]	Total Snow (cm)[a]	Total Precipitation (mm)[a]
Q120309B	-0.8	9.6	-10.3	90 & 240 & 300	41	0	Trace	Trace
Q160409B	4.8	21.2	2.5	40	59	Trace	0	Trace
Q240409B	14.6	27.9	4.8	350-10	115	12.8	0	12.8
Q270409B	12.1	27.5	3.6	140 & 300	69	10.4	0	10.4
Q190509A	17.4	27.6	0.3	180 & 320	59	5.2	0	5.2
Q190509B	17.4	27.6	0.3	180 & 320	59	5.2	0	5.2
Q040609A	14.5	23	6.8	330	39	0	0	0
Q040609B	14.5	23	6.8	330	39	0	0	0
Q190609A	18.1	26.5	11.6	70	39	14.4	0	14.4
Q190609B	18.1	26.5	11.6	70	39	14.4	0	14.4
Q220609APM10	22.8	27.2	16.6	60	17	0	0	0
Q220609BPM2.5	22.8	27.2	16.6	60	17	0	0	0
Q290609B-TOP	14.5	24	14.1	290-300	22	21.6	0	21.6
Q290609B-BOTTOM	14.5	24	14.1	290-300	22	21.6	0	21.6
Q030709A-TOP	21.5	22.1	20.6	330-350	37	0	0	0
Q060709A-TOP	18.3	25.1	17	310	48	0.4	0	0.4
Q060709A-BOTTOM	18.3	25.1	17	310	48	0.4	0	0.4
Q130709A	17.8	25.4	10.6	310	57	0.4	0	0.4
Q150709A	19.1	27.8	11.7	290 & 330	39	0.6	0	0.6

Filter	Average Temp. (^{0}C)[a]	Max Temp. (^{0}C)[a]	Min Temp. (^{0}C)[a]	Wind Direction (^{0})[b]	Max Wind Speed (km h^{-1})[a]	Total Rain (mm)[a]	Total Snow (cm)[a]	Total Precipitation (mm)[a]
Q180709A	18.3	24.8	12	90 & 310	44	Trace	0	Trace
Q180709B	18.7	23.2	14.2	90 & 310	44	Trace	0	Trace
Q190709B	17.5	23	12	90 & 310	35	0	0	0
Q200709B	18.7	24.8	12.5	90 & 310	19	0	0	0
Q270709A	21.5	27.8	14.2	225	52	Trace	0	Trace
Q290709A	20.2	27.7	13.4	230	37	10.6	0	10.6
Q050809A	18.7	24.4	10.9	310-330	37	0	0	0
Q130809B	23.4	29.6	16.8	210	20	0	0	0
Q180809A	23.9	29.5	17.3	0	41	25.6	0	25.6
Q210809A	20.8	27.2	14.7	0	50	1.4	0	0
Q240809A	19	25.8	13.5	250 & 340	35	2.8	0	2.8
Q280809A	16.7	22.3	11.4	350	50	22.2	0	22.2
Q310809A	16.7	23.6	10.5	270 & 340	20	0	0	0
Q040909A	19.3	24.8	14.1	90-160	19	0	0	0
Q150909A	15.5	23.5	8.8	260 & 60	37	0	0	0
Q180909A	13.2	21.2	4.8	270 & 20	48	Trace	0	Trace
Q210909B	20.3	22	13	260-290	46	4.4	0	4.4
Q240909A-TOP	15.3	22.5	8.1	210-230	33	12.8	0	12.8
Q280909A	10.6	18	2.4	350-0	67	22.8	0	22.8
Q011009A	10.1	17.2	2.4	280 & 0	59	13.8	0	13.8
Q051009B	10.6	17.6	5.5	220	72	9.4	0	9.4
Q131009B	3.9	10.7	-1.2	70 & 330	52	0	0	0
Q131009A-AM	7.6	9.7	5.3	0 & 320	33	0	0	0
Q131009A-PM	2	4.5	-0.4	320	22	0	0	0

Filter	Average Temp. (^{0}C)[a]	Max Temp. (^{0}C)[a]	Min Temp. (^{0}C)[a]	Wind Direction (^{0})[b]	Max Wind Speed (km h^{-1})[a]	Total Rain (mm)[a]	Total Snow (cm)[a]	Total Precipitation (mm)[a]
Q141009A-AM	4.7	6.3	1.8	0 & 320-330	20	0	0	0
Q151009A-AM	3.5	4.1	2.4	70 & 330	33	0	0	0
Q151009A-PM	1.7	3.7	-0.2	60 & 330	20	0	0	0
Q191009A	10.9	15.2	0.3	350	41	2.8	0	2.8
Q261009A	8.8	11.8	5.8	160 & 300	39	0	0	0
Q271009A	12.3	16.3	8.2	150-170 & 300	11	1.2	0	1.2
Q281009A	11.3	13	9.6	50 & 110 & 330	24	2.2	0	2.2
Q291009A	10.1	11	9.2	90	17	2.6	0	2.6
Q051109A	4.4	7.5	1.5	300-320	43	1.6	0	1.6
Q061109A	1.9	4.9	-1.1	190 & 320	15	0	0	0
Q071109A	10.3	16.1	4.5	270	41	0	0	0
Q161109A	4.3	8.8	-2.3	230 & 320	37	12.6	0	12.6
Q231109A	7.4	10.6	2.4	230	22	7.4	0	7.4
Q271109A	3.2	7.1	-3	320-330	56	5	0	5
Q101209A	-5.6	1.7	-10.2	180	74	0	1.4	1
Q050110A	-7.4	-2.1	-11.1	350	39	0	3	2
Q060110A	-6.2	-2.1	-10.3	340-350	37	0	Trace	0
Q070110A	-5.2	-7.3	-3	350-0	19	0	Trace	Trace
Q240210A	-2.3	0.9	-7.5	0	61	0	Trace	Trace
Q240210B	-2.3	0.9	-7.5	0	61	0	Trace	Trace
Q020310B-TOP	-0.2	4.4	-3.4	0	32	0	0	0

Filter	Average Temp. (^{0}C)[a]	Max Temp. (^{0}C)[a]	Min Temp. (^{0}C)[a]	Wind Direction (^{0})[b]	Max Wind Speed (km h^{-1})[a]	Total Rain (mm)[a]	Total Snow (cm)[a]	Total Precipitation (mm)[a]
Q020310B-BOTTOM	-0.2	4.4	-3.4	0	32	0	0	0
Q190310B	4.7	19.1	-1.6	280 & 330	50	4	0	4
Q310310A-TOP	7.5	0.3	14.7	210 & 310	19	0	0	0
Q190410A	9.8	16.2	4.4	350-0	39	0	0	0
Q210410A	11.3	19.1	3.4	350-0	48	Trace	0	Trace
Q290410B	11.5	19.5	3.5	240 & 30	32	Trace	0	Trace
Q050510A	19.5	27.2	11.8	250	65	5.4	0	5.4
Q060510A	11.4	15.5	7.2	320	57	0	0	0
Q280510A	22.2	30.7	14.8	210 & 0	41	0	0	0
Q310510A	21.6	27.9	14.5	220 & 300	37	0.6	0	0.6
Q040610A	18.1	25.4	11.4	350-0	48	27.4	0	27.4
Q070610A	14.2	20.3	7.5	280-290	48	11.8	0	11.8
Q070610B	14.2	20.3	7.5	280-290	48	11.8	0	11.8
Q110610A	18.1	23.1	13.2	310 & 60	26	3.6	0	3.6
Q250710A	22.4	29	16.1	210 & 330	41	0	0	0
Q090810A	24.4	28.6	20.2	230 & 300	32	9.8	0	9.8
Q100810A	24.8	30.5	19.9	110 & 230	35	0	0	0
Q160810A	21.3	28.3	15.4	230 & 280	54	0	0	0
Q270810A	20.7	30.9	9.7	220-230	37	0	0	0
Q300810A	27.4	34.5	20	220	46	0	0	0

Filter	Average Temp. (^{0}C)[a]	Max Temp. (^{0}C)[a]	Min Temp. (^{0}C)[a]	Wind Direction (^{0})[b]	Max Wind Speed (km h^{-1})[a]	Total Rain (mm)[a]	Total Snow (cm)[a]	Total Precipitation (mm)[a]
Q130910A	15.6	24.3	8.2	310-320	48	1.8	0	1.8
Q200910A	12.7	18.4	6.9	310-320	19	0	0	0
Q210910A	18.9	26.9	10.8	180-220	48	Trace	0	Trace
Q291010A	6.2	14.1	-1.6	0	52	0.4	0	0.4
Q040211A-TOP	-4.6	0.6	-10.2	230 & 310	59	0	14.2	11.2
Q230211A-TOP	-3	-0.4	-9.9	340-0	17	0	0	0
Q250211A-TOP	-4.3	0.6	-9.1	310-340	50	0	7	4.4
Q090911A	19.5	25.8	12.6	255 & 320	19	0	0	0
Q071011A	17.2	27.5	7.1	150-180 & 350	19	0	0	0
Q181111B	2.8	7.6	-2	230 & 310	50	0	0	0
Q071211B	-0.5	1.3	-2.2	270	19	0	Trace	Trace
Q121211B	2.3	6.8	-2.2	220	20	0	0	0
Q131211B	3	8.6	-2.6	240	13	0	0	0
Q161211B	1.9	5.1	-1.3	330-350	57	0	0.2	0.2
Q140512A	16.2	22.3	10.1	310	15	0	0	0
Q230512A	20.3	24	16.5	130	17	0	0	0
Q300512A	17.6	23.6	11.6	350 & 230	32	0	0	0
Q040612A	13.4	16.7	10	50-70	20	1	0	1
Q040612B	13.4	16.7	10	50-70	20	1	0	1
Q060612A	18.7	24.7	12.7	330 & 50	20	6.8	0	6.8
Q060612B	18.7	24.7	12.7	330 & 50	20	6.8	0	6.8

Filter	Average Temp. (^{0}C)[a]	Max Temp. (^{0}C)[a]	Min Temp. (^{0}C)[a]	Wind Direction (^{0})[b]	Max Wind Speed (km h^{-1})[a]	Total Rain (mm)[a]	Total Snow (cm)[a]	Total Precipitation (mm)[a]
Q130612A	16.1	28.1	10.1	280-300 & 80	22	0	0	0
Q180612A	23.8	27.9	19.7	220-230	22	4.4	0	4.4
Q190612B	26.8	33.4	20.2	230-250	35	0	0	0
Q200612B	29.5	34.6	24.4	220-230	44	0	0	0
Q250612A	17.6	20.8	14.3	270 & 230	52	0	0	0
Q050712A	24	27.8	20.2	250-270	15	0	0	0
Q110712A	22.8	29.5	16	320-330	19	0	0	0
Q120712A	24	32	16	330-340	20	0	0	0
Q240712A	23	27.6	18.4	330-350	48	0	0	0
Q070812A-TOP	22.8	29.9	15.7	250-280	37	0	0	0
X300709B[c]	20.8	27.7	13.4	220 & 320	44	Trace	0	Trace
X050809B[c]	18.7	24.4	10.9	310	37	0	0	0
X070809A[c]	19.8	29.5	12	230-250	32	42.2	0	42.2
X070809B[c]	19.8	29.5	12	230-250	32	42.2	0	42.2
X100809A[c]	22.3	30	16	340-350	115	31.8	0	31.8
X130809A[c]	23.4	29.6	16.8	170-210	20	0	0	0
X210809B[c]	20.8	27.2	14.7	340-350	50	1.4	0	1.4
X280809B[c]	16.7	22.3	11.4	350	50	22.2	0	22.2
X280909B[c]	10.6	18	5.6	340-350	67	22.6	0	22.6
X131109A[c]	4.3	15.8	-1.5	310-320	37	0	0	0
X030211A	-10.5	-3.8	-17.1	240 & 350	50	0	0	0
X030211B	-10.5	-3.8	-17.1	240 & 350	50	0	0	0

Filter	Average Temp. (^{0}C)[a]	Max Temp. (^{0}C)[a]	Min Temp. (^{0}C)[a]	Wind Direction (^{0})[b]	Max Wind Speed (km h^{-1})[a]	Total Rain (mm)[a]	Total Snow (cm)[a]	Total Precipitation (mm)[a]
X040211A-BOTTOM	-1.6	-1.3	-10.2	230 & 310	59	0	14.2	11.2
X040211B-TOP	-1.6	-1.3	-10.2	230 & 310	59	0	14.2	11.2
X040211B-BOTTOM	-1.6	-1.3	-10.2	230 & 310	59	0	14.2	11.2
X230211A-BOTTOM	-3.8	-0.4	-9.9	340-350	15	0	0	0
X250211A-BOTTOM	-5	-0.6	-9.1	290-320	22	0	7	4.4
X030311A-TOP	-7.4	-2.5	-12.3	350-0	32	0	0	0
X030311A-BOTTOM	-7.4	-2.5	-12.3	350-0	32	0	0	0
X250311A-TOP	-8.9	-3	-5.3	350	13	0	0	0
X250311A-BOTTOM	-8.9	-3	-5.3	350	13	0	0	0
X070411A-TOP	3.3	8.3	-1.7	330	13	0	0	0
X070411A-BOTTOM	3.3	8.3	-1.7	330	13	0	0	0
X051011A-TOP	13.2	19.3	7.1	350-20	4	0	0	0
X051011A-BOTTOM	13.2	19.3	7.1	350-20	4	0	0	0
X061011A-TOP	11.1	17.4	4.8	0	32	0	0	0
X061011A-BOTTOM	11.1	17.4	4.8	0	32	0	0	0
X211011A-TOP	8.2	10.5	5.8	270-0	39	Trace	0	Trace
X211011A-BOTTOM	8.2	10.5	5.8	270-0	39	Trace	0	Trace
X281011A-TOP	3.5	8.9	-2	150 & 345	11	0	0	0
X281011A-BOTTOM	3.5	8.9	-2	150 & 345	11	0	0	0
X01111A-TOP	8.2	13.3	3.1	225	19	0	0	0
X01111A-BOTTOM	8.2	13.3	3.1	225	19	0	0	0
X041111A-TOP	4.2	9	-0.6	320	35	0	0	0

Filter	Average Temp. (^{0}C)[a]	Max Temp. (^{0}C)[a]	Min Temp. (^{0}C)[a]	Wind Direction (^{0})[b]	Max Wind Speed (km h^{-1})[a]	Total Rain (mm)[a]	Total Snow (cm)[a]	Total Precipitation (mm)[a]
X041111A-BOTTOM	4.2	9	-0.6	320	35	0	0	0
X08111A-TOP	10.9	13.1	8.6	230	11	0.6	0	0.6
X08111A-BOTTOM	10.9	13.1	8.6	230	11	0.6	0	0.6
X18111A-TOP	2.8	7.6	-2	230 & 310	50	0	0	0
X18111A-BOTTOM	2.8	7.6	-2	230 & 310	50	0	0	0
X071211A-TOP	-0.5	1.3	-2.2	270	19	0	Trace	Trace
X071211A-BOTTOM	-0.5	1.3	-2.2	270	19	0	Trace	Trace
X121211A-TOP	2.3	6.8	-2.2	220	20	0	0	0
X121211A-BOTTOM	2.3	6.8	-2.2	220	20	0	0	0
X131211A-TOP	3	8.6	-2.6	240	13	0	0	0
X131211A-BOTTOM	3	8.6	-2.6	240	13	0	0	0
X161211A-TOP	1.9	5.1	-1.3	330-350	57	0	0.2	0.2
X161211A-BOTTOM	1.9	5.1	-1.3	330-350	57	0	0.2	0.2
X190612A	26.8	33.4	20.2	230-250	35	0	0	0
X200612A	29.5	34.6	24.4	220-230	44	0	0	0
X020812A	22.6	28.8	16.4	250	24	0	0	0
X040812A	27	32	21.9	220	32	Trace	0	Trace
X050812A	23.3	28.9	23.3	340-10	50	0.8	0	0.8
X060812A	20.6	26.2	20.6	250 & 310	17	0	0	0
X070812A-BOTTOM	22.8	29.9	15.7	250-280	37	0	0	0
X090812A-TOP	19.6	20.9	18.3	40	17	26.8	0	26.8
X090812A-BOTTOM	19.6	20.9	18.3	40	17	26.8	0	26.8
X110812A-TOP	18.9	21.1	16.6	330-20	33	10.4	0	10.4
X110812A-BOTTOM	18.9	21.1	16.6	330-20	33	10.4	0	10.4

Filter	Average Temp. (^{0}C)[a]	Max Temp. (^{0}C)[a]	Min Temp. (^{0}C)[a]	Wind Direction (^{0})[b]	Max Wind Speed (km h^{-1})[a]	Total Rain (mm)[a]	Total Snow (cm)[a]	Total Precipitation (mm)[a]
X120812A-TOP	20.5	25.2	15.8	270 & 350	26	0.4	0	0.4
X120812A-BOTTOM	20.5	25.2	15.8	270 & 350	26	0.4	0	0.4

[a] Meteorological data was acquired from Environment Canada: Historical Weather Data, Toronto North York Site
[b] Wind direction was found by looking HYSPLIT (Hybrid Single Particle Lagrangian Integrated Trajectory Model) by Air Resources Laboratory (NOAA)
[c] Sampled and extracted by Busca (2010)

Filters are named according to the following code: ABbCcDdE where:
A is either Q (quartz filter) or X (XAD-coated filter)
Bb is the day
Cc is the month
Dd is the year
E is the air sampler (A or B)

Appendix I: Pollution Data for Sampling Dates

Filter	Average NO_2 (ppb)[a]	Average Daytime NO_2[b] (ppb)[a]	Average O_3 (ppb)[a]	Average PM2.5 ($\mu g\ m^{-3}$)[a]
Q120309B	30	26	15	9
Q160409B	14	13	39	7
Q240409B	17	14	33	7
Q270409B	17	16	26	4
Q190509A	19	20	55	NA
Q190509B	19	20	55	NA
Q040609A	15	10	28	NA
Q040609B	15	10	28	NA
Q190609A	10	12	26	6
Q190609B	10	12	26	6
Q220609APM10	19	13	35	9
Q220609BPM2.5	19	13	35	9
Q290609B-TOP	15	13	16	5
Q290609B-BOTTOM	15	13	16	5
Q030709A-TOP	2	2	22	2
Q060709A-TOP	7	5	18	3
Q060709A-BOTTOM	7	5	18	3
Q130709A	9	7	21	4
Q150709A	12	10	27	6
Q180709A	12	9	16	4
Q180709B	3	9	17	3
Q190709B	11	9	14	5
Q200709B	21	20	16	6
Q270709A	13	12	28	11
Q290709A	16	16	25	9
Q050809A	8	3	19	3
Q130809B	17	13	41	25
Q180809A	12	11	32	8
Q210809A	4	6	9	4
Q240809A	12	9	29	8
Q280809A	9	8	18	2
Q310809A	15	9	18	6
Q040909A	12	6	24	9
Q150909A	12	11	17	3
Q180909A	13	9	18	3
Q210909B	16	16	16	13
Q240909A-TOP	10	10	17	4
Q280909A	5	5	20	1

Filter	Average NO_2 (ppb)[a]	Average Daytime NO_2[b] (ppb)[a]	Average O_3 (ppb)[a]	Average PM2.5 ($\mu g\ m^{-3}$)[a]
Q011009A	15	13	9	4
Q051009B	13	15	13	3
Q131009B	7	11	15	2
Q131009A-AM	8	8	21	3
Q131009A-PM	8	8	12	1
Q141009A-AM	13	13	14	2
Q151009A-AM	18	18	17	3
Q151009A-PM	11	11	20	3
Q191009A	21	22	9	10
Q261009A	21	19	13	3
Q271009A	25	26	8	13
Q281009A	25	18	7	7
Q291009A	19	24	7	6
Q051109A	9	12	18	2
Q061109A	17	13	23	3
Q071109A	16	15	25	13
Q161109A	23	24	9	6
Q231109A	21	23	5	5
Q271109A	14	14	11	5
Q101209A	16	15	20	4
Q050110A	9	13	24	1
Q060110A	9	8	27	2
Q070110A	14	11	23	1
Q240210A	14	8	22	3
Q240210B	14	8	22	3
Q020310B-TOP	13	13	28	3
Q020310B-BOTTOM	13	13	28	3
Q190310B	11	11	26	3
Q310310A-TOP	37	32	16	12
Q190410A	15	9	36	6
Q210410A	17	11	31	4
Q290410B	4	6	31	2
Q050510A	17	19	34	8
Q060510A	6	5	27	0
Q280510A	13	20	29	7
Q310510A	14	12	33	8
Q040610A	7	7	29	4
Q070610A	12	9	21	4
Q070610B	12	9	21	4
Q110610A	15	13	22	7
Q250710A	10	7	27	9

Filter	Average NO_2 (ppb)[a]	Average Daytime NO_2[b] (ppb)[a]	Average O_3 (ppb)[a]	Average PM2.5 ($\mu g\ m^{-3}$)[a]
Q090810A	25	21	19	22
Q100810A	13	12	28	11
Q160810A	13	10	27	5
Q270810A	15	14	40	13
Q300810A	19	23	43	23
Q130910A	10	9	22	2
Q200910A	22	13	13	8
Q210910A	15	17	35	12
Q291010A	8	8	23	3
Q040211A-TOP	24	28	22	9
Q230211A-TOP	27	27	21	6
Q250211A-TOP	14	13	27	4
Q090911A	14	10	19	8
Q071011A	23	21	26	21
Q181111B	14	16	19	6
Q071211B	17	19	15	5
Q121211B	35	30	7	17
Q131211B	42	39	3	26
Q161211B	6	8	21	1
Q140512A	19	18	37	9
Q230512A	15	13	27	9
Q300512A	29	4	4	2
Q040612A	10	11	22	3
Q040612B	10	11	22	3
Q060612A	15	10	24	7
Q060612B	15	10	24	7
Q130612A	10	12	27	3
Q180612A	13	12	45	18
Q190612B	10	9	54	19
Q200612B	10	10	58	19
Q250612A	3	3	28	2
Q050712A	21	14	23	13
Q110712A	14	17	36	11
Q120712A	22	22	45	15
Q240712A	5	5	28	5
Q070812A-TOP	12	12	50	10
X300709B[c]	15	13	28	11
X050809B[c]	8	3	20	3
X070809A[c]	11	10	28	9
X070809B[c]	11	10	28	9
X100809A[c]	9	9	22	7

Filter	Average NO_2 (ppb)[a]	Average Daytime NO_2[b] (ppb)[a]	Average O_3 (ppb)[a]	Average PM2.5 ($\mu g\ m^{-3}$)[a]
X130809A[c]	17	13	40	24
X210809B[c]	6	6	21	4
X280809B[c]	9	8	17	2
X280909B[c]	5	5	20	1
X131109A[c]	20	21	13	4
X030211A	19	20	30	4
X030211B	19	20	30	4
X040211A-BOTTOM	24	28	21	9
X040211B-TOP	24	28	21	9
X040211B-BOTTOM	24	28	21	9
X230211A-BOTTOM	29	27	19	7
X250211A-BOTTOM	14	13	27	4
X030311A-TOP	26	29	21	4
X030311A-BOTTOM	26	29	21	4
X250311A-TOP	20	20	23	3
X250311A-BOTTOM	20	20	23	3
X070411A-TOP	26	29	22	6
X070411A-BOTTOM	26	29	22	6
X051011A-TOP	18	12	13	7
X051011A-BOTTOM	18	12	13	7
X061011A-TOP	28	22	8	12
X061011A-BOTTOM	28	22	8	12
X211011A-TOP	7	6	11	3
X211011A-BOTTOM	7	6	11	3
X281011A-TOP	29	24	5	10
X281011A-BOTTOM	29	24	5	10
X01111A-TOP	27	29	12	15
X01111A-BOTTOM	27	29	12	15
X041111A-TOP	18	13	13	5
X041111A-BOTTOM	18	13	13	5
X08111A-TOP	27	30	3	18
X08111A-BOTTOM	27	30	3	18
X18111A-TOP	14	16	19	6
X18111A-BOTTOM	14	16	19	6
X071211A-TOP	17	19	15	5
X071211A-BOTTOM	17	19	15	5
X121211A-TOP	35	30	7	17
X121211A-BOTTOM	35	30	7	17
X131211A-TOP	42	39	3	26
X131211A-BOTTOM	42	39	3	26
X161211A-TOP	6	8	21	1

Filter	Average NO_2 (ppb)[a]	Average Daytime NO_2[b] (ppb)[a]	Average O_3 (ppb)[a]	Average PM2.5 ($\mu g\ m^{-3}$)[a]
X161211A-BOTTOM	6	8	21	1
X190612A	10	9	54	19
X200612A	10	10	58	19
X020812A	12	12	44	19
X040812A	7	7	56	19
X050812A	4	5	36	6
X060812A	7	4	28	3
X070812A-BOTTOM	12	12	50	10
X090812A-TOP	9	12	14	6
X090812A-BOTTOM	9	12	14	6
X110812A-TOP	8	7	20	4
X110812A-BOTTOM	8	7	20	4
X120812A-TOP	4	4	22	3
X120812A-BOTTOM	4	4	22	3

[a] Pollution data acquired from Ontario Ministry of the Environment: Historical Pollutant Data, Toronto North Site and values are averaged over the sampling time.
[b] NO_2 values were averaged between 8 am and 5 pm, local time.
[c] Sampled and extracted by Busca (2010)

Filters are named according to the following code:

ABbCcDdE where:
A is either Q (quartz filter) or X (XAD-coated filter)
Bb is the day
Cc is the month
Dd is the year
E is the air sampler (A or B)